Comprehensive analysis of WRN protein interaction network by Mass Spectrometry

Veronika A. Glukhova

A dissertation

submitted in partial fulfillment of the

requirements for the degree of:

Doctor of Philosophy

University of Washington

2014

Reading Committee:

Raymond J. Monnat Jr., Chair

Michael J. MacCoss

Toshiyasu Taniguchi

Program Authorized to Offer Degree:

Pathology

University of Washington

Abstract

Comprehensive analysis of WRN protein interaction network by Mass Spectrometry

Veronika A. Glukhova

Chairperson of the Supervisory Committee:

Professor Raymond J. Monnat Jr.

Department of Pathology

Cells that have lost WRN function exhibit a shortened replicative lifespan, accumulation of chromosomal aberrations, and demonstrate sensitivity to a number of chemotherapeutic agents, including DNA Topoisomerase I inhibitor camptothecin (CPT). On organismal level, the lack of this protein results in the progeroid syndrome Werner Syndrome, which is characterized by increased incidence of cancers, cardiovascular disease, cataracts, and other age-associated pathologies.

In this study we examined the network of proteins that associate with WRN protein, and then expanded this picture when the cells were challenged with CPT. We detail the profiling analysis used for unbiased detection of all interacting proteins using LC-MS/MS, followed by data analysis and selection of targets for follow-up.

We then focus on the method development, complexities of data analysis, and

application of selected reaction monitoring (SRM), a method for targeted MS. Using RNAi we demonstrate the power of this technique for relative protein quantitation of human proteins WRN and TP53, and a number of small, low-abundance seminal fluid proteins from *D.melanogaster* flies.

SRM was applied for two studies of the WRN interactome: 1) to partially validate findings of the profiling screen after short-term treatment with CPT, and 2) to describe the dynamics of association of these proteins with WRN as a function of time, by expanding the treatment time course to 6 and 12 hours.

We report on our description of WRN protein interaction complexes in unperturbed cells, and how these interaction complexes become reorganized in response to DNA damage. Our results demonstrate that the newly recruited proteins participate in chromatin remodeling, negative regulation of cell cycle progression, and double-strand break repair. We focus on 40 proteins to test their differential interaction with WRN after 1, 6, and 12 hours of treatment with CPT. We specifically focus on the functional importance of the chromatin-remodeling factors, and present the list of WRN interacting proteins that have emerged as high-priority targets for functional validation. Finally, we discuss how our work has expanded the understanding of the functional roles of WRN, and how targeted, hypothesis-driven application of mass spectrometry can be used to answer complex questions about protein interaction.

Table of Contents

List of Figures

List of Tables

Acknowledgements

I am grateful for the opportunities I had, which showed me that indeed, I was doing what I liked, even when the process itself was not pleasant. This is what in climbing we call “Type 2 fun”.

I am grateful for the many friends who kept me sane during my years in graduate school. I received a lot of support from people who have gone through this process, and from those who decided that it was not for them. Whether it was a recharging run, an arduous climb, or regular 5 a.m. rowing sessions, my partners in physical pursuits kept me afloat.

I am thankful for the mentorship I received from many people over the years, including my undergraduate advisor Dr. Jeff Young, and some of my favorite professors, Drs. George Kriz and Emily Peele. My first undergraduate research mentors outside of the university, microbiologists Dr. Yuri Gorby and Jeff MacLean, really showed me that laboratory research was fun and engaging. Collecting bacterial samples from the bioreactor in the middle of the night made me feel important, and science assumed an urgency that I never experienced in the classroom.

I am thankful to my graduate advisors Ray and Mike, who have attempted many times to give up on me, but somehow have kept scheduling meetings, replying to emails, and answering questions. I learned a lot about what types of encouragement and pressure work best for me because of the people who were constantly providing me with the opportunity to test the myriad of different approaches get me to finish what I started. I am infinitely thankful to our graduate

program administrator Steve Berard, who is every student's biggest cheerleader, tireless advocate, and a priceless colleague.

Finally, I could not have done this without the support of my family. I heard from a young age that higher education was not optional. I always knew that I would at least finish an undergraduate degree, and my parents backed that knowledge with full support of my studies. My parents and brother Pavel love hearing about my work, and enjoy learning about advancements in modern research. The pride that my grandparents, who are in their 80s, express when they understand something about genetics and biochemistry from my drawings and explanations, gives me hope that someday I will have the opportunity to teach, or to communicate science to a wider audience in some capacity.

My daily struggles, successes, and stresses are seen by no one better than my most steadfast partner, my husband Doug. He is the one who gets to hear about the hard day in the lab, the failed experiments, and he is the one who gets to make dinner when I stay at work too late. He and our son Silas give me all the reasons to try harder, and for this I am so very grateful.

Dedication

To my parents, to Pavel, Doug, and Silas

Chapter 1 – Werner Protein, its structure, known functions and importance in human aging and the Werner Syndrome

Deficiency in the Werner protein (WRN) results in the Werner syndrome (WS), which is characterized by accelerated rate of mutation and the organism's inability to resolve a variety of genome-damaging events. Clinically, WS resembles premature aging, and activity of proteins such as WRN suggests that the complex process of aging may be controlled in part by the action of individual genes such as *WRN*. Aging research is extremely important considering the changing demographics worldwide, increased overall longevity and rise in elderly population. Understanding of the mechanisms that underlie aging and development of age-related disease due to genomic aberration can lead us to improved treatment, prevention, and alleviated burden of age-related disease.

To determine what role mechanistic role WRN plays in aging and age-related pathologies, we study protein function in normal and diseased states using proteomics. Resources that are currently available to us include modern analytical instrumentation, support from computational sciences, and access to rare biological samples. Our work is aimed at defining proteins consistently associated with WRN, and post-translational modifications of WRN that are required, or are causal, for its function in human cells. This knowledge will increase our understanding of WS pathogenesis and provide insight into novel strategies to alter the progression of WS or associated diseases such as atherosclerotic cardiovascular disease, cancer, diabetes, and osteoporosis.

Section 1: WRN protein, its biology and role in disease

Werner Syndrome

Werner syndrome (WS) as an uncommon autosomal recessive disease whose phenotype includes features of premature aging, genetic instability, graying and loss of hair, loss of subcutaneous fat and the development of several age-associated diseases such as ocular cataracts, cancer, cardiovascular disease, diabetes mellitus and osteoporosis (1,2). Tumors in WS are predominantly of five types that are uncommon in general population: soft tissue sarcomas, osteosarcoma, thyroid carcinoma, acral lentigenous melanoma and meningioma (2,3). Werner patient mutations are usually nonsense or frameshifts that result in a truncated form of the protein that fails to localize to the nucleus and becomes degraded (3–6) . On cellular level, loss of WRN function manifests itself as accelerated rate of mutation and the organism's inability to resolve a variety of genome-damaging events; it suppresses cell division, confers DNA damage hypersensitivity, and promotes genetic instability (7).

Phenotypic expression of the WRN mutation suggests that it is a sensitizing mutation. Initial development in the affected individual is normal, and delayed onset of the disease may require damage accumulation, or indicate a threshold for accumulation of sufficient hits to the genome integrity, or a switch in the proliferative capacity of cells. The lack of DNA damage management may leave unresolved recombination products that are allowed to persist, and which then may promote mutations or gene rearrangements.

WRN helicase overview

Helicases are enzymes vital to all living organisms. They are motor proteins that move directionally along a nucleic acid phosphodiester backbone, separating two annealed nucleic acid strands (i.e. DNA, RNA, or RNA-DNA hybrid) using energy derived from nucleotide hydrolysis. There are many helicases (14 confirmed in *E. coli*, 24 in human cells) resulting from the great variety of processes in which strand separation must be catalyzed. Although separation of the strands initially appears to be an essential process due to necessity of transcription and replication of nucleic acids, many helicases are specialized to perform additional functions in nucleic acid metabolism and repair, translation, recombination, DNA repair, and ribosome biogenesis.

Multiple superfamilies of helicases have been identified, and the individual members have been characterized. Helicases are separated into superfamilies based on primary sequence and homology, sequence motifs, presence of additional domains that function in unwinding and substrate selectivity. There are superfamilies (SF) I, II, and III, as well as the DnaB-like family, and Rho- like family. WRN protein is classified as a member of the superfamily II, RecQ family of helicases (8).

The RecQ family of proteins is conserved across prokaryotes and eukaryotes. In eukaryotes, 5 members of this family are currently known, all of which share a $3' \rightarrow 5'$ DNA helicase activity, as well as structural features including the RQC (RecQ consensus) and HRDC (Helicase and RNase C-terminal) domains that play roles in substrate recognition or binding ((9). WRN (also referred to as RECQ3 or RECQL2) is unique within this family in possessing

additional 3′ → 5′ DNA exonuclease activity. A closely related protein, E. coli RecQ, is involved in DNA repair mechanisms (10), implying that WRN performs a similar function.

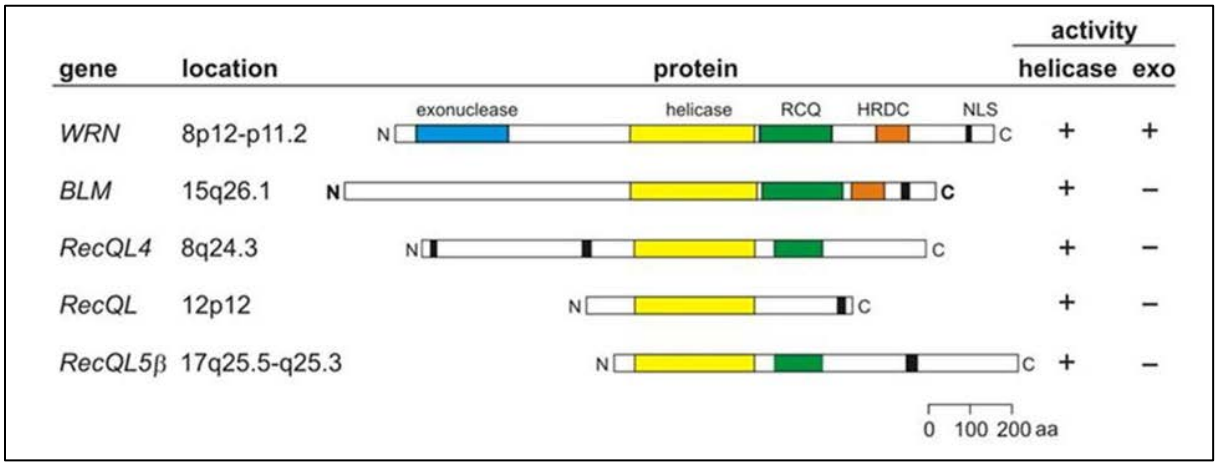

Figure 1.1: The five known members of the RecQ family.

The five known members of the RecQ helicase family share several structural features, but differ vastly in size, tissue distribution, and disease association.

It has been recently determined that helicases do not merely wait passively for the fork to widen, but play an active role in forcing the fork to open (11), acting as a motor unwinding its substrate. Recent studies have shown that WRN is important in replication fork progression after DNA damage with the removal of DNA lesions or structural obstacles was extensively covered in a recent review (12), while family members RecQL4 and BLM have been suggested to play roles in replication initiation and in replication fork restart after DNA damage, respectively(5,13).

In addition, helicases engage in a large number of molecular interactions, and experimental evidence shows that helicases may process much faster *in vivo* than *in vitro* due to the presence of accessory proteins that aid in the destabilization of the fork junction. Helicases

rarely operate in isolation, and WRN association with proteins involved in maintenance of genome stability, repair, and scaffolding, suggest some of its *in vivo* functions.

WRN protein structure

WRN gene is located at locus 8p12-p11.2 on the human chromosome 8 (OMIM, 2003). The transcript of the gene is 140.5 kb long with many introns and exons, and the protein product is 162 kDa in size. WRN helicase is localized to the nucleus, and consists of several major structural domains (Figure 1.2).

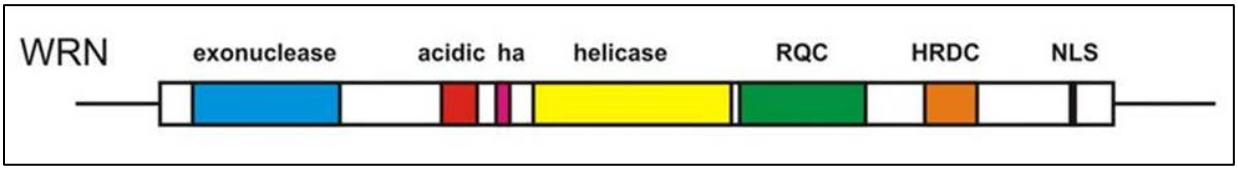

Figure 1.2: Domain structure of the Werner protein.

Werner protein contains a number of characterized domains, including its two main catalytic domains: helicase and exonuclease, RecQ C-terminal (RQC), helicase-and-RNaseD-like-C-terminal (HRDC), and nucleolar localization sequence (NLS).

At the N-terminus of the WRN protein is the 171 amino acid-long exonuclease region. It is highly similar to the exonuclease regions of proteins, such as DNA polymerase, that have DNA proofreading activity. When exposed to double-stranded DNA, these exonuclease residues form a hexamer around the end of the strand and remove DNA bases toward the 5'. In previous studies involving removal of N-terminal residues of WRN, protein function was, suggesting that it contains the catalytic domain (14).

The DEAD box domain of WRN is highly conserved among DNA and RNA helicases.

DEAD box helicases are involved in various aspects of RNA metabolism, including nuclear transcription, pre mRNA splicing, ribosome biogenesis, nucleocytoplasmic transport, translation, RNA decay and organellar gene expression. Along with the helicase-C (carboxy-terminal helicase) domain, this region of the protein is thought to be essential to helicase activity of WRN (Sanger Institute- Ensembl Protein Report, 2003).

On the C-terminal end of the protein reside the nucleolar localization sequence(15), the RecQ helicase C-terminal region (RQC), and the helicase-and-RnaseD-C-terminal conserved region (HRDC) (16). The HRDC domain spans 80 amino acids and contains five helices connected by short turns or hydrophobic loops. Certain hydrophobic residues within the loops are necessary for the packing of this domain into a bundle. This portion of the protein has been shown to interact with DNA in a non-sequence specific manner, suggesting that this domain may contribute to the interaction between the WRN protein and the double stranded DNA as it performs its helicase function (17). Multiple studies have shown that both of these regions are involved in substrate recognition and binding.

In addition to these regions, the WRN protein, like other helicases, has two conserved Mg-dependent ATP binding. Binding and hydrolysis of ATP by these regions provides the energy necessary for the DNA helicase to break the hydrogen bonds between the bases of the double stranded DNA and unwind the helix (10,18).

Due to the variety of functions performed and substrates utilized, helicases adapt different morphologies and oligomerization states, and can function as monomers, dimers, and up to hexamers. It has been shown that mouse WRN appears to work as a multimer(19), while human WRN forms a trimer (20), a dimer of the full-length protein in solution and a tetramer

when bound to DNA (21). Additional studies of WRN exonuclease domain (WRNexo) have shown that it forms a hexamer (5). Comparison between exonuclease domains of mouse and human WRN revealed differences in coordination of three residues, all of which were shown to be essential for WRNexo function by mutational analysis(19). Similar to other essential proteins, many helicases have redundant functions. The fact that *WRN* is not an essential gene has long suggested that WRN function may be partially redundant with the function of other proteins, such as other RecQ helicases.

WRN protein in DNA damage management and repair

WRN protein has been reported to promote recombination, replication restart, or other aspects of cellular DNA metabolism, such as telomere maintenance, that may require resolution. WRN has been shown to interact physically or functionally with replication protein A, proliferating cell nuclear antigen, DNA polymerase δ, tumor protein p53, topoisomerases I and III, FEN-1/flap endonuclease, RAD51, and the nonhomologous-end-joining (NHEJ) components Ku and DNA-PK (4,6,7). We discuss the previously reported interacting proteins in further detail in Chapter 4. Table 4.1 is a referenced summary of all previously reported WRN-interacting proteins to date.

In damaged DNA, the Ku heterodimer, consisting of Ku70 (XRCC6) and Ku86 (XRCC5), binds to the exposed ends of the broken DNA molecule, and it recruits DNA-PKcs, which phosphorylates other proteins and activates the repair machinery(22,23). Previous data, including ours, suggests physical interaction between WRN, Ku, and DNA-PKcs, implicating WRN participation in NHEJ repair mechanism (24,25). While it has been shown that WRN has a

role in NHEJ in the absence of a functional Fanconi Anemia pathway (26), there is no direct data suggesting that WRN deficient cells have an NHEJ defect.

The requirement for WRN in the cell appears to be strongly driven by replication stress, and it is important to understand how activity of WRN is modulated by recruitment of additional biochemical factors to perform all of its activities. Cells harboring mutations in the *WRN* gene display an increased rate of spontaneous sister chromatid exchange and other aberrations.

WRN protein has also been shown to play a role in recombination *in vitro* and *in vivo* (7,26–29), and human cells deficient in WRN are hypersensitive to a number of chemical agents, where the resolution of inflicted damage necessitates repair by homologous recombination (HR). Cells that lack WRN are highly sensitive to DNA cross-linking drugs such as 8-methoxypsoralen (30) and cis-Platinum (*cis*-Pt) (31), and DNA topoisomerase I inhibitor Camptothecin (32,33). WRN deficiency also leads to sensitivity to the DNA damaging agent 4- nitroquinoline-1-oxide (4NQO), which induces DNA lesions usually corrected by nucleotide excision repair (30), although other NER damage classes appear unaffected by WRN loss.

Some research suggests that the WRN protein performs DNA repair when problems occur at the replication fork, preventing the progression of replication (12,34,35). This may occur when the helicase associates with a topoisomerase during DNA replication or recombination. The topoisomerase protein transiently cuts the DNA at regular intervals as it is unwound, allowing DNA to unwind smoothly without becoming tightly coiled at the end of the strand. The helicase may associate with topoisomerase to correct mistakes which are made in this cutting process allowing smooth progression of the replication fork, and ensuring efficient recombination or replication (36).

Section 2: Analysis of multi-protein complexes using Affinity Purification and Mass Spectrometry (AP-MS)

Analysis of proteins by Mass Spectrometry (MS)

Mass spectrometry (MS) is an analytical technique that measures mass to charge ratios (*m/z*) of analyte molecules that can provide both qualitative and quantitative information on molecular mass, the concentration of the analyte, elemental composition, and structure. Development of soft ionization techniques, advancements in separation, increased power of mass analyzers, and improved data interpretation tools have all enabled the extension of this powerful technique to the analysis of proteins.

In 2002, the Nobel Prize in Chemistry was awarded for the development of methods for identification and structure analyses of biological macromolecules". Two of the awards were given for development of electrospray ionization (ESI) (37) and matrix-assisted laser desorption ionization (MALDI) (38,39). These two soft-ionization approaches truly opened up the realm of analysis of large, fragile molecules by transferring them into gas phase, and enabled interfacing between peptides or proteins in solution and powerful mass analyzers that help determine their identity.

The combination of liquid chromatography and mass spectrometry (LC-MS) enables the separation of complex mixtures with downstream analysis by MS, and is a technique that has achieved unprecedented sensitivity and selectivity. Chromatographic separation can be

performed on the protein level (40), peptide level following proteolytic digestion in one (41,42) or two, chromatographic dimensions (43,44), or by a combination of the two approaches (45). The typical approach used in our experiments is a “bottom-up” approach of digesting proteins into peptides, separating them in one dimension by reversed-phase (RP) liquid chromatography, and ionizing by ESI prior to introduction to the MS instrument. This scheme is summarized in Figure 1.3.

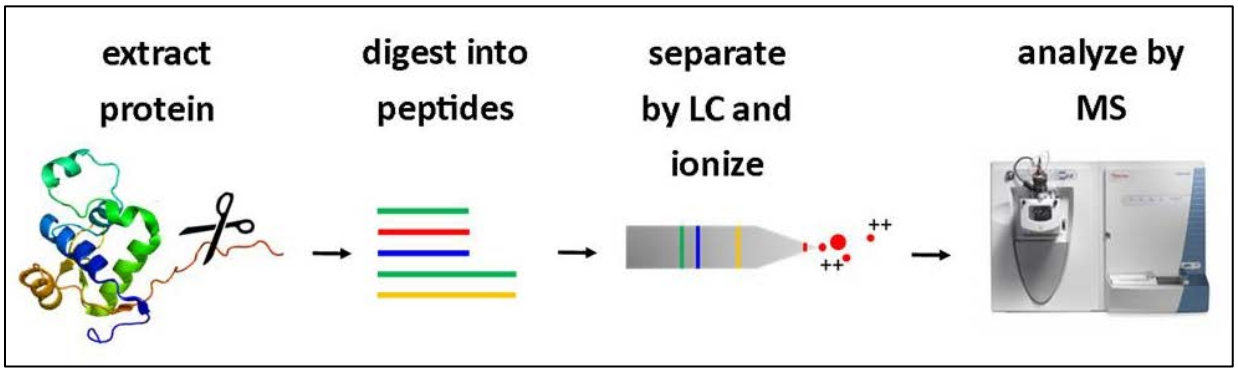

Figure 1.3: Typical proteomic workflow.

Protein extracts are reduced, alkylated and digested with proteolytic enzyme such as Trypsin, and the peptides are separated by liquid chromatography, typically by reversed phase. The eluates are ionized in line by ESI, and introduced into the mass spectrometer for mass analysis.

Sample preparation, separation, introduction into the mass spectrometer, and subsequent analysis all result in rich and extensive datasets. Development of the SEQUEST algorithm revolutionized the interpretation of mass spectra by rapid assignment of peptide sequence via correlation of experimental MS/MS patterns with a library of theoretical MS/MS spectral patterns (46). This approach automated interpretation of hundreds of thousands of spectra produced by MS instruments, and with ever-increasing scanning speed and richness of datasets has become an invaluable tool in proteomics. All profiling MS data in our work was analyzed

using SEQUEST.

Affinity Purification and Mass Spectrometry (AP-MS)

Understanding the composition of protein complexes surrounding a target protein of interest (bait) is often an important part in describing its function. Changes in composition of the interaction network in response to perturbations may reflect changes in the functional role of the target protein. Affinity purification coupled to mass spectrometry (AP-MS) has become a popular approach to isolate and analyze protein complexes. This technique is especially valuable for determining functional roles of unknown proteins bound to proteins of known function (47).

Individual proteins can be isolated from complex mixtures by exploiting native epitopes on endogenous proteins and using targeting immunoreagents (such as in antibody immunoprecipitation). Another approach involves encoding affinity tag sequences to be coexpressed along with coding genes of interest, and using reagents that selectively target the affinity tag (48). The latter approach is generally cheaper, and allows to use a single affinity approach to isolate and analyze multiple baits with the same tag, minimizing variability inherent in antibody immunoprecipitation studies. In our study we use the epitope tag approach, and will focus on AP-MS in context of tagged protein isolation.

In the course of our preliminary studies in isolation of WRN interacting proteins, we tested three epitope tag systems as shown schematically in Figure 1.4 and summarized thereafter.

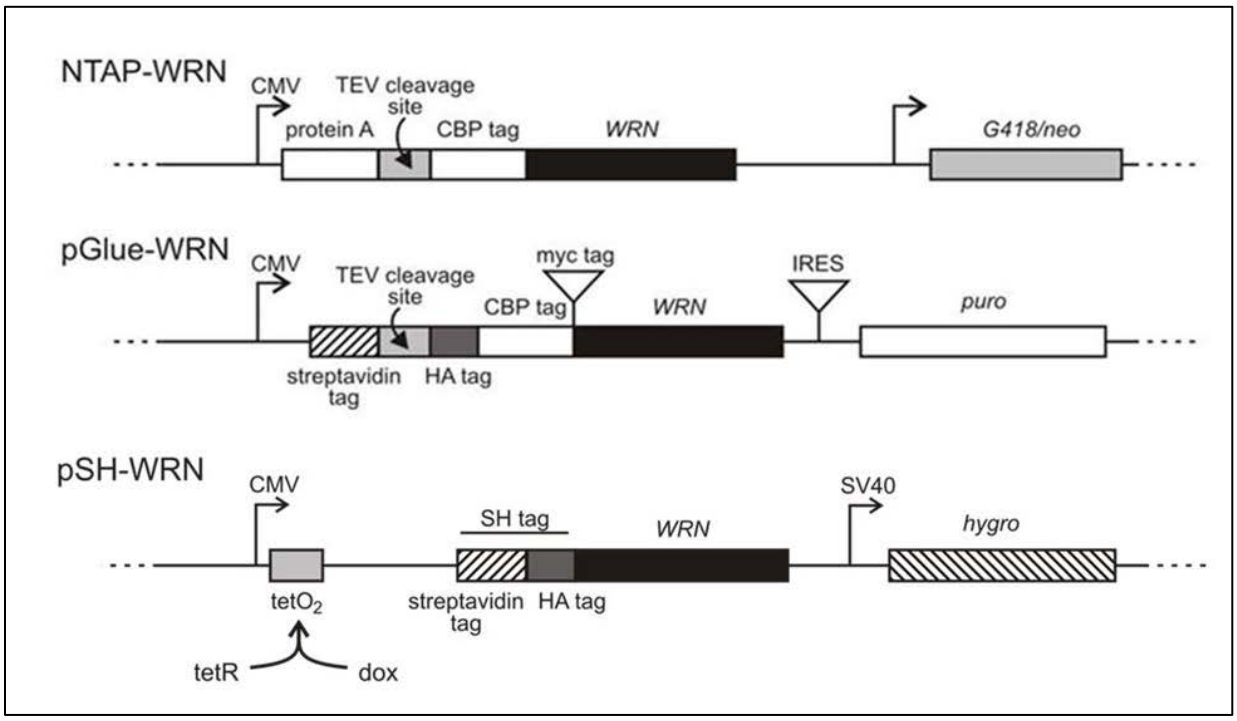

Figure 1.4: Schematic representation of three types of affinity tags used in our studies, the N-terminal tandem affinity purification (NTAP) tag, pGlue TAP tag, and a tetracycline-inducible Streptavidin and Haemagglutinin (SH) tag.

NTAP-WRN. An early version of the tag encoded a Protein A domain, a Tobacco Etch Virus (TEV) cleavage site, and a Calmodulin-Binding Protein (CBP). The selection of stable transfectants is performed with antibiotic G418.

pGlue-WRN. Tandem affinity tag pGlue (49,50) contains Streptavidin-Binding Protein (SBP), CBP, and the haemagglutinin (HA) epitope. This tag is smaller in size, tends to provide more reliable binding and release due to superior properties of SBP, and allows selection of transfectants with puromycin.

pSH-WRN (later referred to as SH-WRN). Tandem affinity tag SH (51) was constructed by Gateway cloning, and contains streptavidin tag and HA epitope, both of which can be used for

affinity purification. In our studies we used the streptavidin tag for isolation and HA tag for immunodetection.

Briefly, the experimental setup of an AP-MS experiment involves harvesting biological material, such as cells that express one of many available affinity tags, isolating the tagged proteins and their interacting partners, enzymatically digesting the whole sample, and performing mass spectrometric analysis. This protocol is outlined in Figure 1.5.

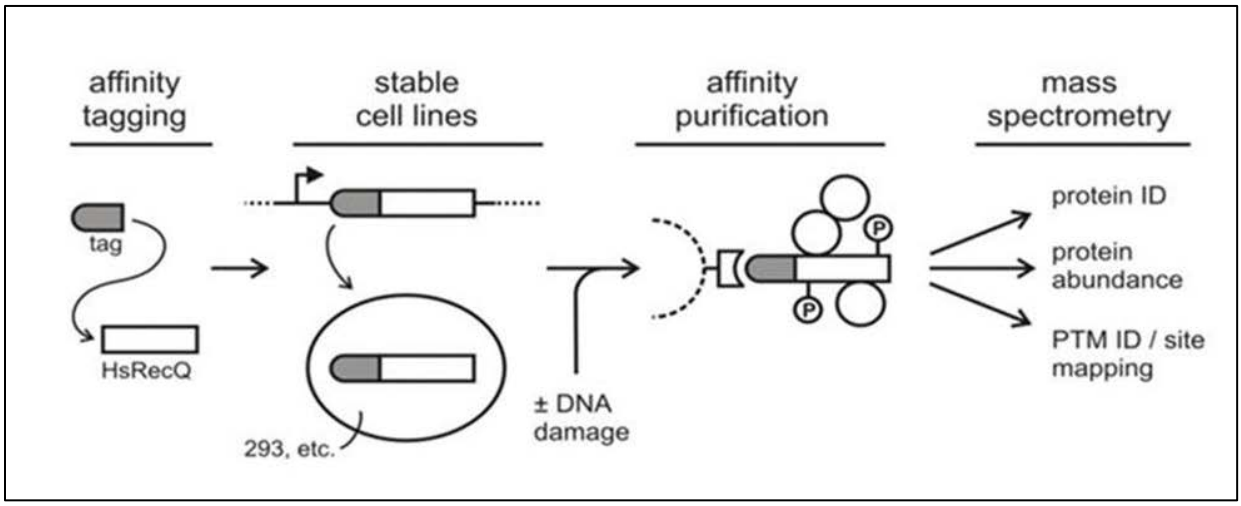

Figure 1.5: The experimental workflow of AP-MS experiment.

Tagged protein (bait) is stably expressed in cells, and isolated from the lysate by affinity purification. The resulting samples are analyzed by MS to identify components of the protein complex.

Based on extensive preliminary studies, all data reported in further chapters uses SH-tagged Werner protein (SH-WRN) expressed at 2-10x physiologic levels in human cells and then enriched by well- established methods for MS analysis (51–53). While many interaction studies are conducted by using immobilized bait out of its normal cellular environment, the benefit of the AP system is in its ability to capture protein interactions as they occur in specific cellular

microenvironments, which may be dependent on modifications or small molecules. As a method, AP results in production of a complex that is sufficiently clean from nonspecifically bound species, while minimizing the loss of legitimate interactors through the use of mild washing conditions.

Because a typical MS experiment will result in hundreds to thousands of protein identifications, inclusion of proper control samples is critical. Side-by-side affinity purifications of bait protein and identically tagged control proteins serve as ideal control experiments, and computational tools such as SAINT (Significance Analysis of INTeractome) are based on this experimental scheme (54).

Targeted Mass Spectrometry by Selected Reaction Monitoring (SRM)

Targeted MS and selected reaction monitoring (SRM), and it applications are described in detail in Chapter 2. Briefly, selected reaction monitoring (SRM) mass spectrometry is an approach to target specific peptides for mass analysis. In data-dependent acquisition (DDA) peptide ions are introduced into the instrument, and the most abundant precursor ions are chosen for MS2 fragmentation and sequencing from each scanned MS1 mass window, typically in the *m/z* range of 400-1200. This approach is often referred to as “shotgun proteomics”, describing the stochastic nature of identification. In SRM, a selected peptide is targeted by manipulating instrument settings to choose species of defined *m/z*. This approach is highly sensitive, selective, and reproducible. It is also highly quantitative, a feature that we exploit in our studies, further described in Chapters 2 and 5.

Notes to Chapter 1

Figures 1.1, 1.2, 1.4 and 1.5 were generated with help from Alden Hackmann.

Chapter 2 – Development of targeted methods to detect and quantify relative protein abundance, and their successful application for study of RNAi-mediated Protein Depletion.

Section 1: Introduction

We describe the use of a targeted proteomics approach, Selected Reaction Monitoring (SRM) mass spectrometry, to detect and assess RNAi-mediated depletion or 'knockdown' of specific proteins from human cells and from *Drosophila* flies. This label-free approach does not require any specific reagents to confirm the depletion of RNAi target protein(s) in unfractionated cell or whole organism extracts. The protocol described here is general, can be developed rapidly and can be multiplexed to detect and measure multiple proteins at once. Furthermore, the methodology can be extended to any tandem mass spectrometer - making it widely accessible. This methodology will be applicable to a wide range of basic science and clinical questions where RNAi-mediated protein depletion needs to be verified, or where differences in relative abundance of target proteins need to be rapidly assessed between samples.

RNA interference (RNAi) has established itself as a particularly powerful methodology for large scale loss-of-function screens to identify genetic determinants of development, aging or disease processes such as cancer. The genes, proteins and pathways identified by RNAi screens can serve as an immediate focus for additional experiments to elucidate mechanisms of action or,

in the case of disease, identify genes or proteins with the potential to serve as diagnostic or therapeutic biomarkers or targets. Libraries of RNAi reagents, such as short hairpin (sh) and short interfering (si) RNAs, are now available for many organisms to perform genome-scale screens or more targeted analyses of specific families of proteins, such as kinases (55–59).

Several practical approaches have been developed to validate RNAi screens and identify off-target and other confounding effects. These approaches include the use of multiple RNAi reagents predicted to target the same gene, and organism-specific "scrambled sequence" or nonspecific RNAi controls; RT-PCR or Western blot assays to demonstrate reduced expression of the targeted RNA or protein; and biochemical or biological "rescue" by expressing an RNAi-resistant target gene or cDNA (57,60). Direct verification of target protein depletion is desirable, as protein – rather than mRNA – depletion is the goal of many RNAi experiments. Direct analysis of protein abundance also allows researchers to account for the widely differing biological half-lives of proteins that may affect the interpretation of RNAi screen results. Despite the need for protein-based verification in RNAi experiments, high quality antibodies are not available for most proteins even in well-studied organisms. Moreover, proteins of high biological interest in any organism may be refractory to antibody development, and antibody-based analytical methods such as Western blotting are difficult to multiplex to enable the detection and quantitation of multiple proteins in single analyses. Mass spectrometry (MS) is a versatile alternative to detect and measure the difference in abundance of individual peptides from a digest of a protein mixture between conditions or states. Selected reaction monitoring (SRM) mass spectrometry, which has historically been used for small molecule analyses and is also well established for peptides absolute quantitation (61), represents a particularly promising

approach to validate the depletion or “knockdown” of a protein by RNAi. Due to its sensitivity and selectivity, SRM can detect specific target proteins, including low abundance proteins that may be missed or proteins intrinsically difficult to detect by “shotgun” proteomic profiling methods (62–65). Moreover, SRM can be applied to protein targets regardless of immunogenicity, can be used to detect and quantify specific proteins or modifications over a wide range of protein abundances with high accuracy (64,66), and can be multiplexed to detect and quantify multiple protein targets in single experiments. Additionally, multiplexing may be accomplished by implementing scheduling, where a larger number of transitions could be monitored by breaking the chromatographic space into windows.

Here, we describe a general SRM-based methodology that can be used to detect low abundance peptides that can be used as a proxy of a target protein and demonstrate the use of this method to measure RNAi-mediated depletion of specific proteins from human cells and from the fruit fly Drosophila melanogaster. We deliberately chose target proteins for these analyses that represent analytical challenges. The multifunctional human tumor suppressor protein TP53 is variably expressed and is modified across a wide range of residues by post-translational modifications that include phosphorylation, acetylation, ubiquitination, sumoylation, neddylation, methylation and glycosylation (67,68). Our two Drosophila target proteins, in contrast, are short accessory gland seminal fluid proteins that are among >130 seminal fluid proteins transferred from males to females during mating (69,70). Acp70A is a processed protein that in mature form is a 36 residue lysine- and arginine-rich peptide (69,71). Acp53C14a is a processed protein of 98 residues with no homology to known proteins, and for which there is no good antibody. WRN protein is a low-abundance, DNA-binding protein that belongs to the RecQ

family of helicases. Its loss causes Werner Syndrome, which is characterized by premature aging and genomic instability (72). Previous analysis by quantitative immunoblots has shown that lymphoblastoid cells lines and fibroblasts contain 6 × 104 WRN molecules per cell (73), and a more recent report using SRM estimates WRN abundance at <5 × 102 copies per cell in U-2 OS cells (74).

In this work we demonstrate the development of a common SRM protocol to detect and identify differences in abundance for these four target proteins in the context of RNAi-mediated depletion experiments in human cells or in whole flies. Our results show excellent agreement between SRM and Western blot-based detection and quantitation methods where a direct comparison was possible. Using different proteins as examples, we validate our peptide selection by utilizing publically available NIST spectral library for verification of our chosen transitions, using commercially available recombinant protein, and incorporating stable isotope labeled (SIL) peptides in the analysis.

Section 2: Experimental

Cell Culture and Fly Rearing

The SV40-transformed human fibroblast cell lines GM639 and HEK-293T cell line were obtained from the Coriell Institute Cell Repositories (Camden, NJ). Cells were grown in Dulbecco-modified Eagle's medium (MediaTech CellGro, Manassas, VA) containing 4500 mg/L glucose and supplemented with 10% fetal bovine serum (Hyclone, Logan, UT), penicillin and streptomycin sulfate (100 U/mL and 100 mg/mL, respectively; Invitrogen, Carlsbad, CA) in a

humidified 37 °C, 7% incubator. Drosophila melanogaster RNAi lines were obtained from the Vienna DrosophilaRNAi Center (VDRC; www.vdrc.at) (75). Flies were reared at 25 °C on yeast-cornmeal-molasses medium.

siRNA-mediated Depletion of TP53

TP53 depletions were performed using two methods, and differentially treated cells were used as indicated. Cells were initially transfected with a TP53-specific siRNA (Silencer Select s606) or Silencer Negative Control #1 siRNA (Applied Biosystems, Foster City, CA). In brief, cells were grown in 6-well plates (Nunc, Denmark) and transfected when 50% confluent with either 50 or 100 pmol of siRNA using Lipofectamine 2000 (Invitrogen, Carlsbad, CA) according to the manufacturer's instructions. Transfection efficiency was consistently >90% as estimated from the transfection of a Cy3-labeled control oligonucleotide of sequence 5′-Cy3-CCTAAGGTTAAGTCGCCCTCGCTCTAGCGAGGGCGACTTAACCTTAGG-3′ (Operon, Valencia, CA) followed by fluorescence microscopy. Cells were harvested by addition of trypsin 40 h after transfection, and used for Western blot analysis and mass spectrometry as described in following sections.

shRNA-mediated Depletion of TP53

Depletion of TP53 was additionally achieved by viral transduction of shp53 pLKO.1 puro plasmid (plasmid 19119; Addgene) or pLKO.1 expressing a scrambled shRNA with no known target sequence in the human genome (plasmid 1864, "scramble shRNA"; Addgene). The cells

were grown under puromycin selection (1 μg/mL) for 48 h prior to collection. The reduced level of protein was verified by Western blot.

Protein Depletion in Drosophila

The VDRC fly line #52425(21) contains a chromosome III P-element insertion from which an inverted repeat (IR)-Acp70A is expressed under the control of the UAS promoter. To generate RNAi flies, line #52425 males (genotype: w1118; +/+; UAS-IR-Acp70A/UAS-IR-Acp70A) were crossed to virgin females harboring the GAL4 transcription factor gene under control of aDrosophila tubulin promoter (genotype: w1118/w1118; +/+; tubulin-GAL4/TM3, Sb). The tubulin-GAL4 driver causes UAS-IR expression, resulting in RNAi-mediated knockdown of the Acp70Atarget gene in all adult tissues (76). Knockdown males were identified by the lack of the Sb marker; control males inherited and expressed the Sb marker. RNAi-mediated depletion of a second transferred and readily identifiable accessory gland protein, Acp53C14a (70,77), was also performed using the corresponding VDRC line for this gene, #44789, in crosses and sample preparation in parallel with Acp70A flies.

shRNA-mediated Depletion of WRN

Depletion of WRN protein from human GM639-cc1 cells was previously described by Mao et al (78). In brief, cells that stably express the lentiviral shRNA plasmid were grown under puromycin selection (1 μg/mL) for 48 h prior to collection. Decreased protein expression was verified by Western blot. Controls included cells transduced with pLKO.1 vector DNA alone or

with pLKO.1 expressing a scrambled shRNA with no known target sequence in the human genome (plasmid 1864, “scramble shRNA”; Addgene).

Generation of Expression Constructs and Tetracycline-inducible Cell Lines

The tet-inducible expression vector for N-terminally SH-tagged human WRN, pFTSH-WRN (originally named pcDNA5/FRT/TO/SH/GW/WRN) was a gift from Dr. Alessandro Vindigni (St. Louis University, MO, USA). It was constructed by Gateway cloning using human WRN ORF in pDONR223 vector for LR recombination with Flp-In tet-inducible expression vector pcDNA5/FRT/TO/SH/GW (51).

The Flp-In T-REx-293 cells (Invitrogen, NY, USA) containing genomic FRT sites and stably expressing the tet repressor were maintained in DMEM (4.5 g/L glucose, 10% FBS, 2 mM L-glutamine, 50 U/ml penicillin, 50 μg/mL streptomycin) containing 100 μg/mL zeocin and 15 μg/mL blasticidin. For generation of tet-inducible WRN expressing cell line, 1.5 × 106 Flp-In T-REx-293 cells were seeded in 6-cm Petri dish in culture medium without zeocin for 16–24 h, cotransfected with 1 μg of pFTSH-WRN and 2 μg of the Flp-recombinase expression vector pOG44 (Invitrogen, NY) using calcium phosphate transfection. Two days after transfection, cells were reseeded in a 10-cm Petri dish and selected in DMEM containing 100 μg/mL hygromycin and 15 μg/mL blasticidin for 2 weeks, with medium change every 3–4 days. Pooled hygromycin-resistant cells were treated with doxycycline, a tetracycline analog with a longer half-life, as inducing agent at 1 μg/mL for at least 24 h and inducible expression of SH-tagged WRN was assessed by Western blotting and IHC using anti-HA antibodies (Covance Inc., NJ, USA).

Stable Isotope Labeled Peptides

Mass labeled peptides from TP53 sequence were purchased at AQUA QuantPro quality level from Thermo Fisher Scientific (Thermo Fisher Scientific Production team, Ulm, Germany): ALPNNTSSSPQP[Lys(13C6; 15N2)], 100.00% measured purity and ELNEALEL[Lys(13C6;15N2)], 99.01% measured purity. Peptides were provided in solution of 5 pmol/uL, and serially diluted to generate the limit of quantitation and detection (LOQ/LOD) curves.

SRM Methods Development

SRM methods development was done using the freely available Skyline software package (skyline.maccosslab.org)(79). In brief, protein sequences were trypsin-digested in silico, and all predicted y-ion fragments from y3 to yn–1 for peptides of 7–25 amino acids were used to experimentally validate ion ratios and predicted retention times (80).Methods were exported directly from Skyline to a ThermoFisher TSQ Quantum Ultra triple quadrupole (QqQ) mass spectrometer to guide data acquisition. Step-by-step tutorials for method refinement can be found on the Skyline Web site.

The reference sequence of human tumor protein 53 (TP53, p53; UniProt accession numberP04637; Swiss Institute of Bioinformatics) was used to predict transitions as described above. Two experimentally verified peptides, ALPNNTSSSPQPK (residues 307–319) at m/z 670.8 and ELNEALELK (residues 342–351) at m/z 529.8, were monitored together with two internal control peptides derived from GAPDH (accession P04406): IISNASCTTNCLAPLAK (residues 146–162, 5 fragments) at m/z 917.5 and VPTANVSVVDLTCR (residues 235–248, 6

fragments) at m/z 765.9. Recombinant TP53 (BD Pharmingen, San Jose, CA) protein was used during methods development to select peptides, identify the most useful transitions and confirm predicted chromatographic retention times. The five most abundant transitions for each peptide were selected for final data acquisition, and were monitored using an unscheduled protocol in three analytical replicates. Additionally, the stable isotope-labeled form of each peptide was purchased for validation and quantitation, as noted previously.

The mature Drosophila accessory gland seminal fluid protein Acp70A protein product is a 36 residue lysine- and arginine-rich peptide from which only the tryptic peptide LNLGPAWGGR atm/z 520.8 could be readily detected (77). As a positive control we used the readily detected semitryptic peptide KEDMLLGVSNFK, at m/z 690.8, derived from accessory gland protein Acp62F (77). All y-ions, from y3 through yn-1 were monitored for selected peptides.

Two semitryptic peptides were used to monitor Acp53C14a in SRM analysis of strain #44798: AISSELDHYLR at m/z 652.3 and SSELDHYLR at m/z 560.3. Both peptides were consistently identified in previous experiments. Although the entire sequence of the m/z 560.3 peptide is contained within the m/z 652.3 peptide, both peptides provided good confirmation of depletions in which peptide KEDMLLGVSNFK, from control protein Acp62F, was used as an internal control.

The reference sequence of human Werner protein (WRN; RecQ3; RecQL2; UniProt accession number Q14191; Swiss Institute of Bioinformatics) was used to predict transitions as described above. Three fully tryptic, experimentally verified peptides, CTETWSLNSLVK (residues 170–181),m/z 719.3558, LLSAVDILGEK (residues 965–975), m/z 579.3424, and AAMLAPLLEVIK

(residues 1208–1219), m/z 634.8860 were monitored concurrently with the GAPDH control peptides referenced above.

Assigned peptides were cross-correlated to MS spectral libraries from the National Institute of Standards and Technology (NIST) (81), downloaded from http://peptide.nist.gov.

MS Sample Preparation

Whole cell extracts from RNAi-depleted or control GM639 cells containing 500 μg of total protein were diluted to 1 mL with ammonium bicarbonate buffer (50 mM, pH 8). Samples were reduced by the addition of 10 μL of 500 mM dithiothreitol followed by incubation at 60 °C for 30 min, then alkylated by the addition of 15 μL of 500 mM iodoacetamide at room temperature for 30 min in the dark. The resulting protein samples were digested with trypsin (50 μg/sample; Promega, Madison, WI) at 37 °C for 1 h. Trypsin digests were stopped by adding 10 μL of formic acid (90%, J.T. Baker, Phillipsburg, NJ), cleared of insoluble debris by centrifugation at 14000 rpm for 10 min at 4 °C in a tabletop microcentrifuge (Eppendorf 5417R) and then run on Oasis MCX mixed phase columns (Waters Corporation, Milford, MA) according to manufacturer's instructions in order to remove detergent. Samples were resuspended in 0.1% formic acid in water and stored at −80 °C until analysis.

Drosophila extracts were prepared by homogenizing 5 whole RNAi depleted or control male flies in 70 μL of 50 mM ammonium bicarbonate, then centrifuging for 5 min at 18000× g to clear insoluble debris. The protein content of supernatants containing soluble accessory gland proteins (77) was quantified using a BCA assay (Pierce), and 40 μg aliquots were denatured, reduced, alkylated and digested with trypsin as previously described (82).

Liquid Chromatography

Fused silica capillary tubing (75 μm i.d., Polymicro Technologies) was pulled to a 5 μm tip, then packed with 25 cm of Jupiter Proteo reversed-phase chromatography material (Phenomonex, Torrance, CA). Nanoflow liquid chromatography was performed using an Eksigent nanoLC-1D system (Dublin, CA). Samples were injected into a 5 μL loop using an autosampler, and washed directly onto the column. Solvents A and B for gradient elutions were water/acetonitrile (95%/5% v/v), and water/acetonitrile (20%/80% v/v), respectively. Both contained 0.1% formic acid. In order to better separate GM639 lysates, solvent B was increased from 3% to 15% acetonitrile over 8 min, followed by an increase to 35% over the subsequent 52 min; a step to 90% for 10 min; then a return to Solvent B at 3% for 20 min. The total gradient time was 90 min at a flow rate of 350 nL/min. Drosophila peptides were eluted using a 60 min linear gradient of 5% to 25% solvent B.

Mass Spectrometry

Eluting peptides were ionized via electrospray with the emitter held at 2.4 kV using a home-built ESI source, and directed into a Thermo Scientific TSQ Quantum Ultra triple quadrupole mass spectrometer. Transitions developed in Skyline were used to monitor precursor-fragment ion pairs defined previously. Resolution in Q1 and Q3 was 0.7 in all experiments. Skyline was used to calculate peak areas by integrating total ion chromatograms. In order to normalize signal intensity, total peak areas for individual peptides from each target protein were divided by total peak areas for each internal control peptide. Differences in protein abundance were calculated by

dividing the normalized peak areas of experimental samples by the analogous peak areas of control samples in the same experiment.

Standard Curve Generation

Heavy peptides were added to a buffer solution of 50 mM ammonium bicarbonate (pH 7.5) at the final concentration of 1 amol/μL, 10 amol/μL, 100 amol/μL, 1 fmol/μL, 10 fmol/μL, 100 fmol/μL, and 1 pmol/μL. Five microliters of each sample was injected onto column for the analysis, and three analytical replicates were taken.

Heavy peptides of these concentrations were then added to the digest of whole cell lysate from GM639-cc1 cells, and analyzed as described above. Peak area values were extracted using Skyline.

Western Blot Analyses

Whole cell extracts of GM639 and HEK-293T cells were prepared by resuspending cells in lysis buffer (15 mM Tris pH 8, 15 mM NaCl, 60 mM KCl, 1 mM EDTA, 0.5 mM EGTA, 0.5 mM spermidine, 0.5% NP-40 supplemented with Sigma protease inhibitor cocktail 1) followed by incubation on ice for 30 min. Nucleic acids were digested by adding Benzonase nuclease (EMD Biosciences, Darmstadt, Germany; 0.375 U/μL) and incubating for 15 min on ice, followed by the addition of DNase I (Sigma-Aldrich, St. Louis, MO; 180 U/mL) and incubation at 37 °C for 15 min with periodic mixing. Protein concentrations of extracts were determined by Bradford assay (Bio-Rad, Hercules, CA), and 50 μg aliquots were resolved by SDS-PAGE electrophoresis (Invitrogen, Nu-PAGE) prior to transfer onto PVDF membrane (Bio-Rad, Richmond, CA). TP53

protein was detected using a mouse monoclonal anti-p53 primary antibody (AHO0112, Invitrogen). Endogenous WRN protein was detected using a mouse monoclonal anti-WRN primary antibody (W0393, Sigma), inducible tagged WRN was detected using a mouse monoclonal anti-HA antibody (MMS-101P, Covance Inc., NJ, USA). GAPDH, an internal control protein, was detected using a mouse monoclonal anti-GAPDH primary antibody (MAB374, Millipore). Bound primary antibodies were detected using Alexa Fluor 647 donkey antimouse polyclonal antibody (A-31571, Invitrogen), and quantified on an Alpha Innotech FluorChemQ Imager (Alpha Innotech Corporation, San Leandro, CA).

Western blot analyses of Drosophila samples were performed using extracts from RNAi-expressing and control males of line #52425. Triplicate samples from depleted and control flies containing 40 μg of reduced protein were separated on 15% polyacryl-amide gels. One set of replicates was stained with Coomassie blue to verify equal protein abundance in samples from RNAi and control flies (data not shown). The second and third sets of replicates were Western blotted to identify target proteins: one replicate was probed with a 1:2000 dilution of an anti-Acp70A antibody (83), the other with a 1:4000 dilution of an anti-Acp62F antibody. Both primary antibodies were generously provided by M. F. Wolfner (Cornell University). Bound primary antibodies were detected and quantified by incubating membranes with a 1:10000 dilution of a goat antirabbit secondary antibody (Jackson ImmunoResearch) followed by enhanced chemiluminescence detection (GE Healthcare).

Section 3: Results

We developed a general SRM protocol (Figure 2.1) to detect and quantify RNAi-mediated depletion of four target proteins: the human TP53 tumor suppressor protein, the human Werner (WRN) protein, and the Drosophila accessory gland seminal fluid proteins Apc70A and Apc53C14a. To improve measurement precision, we selected organism-specific internal controls to account for sample preparation and sample loading differences. We used the human glycolytic enzyme glucose-6-phosphate dehydrogenase (GAPDH), and the Drosophila accessory gland protein Apc62F.

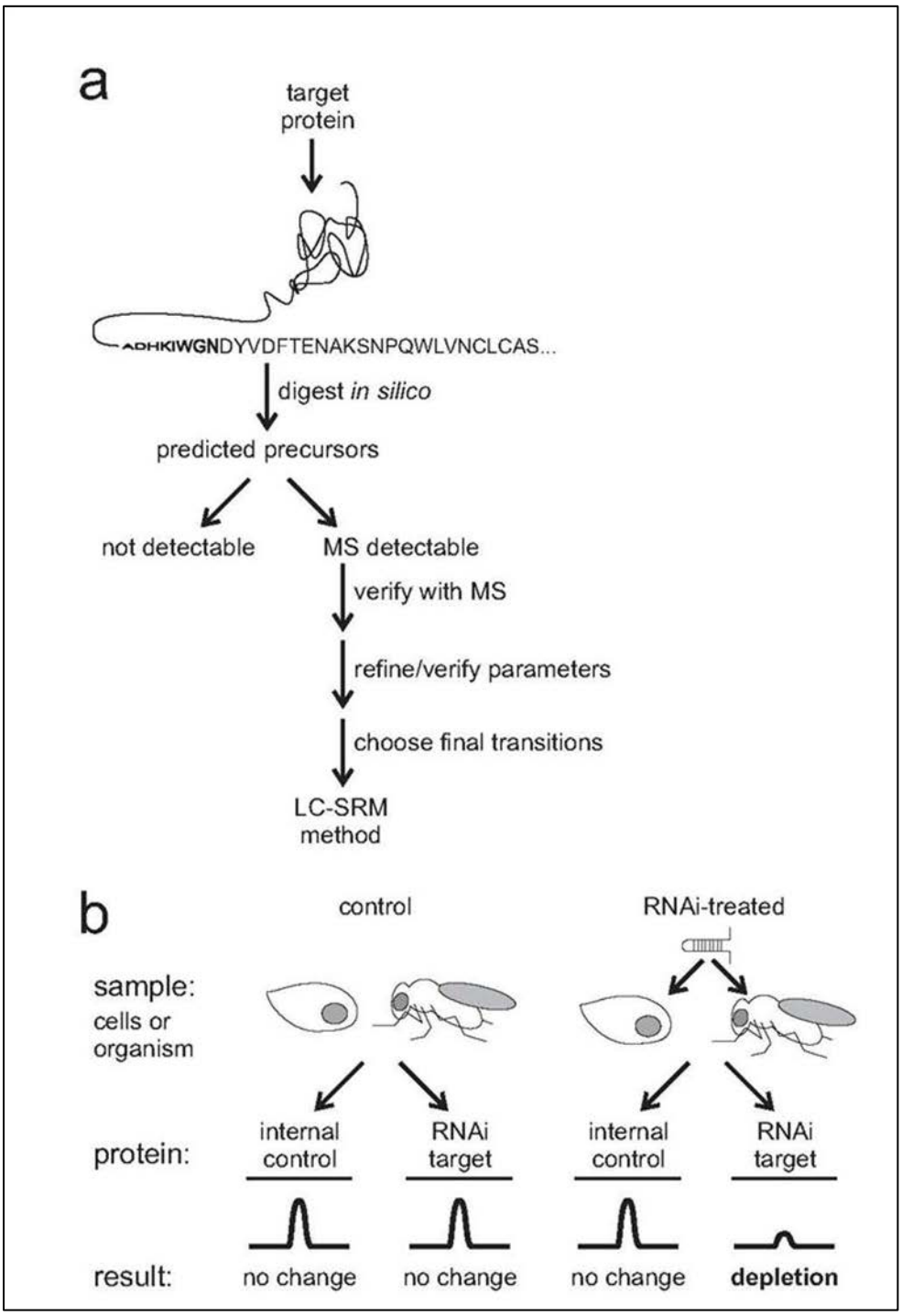

Figure 2.1: Outline of selected reaction monitoring mass spectrometry (SRM) workflow.

(a) SRM protocol used to detect and quantify a specific target protein versus a control. (b) Experiment design of an SRM experiment to detect and quantify depletion of a target protein in an RNAi experiment using cells or whole organisms.

SRM analysis of unfractionated cell extracts from a human fibroblast cell line GM639, depleted of TP53 by transfecting a *TP53*-specific siRNA, revealed TP53 depletions ranging from 70 to 93% in independent experiments across several peptides. There was excellent agreement between the extent of depletion derived by measuring peak area ratios from individual peptides in SRM data (Figure 2.2), and the extent of depletion estimated by Western blot analysis (Figure 2.3).

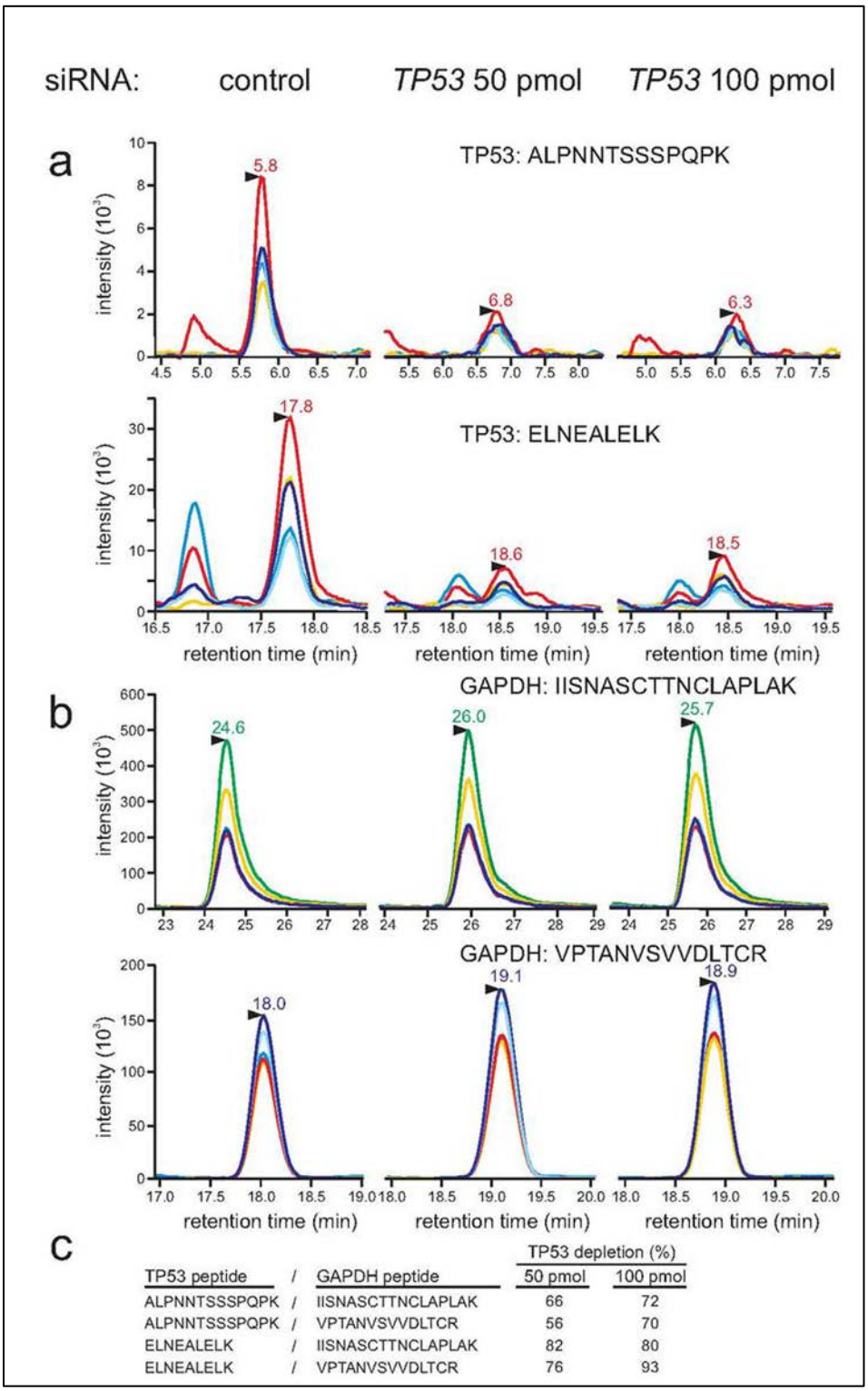

Figure 2.2: RNAi-mediated TP53 depletion quantified by Selected Reaction Monitoring (SRM) mass spectrometry.

The chromatograms show sets of transitions for specific peptides derived from target protein TP53 (a) or loading control GAPDH (b) in human cell RNAi depletion experiments. Samples were treated with a control RNAi or with 50 or 100 pmol of a TP53-specific siRNA prior to SRM analysis. Specific peptides detected and quantified from TP53 were ALPNNTSSSPQPK and ELNEALELK, and from GAPDH VPTANVSVVDLTCR and IISNASCTTNCLAPLAK. (c) TP53 depletion was quantified from individual peak area ratios determined for all measured peptides and normalized against an internal standard GAPDH as described in Methods. Normalized peptide intensities in depleted and control samples were used to estimate target protein depletion in the RNAi experiment depicted in panels (a) and (b).

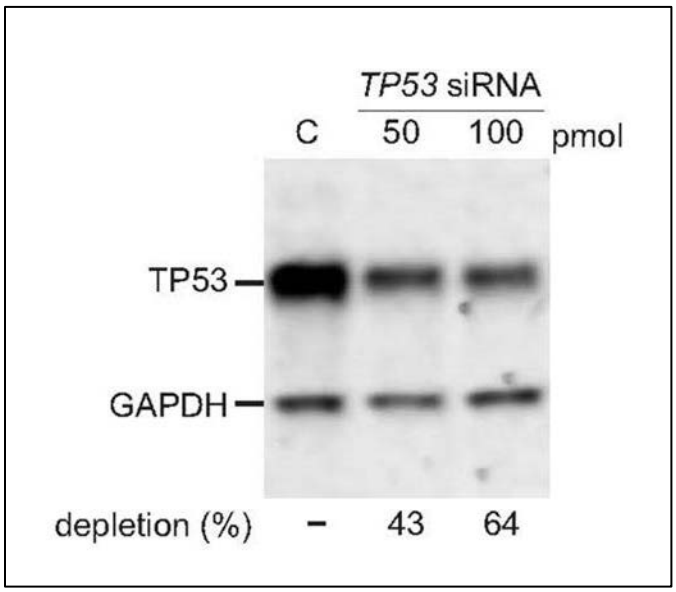

Figure 2.3: Western blot verification of TP53 depletion from human cells.

Cells were transfected with TP53-specific or control (C) siRNAs prior to preparing whole cell extracts. TP53 and GAPDH were detected by Western blot analysis. Band intensities for TP53 versus GAPDH were normalized against the blot background, then used to estimate percent TP53 depletion as a function of siRNA dose.

In addition to Western blot analysis, we purchased the recombinant protein and stable isotope labeled peptide standards to corroborate our findings in TP53. We also determined the limit of quantitation for each of the labeled peptides by isotope dilution curves, and provided ion fragment ratio data for every measured peptide. These are presented in Figure 2.4 and show how

individual ion fragments contribute to the total signal received from a given precursor. This confirms that we specifically identify the peptides of interest using our method by comparing the fragmentation patterns of our analyte in whole cell lysate to peptides from a recombinant protein. Recombinant human TP53 protein was used to verify peptide elution times and confirm the relative ratios of contributing fragments. The consistency in absolute and normalized ion ratios for the TP53 and GAPDH tryptic peptides in independent siRNA depletion experiments are illustrated in Figure 2.4. These results demonstrate the proportionally consistent contribution of different fragments to the total peak area regardless of absolute peptide abundance in the given sample and confirm that all measured transitions were derived from TP53 target peptides as opposed to contaminants.

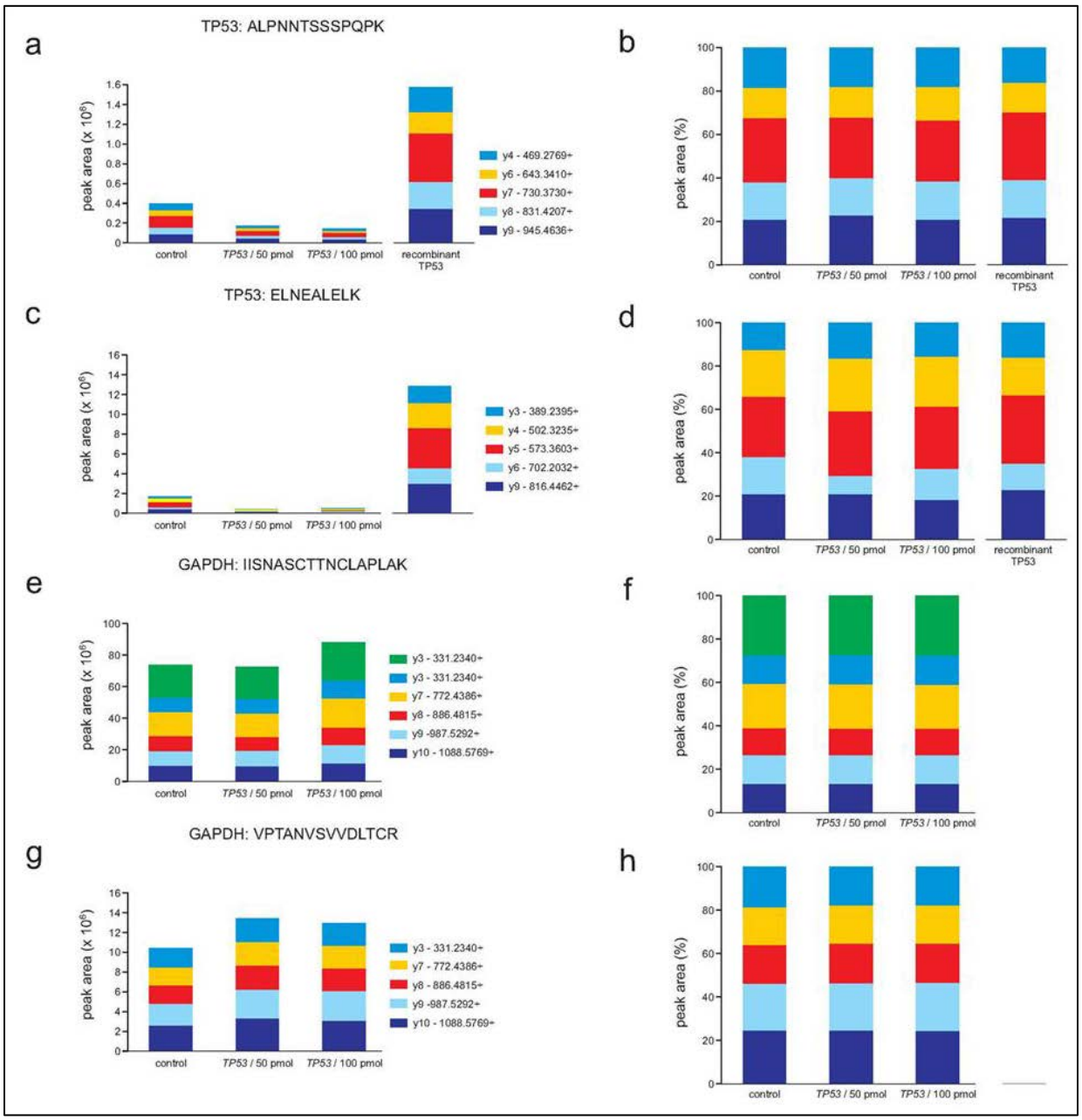

Figure 2.4: Target protein-specific ion ratios are maintained in samples having different protein abundances.

Absolute (a) and normalized (b) ion ratios from TP53 peptide ALPNNSSSPQPK are shown for samples having substantially different amounts of TP53 protein. The first three samples in each panel are unfractionated cell extracts, whereas the final sample (right) in each panel consisted of purified recombinant human TP53 protein. siRNA key indicates transfection of cell samples with a control siRNA or with two different concentrations of TP53-specific siRNA. Panels (c) and (d) show ion ratios for TP53 peptide ELNEALELK, (e) and (f) show ion ratios for GAPDH peptide IISNASCTTNCLAPLAK, and (g) and (h) show ion ratios for GAPDH peptide VPTANVSVVDLTCR. Note that because GAPDH peptides are not present in TP53, their signal is absent in the recombinant TP53 digest.

We also demonstrate a linear quantitative range for the spiked-in peptides over 6 orders of magnitude (Supplementary Figure 1, Appendix A). Supplementary Figure 2, Appendix A, shows that when added to a complex background of whole cell extract (WCE), the peptides show a higher LOQ, but still maintain a similar pattern of ion fragments at lower spiked-in concentrations, confirming detection. Importantly, as demonstrated in panels (a) and (h), the endogenous level of the peptide is well within the quantitative range of 2 orders of magnitude. Therefore, signal reduction by 99% would still fall within the LOQ.

All five proteins were trypsin-digested *in silico* using Skyline, a software tool for SRM method development and data analysis (79). The resulting predicted tryptic peptides were sorted to identify peptides of 7–25 residues that had a high likelihood of being detected by MS. Detection of these peptides was then verified to identify the subset of peptides that gave strong MS signal intensities. Specific transitions (i.e., sets of specific precursors and fragmentation products) were then selected for each target peptide and verified to demonstrate that target and control proteins could be reliably measured by MS in unfractionated cell extracts.

The reproducibility of SRM and Western blot quantitation were compared by performing technical replicates for each sample and method. For SRM we used 6 technical replicates in which 4 different peptides were analyzed and the relative signal intensities were compared. Western blot analyses of TP53 protein using the same samples allowed us to assess the reproducibility of TP53 depletion relative to a within-lane loading control (GAPDH; Supplementary Figure 3a, Appendix A). Both methods detected comparable levels of protein

depletion, with SRM-based measures having the lower coefficient of variation (CV) (Supplementary Figure 3b, Appendix A).

An independent set of TP53 depletions was performed to demonstrate that the depletion levels could be verified using synthetic SIL peptides. The depletion was achieved by the lentiviral shRNA plasmid transduction, and cells were grown under puromycin selection (1 μg/mL) prior to analysis. The results indicate that knockdown was much higher, and estimated to be approximately 90% by quantitation of fluorescent signal in Western blots (Supplementary Figure 4, Appendix A) and by using SRM (Supplementary Figure 5, Appendix A). Ion fragment analysis for all peptides is presented in Supplementary Figure 6,Appendix A.

In this set of experiments, in addition to normalization to internal standard GAPDH, SIL peptides were used as a verification of the level of depletion. Our results indicate that both normalization measurements show high level of agreement within 10% for all measured peptides.

Prior to addition of SIL peptides to the lysates, we determined the limit of detection (LOD) and limit of quantitation (LOQ) for each peptide both in loading buffer and in WCE. The data are presented in Supplementary Figures 1 and 2, Appendix A. Each measurement was recorded on an absolute and logarithmic scale, and relative ion fragment contributions are also presented. The acquired SIL peptide data guided our decision to load protein amounts that fell well within our LOQ.

Human WRN protein has been previously shown to be a very low abundance protein in a number of cell lines (73,74), and we successfully used it in this study. We employed a series of cell preparations containing different relative amounts of WRN: a tetracycline-inducible Flp-In

T-REx-293 cell line with and without induction, and a GM639 fibroblast cell line that stably expresses a nontargeting control shRNA and an anti-WRN shRNA (Supplementary Figure 7,Appendix A). We reliably show that we can identify peptides that are suitable for SRM, we can verify identity of these peptides by comparing ion fragmentation to publically available NIST peptide tandem mass spectral library, and we can quantify extent of knockdown even at low signal intensity. Supplementary Figure 8, Appendix A, shows chromatographic traces extracted directly from Skyline, demonstrating relative intensities of WRN peptides and control peptides from GAPDH. Supplementary Figure 9, Appendix A, shows that not only do our selected peptides match the library spectra within the dot product cut off of 0.9, but that with decreasing signal intensity the overall pattern of ion fragment contribution is largely maintained.

In vivo RNAi-mediated protein depletions were performed in Drosophila by crossing flies that contained target gene-specific UAS-IR RNAi cassettes under control of a tubulin-GAL4 driver. RNAi expression caused almost complete (>99%) knockdown of both targeted seminal fluid accessory proteins as demonstrated by SRM analyses and, in the case of Acp70A where an antibody was available, by Western blot analysis (Supplementary Figures 10–12, Appendix A). Again, there was excellent concordance of depletion estimates of Acp70A by SRM and Western blot analysis. The potential residual Acp53c14 protein shown in Supplementary Figure 12, Appendix A, was shown to be an unrelated, coeluting peak that could be distinguished from target fragments on the basis of ion fragment ratios. This illustrates the ability of SRM to discriminate between coeluting target and contaminating proteins. For all analyses, relative ion fragment ratios were determined. Absolute, log-transformed, and normalized ion ratios are

reported for all measurements, and demonstrate that even at lower signal intensities the ratios are preserved.

Section 4: Discussion

We have developed a general, targeted mass spectrometry approach based on selected reaction monitoring (SRM) to detect and quantify specific target proteins in unfractionated extracts from cells or whole organisms. The applicability of this method was demonstrated by using SRM analysis to detect and assess the abundance of target protein depletion relative to internal, organism-specific controls in cell-based and whole organism RNAi-mediated depletion experiments. Where good antibodies existed for both target and control proteins, we demonstrated excellent agreement between SRM and Western blot-based quantitation of target protein depletion.

The SRM approach described here has several advantages when compared with antibody-based protein detection or quantitation methods. SRM is a transparent detection protocol that uses defined and experimentally validated precursor-fragment ion pairs for detection and quantitation. Immunologic approaches, in contrast, may depend on antibodies whose epitope(s) are often not known in any detail. Thus, an advantage of SRM for targeted peptide measurement is that it provides unambiguous structural specificity of a target peptide. Additionally, precursor-fragment ion pair transitions can be chosen to detect specific protein regions, isoforms or post-translational modifications. For example, we show that SRM can be used to detect and measure even very small proteins and peptides such as the 36-residue Apc70A protein that may be

challenging targets for antibody development. Once a robust set of transitions are identified for a specific protein, they can be applied immediately in subsequent experiments and combined with additional target protein-specific transition sets to allow the simultaneous detection and quantitation of multiple proteins within single experiments and samples. Dozens of different proteins, represented by as many as a hundred or more specific transitions, can in principle be detected in single experiments using a common protocol and reagents. In our multiplexed scheme, using scheduling, we typically detect 8-10 proteins per run, with each injection of only 1-1.5 µg of protein onto the column.

In contrast to immunodetection-based methods such as Western blotting, information about full-length proteins is lost in SRM analyses. This occurs because proteolytic digestion is performed prior to MS analysis. However, as noted above, careful peptide selection and verification can be used to compensate for this potential disadvantage and may be used to distinguish between protein isoforms or post-translational modifications that are difficult or impossible to detect by conventional immunologic methods. The protein quantitation performed here by SRM is analogous to quantitation in antibody-based blotting in that it is relative to a selected standard or “loading control”. This approach allows even small differences in protein abundance to be detected and precisely measured. We demonstrate that there is no appreciable difference when normalizing endogenous peptide signal intensities to other endogenous protein chosen as a control, rather than SIL forms of each peptide. Thus, our analysis agrees with Hoofnagle et al. (84), who had demonstrated that a single protein internal standard applied to all proteins performed as well as multiple protein-specific peptide internal standards. Absolute

quantitation can also be performed by SRM, as is the case with antibody-based detection, by using known controls with appropriate calibration (85).

The general workflow outlined in Figure 2.1 should be applicable to a wide range of proteins from diverse taxa. The instrumentation and software to enable large-scale SRM analyses are readily available and becoming increasingly commonplace in protein mass spectrometry laboratories. Thus, SRM methods based on genomic data should facilitate quantitative proteomic analyses in well-characterized organisms where many good immunologic reagents are available, as well as other organisms of high biological or medical interest where few or no protein or immunologic resources exist. The validation of RNAi-mediated protein depletion will minimize false negatives and assist in the curation and use of increasingly large RNAi reagent libraries.

Notes to Chapter 2

All Supplementary data to Chapter 2 can be found in Appendix A, as noted.

All Figures were generated with help from Alden Hackmann.

This work is published:

Rapid Assessment of RNAi-mediated Protein Depletion by Selected Reaction Monitoring Mass Spectrometry

Veronika A. Glukhova, Daniela M. Tomazela, Geoffrey D. Findlay, Raymond J. Monnat, Jr., and Michael J. MacCoss. Journal of Proteome Research **2013** 12 (7), 3246-3254

All skyline files incorporating RAW data files are provided here:

http://proteome.gs.washington.edu/software/panorama/spionin_RNAi_SRM.html.

Chapter 3 – Affinity purification of Werner protein and its interacting partners.

Section 1: Introduction

Although WRN activity has been implicated in several different mechanisms of DNA repair (7,24,86), these mechanisms are based on specific *in vitro* phenotypes, and the subsequent biochemical characterization has provided limited clarification and expansion on the specifics of WRN activity. Furthermore, the number of processes that WRN protein is involved in suggests that its functions are context-dependent, and altered by differential interaction with other proteins. The number of putative interaction partners and the diverse functional roles assigned to WRN suggest that WRN may exist in many different protein complexes. To date, a number of WRN interaction partners have not been confirmed by a single comprehensive method, or even a single type of analysis.

Our goal was to provide a detailed proteomic picture of the WRN protein interactome in the context of human cell. Current entries for WRN in protein interaction databases were assembled from data generated by several different groups on several types of instruments, utilizing methods that are difficult to compare. We aimed to collect single-source MS data to validate existing information and to potentially expand the current list of WRN interaction partners. When considered in the context of the confirmed functions of identified interaction partners, we anticipate that the association studies will help us link the loss of function of WRN protein to the loss or gain of specific interactions, and more broadly, to specific molecular and

cellular defects.

To elucidate the biochemical pathways involving WRN we characterized its interacting proteins in normal cells and DNA damage states via AP-MS. In this chapter we focus on the characterization studies of the epitope-tagged baits WRN and control protein LacZ. Bacterial protein LacZ was fused to a nuclear localization sequence, and tagged identically to WRN. This protein is not expected to have shared functional interactors with WRN, while being comparatively large, and thus a good target for nonspecific interactions with abundant or sticky proteins, making it an ideal control. The integration of this control sets our analysis apart from similar studies because the common approach is to use the affinity tag as a control, and the tags tend to localize to the cytoplasm, thus controlling for nonspecific interactions in the wrong compartment. In this chapter we demonstrate protein induction patterns, validate proper protein localization, and show results of isolation of these proteins from the complex cell lysates.

Section 2: Experimental

Generation of expression constructs and tetracycline-inducible cell lines.

Vector pIRESpuro-GLUE (pGlue) was a gift from the laboratory of Randall Moon (University of Washington, HHMI, Department of Pharmacology), and was created by using the pIRES–puro (Clontech, Mountain View, CA) backbone vector, and constructing the dual affinity tag using PCR (50). The WRN ORF was obtained from a plasmid containing both the IgG and calmodulin binding domains. The ORF was excised using NotI and AscI sites, and contains a myc-tag at the N-terminus of the WRN gene.

The tet-inducible expression vector for N-terminally SH-tagged human WRN, pFTSH-WRN (originally named pcDNA5/FRT/TO/SH/GW/WRN), was a gift from Dr. Alessandro Vindigni (St. Louis University, MO, USA). It was constructed by Gateway cloning using human WRN ORF in pDONR223 vector for LR recombination with Flp-In tet-inducible expression vector pcDNA5/FRT/TO/SH/GW ((51). Control vector pFTSH-nLacZ was constructed by replacing a BsrGI fragment containing WRN ORF in pFTSH-WRN with a PCR generated BsrGI fragment containing bacterial beta-galactosidase gene with N-terminally fused SV40 large-T antigen nuclear localization sequence.

The Flp-In T-REx-293 cells (Invitrogen, NY, USA) containing genomic FRT sites and stably expressing the tet repressor were maintained in DMEM culture medium (4.5 g/L glucose, 10% FBS, 2mM L-glutamine, 50 U/ml penicillin, 50 µg/ml streptomycin) containing 100 µg/ml zeocin and 15 µg/ml blasticidin. Tet-inducible WRN expressing cell line was generated. Briefly, 1.5x106 Flp-In T-REx-293 cells were seeded in 6-cm Petri dish in DMEM culture medium without zeocin for 16-24 hours, and co-transfected with 1 µg of pFTSH-WRN and 2µg of the Flp-recombinase expression vector pOG44 (Invitrogen, NY, USA) using calcium phosphate transfection protocol (Kingston et al. Curr protoc Mol Biol 2003). Two days after transfection, cells were reseeded in a 10-cm Petri dish and selected in DMEM containing 100 µg/ml hygromycin and 15 µg/ml blasticidin, and maintained for 2 weeks, with a medium change every 3-4 days. Pooled hygromycin-resistant cells were treated with doxycycline, a tetracycline analog with a longer half-life, as inducing agent at 1 µg/ml for at least 24 hours. Expression of SH-tagged WRN was assessed by immune-blotting and IHC using anti-HA antibodies (Covance Inc., NJ, USA).

Cell culture and drug treatment.

The Flp-In T-Rex-293 cells expressing either pFTSH-WRN or pFTSH-nLacZ were grown in DMEM culture medium, in a humidified 37°C, 7% incubator.

Stock solution of Camptothecin (Sigma-Aldrich) was prepared at 10 µg/mL in DMSO, and added directly to cell plates at the time of treatment. Volume equivalent of DMSO alone was added in controls.

Protein expression and affinity purification.

Cells were grown as described in prior section, and induced using 1 µg/uL doxycycline 24 hours prior to start of the experiment. Cells were lysed in lysis buffer (100mM Tris pH 8, 125 mM NaCl, 2.5 mM MgCl, 0.5 mM Spermidine, 0.2% NP-40, supplemented with protease inhibitor cocktail for mammalian cells (P8340, Sigma-Aldrich), and phosphatase inhibitor cocktail against Ser/Thr phosphatases (P2850, Sigma-Aldrich) followed by incubating on ice for 30 min. Nucleic acids were digested by adding Benzonase nuclease (EMD Biosciences, Darmstadt, Germany; 0.375 U/µl) followed by incubation for an additional 15 min on ice. Insoluble material was removed by centrifugation at 14,000× *g* for 10 minutes at 4^{o}C, and cleared lysates were loaded into large spin columns (Thermo Scientific, Rockford, IL) containing 800 µL of packed Strep-Tactin beads (IBA GmbH, Göttingen, Germany). Prior to addition, the beads were equilibrated by washing 3 times with 4 bead volumes of lysis buffer, and spun briefly to allow the buffer to flow through. After addition of lysate, binding was accomplished by gravity flow through the column. Beads were washed three times with four volumes of lysis buffer, and eluted with 1 mL of 2.5 mM desthiobiotin solution in lysis buffer.

Western Blots.

Whole cell extracts were prepared as described in previous section. Protein concentration of extracts was determined by Bradford assay (Bio-Rad, Hercules, CA), and aliquots of each sample (70 µg total protein) were resolved by SDS-PAGE electrophoresis (Invitrogen, Nu-PAGE) prior to transfer onto PVDF membrane (Bio-Rad, Richmond, CA, USA). Tagged protein was visualized by incubation with an anti-HA (clone 16B12) mouse mAb (MMS-101P; Covance Inc., NJ, USA). Nucleolin was used as a loading control, and was detected with an anti-Nucleolin antibody (Life Technologies Corporation, Grand Island, NY). Additional analysis was performed with anti-Phospho-ATM (Ser1981) Mouse mAb (4526S; Cell Signaling Technology, Danvers, MA). Bound primary antibodies were detected using Alexa Fluor -conjugated secondary antibodies (Life Technologies Corporation, Grand Island, NY) followed by fluorescence detection. Band intensities were quantified using an Alpha Innotech FluorChem Imager (Alpha Innotech Corporation, San Leandro, CA).

Immunofluorescence microscopy.

Cells of interest were grown to near confluency using uncoated multichamber slides (Millicell EZ slides, EMD Millipore, Billerica, MA), and treated depending on the experiment, prior to fixing. Briefly, the cells were fixed using 4% Paraformaldehyde in PBS for 25 minutes, permeabilized with 0.1% Triton-X in PBS, and incubated using primary antibodies appropriate for given experiments: anti-HA (Covance Inc., NJ, USA), anti-Phospho-H2AX (Ser139) (Millipore, Tellecula, CA), and counter-stained using DAPI. Alexa Fluor conjugated secondary antibodies were used for fluorescence detection (Life Technologies Corporation, Grand Island,

NY). All washes were done in 1x PBS. Slides were visualized using Nikon Eclipse E600 microscope.

Immunohistochemistry.

Cells of interest were attached to uncoated glass slides by cytocentrifugation with Cytopro 7620 (Wescor Inc., Logan, UT). Cells were spun onto the slide at 3500 rpm for 3 minutes, fixed with 4% Paraformaldehyde in PBS for 25 minutes, and permeabilized with 0.1% Triton-X in PBS. All procedures were conducted according to manufacturer's instructions for the Vectastain ABC kit (Vector Laboratories, Inc. Burlingame, CA). Samples were blocked for 1 hour in 10% horse serum, corresponding to the secondary antibody for the assay, followed by 1 hour incubation in anti-HA antibody (Covance Inc., NJ, USA) diluted in 10% horse serum. Slides were then washed and incubated with biotinylated secondary antibody and the Vectastain ABC reagent. Visualization was achieved after incubation in peroxidase substrate solution. All washes were done in PBS, and rinses were done in water.

Biochemical analysis of WRN protein function.

Biochemical analysis was performed as described previously (73,87). Briefly, frozen cells (~10^8; wet vol 0.1 ml) were resuspended in 4 vol of ice-cold extraction buffer (20 mM Tris–HCl, pH 8.0, 0.5 M NaCl, 1 mM EDTA, 0.5 mM DTT, 0.5% NP-40, 25% glycerol, 0.2 mM PMSF and 10 µg/ml each of aprotinin, pepstatin and leupeptin), incubated, homogenized, and subjected to immunoprecipitation. Either total WRN was precipitated by using WRN antiserum (as described previously) or only epitope-tagged WRN was purified using an anti-HA antibody (Covance Inc., NJ, USA). The suspension was assayed immediately for helicase and exonuclease activity,

detected by the displacement of a ^{32}P-5′-labeled 20mer oligonucleotide from a 20mer/46mer partial DNA duplex as previously described. This experiment were done by Ashwini Kamath.

Sucrose density gradient centrifugation.

7-47% buffered sucrose gradient was formed by preparing two solutions of sucrose of 7% and 47% Tris (pH 7.0), and layering to form a gradient (2 mL each, 7%, 17%, 27%, 37%, and 47%) . A concentrated whole cell lysate was prepared as described previously, and was layered on top. Centrifugation was performed at 35,000×*g* for 2 hours at 40^{o}C, and 12 1- mL fractions were then collected. Fractionated lysate was loaded on polyacrylamide gels and protein was detected using silver staining for total protein in all fractions, and by Western blotting for detection of WRN protein.

Section 3: Results

Proof-of-concept experiments and initial MS results.

The feasibility of our approach was initially assessed using affinity tags NTAP and pGlue, as described in Chapter 1 and summarized in Figure 1.4. We tested both transient transfection and stable cell lines, in background of cell lines HEK293T and HT1080. In both cases, we showed that the fusion protein is generated, although HEK293T cells achieved a higher rate of transfection, and protein expression was more consistent. In all cases, an empty vector was also transfected into cells to be used as a control. The merit of this system over untransfected cells as a negative control includes required exposure to selection agents (G418 or puromycin,

depending on the epitope tag), and presence of tag in the cell to test cytotoxicity. However, a superior negative control was used in further experiments, where a tagged protein with no known overlap in interacting partners with WRN, was used. Transfected cells were exposed to the selection agent puromycin and stable cell lines were successfully derived from HEK293T cells. These lines have grown continuously, and have expressed a constant amount of the fusion protein and tag alone in the controls.

Figure 3.1 shows the expression of endogenous and transfected WRN as visualized by an anti-WRN antibody. The lysates were used to perform initial MS profiling experiments, and the results in terms of a number of protein identifications, are summarized in Figure 3.2.

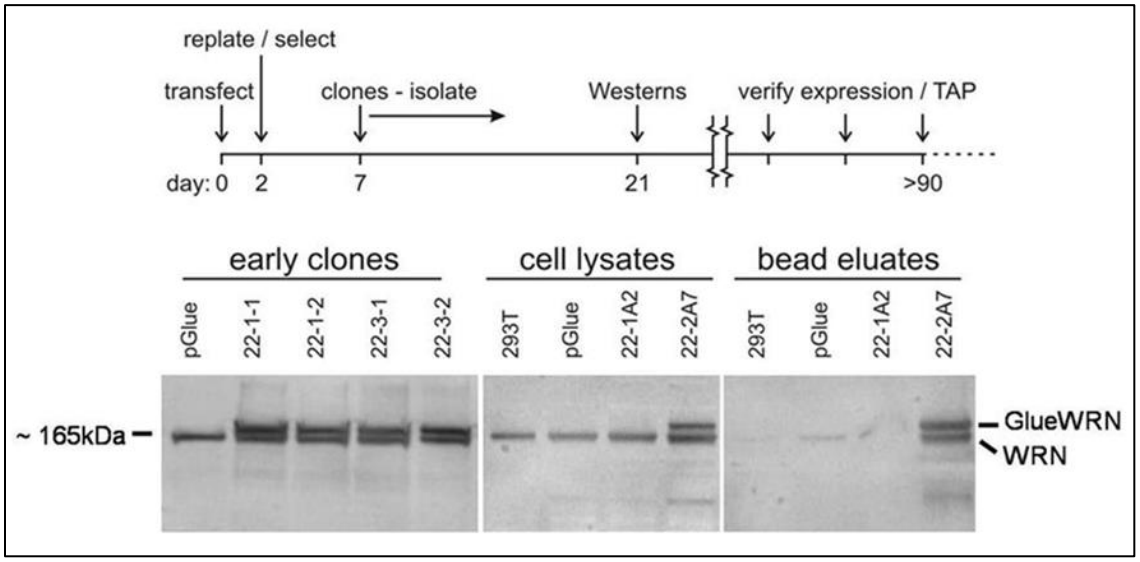

Figure 3.1: HEK293T cell line expressing tagged WRN was successfully established for proof-of-concept experiments.

Expression has been confirmed by a timed series of experiments, and has proven to be consistent. As demonstrated by clone 22-1A1, not all cultures maintained resistance to puromycin express pGlue-WRN. These cells have been successfully maintained in culture while expressing tagged WRN for >180 days.

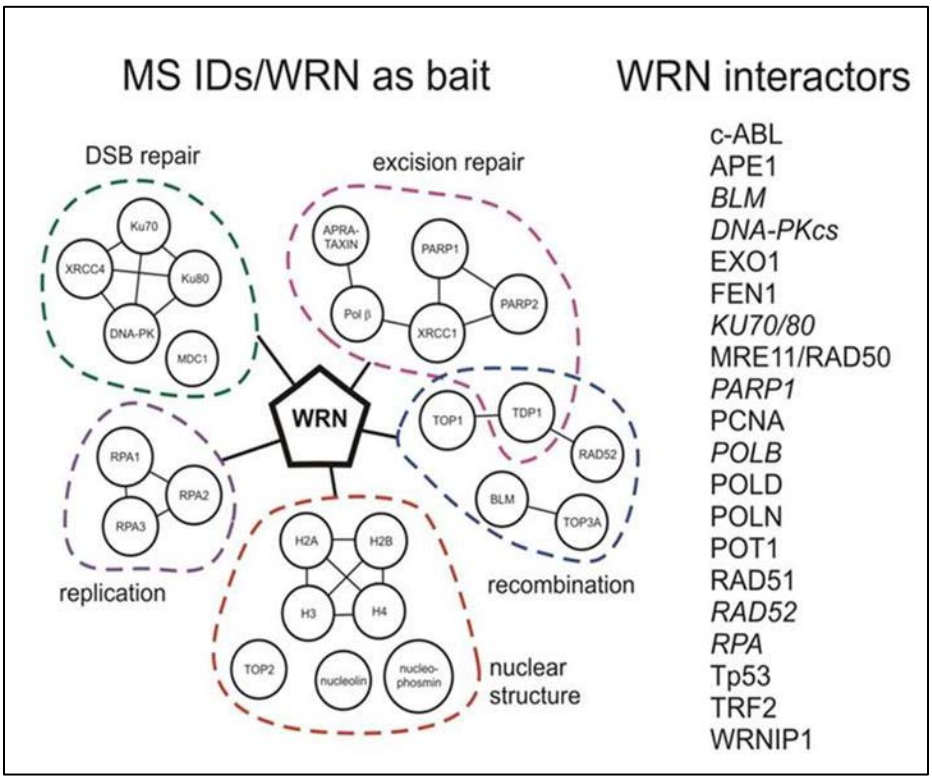

Figure 3.2: Proof-of-concept experiments using pGlue-WRN confirm a number of previously identified WRN-interacting proteins. Here, detected interacting proteins are organized by primary biological function.

Identification of many of these interacting proteins supports that WRN contributes to different aspects of genomic integrity. The presence of the 70/86 Ku heterodimer (Ku), participating in the repair of double-strand breaks (DSBs), alleviates WRN exonuclease blockage imposed by the oxidatively induced DNA lesions. It has been reported that Ku stimulates the WRN exonuclease to bypass these lesions (88). Both Ku and WRN have been shown to localize to telomeres. The G-rich regions of telomeres are particularly susceptible to oxidative damage (89,90) and may contribute to accelerated telomere shortening. As short telomeres are related to aging, the ability of Ku to stimulate the WRN exonuclease to bypass oxidative stress-induced lesions is likely important during DNA repair events and further supports the essential role of

WRN and Ku in the maintenance of genome stability.

Generation of SH-tagged WRN and control nLacZ, expression and localization

WRN cDNA was cloned into a commercially-available dual-specificity tag TRex (Invitrogen). The tag encodes a streptavidin-binding peptide and Haemagglutinin epitope, both of which can be used for affinity isolation. The HA epitope is particularly attractive for many types of immunodetection, as excellent antibodies are commercially available (Covance Inc., NJ, USA). This system was used to rapidly generate stable cell lines for WRN and control protein nLacZ in isogenic HEK 293T background by applying Hygromycin and Blasticidin selection. Expression of tagged protein was induced by addition of doxycycline, and desired experimental treatments were applied prior to affinity pulldown and downstream analysis by MS (workflow previously summarized in Figure 1.3).

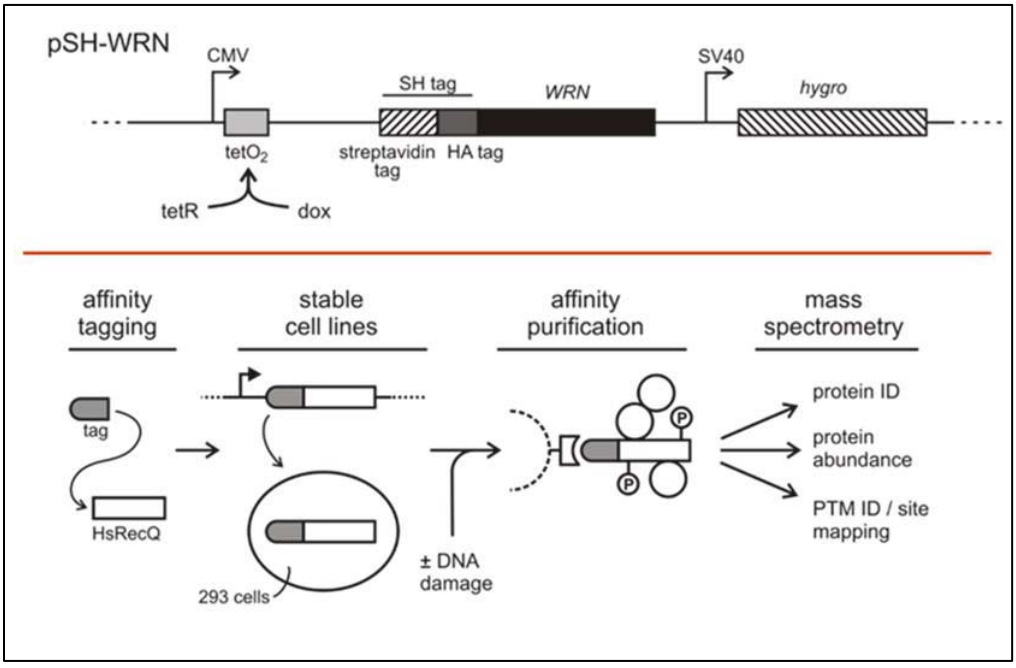

Figure 3.3: General overview of the tagging process, tag structure used in this experiment, and flowchart of Affinity purification process.

Tagged protein expression and localization was assayed by immunodetection using the HA epitope. Western blotting of SH-WRN induction time course (Figure 3.4) shows that the highest level of overexpression is achieved at or around 24 hours post-addition of doxycycline. While lower levels of overexpression may be desirable in some studies, we found that at other time points the level of overexpression was less consistent. The results of this analysis led us to perform all our experiments 24 hours post-induction to maintain consistency.

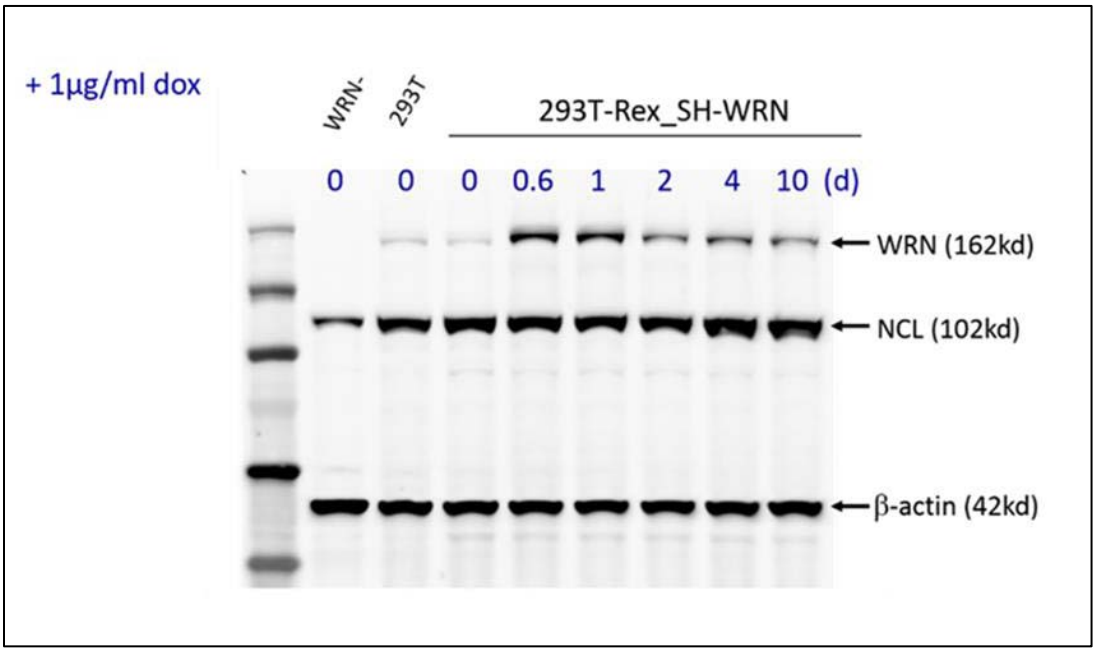

Figure 3.4: Expression of SH-tagged WRN over time.

Dynamics of induction and expression of SH-WRN are demonstrated over a time course of 10 days. Cells that are not induced show expression of endogenous WRN, which runs a little lower than the more intense band after induction. The optimal time of induction was determined to be between 16 and 24 hours, and 5-10 fold overexpression was consistently achieved. All experiments were conducted 24 hours post-induction. Titrating amount of doxycycline failed to fine-tune level of over-expression of SH-WRN, and we selected the lowest dose that provided the most consistent results, 1 µg/mL (Weiliang Tang)

Immunohistochemistry and immunofluorescence were used to verify the correct localization of tagged WRN and control protein nLacZ (Figure 3.5 and 3.6). Immunohistochemistry results showed a more diffuse nuclear staining for SH-WRN, and importantly, demonstrated that majority of the cells in the culture stably express the tagged protein. The uniform density of staining also suggests that the individual cells express SH-WRN at approximately even level. Immunofluorescence analysis was performed on SH-WRN and SH-nLacZ cells to compare patterns of localization. Anti-HA antibody shows that the tagged WRN mostly localizes to nucleolar foci, and to a minor degree to the nucleoplasm. Majority of the tagged nLacZ localizes to the nucleus, and minor cytoplasmic staining is also visible. The results of this analysis demonstrate that SH-nLacZ localizes to the same subcellular compartment as SH-WRN, and is therefore expected to be a suitable control.

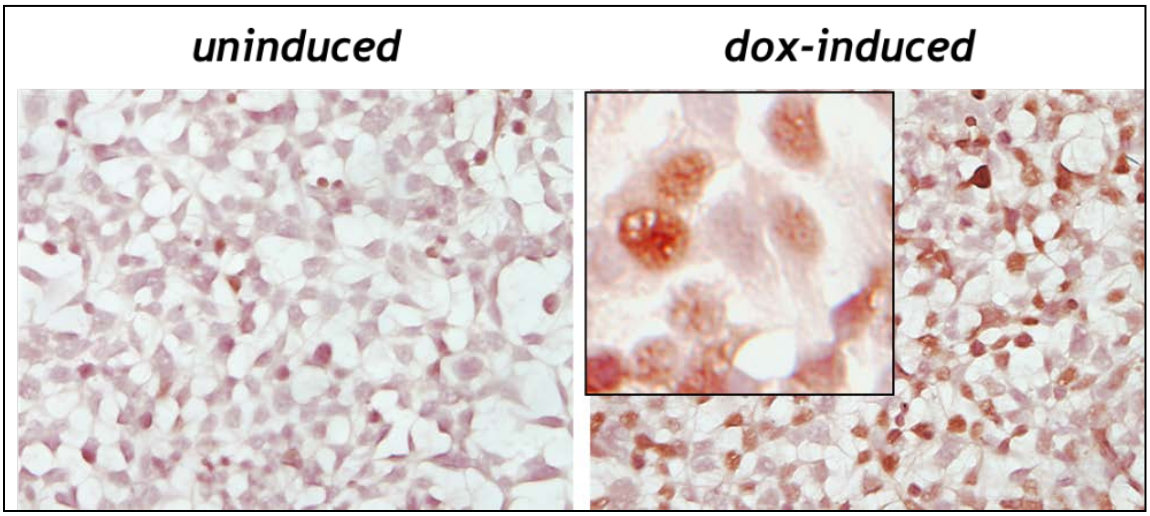

Figure 3.5: Immunohistochemistry verifies correct localization of tagged proteins.

Both, SH-WRN and SH-nLacZ localize to the nucleus (Weiliang Tang)

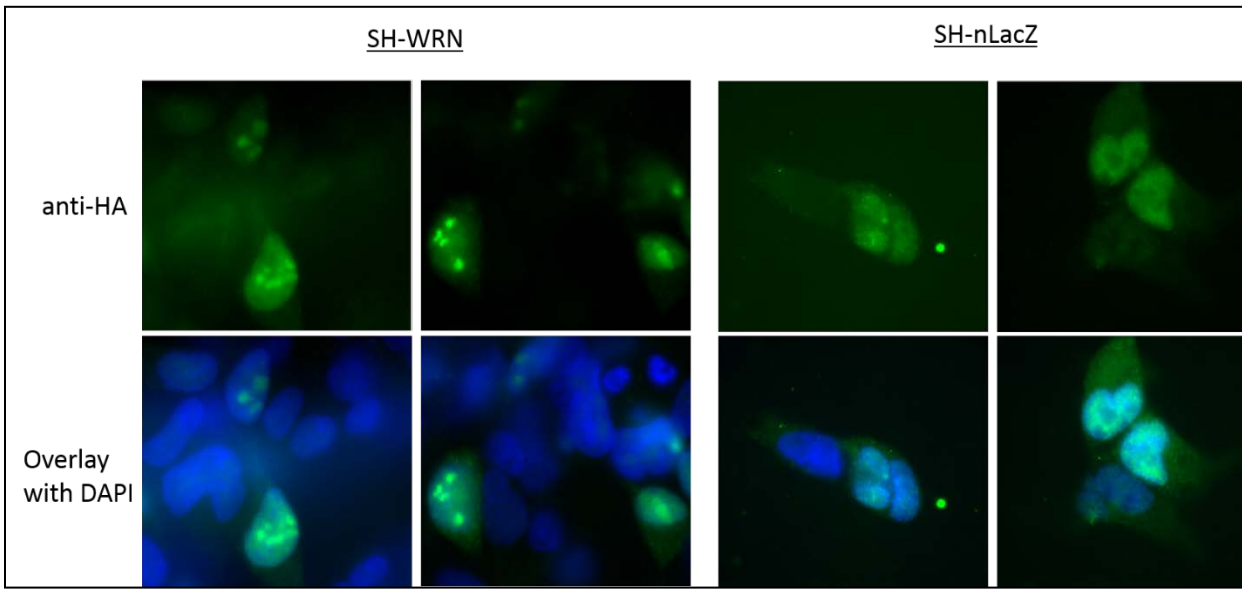

Figure 3.6: Immunofluorescence study of localization of SH-WRN and SH-nLacZ.

Immunofluorescence demonstrates that WRN localizes to the nucleus in the distinct focal pattern, as described previously, and approximately 35% of all cells showed staining at the time of analysis. SH-nLacZ localizes mostly to the nucleus, but cytoplasmic staining is also visible. Expression of tagged allele is uniform in most cells.

Analysis of the two biochemical functions of WRN, as a helicase and an exonuclease showed that both activities are intact in the tagged protein (Figure 3.7). Functionality of the tagged protein was tested using an autoradiography approach, where immunoprecipitated proteins were assayed by detection of displacement of a ^{32}P-5'- labeled 20mer oligonucleotide from a 20mer/46mer partial DNA duplex. If the helicase and the exonuclease domains are active, distinct labeled products are detected. The negative control lane shows that the intact heteroduplex runs as a larger product. The positive control lane shows creation of a helicase and an exonuclease product. Both, immunoprecipitation of total (endogenous and tagged) WRN as well as SH-WRN alone shows unwinding capacity. An additional product is generated due to exonuclease activity, and is visible as a second band.

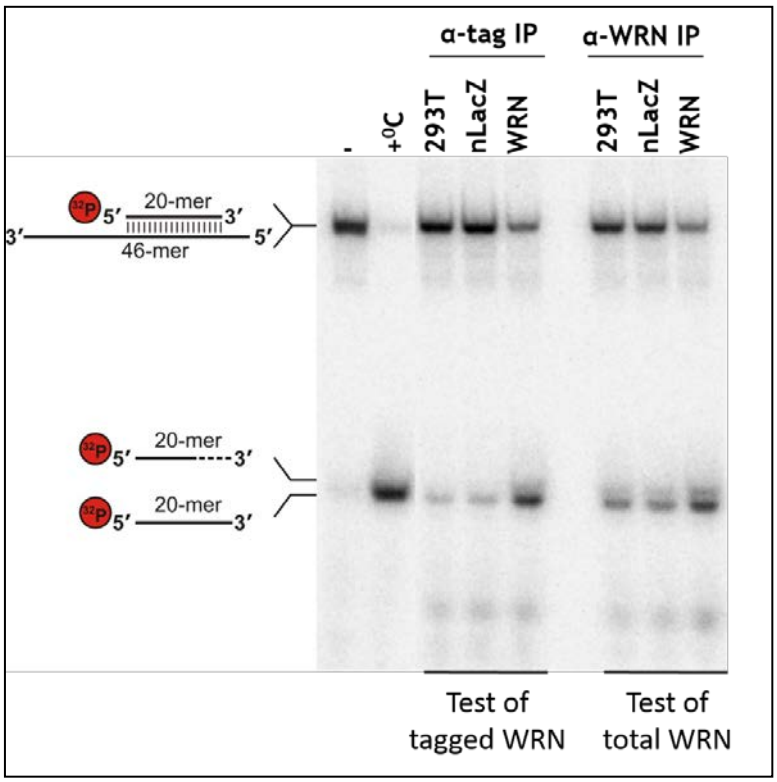

Figure 3.7: Helicase/exonuclease biochemical assay.

Functionality of the tagged protein was tested using an autoradiography approach. An immunoprecipitated protein is assayed by detection of displacement of a ^{32}P-5'- labeled 20mer oligonucleotide from a 20mer/46mer partial DNA duplex. If the helicase and the exonuclease domains are active, distinct labeled products are detected. The negative control lanes with untransfected and SH-nLacZ expression show that the intact heteroduplex runs as a larger product. The positive control lane shows creation of a helicase and an exonuclease product.

To assess the possibility of WRN forming a number of diverse protein interaction complexes we separated whole cell extract by sucrose gradient, and immunoblotted each fraction for WRN and some of its previously reported interacting partners (Figure 3.8). The results of the Western blot clearly show that WRN is distributed across many of the 12 fractions, and co-blotting for some of the interacting proteins demonstrates that they occur in distinct, not necessarily overlapping fractions, as well.

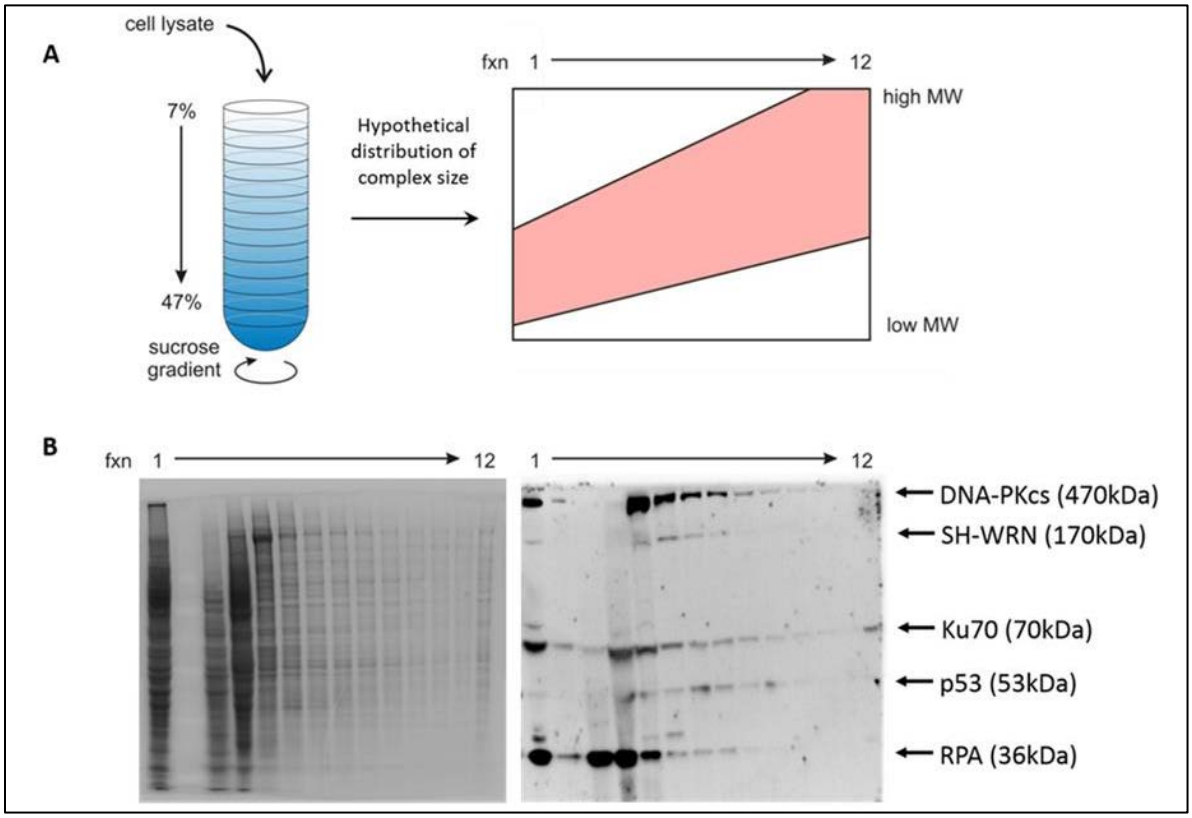

Figure 3.8: Schematic representation of sucrose gradient fractionation and its application to separate whole cell extract containing SH-WRN.

Same lysis conditions were used as in our affinity pulldown protocol to maintain stable protein-protein interactions. Hypothetical protein complex distribution by size is presented. Small complexes and individual proteins are likely to be retained in the fractions of lowest sucrose concentration, while larger complexes are expected to have a higher sedimentation rate. (B) Whole protein stain and Western blot were performed on a separated whole cell extract containing SH-WRN. Blotting against bait, SH-WRN, and its known interaction partners DNA-PKcs, XRCC6 (Ku70), p53, and RPA shows varied distributions of all these proteins in their individual complexes. Whole protein stain with SYPRO ruby shows that protein content is highest in fractions with lowest concentration of sucrose, and that fractions with highest overall protein content are not always the same fractions containing the proteins we detected by Western blot.

Section 4: Discussion

We demonstrate successful generation of stable cells lines that express SH-tagged WRN (SH-WRN) and SH-tagged, nuclear-localized control protein LacZ (SH-nLacZ). Predictable expression of these proteins under a tet-inducible promoter, their consistent localization to nucleus and nucleolus, and efficient isolation by our established AP protocol leads us to conclude that we have successfully established an experimental platform for subsequent MS experiments.

Isolation of proteins by AP can be performed as a single- or double-step enrichment, in either native or denaturing conditions. Single-step protocol to maximizes recovery and has the ability to retain even transient interactors. Double -step enrichments were performed to assess their value as complementary analyses and to validate interactions, however the low recovery and decreased reproducibility led us to make single-step AP the standard protocol.

Addition of chaotropes and denaturing agents while performing AP can lead to an isolated bait devoid of any interacting proteins, or to largely purified complex where only the most stable interactions persist. In our study we used very mild conditions to perform AP, relying instead on downstream computational tools to help us identify proteins that are enriched in bait-dependent fashion.

Notes to Chapter 3

Figures 3.1, 3.2, 3.3, and 3.8 were generated or assembled with the help from Alden Hackmann.

Figures 3.4 and 3.5 were generated by Weiliang Tang.

Figure 3.7 was generated by Ashwini Kamath and Alden Hackmann.

Chapter 4 – Proteomic profiling of WRN protein and changes in its interactome in response to treatment with Topoisomerase I inhibitor Camptothecin (CPT).

Section 1: Introduction

Aiming to understand how WRN protein does its work in the cell, and when is it that the cell needs it, we conducted a series of experiments challenging cells with mutagenic compounds. In response to DNA-damaging events cells undergo a multi-step process that includes sensing, signaling, and repair (91–93). At each of these steps a cell is presented with a number of choices, which can ultimately result in successful repair of a lesion and continued function, an unsuccessful repair or bypass and abnormal function or oncogenesis, or death. While the importance of WRN protein in resolution of stalled replication forks and in later stages of recombinational repair has been previously appreciated, in our study we sought to characterize the protein interaction networks of WRN at the early stages of DNA damage response and to contrast them with the protein complexes that occur at steady, undamaged cell state.

It is known that WRN-deficient cells are specifically sensitive to a number of chemotherapeutic agents (reviewed in more detail in Chapter 1), one of which is camptothecin (CPT), a DNA topoisomerase I (TOP1) inhibitor. Our studies of cells exposed to this drug were aimed at understanding the mechanisms cells employ to resolve the resulting damage, and how WRN protein is involved in these mechanisms.

The mechanism of CPT is well understood, and its derivatives have been successfully

used in chemotherapy (94), making it excellent for our experiments. CPT targets nuclear TOP1, and reversibly traps it on DNA. TOP1 is an essential and ubiquitous enzyme that helps relieve the torsional strain on separated strands of double-stranded DNA by cutting a single strand, relaxing negatively supercoiled DNA, and reannealing it. Complexing with CPT prevents TOP1 from reannealing the DNA, leading to formation of single-strand breaks (SSBs) that can be converted to double-strand breaks (DSBs) upon collision with the replication apparatus (95). The DSBs generated by CPT are generally repaired by homologous recombination, although alternative pathways involving tyrosyl-DNA-phosphodiesterase excision pathway and the fork-regression pathway centered on the Bloom (BLM) helicase have also been described (94).

To describe the changes in WRN protein interactome in response to CPT we employed the combination of affinity purification and mass spectrometry, as described previously. While preparation of cells, enrichment of the bait protein, and generation of many replicates is a tedious and labor-intensive process, it is commonly under-appreciated that large experiments produce large amounts of data. And the complexity of data interpretation has inspired the development of robust computational tools to analyze and compare data sets from large-scale proteomic studies (48). In this chapter we describe the data analysis workflow that we developed to describe the data from our profiling analysis of WRN and its interacting proteins, to organize this data by gene ontology (GO) annotation, and to identify the categories enriched in treatment-dependent manner by cross-referencing our observations to previous reports.

To explore the functional categories that may join the most significantly represented proteins in our analysis, we used gene ontology (GO) analysis. Analysis of protein lists in Supplementary Tables 1A and 1B (Appendix B) in isolation resulted in lists of significantly represented functional categories. However, the relationship between categories in each list was

not always clear. We made use of an existing GO explorer tool at the Yeast Resource Center (YRC) (www.yeastrc.org), which shows individual GO categories in tree format, showing the "parent" terms as well as the "daughter" terms. We expanded on this existing explorer and developed a new tool, which we call CompGO, for either exploration of a single list in tabular or tree format, or comparison of two lists.

We used publically available protein network analysis tools such as the BioGRID, GeneGO, STRING, and BOND to further validate our MS findings, and make inferences about the functional importance of newly discovered interacting proteins. These databases give us information about involvement of proteins in known pathways, and we further investigated the proposed interactions, as described in Chapter 5.

Profiling analysis such as provided by modern MS typically delivers a comprehensive list of interacting proteins functions of which may be known. A suggestion of the function of the entire complex may be inferred. Results of the profiling experiments can generally be split into three descriptive categories:

1) Known knowns. These interacting proteins are those that have previously been reported to interact with bait. Presence of these proteins works as an internal control and a validation of the method. The importance of this finding is less novel, but exhaustive. Additional information is gained by measures of abundance and contingency on damage.

2) Unknown knowns. This is a group of proteins that have known functions but have not previously been linked to the bait. This group has the highest immediate importance, especially if a functional link can be established and tested. Identification of such interacting partners can be followed with studies of exact mode of interaction, cross-linking, and shared kinase regulation.

3) Unknown unknowns. These are proteins with unknown or uncertain function and no known link to repair or senescence. Validation may require more in-depth study to prove association and development of new assays. Identification of an interacting partner can have a number of immediate lead-outs, depending on potential functional significance.

Traditional methods of experimental follow-up include validation of interaction by orthogonal methods such as Western blotting, immunofluorescence, or targeted MS. Functional validation may include reciprocal AP to test for concordant enrichment of shared interacting proteins, knockdown of potential interacting proteins and phenotyping, or targeted disruption of the proposed interaction.

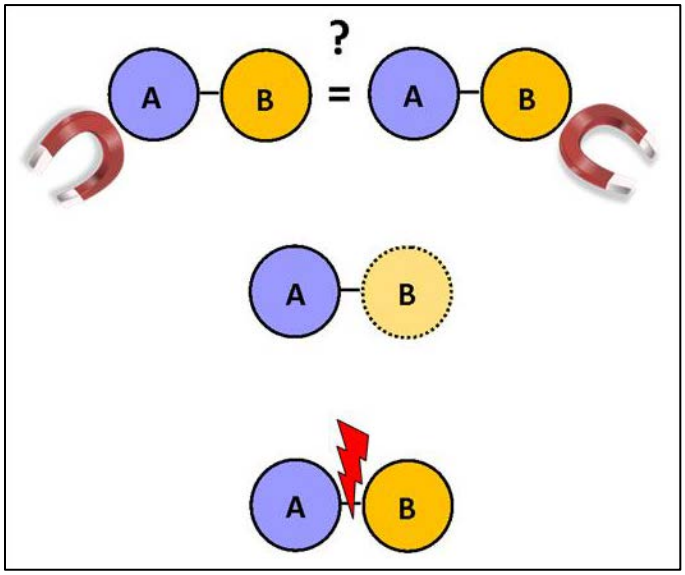

Figure 4.1: General schematic showing some ways of confirming physical protein interactions: by reciprocal purification, knockdown, or interference with interaction by inhibitory small molecules or disruption of protein interaction sequence..

Section 2: Experimental

Cell culture and drug treatment.

The Flp-In T-Rex-293 cells expressing either pFTSH-WRN or pFTSH-nLacZ were grown in Dulbecco-modified Eagle's medium (MediaTech CellGro, Manassas, VA), containing 4.5 g/L glucose and supplemented with 10% FBS (Hyclone, Logan, UT), penicillin and streptomycin sulfate (100 U/ml and 100 mg/ml, respectively; Invitrogen, Carlsbad, CA). Cells were grown in a humidified 37°C, 7% incubator. Stock solution of Camptothecin (Sigma-Aldrich) was prepared at 10 µg/mL in DMSO, and added directly to cell plates at the time of treatment. Volume equivalent of DMSO alone was added in controls.

LIVE/DEAD Assay.

Short-term toxicity and death was assayed using LIVE⁄DEAD® Viability⁄Cytotoxicity Kit (Life Technologies Corporation, Grand Island, NY) in combination with fluorescent microscopy according to manufacturer's instructions. Cells were treated with 16 uM CPT or volume equivalent of DMSO for 1 hour before assay. Negative control was not treated, and positive control cells were treated with 0.1% and 0.5% bleach solution for 5 minutes prior to analysis. Concentration of bleach >0.5% were found to result in complete and immediate killing.

MS Sample preparation.

Full aliquots of the eluate were diluted to 1 mL total volume with Ammonium Bicarbonate buffer (50 mM, pH 8). Samples were reduced by the addition of 10 μL of 500 mM dithiothreitol followed by incubation at 60^{o}C for 30 min, then alkylated by the addition of 15 μL of 500 mM

iodoacetamide followed by incubation at room temperature for 30 min in the dark. The resulting protein samples were then digested into peptides by the addition of trypsin (20 μg/sample; Promega, Madison, WI) and incubation at 37^{o}C for 1 h with agitation. Trypsin digestion was stopped by the addition of 10 μL formic acid, and samples were cleared of insoluble debris by centrifugation at 14,000 rpm for 10 min at 4^{o}C in a tabletop microcentrifuge (Eppendorf 5417R). Detergent was removed from the supernatant by solid phase extraction on Oasis MCX mixed phase columns (Waters Corporation, Milford, MA) according to manufacturer's instructions. The resulting samples were resuspended in 0.1% formic acid in water and stored at -80^{o}C until analysis.

Data Acquisition via LC-MS/MS.

Fused silica capillary tubing (75 μm i.d., Polymicro Technologies) was pulled to a tip of 5 μm at one end, then packed with 25 cm of Jupiter Proteo C12 reversed-phase chromatography material (Phenomonex, Torrance, CA). Nanoflow liquid chromatography was performed using an Agilent 1100 LC system. Samples were injected into a 5 μL loop using an autosampler, and washed onto a trap prior to elution onto the column. Solvents A and B for gradient elutions were water/acetonitrile (95%/5% v/v), and water/acetonitrile (20%/80% v/v), respectively. Both contained 0.1% formic acid. Solvent B was held at 3% for 10 min, then increased to 35% over the subsequent 50 min prior to a step to 90% for 10 min before returning to Solvent B at 3% for 20 min. The total gradient time was 90 min at a flow rate of 350 nL/min.

Eluting peptides were ionized via electrospray with the emitter held at 2.4 kV using an ESI source, and directed into a Thermo Scientific LTQ-Velos Linear Ion Trap mass spectrometer. Each precursor scan covered 400-1400 *m/z* range and was followed by 10 DDA scans. Dynamic

exclusion was used with a list size of 100 and a duration of 120 s. A normalized collision energy (CE) of 35 was used. A commercial digest consisting of six bovine proteins (Bruker Michrom, Auburn, CA) was run every five injections and was used to evaluate chromatographic peak shape, retention time reproducibility, and peak intensity.

Protein Identification and SAINT analysis.

Following LC-MS/MS analysis, .RAW data files were converted into compressed MS2 format, MS/MS spectra were searched by SEQUEST (version 27) (46) against a human IPI database (human-ipi-250309-contam.fasta) with semi-tryptic specificity, a static modification of 57.021 on Cysteine residues, and a variable modification of 15.995 on Methionine residues. Peptide spectrum match false discovery rates were determined by the Percolator algorithm (96) with a threshold of 0.01. Parsimonious protein inference was determined using the IDPicker algorithm (97). The results were loaded into our in-house data storage and viewing platform, MSDaPl (98). Data is publically available on PRIDE at http://www.ebi.ac.uk/pride (99).

Scoring of specific interacting proteins for SH-WRN in comparison to SH-nLacZ was performed using the statistical tool SAINT (Significance Analysis of INTeracome). For each bait AP, SAINT converted spectral counts corresponding to each prey protein identified, into the probability of true interaction between the two proteins (54,100). SAINT normalizes spectral counts to the length of the proteins and to the total number of spectra in the purification, and can calculate a probability of an interaction even for highly abundant or commonly detected proteins, based on quantitative enrichment (101).

For each bait and treatment condition, three biological replicates were used, and for each sample 2-3 analytical replicates were performed. Samples for each biological replicate were processed in parallel. Files initially searched with SEQUEST were converted to pep.xml and prot.xml files for direct importing into SAINT. SAINT analysis was performed in pairwise fashion between samples of the same treatment. Anti-SH-WRN was selected as an experimental sample, and anti-SH-nLacZ +DMSO AP – the control, in +DMSO and +CPT treatments. SAINT calculated an enrichment score for each identified protein, and a cutoff of 0.9 was selected. Data was exported directly from SAINT and used for further analysis.

Using CRAPome.

CRAPome (102) is a public repository of proteins that are commonly detected in AP-MS experiments. The repository was constructed by aggregating results of multiple negative controls in AP-MS experiments. We cross-referenced all proteins identified in our analysis with high confidence (SAINT score ≥0.9, 5+ Spectral Counts) with CRAPome database, and report the score in Results.

Development of Gene Ontology Comparison Tree Viewer CompGO.

We expanded on the current implementation of the Gene Ontology term explorer at the Yeast Resource Center (http://www.yeastrc.org/pdr/pages/go/goTermSearchForm.jsp) (103), and developed a GO term Comparison viewer, called CompGO for analysis of significantly represented GO categories in one or two samples, and can be found at http://www.yeastrc.org/compgo/. (*temporarily at http://yrc-apollo.no-ip.biz:8080/vg/pages/goAnalysisForm.jsp)

CompGO p-value Calculation. A p-value representing the statistical significance of the representation of a Gene Ontology (GO) term in a set of proteins was calculated using the hypergeometric distribution using the following formula:

$$P(I) = \frac{\binom{A}{I} * \binom{T-A}{B-I}}{\binom{T}{B}}$$

Where *A* = total number of proteins submitted that have GO annotations, *B* = the total number of proteins annotated with the given GO term (or any of its descendants), I (intersection of *A* and *B*) = the total number of submitted proteins annotated with the given GO term (or any of its descendants), and *T* = the total number of annotated proteins. Note: only UniProtKB GO annotations of human proteins were used in the calculation.

Then, the p-value describing the chance of having an intersection of size *I* or larger by chance may be computed as:

P-value = $\sum_{i=I}^{\min(A,B)} P(i)$, where min (*A,B*) is the minimum of values *A* and *B*.

CompGO Graph Assembly and Filtering. A p-value was calculated for every GO term represented in the protein set and for all ancestor terms up to the root term. The result is a complete directed acyclic graph (DAG) that represents a subset of the whole GO DAG where every term has an associated p-value. This DAG was then filtered by removing all terms with no children with an associated p-value >= some p-value cutoff. The resulting DAG was then filtered using the same method, and this process repeated until no childless terms remained with a p-value >= the cutoff. The final result is a filtered subset of the GO DAG that contains no leaf

nodes with a p-value greater than the cutoff, but where a given term is guaranteed to have all of its ancestor terms, even if those terms have a p-value greater than the cutoff. Having the ancestor terms present is critical to visualization as they provide context for interpreting the results.

CompGO Visualization Application. An application was developed for visualizing and reporting the resulting GO DAG, and for comparing and contrasting the GO DAG resulting from two separate protein sets. The application was developed as a web application using the Java, HTML, and Javascript; built utilizing the Struts web application framework and runs on the Apache Tomcat servlet container. All data is stored in an instance of the MySQL relational database management system (RDBMS). The application, dubbed "CompGO" is available for public use at http://www.yeastrc.org/compgo/.

Visualization is accomplished by generating a graphical representation of the GO DAG, where each node represents a GO term and each node is color-coded according to its calculated p-value. The nodes are labeled and color-coded according to p-value. If found in the first set (or if only a single set is submitted), they are colored by shades of red where darker red indicates more significant p-values. If found only in the second set, they are colored by shades of blue. If found in both sets, the coloring is inversed (dark background, white text) to clearly distinguish the terms from terms only found in one set or the other. In this case, the contribution of red and blue intensities is linked to the p-values from their respective sets. The result is that terms that are redder or bluer, depending on which set has the more significant p-value. In the case of somewhat equal p-values, the terms will be some shade of magenta (red combined with blue).

Data Analysis by CompGO.

SAINT results with score >0.9 were considered for analysis by Gene Ontology. IPI identifiers were converted to UniProt accessions, and imported directly into CompGO for comparative analysis. Maximum p-value of 10E-2 was selected as a significance cutoff for analysis by Cellular Component, and p-value of 10E-5 was selected as a significance cutoff by Biological Process. Graphical representation of results was exported directly from CompGO. Results in tabular format were subsequently used to identify proteins that supported assignment of a specific GO category were exported in tabular format to identify

Design of Protein interaction Networks.

Proteins identifications in support of every assigned GO category were extracted directly from CompGO and imported into STRING (104). Known interactions were mapped with the highest confidence score of 0.900 to allow only interactions substantiated by direct biochemical evidence to be displayed. The network was then expanded to display known interacting proteins that may act as connecting physical links, and to provide direction for validation studies. Resulting protein networks were exported and redrawn in Corel Draw for figures. Summary figure for WRN protein interaction networks as grouped by function was drawn in Microsoft Publisher.

Section 3: Results

Treatment with CPT

We performed extensive characterization of protein expression, localization, short-term cell toxicity when treated with CPT. DDR activation is shown by a rapid and robust phosphorylation of ATM, one of the earliest markers of DDR (Figure 4.1). This experiment guided our decision to select the treatment dose. We then tested the formation of γ-H2AX foci, a signature of DDR whereby histone H2AX is phosphorylated at Ser139. The result of the immunofluorescence analysis shows the characteristic staining of the phosphorylated histone (Figure 4.2).

The re-localization of WRN protein from primarily nucleolar location to the nucleoplasm was previously reported (105,106), and we tested for this response with our experimental treatment conditions after 1 hour at 16 μM CPT. The result shows that SH-WRN leaves nucleoli after treatment (Figure 4.3).

To determine whether the treatment caused acute toxicity or caused an increase of cell death, we used the LIVE/DEAD assay, which uses dual staining of the cells (Figure 4.4). The membrane-permeable dye stains all cells, which are shown on the immunofluorescence image in green. The cell-impermeable dye can only stain if the membrane is compromised, such as in cell death, and the cell appears as red on the image. The results indicate that neither CPT, nor control treatment solution of DMSO, nor induction agent doxycycline cause an increase of background level of dead cells. As a positive control we demonstrate the use of two solutions of common bleach, 0.1% and 0.5% for 5 minutes, and the massive cell death is immediately visible.

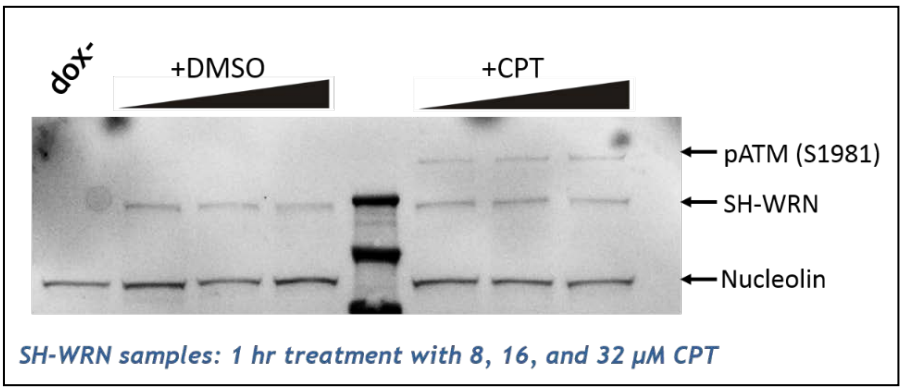

Figure 4.2: Demonstration of induction of damage-dependent response by WB: PO4-ATM.

Induction of DNA damage response was detected by Western blot against phosphorylated ATM. Range of CPT used for analysis: 8, 16, and 32 uM. Volume equivalent of DMSO was used in paired controls. Results indicate that a specific and robust response by pATM was achieved.

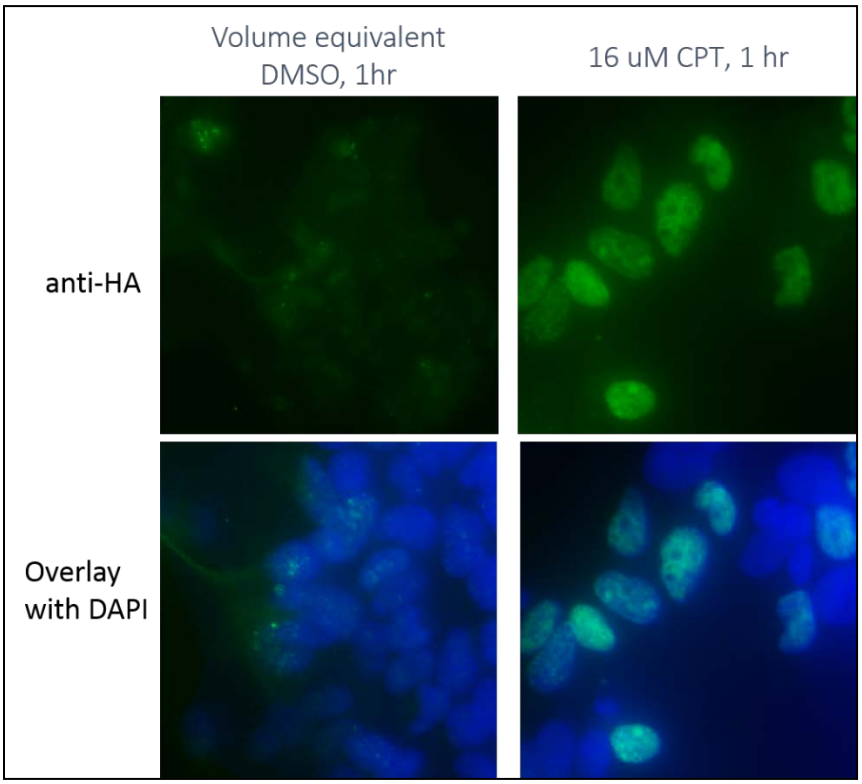

Figure 4.3: Induction of damage-dependent response by IF: γ-H2AX staining in S-phase cells.

This analysis has allowed us to determine that 1 hour treatment with 16 uM CPT is sufficient to induce focus formation. We delineated the conditions for the study to help us determine the role of WRN in immediate response to damage.

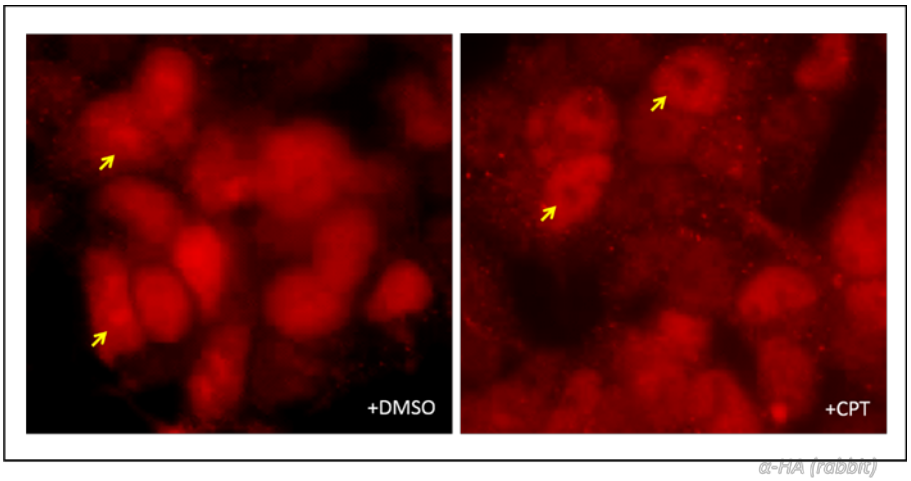

Figure 4.4: Relocalization of WRN from nucleoli to nucleoplasm after CPT treatment

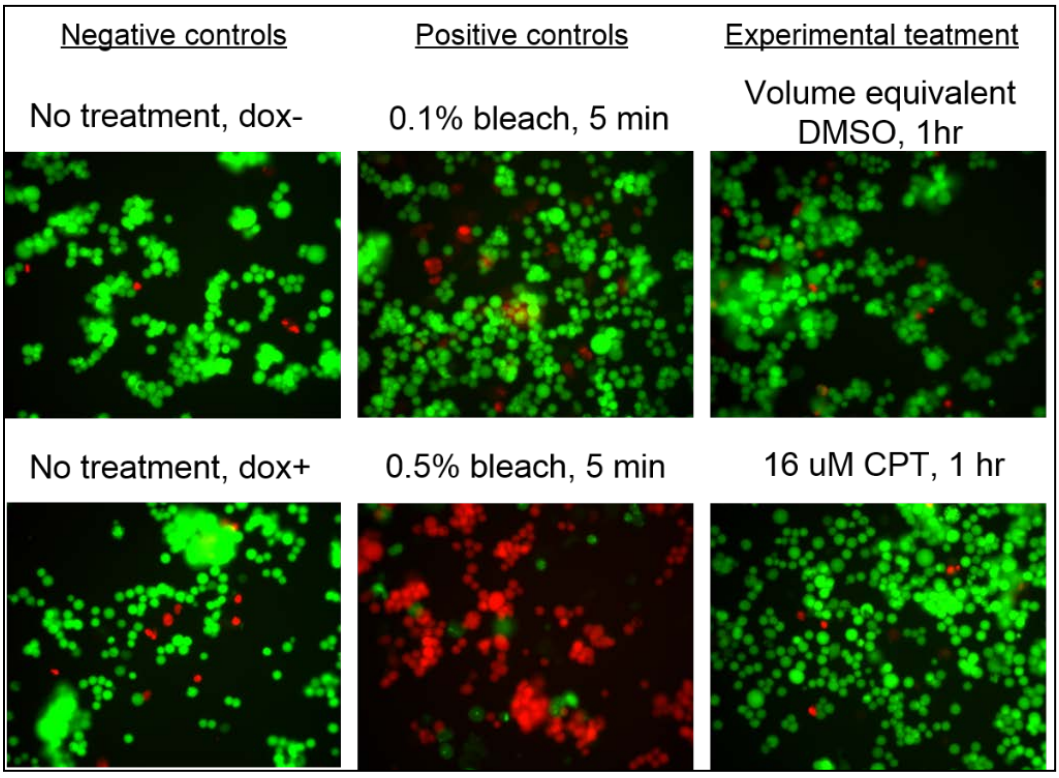

Figure 4.5: Acute toxicity analysis using Live/Dead stain to demonstrate that our selected dose and timepoint of treatment do not cause massive cell death.

SH-WRN and SH-nLacZ cells were seeded into 12-well plates for the analysis, and three fields were imaged per sample. Representative fields are shown. No difference was detected between different cell lines without treatment, and no difference in cell death was detected between dox+ and dox- cells. Experimental conditions were tested to determine whether drug treatment or negative control treatment by DMSO would cause cell death or elicit a nonspecific response. Treatments were as follows: 16 uM CPT for 1 hr, DMSO (16 uM volume equivalent, 0.16%

by volume) for 1 hr. Results show that addition of DMSO or CPT does not cause cell death as compared to untreated control. Doxycycline does not cause cell death after 24 hr treatment prior to analysis, and does not affect cell survival after treatment with CPT or DMSO. Bleach is an adequate positive control if cells are treated with it for 5 minutes.

Identification of WRN-interacting proteins and data analysis

The scheme in Figure 4.5 shows that once isolated, the protein complex containing the bait protein (SH-WRN or control SH-nLacZ) and its bound milieu is subjected to standard proteomic preparation (as described in Figure 1.3). We analyzed the results of the profiling MS analysis using SAINT, which identified subsets of all protein identifications that were enriched in bait- and treatment-specific manner. These results between two sets of proteins enriched by treatment were then compared by Gene Ontology annotations using our new program CompGO, and verified against known protein-protein interactions using STRING.

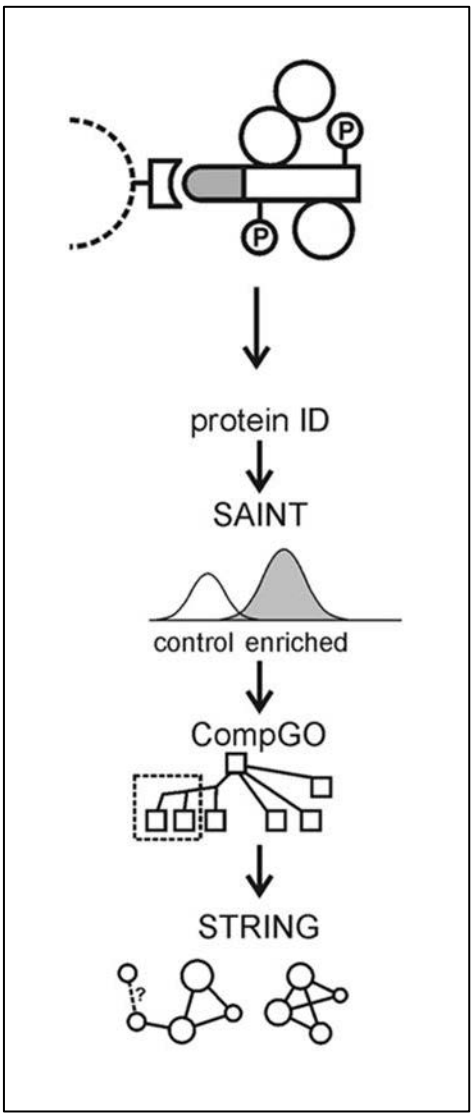

Figure 4.6: Isolation of the protein complex and subsequent steps of protein identification and data mining.

Enrichment and recovery of bait proteins, SH-WRN and SH-nLacZ was assessed. The level of expression of SH-WRN was consistently higher than that of SH-nLacZ, but relative levels of protein within cell line did not change whether the cell was treated with CPT or control DMSO (Figure 4.6). The results also demonstrate that the recovery of baits did not change depending on treatment. The total protein stain by SYPRO ruby shows that many bands

are present in the eluted samples, and the abundance of bands is approximately equal in all four lanes. This indicates an intermediate level of enrichment. In our analysis, the selection of a proper control protein that localizes to the same compartment, as well as using stringent criteria for enrichment, was crucial to maintain a high level of sensitivity and specificity in downstream protein identification. This is further reviewed in the Discussion section.

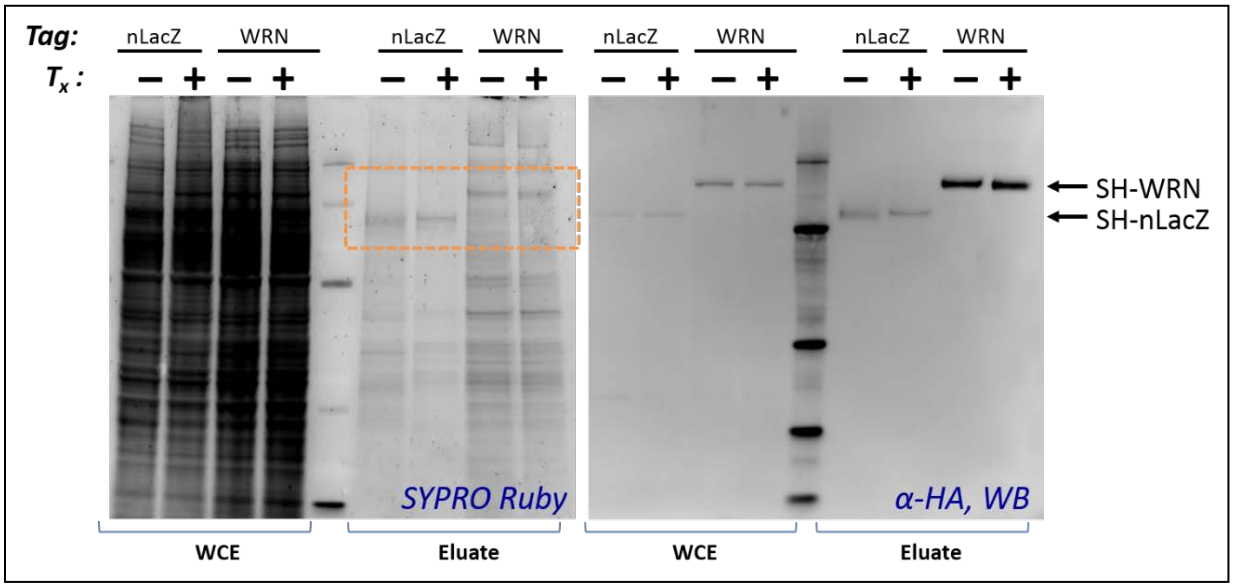

Figure 4.7: Western blot and total protein (SYPRO ruby-stained polyacrylamide gel) stain demonstrating recovery and enrichment of bait.

We demonstrate that relative protein expression and recovery are not dependent on drug treatment. Bait recovery was estimated to be 60-90% based on load/eluate proportion.})

MS data was analyzed by SAINT in pairwise manner, where proteins identified in anti-SH-nLacZ +DMSO AP were identified as controls for anti-SH-WRN +DMSO AP, and analogously for the pair treated with CPT.

Table 4.1 is a referenced summary of proteins that were previously shown to interact with WRN. This table demonstrates the breadth of different interactions that have been determined for WRN,

based on methods such as affinity purifications and immunoprecipitations, co-localization studies, yeast two-hybrid (Y2H), reconstituted complex assay, MS profiling studies, and *in vitro* assays. We indicate the overlap with our findings, provide supporting SAINT score and spectral counts, and identify proteins that were further analyzed by SRM, as discussed further in Chapter 5.

protein name	description	SAINT				SRM	
		WRN vs nLacZ (+DMSO)		wrn-WRN vs nLacZ (+CPT)			
		SAINT score	SC	SAINT score	SC		Ref.
ABL	c-Ableson tyrosine kinase						(107,108)
ATR	Serine-protein kinase ATM-related						(109–112)
ATRX	alpha thalassemia/mental retardation syndrome X-linked						(109)
ATM	Serine-protein kinase ATM						(110)
BAT1	Spliceosome RNA helicase BAT1						(111)
BLM	Bloom syndrome protein			0	1	x	(111,113,114)
BRCA1	Breast Cancer susceptibility Region 1						(27)
C1orf77	CHTOP chromatin target of PRMT1						(111)
CCT2	Chaperonin Containing TCP1, Subunit 2	0	126	0.008	109		(111)
CCT3	Chaperonin Containing TCP1, Subunit 3						(111)
CCT8	Chaperonin Containing TCP1, Subunit 8	0.392	104	1	98		(111)
CDC5L	CDC5 cell division cycle 5-like (S. pombe)	0.674	6	0	5		(115)
CDKN2A	Cyclin-dependent kinase inhibitor 2A (p14ARF)	0	1	0.554	3		(116)
CHD1	Chromodomain Helicase DNA Binding Protein 1						(111)

protein name	description	SAINT				SRM	Ref.
		WRN vs nLacZ (+DMSO)		wrn-WRN vs nLacZ (+CPT)			
		SAINT score	SC	SAINT score	SC		
CHD4	Chromodomain Helicase DNA Binding Protein 4	0.958	40	0	28	x	(111)
CHAF1A	Chromatin assembly factor 1 subunit A					x	(117,118)
DDX1	ATP-dependent RNA helicase DDX1	0	107	0	104		(111)
DDX17	Probable ATP-dependent RNA helicase DDX17	0	60	0	64		(111,119)
DDX3X	ATP-dependent RNA helicase DDX3X			0	204		(111)
DDX5	Probable ATP-dependent RNA helicase DDX5	0	76	0	71		(111)
DDX21	DDX21 DEAD (Asp-Glu-Ala-Asp) box helicase 21	0.926	37	0.25	18		(111)
DHX9	RNA helicase A	0	300	0	299		(120,121)
EIF4A3	Eukaryotic initiation factor 4A-III	0	9	0	7		(111)
ELAV1	ELAV Like RNA Binding Protein 1						(111)
EMD	Emerin	0	13	0	10		(111)
EXO1	Exonuclease 1						(122)
FEN1	Flap structure-specific endonuclease 1	0.114	4	0.692	11	x	(119,123–125,125,126)
FYTTD1	Forty-Two-Three Domain Containing 1						(111)
GIS1	JmjC domain-containing histone demethylase and transcription factor						(127)
H2AFX	Histone H2AX	0.906	17			x	(128,129)
HERC2	Probable E3 ubiquitin-protein ligase HERC2	0.588	4	0.386	2		(111)
HIST1H1E	Histone Cluster 1, H1e	0.086	4	0.764	6		(111)
HIST1H2AB	Histone Cluster 1, H2ab						(111)
HIST1H2BK	Histone Cluster 1, H2bk						(111)
HIST1H4A	Histone Cluster 1, H4a						(111)

protein name	description	SAINT				SRM	
		WRN vs nLacZ (+DMSO)		wrn-WRN vs nLacZ (+CPT)			
		SAINT score	SC	SAINT score	SC		Ref.
HNRNPA2 B1	Heterogeneous Nuclear Ribonucleoprotein A2/B1	0.998	614	0	365		(111)
HNRNPM	Heterogeneous Nuclear Ribonucleoprotein M	0	300	0	314		(111)
HNRNPU	Heterogeneous Nuclear Ribonucleoprotein U (Scaffold Attachment Factor	0	434	0	514		(111)
HNRNPUL2	Heterogeneous Nuclear Ribonucleoprotein U-Like 2	0	236	0	242		(111)
HSPA5	Heat Shock 70kDa Protein 5	0	172	0	156		(111)
ILF2	Interleukin Enhancer Binding Factor 2	0	179	0	194		(111)
LIG1	Ligase I, DNA, ATP-dependent	0.386	2			x	(130)
LIG3	Ligase III, DNA, ATP-Dependent	0.748	7	0.248	5		(111)
LMNA	Lamin A/C	0.312	15	0.01	11		(111)
MDC1	Mediator Of DNA-Damage Checkpoint 1	0	4	0.864	5	x	(131)
MRE11	MRN complex member MRE11	0	40	0	45	x	(132,133)
MSH2	DNA mismatch repair protein MSH2	0.188	2	0.916	5		(111)
MSH3	DNA mismatch repair protein MSH3	0	1				(111)
NBS1	Nibrin, MRN complex member	0	1	0.454	8		(128,134)
NEIL1	DNA glycosylase (endonuclease VIII-like 1)						(135)
NOP2	Proliferating-Cell Nucleolar Antigen P120	0.606	3				(111)
NPM1	Nucleophosmin	0	64	0	63		(111)
NSD1	nuclear receptor binding SET domain protein 1						(111)

protein name	description	SAINT				SRM	
		WRN vs nLacZ (+DMSO)		wrn-WRN vs nLacZ (+CPT)			
		SAINT score	SC	SAINT score	SC		Ref.
PARP-1	Poly (ADP-ribose) polymerase-1	0	329	0	318	x	(119,136–138)
PCNA	Proliferating cell nuclear antigen	0	31	0.606	33	x	(111,134,139–142)
PELP1	Proline, Glutamate And Leucine Rich Protein 1	0	8	0.056	15		(111)
PHB	Prohibitin	0.01	2	1	35		(111)
PML	tripartite motif-containing protein 19	0	1	0.448	4		(143)
POLB	DNA polymerase beta subunit	0.392	2			x	(117,118,144)
POLD1	DNA polymerase delta 1 subunit	0.604	3	0.578	3	x	(145)
POLD2	DNA polymerase delta 2 subunit	0	1	0.448	2		(145)
POLR1C	DNA-directed RNA polymerases I subunit RPAC1	0.052	36	0.512	32		(146)
POT1	Protection of telomere homologue 1						(147)
PRKDC	DNA dependent protein kinase catalytic subunit	0.998	406	0.954	342	x	(110,111,148)
Rad50	MRN complex member RAD50	0	45	0.002	55		(111)
RAD51	DNA repair protein RAD51	0.998	41	0.926	33		(109,149)
RAD52	DNA repair protein RAD52						(109,140)
RAD54	DNA repair protein RAD54						(109)
RALY	RALY Heterogeneous Nuclear Ribonucleoprotein	0.944	118	0.31	127	x	(111)
RBMX	RNA binding motif protein, X-linked	0.002	46	0.004	42		(111)
RECQL	ATP-dependent DNA helicase Q1	0.356	4	0.75	6		(150)
RFC1	Replication factor C 1						(111)
RFC4	Replication factor C 4	0.194	4	0.424	7		(111)

protein name	description	SAINT				SRM	
		WRN vs nLacZ (+DMSO)		wrn-WRN vs nLacZ (+CPT)			
		SAINT score	SC	SAINT score	SC		Ref.
RFC5	Replication Factor C (Activator 1) 5,	0.412	4	0.72	4		(111)
RPA1	Replication protein A 70 kDa DNA-binding subunit	0	12	0.522	23	x	(111,151–153)
RPA2	Replication protein A2, 32 kDa	0.004	4	0.826	7		(129)
RPL11	Ribosomal Protein L11	0.36	9	0.224	15		(111)
RPL5	Ribosomal Protein L5	0	25	0.004	24		(111)
RPS19	ribosomal protein S19	0	33	0.006	37		(111)
RPS3A	Ribosomal Protein S3A	0.914	88	0.396	84		(111)
RPS6	Ribosomal Protein S6	0.194	46	0.282	43		(111)
RPS9	Ribosomal Protein S9	0.012	37	0.36	40		(111)
RSL1D1	ribosomal L1 domain containing 1						(111)
SATB2	Special AT-Rich Sequence-Binding Protein 2						(111)
SFRS1	serine/arginine-rich splicing factor 1						(111)
SFRS7	Serine/arginine-rich splicing factor 7						(111)
SIRT1	Sirtuin 1						(154)
SNRNP200	Small Nuclear Ribonucleoprotein 200kDa	0	176	0	202		(111)
SSRP1	structure specific recognition protein 1	0.998	16	1	17	x	(111)
SUMO1	SMT3 suppressor of mif two 3 homologue 1 (*S. cerevisiae*)	0.538	3	0.19	2	x	(116,155)
SUMO2	Small ubiquitin-related modifier 2						(156)
SUPT16H	Suppressor Of Ty 6 Homolog (S. Cerevisiae)	0.078	117	0.994	136	x	(111,119)
TCP1	t-complex 1	0.18	83	0.756	97		(111)
TFAM	Mitochondrial transcription factor A						(111)

protein name	description	SAINT				SRM	
		WRN vs nLacZ (+DMSO)		wrn-WRN vs nLacZ (+CPT)			
		SAINT score	SC	SAINT score	SC		Ref.
THOC1	THO Complex 1						(111)
THOC2	THO Complex 2						(111)
THOC6	THO Complex 6						(111)
TMPO	thymopoietin	0.678	23	0.014	28		(119)
TOP1	topoisomerase 1	0.538	3	0.004	2	x	(119,141)
TP53	Tumour Protein p53	0	89	0	76	x	(111,151,157–159)
TRF1	Telomeric repeat binding factor 1						(160)
TRF2	Telomeric repeat binding factor 2	0	1	0	1		(160,161)
TRIM28	Tripartite Motif Containing 28, KAP1	0	126	0	123		(111)
UBC	ubiquitin protein c						(144,162)
UBC9	SUMO-conjugating enzyme						(163)
UBTF	Nucleolar transcription factor 1						(111)
VCP	Transitional endoplasmic reticulum ATPase	0	582	0	642		(111,147,164)
VRK3	Vaccinia Related Kinase 3						(111)
WDR48	WD repeat-containing protein 48						(165)
WRNIP1	Werner helicase-interacting protein 1 (WHIP)	0.048	6	0.526	3	x	(166)
XRCC1	X-ray repair cross-complementing protein 1						(111)
XRCC5	Ku86	0	380	0	374	x	(25,111,119,136,137,148,164,167,168)
XRCC6	KU70	0	383	0.99	416	x	(25,111,119,136,137,148,164,167,168)
YBX1	Y box 1 transcription factor					x	(111,169)

Table 4.1: Abbreviated list of previously reported interaction partners of WRN, as determined by a variety of biochemical and genetic approaches.

Figure 4.8 summarizes the numbers of proteins that were previously reported to interact with WRN, and the overlap of these studies with ours. (A) In the context of previously reported WRN-interacting proteins, results of shotgun proteomic analysis of WRN-associated complexes on three biological replicates show significant overlap in protein identification (77/118 proteins). After filtering our results by SAINT score (≥0.9), spectral counts (≥5), and nuclear localization, we identify 14 proteins in our dataset that were previously reported in other studies. (B) This panel presents the list of previously identified WRN-interacting proteins in the context of our study. The entire set of proteins that we determined to be significantly enriched in association with WRN, and which passed our stringency cut-offs is shown. Yellow circle and blue oval represent proteins that were shown as enriched in association with WRN after treatment with DMSO (control) and 16 uM CPT for 1 hour, respectively.

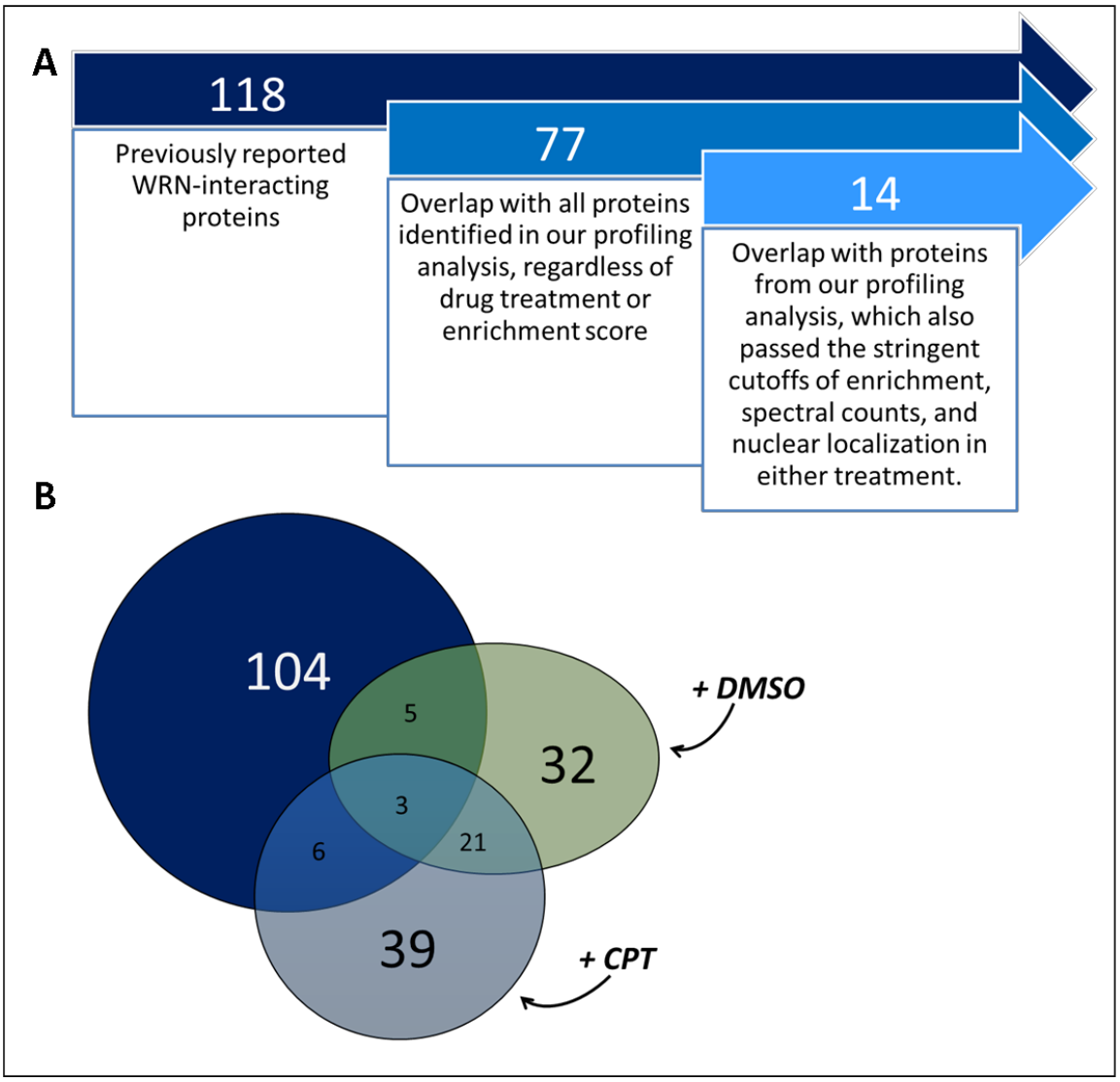

Figure 4.8: The extent of overlap in identification of WRN-associated proteins between our study and previous studies is shown.

Figure 4.8 demonstrates that regardless of the drug treatment, proteins that were identified as significantly interacting with SH-WRN fall into the major subcellular categories in very close proportion. We used Gene Ontology analysis by cellular component (GO_CC) of all proteins found in our analysis to separate them into major categories. Proportion of proteins

annotated to a selected category of the total was calculated and graphed. Results show that proteins from non-nuclear compartments constitute a very close proportion of identified proteins regardless of treatment type. However, breakdown of proteins that were categorized as nuclear, shows that a significant difference between nucleolar, nucleoplasmic, and chromosome-associated fractions depending on sample treatment. It should be noted that many proteins are annotated to multiple subcellular compartments, and therefore the totals add up to over 100%.

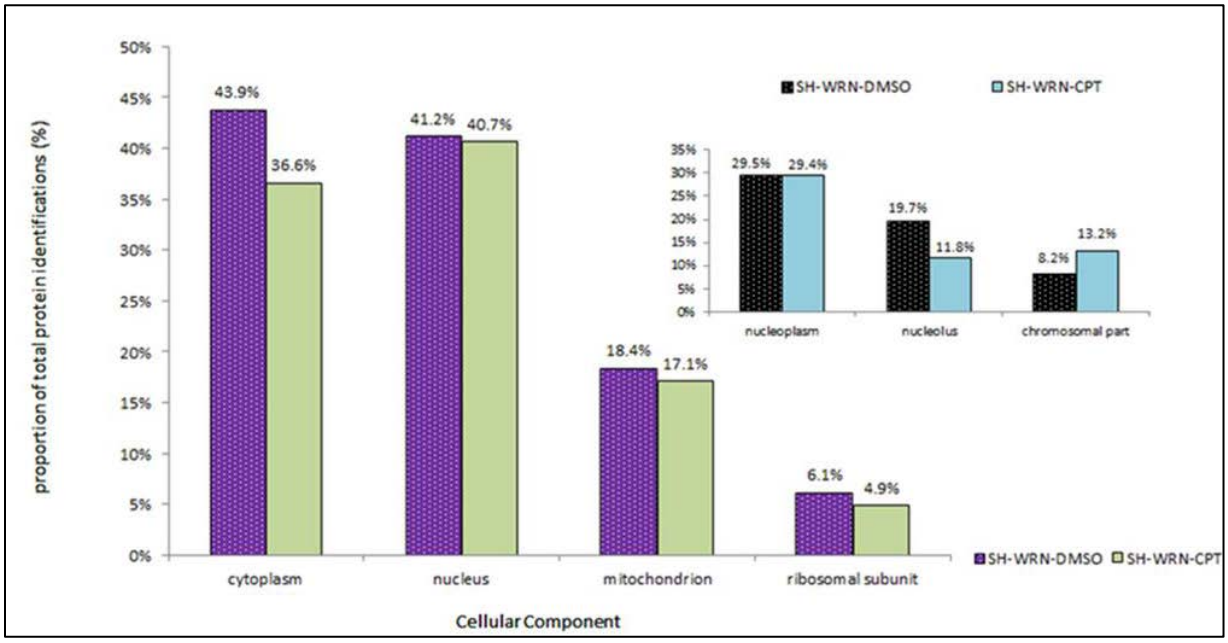

Figure 4.9: Overview of results based on subcellular localization – demonstration of equal contamination of pulldowns by proteins from non-nuclear compartments regardless of bait or treatment.

The figure shows that numbers of proteins from non-nuclear compartments that associate with WRN are even between differentially treated samples. However, a further breakdown of nuclear proteins reveals that drug treatment results in significant differences between numbers of nucleolar and chromatin-associated, but not nucleoplasmic proteins that bind to SH-WRN.

In agreement with IF results in Figure 4.3, WRN associates with fewer proteins that are

assigned as nucleolar in samples that were treated with CPT. The novel finding from our results shows that WRN associates with a larger number of proteins that are annotated to associate with chromatin. This observation is further substantiated by the results of GO analysis by Biological Process, which identifies chromatin organization as a significant functional category (p-value: 1.79E-7).

Eight proteins that are annotated to the nucleolus were found to interact with WRN in the CPT-treated sample. 4 of these are also annotated to the nucleoplasm, reminding us that the assignments are never exclusive, and that annotations should only be used as a guide rather than a definitive characterization of the protein's localization or function. Furthermore, because WRN is normally localized to the nucleolus, the detection of nucleolar proteins may be due to detection of interacting proteins with the remaining population from the nucleolus, or those that shuttle to the nucleoplasm with WRN during CPT-induced relocalization.

As summarized in Table 4.1, our results show overlap with some of the previously reported interactors or WRN. This table also highlights the large number of proteins that have been shown to interact with WRN, and the methods by which each interaction was determined or inferred.

To explore the functional categories that may join the most significantly represented proteins in our analysis; we used CompGO, a tool we developed for comparative analysis of two samples by Gene Ontology. For analysis by cellular component, GO_CC, we chose a p-value cutoff of 1E-2, and were able to easily show that although nucleoplasmic proteins were represented with very high confidence in both treatments (p-value 4.42E-13 when treated with DMSO, and 5.28E-15 when treated with CPT), assignment of proteins that are annotated to the nucleolus was only significant in DMSO-treated samples (p-value 1.27E-3). Figure 4.10 shows

how a single parent category (nuclear part) as well as one of the two “daughter” categories (nucleoplasm) are both representative of proteins in both samples, while “daughter” category nucleolus is only significantly representative of one of the samples. The inputs are readily distinguished based on color of the categories.

The entire figure, directly as imported from CompGO is included here, and attached in full resolution in the supplement (Figure 4.11).

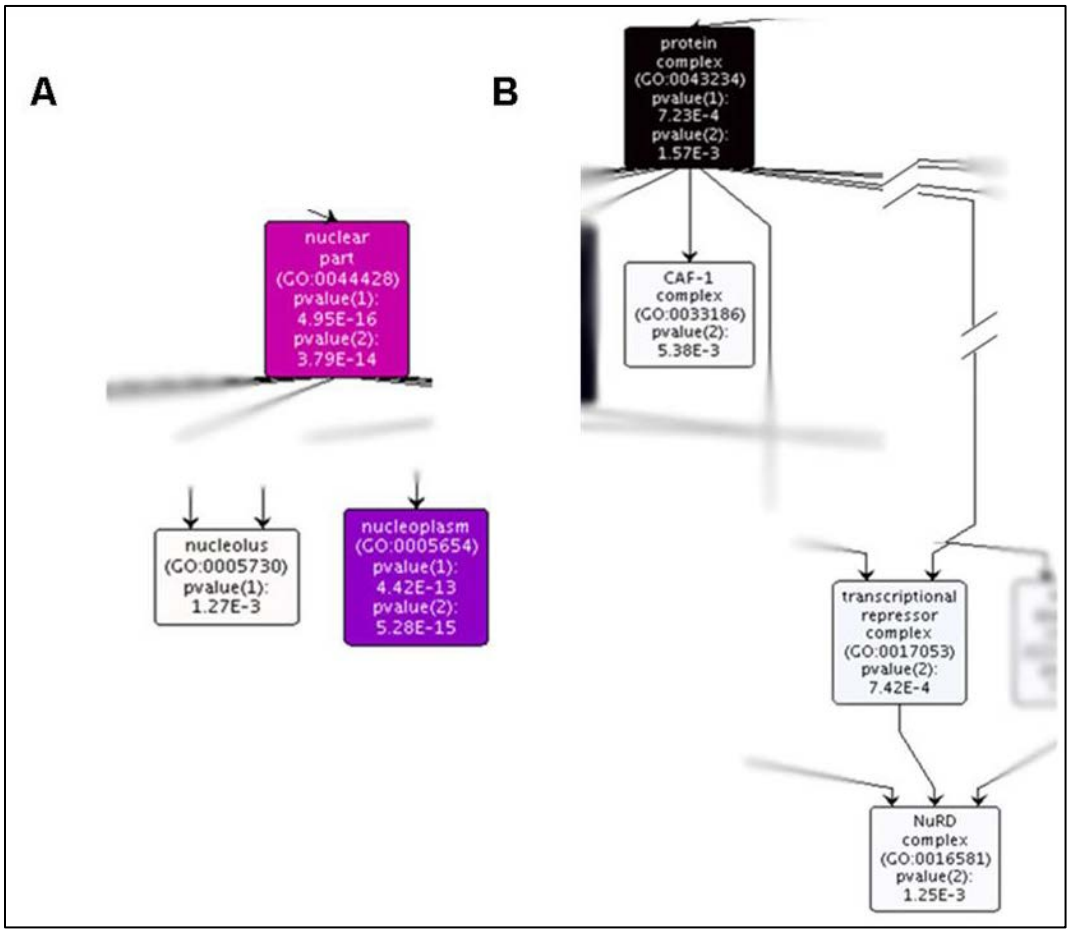

Figure 4.10: An abbreviated form of GO_CC dendrogram (p-value cutoff 1E-2), which is focused on a few chosen examples of where the identifications by GO diverge in treatment-specific manner.

(A) The focused divergence between nucleoplasmic and nucleolar annotatation in our samples. (B) The assignment of significance to a number of protein complexes that are known to participate in chromatin remodeling.

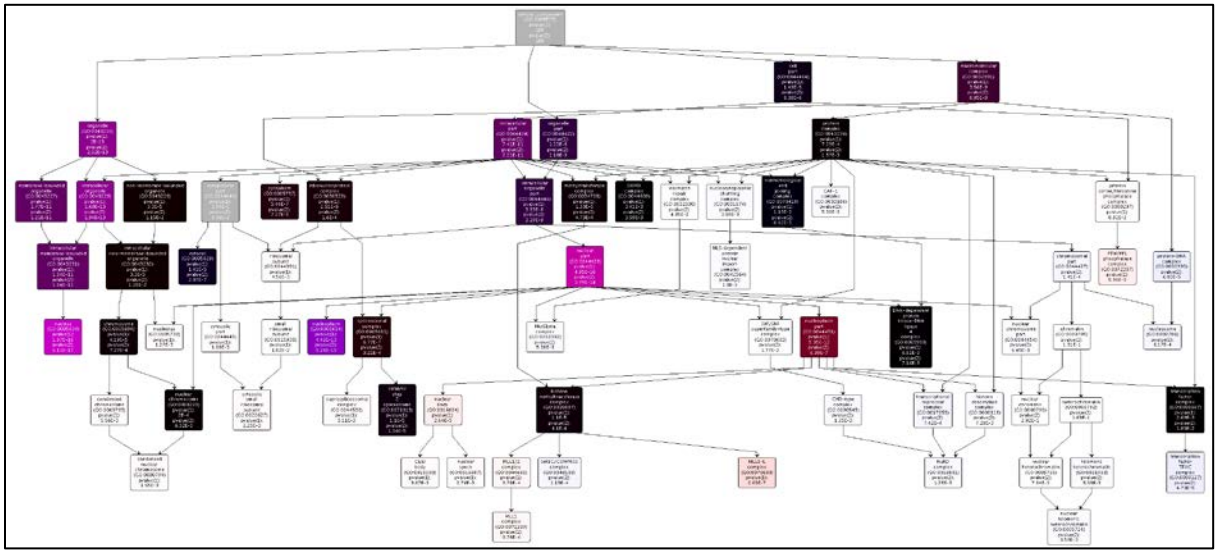

Figure 4.11: Complete GO_BP dendrogram (p-value cutoff 1E-5), as imported from CompGO. Complete input data is presented in Supplementary Table 1A as sample (1) and Supplementary Table 1B as sample (2). Full-scale image is available in Appendix B, Figure B2.

We summarize our findings of most dominant functional categories represented by sample treatment in Figure 4.11. Protein identifiers, as extracted from **Supplementary Tables 1A and 1B,** were entered into CompGO. Categories significantly represented in treatment-specific manner are summarized. These categories, and the proteins contributing to the assignment, were used as a guide for exploration of specific biological processes, and further validation.

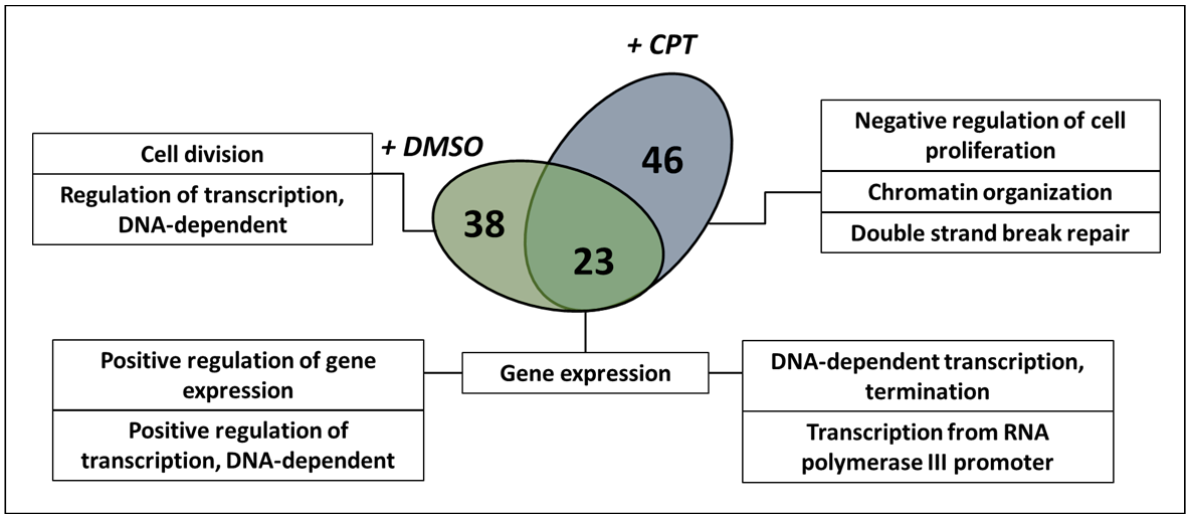

Figure 4.12: Summary of GO_BP results by drug treatment – demonstrating breakdown of major biological processes and sub-processes

Abbreviated results that contributed to Figure 4.10 are presented in Table 4.2. The table identifies new as well as previously reported interacting proteins of WRN, the SAINT scores calculated to support the enrichment in WRN-dependent manner, as well as an overlay with CRAPome database.

New interacting partner	Frequency of CRAPome detection	Gene Name	Description	(+DMSO) SAINT score	(+CPT) SAINT score
*	126 / 343	PCBP2	poly(rC) binding protein 2		1
*	129 / 343	HNRNPR	heterogeneous nuclear ribonucleoprotein R		1
*	8 / 343	GTF3C3	general transcription factor IIIC, polypeptide 3, 102kDa		1
*	85 / 343	SRRM2	Isoform 1 of Serine/arginine repetitive matrix protein 2		1
*	96 / 343	TAGLN2	transgelin 2	0.922	1
*	96 / 343	PRDX6	peroxiredoxin 6	0.956	1

New interacting partner	Frequency of CRAPome detection	Gene Name	Description	(+DMSO) SAINT score	(+CPT) SAINT score
*	62 / 343	RARS	arginyl-tRNA synthetase	1	1
*	25 / 343	KPNA4	karyopherin alpha 4 (importin alpha 3)		0.998
*	3 / 343	STRN	striatin, calmodulin binding protein		0.998
*	164 / 343	HIST2H2AB	histone cluster 2, H2ab		0.998
*	21 / 343	UBR4	ubiquitin protein ligase E3 component n-recognin 4	0.916	0.998
*	26 / 343	HCFC1	host cell factor C1 (VP16-accessory protein)	0.996	0.998
*	160 / 343	HIST1H2BL	histone cluster 1, H2bl		0.996
*	155 / 343	ENO1	enolase 1, (alpha)	0.926	0.996
*	35 / 343	AIMP2	aminoacyl tRNA synthetase complex-interacting multifunctional protein 2; stromal antigen 3-like 3	0.998	0.996
*	24 / 343	SUPT6H	suppressor of Ty 6 homolog (S. cerevisiae)		0.994
*	70 / 343	MYBBP1A	MYB binding protein (P160) 1a		0.988
*	11 / 343	PCNP	PEST proteolytic signal containing nuclear protein		0.988
*	24 / 343	TSR1	TSR1, 20S rRNA accumulation, homolog (S. cerevisiae)		0.986
*	230 / 343	KRT14	keratin 14	0.948	0.986
*	206 / 343	HIST2H2AA4	histone cluster 2, H2aa3; histone cluster 2, H2aa4		0.984
*	75 / 343	TPI1	TPI1 pseudogene; triosephosphate isomerase 1		0.98
*	18 / 343	PPP1R10	protein phosphatase 1, regulatory (inhibitor) subunit 10		0.978
*	22 / 343	FUBP1	far upstream element (FUSE) binding protein 1		0.976
*	131 / 343	PPIA	Peptidyl-prolyl cis-trans isomerase A		0.972
*	1 / 343	RALGAPA1	GTPase activating Rap/RanGAP domain-like 1		0.972
*	36 / 343	CPSF7	cleavage and polyadenylation specific factor 7, 59kDa		0.97
*	1 / 343	EPN1	epsin 1		0.97
*	48 / 343	PGAM2	phosphoglycerate mutase 2 (muscle)		0.968

New interacting partner	Frequency of CRAPome detection	Gene Name	Description	(+DMSO) SAINT score	(+CPT) SAINT score
*	71 / 343	KHSRP	KH-type splicing regulatory protein		0.968
*	6 / 343	CTBP2	C-terminal binding protein 2	0.998	0.968
*	116 / 343	MATR3	matrin 3	0.912	0.966
*	37 / 343	HSPA4L	heat shock 70kDa protein 4-like		0.964
*	7 / 343	TNKS1BP1	tankyrase 1 binding protein 1, 182kDa		0.964
*	109 / 343	TAF15	TAF15 RNA polymerase II, TATA box binding protein (TBP)-associated factor, 68kDa		0.962
*		NFKBIE	nuclear factor of kappa light polypeptide gene enhancer in B-cells inhibitor, epsilon		0.962
*		PKM	similar to Pyruvate kinase, isozymes M1/M2, CTHBP	0.902	0.96
*	127 / 343	HNRNPC	heterogeneous nuclear ribonucleoprotein C (C1/C2)	0.972	0.958
*	201 / 343	HNRNPA1	heterogeneous nuclear ribonucleoprotein A1		0.956
*	182 / 343	H2AFZ	H2A histone family, member Z		0.954
*	14 / 343	EDC4	enhancer of mRNA decapping 4	0.95	0.954
*		POLR3D	polymerase (RNA) III (DNA directed) polypeptide D, 44kDa		0.952
*	92 / 343	RBBP4	hypothetical LOC642954; retinoblastoma binding protein 4		0.952
*	12 / 343	NUP160	nucleoporin 160kDa		0.948
*	10 / 343	GTF3C1	general transcription factor IIIC, polypeptide 1, alpha 220kDa		0.942
*		FAM175B	family with sequence similarity 175, member B		0.938
*	31 / 343	ZNF326	zinc finger protein 326		0.932
*	16 / 343	ZCCHC8	zinc finger, CCHC domain containing 8		0.932
*	113 / 343	RPL3	ribosomal protein L3; similar to 60S ribosomal protein L3 (L4)	0.924	0.932
*	4 / 343	NOTCH2	Notch homolog 2 (Drosophila)		0.93
*		DMRT3	doublesex and mab-3 related transcription factor 3	0.998	0.928

New interacting partner	Frequency of CRAPome detection	Gene Name	Description	(+DMSO) SAINT score	(+CPT) SAINT score
*	12 / 343	MDN1	MDN1, midasin homolog (yeast)		0.926
*	45 / 343	PSMA3	proteasome (prosome, macropain) subunit, alpha type, 3		0.926
*	7 / 343	ANXA7	annexin A7	1	0.924
*		HNRNPA1P10	heterogeneous nuclear ribonucleoprotein A1-like		0.922
*	13 / 343	PTRF	polymerase I and transcript release factor		0.91
*	21 / 343	DPY30	dpy-30 homolog (C. elegans)		0.906
*	61 / 343	NOLC1	nucleolar and coiled-body phosphoprotein 1	0.902	
*		BAT2	HLA-B associated transcript 2	0.906	
*	84 / 343	DDX39B	Isoform 2 of Spliceosome RNA helicase DDX39B	0.914	
*		MED4	mediator complex subunit 4	0.916	
*	75 / 343	PPP1CA	protein phosphatase 1, catalytic subunit, alpha isoform	0.918	
*	7 / 343	CDCA2	cell division cycle associated 2	0.926	
*	88 / 343	HIST1H3F	histone cluster 1, H3	0.928	
*	1 / 343	IQSEC1	IQ motif and Sec7 domain 1	0.942	
*	20 / 343	DDX42	DEAD (Asp-Glu-Ala-Asp) box polypeptide 42	0.944	
*	197 / 343	HNRNPA2B1	heterogeneous nuclear ribonucleoprotein A2/B1	0.948	
*	112 / 343	KIF11	kinesin family member 11	0.952	
*	144 / 343	HNRNPAB	heterogeneous nuclear ribonucleoprotein A/B	0.952	
*	31 / 343	ZNF326	zinc finger protein 326	0.952	
*	1 / 343	RELA	v-rel reticuloendotheliosis viral oncogene homolog A	0.956	
*	93 / 343	PFN1	profilin 1	0.964	
*		EPS15L1	epidermal growth factor receptor pathway substrate 15-like 1	0.976	
*	201 / 343	HNRNPA1	heterogeneous nuclear ribonucleoprotein A1	0.976	
*		SSBP3	single stranded DNA binding protein 3	0.98	

New interacting partner	Frequency of CRAPome detection	Gene Name	Description	(+DMSO) SAINT score	(+CPT) SAINT score
*	12 / 343	RNF2	ring finger protein 2	0.988	
*	3 / 343	TFDP1	transcription factor Dp-1	0.988	
*	95 / 343	NME2	non-metastatic cells 2, protein NM23B	0.99	
*	30 / 343	ADAR	adenosine deaminase, RNA-specific	0.994	
*	18 / 343	PDCD6	aryl-hydrocarbon receptor repressor; programmed cell death 6	0.994	
*	33 / 343	CPSF1	cleavage and polyadenylation specific factor 1, 160kDa	0.994	
*	143 / 343	RPS2	ribosomal protein S2	0.996	
*	42 / 343	SARNP	SAP domain containing ribonucleoprotein	0.996	
*	13 / 343	SMARCE1	SWI/SNF related, matrix associated, actin dependent regulator of chromatin, subfamily e, member 1	0.996	
*		SOX9	SRY (sex determining region Y)-box 9	0.998	
*		MEIS1	Meis homeobox 1	0.998	
*	84 / 343	SRSF6	splicing factor, arginine/serine-rich 6; similar to arginine/serine-rich splicing factor 6	0.998	
*	5 / 343	POLR2J	polymerase (RNA) II (DNA directed) polypeptide J, 13.3kDa	1	
*	75 / 343	PPP1CC	protein phosphatase 1, catalytic subunit, gamma isoform	1	
*	8 / 343	POLR2D	polymerase (RNA) II (DNA directed) polypeptide D	1	
*	17 / 343	ANP32B	similar to Acidic leucine-rich nuclear phosphoprotein 32 family member B, PHAPI2 protein, protein SSP29	1	
	58 / 343	PHB	prohibitin		1
	136 / 343	DDX3Y	DEAD (Asp-Glu-Ala-Asp) box polypeptide 3, Y-linked	0.954	1
	13 / 343	TFAM	transcription factor A, mitochondrial	0.996	1
	44 / 343	SSRP1	structure specific recognition protein 1	1	1
	114 / 343	XRCC6	X-ray repair complementing defective repair in Chinese hamster cells 6, Ku70		0.99

New interacting partner	Frequency of CRAPome detection	Gene Name	Description	(+DMSO) SAINT score	(+CPT) SAINT score
	28 / 343	CHD4	chromodomain helicase DNA binding protein 4		0.958
	114 / 343	PRKDC	Protein kinase, DNA-activated, catalytic polypeptide	0.954	0.954
	84 / 343	DDX39A	ATP-dependent RNA helicase DDX39		0.934
	39 / 343	SPT16H	suppressor of Ty 16 homolog (S. cerevisiae)	0.99	0.93
	23 / 343	THOC2	THO complex 2		0.926
	1 / 343	RAD51	RAD51 homolog (RecA homolog, E. coli)	0.986	0.926
	19 / 343	MSH2	mutS homolog 2, colon cancer, nonpolyposis type 1 (E. coli)		0.916
	141 / 343	RPS3A	ribosomal protein S3A	0.942	
	171 / 343	H2AFX	H2A histone family, member X	0.96	
	123 / 343	DDX21	DEAD (Asp-Glu-Ala-Asp) box polypeptide 21	0.996	
	37 / 343	RALY	RNA binding protein, autoantigenic (hnRNP-associated with lethal yellow homolog)	0.998	

Table 4.2: Abbreviated results of all proteins found to be enriched in WRN AP samples.

Table is abbreviated to include only nuclear proteins that were found to interact with SH-WRN when sample was treated with DMSO and CPT, as indicated. These proteins were identified in profiling analysis, and then analyzed by SAINT to identify interacting partners that passed a significance threshold of Max SAINT score >=0.9. Nuclear localization was determined by Gene Ontology filtering. Proteins that are novel and were not previously reported to interact with WRN are identified in column "New ID", and are marked with an *. The protein results were cross-validated using CRAPome to determine overlap with frequently detected proteins in proteomics experiments. The overlap is presented, and marked with #. Full results can be found in Supplementary Tables 1A and 1B (See Appendix B).

Upon determination of dominant functional categories, CompGO was further used to extract lists of proteins that contributed to assignment of significantly represented GO_BP categories. These proteins were used as a guide for further investigation by examining known

protein-protein interactions between them. The proteins within each selected GO_BP category were entered into STRING v9.1 (http://string-db.org, (104) to determine whether they have been previously shown to physically interact. The confidence score of 0.9 (highest confidence) was selected as a filter, and a number of interacting proteins was gradually increased to allow the connections between proteins to appear. Only proteins that were identified in our analysis, even if they did not meet the SAINT score threshold, were kept. The resulting networks show proteins that are identified with SAINT score >0.9 and contribute to annotation to the given category are circled with a dotted line, and are highlighted in yellow in the table legend. The table contains information about the SAINT score in for each identified protein, and number of spectral counts with which it was identified. Interestingly, when the created network for chromatin organization was analyzed by GO_BP with the advanced features of STRING v9.1, all of the proteins in the network except SSRP1 and HIST2H2AB contributed to assignment of GO category “chromosome organization”, and were given a p-value of 3.899E-24. The protein networks generated for functional categories of double-strand break repair, chromatin organization, transcription from RNA polymerase III promoter, transcription from RNA polymerase II promoter, and cell cycle from our identifications are shown in Figures 4.12-4.16, respectively. In Figure 4.13, especially, we noted that many of the proteins that are identified with high confidence in our analysis have not been previously shown to interact among themselves, or to participate in the larger complex. These proteins present a particularly intriguing subset of targets for further analysis, and are discussed in further detail in Chapter 5.

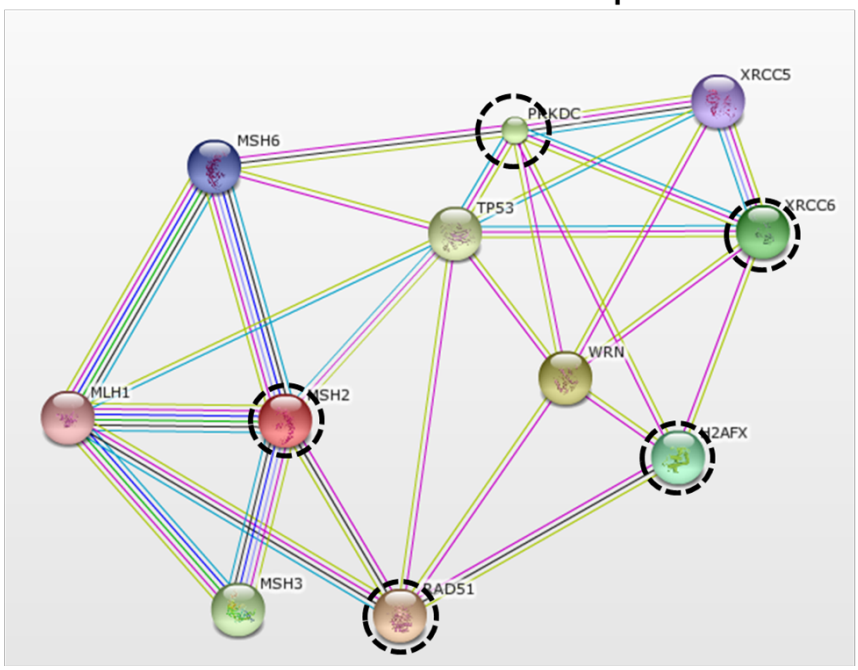

Protein Name	(+CPT) Total spec	(+CPT) SAINT	(+DMSO) Total spec	(+DMSO) SAINT
XRCC6	416	0.99	383	0
PRKDC	342	0.954	406	0.998
RAD51	33	0.926	41	0.998
MSH2	5	0.916	2	0.188
MLH1	2	0.408	\N	\N
MSH6	26	0.348	22	0
TP53	76	0	89	0
XRCC5	374	0	380	0
MSH3	\N	\N	1	0
H2AFX	\N	\N	19	0.906

Figure 4.13: Protein network for proteins annotated to participate in double-strand break repair, as directly reported by STRING.

The number of lines connecting individual nodes (proteins) reflects the lines of evidence that support the interaction. High-stringency criteria were selected in our analysis.

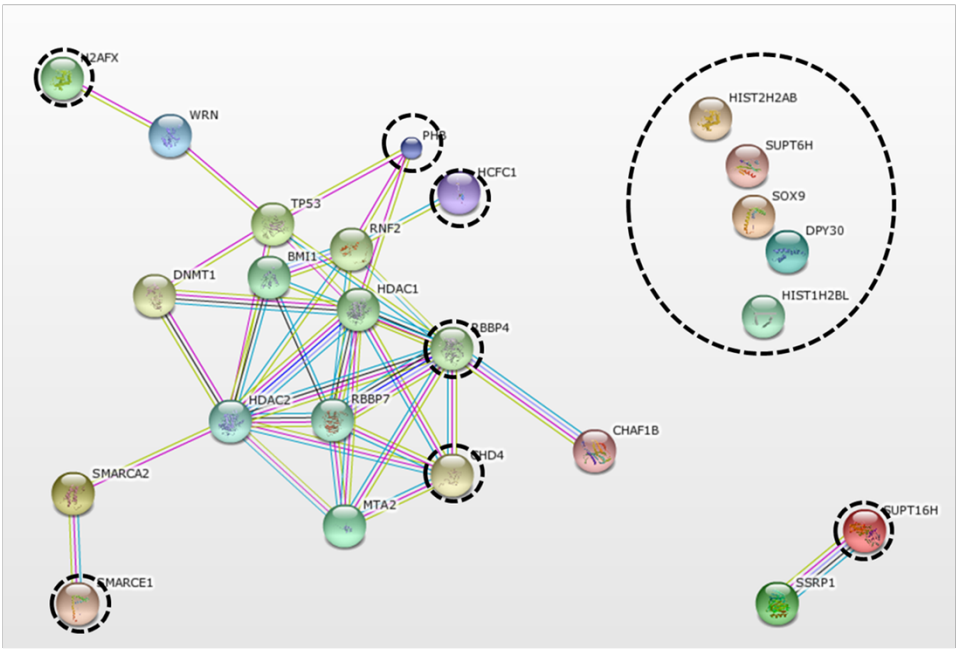

Protein Name	(+CPT) Total spec	(+CPT) SAINT	(+DMSO) Total spec	(+DMSO) SAINT
PHB	35	1	35	0.01
SSRP1	17	1	16	0.998
HCFC1	19	0.998	11	0.972
HIST2H2AB	23	0.998	26	0.182
HIST1H2BL	70	0.996	122	0
SUPT6H	136	0.994	117	0.078
CHD4	40	0.958	28	0
RBBP4	7	0.952	20	0.122
SUPT16H	17	0.93	25	0.986
DPY30	9	0.906	11	0.796
HDAC2	17	0.888	16	0.078
SOX9	7	0.798	11	0.996
CHAF1B	4	0.724	2	0.212
SMARCA2	2	0.41	2	0.19
MTA2	17	0.382	12	0
KDM1A	11	0.206	6	0.024
DNMT1	3	0.176	\N	\N
RBBP7	31	0.158	17	0.012
SMARCE1	9	0.126	15	0.902
HDAC1	5	0	5	0
TP53	76	0	89	0
RNF2	2	0	5	0.942
SIN3A	\N	\N	1	0
H2AFX	\N	\N	19	0.906
BMI1	\N	\N	1	0

Figure 4.14: Protein network for proteins annotated to participate in chromatin remodeling, as directly reported by STRING.

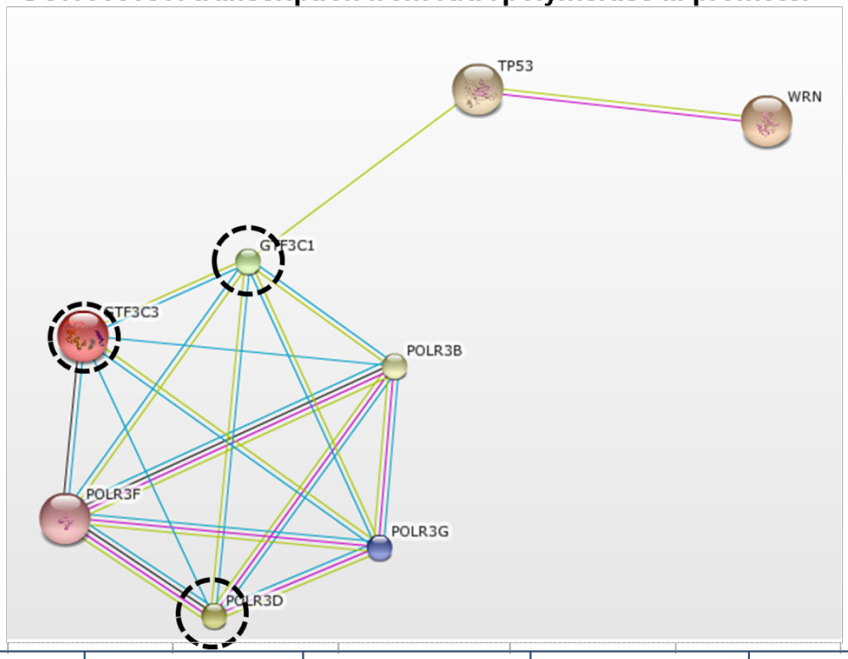

Protein Name	(+CPT) Total spec	(+CPT) SAINT score	(+DMSO) Total spec	(+DMSO) SAINT score
GTF3C3	12	1	6	0.608
POLR3D	13	0.952	10	0.62
GTF3C1	17	0.942	17	0.62
POLR3C	24	0.882	25	0.178
POLR3B	14	0.456	16	0.072
POLR3G	2	0.14	5	0.834
POLR3F	6	0.126	8	0.008
TP53	76	0	89	0

Figure 4.15: Protein network for proteins annotated to participate in transcription from RNA polymerase III promoter, as directly reported by STRING.

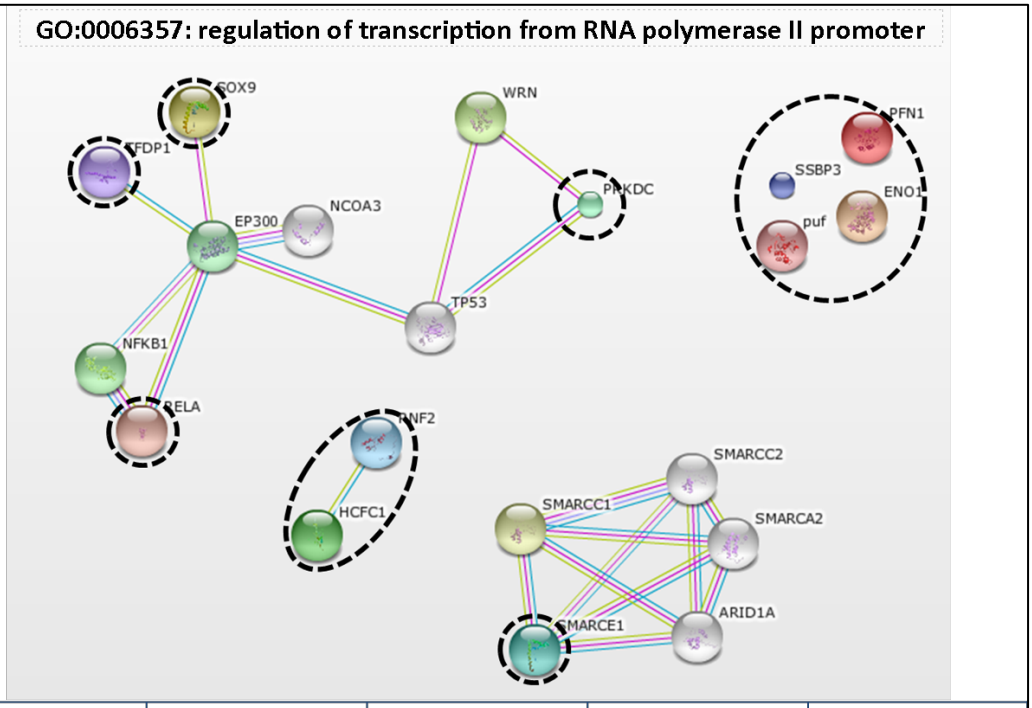

Protein Name	(+CPT) Total spec	(+CPT) SAINT score	(+DMSO) Total spec	(+DMSO) SAINT score
HCFC1	19	0.998	11	0.972
ENO1	27	0.996	28	0.956
PRKDC	342	0.954	406	0.998
SOX9	7	0.798	11	0.996
PFN1	16	0.758	18	0.988
SSBP3	11	0.59	10	0.916
SMARCA2	2	0.41	2	0.19
NFKB1	53	0.262	48	0
TFDP1	2	0.138	7	0.924
SMARCE1	9	0.126	15	0.902
SMARCC2	7	0.002	11	0.022
ARID1A	1	0	2	0
SMARCC1	4	0	7	0
NCOA3	12	0	20	0.004
RNF2	2	0	5	0.942
TP53	76	0	89	0
RELA	40	0	121	1
EP300	\N	\N	1	0
NME2 (puf)	\N	\N	9	0.994

Figure 4.16: Protein network for proteins annotated to participate in regulation of transcription from RNA polymerase II promoter, as directly reported by STRING.

GO:0007049: cell cycle

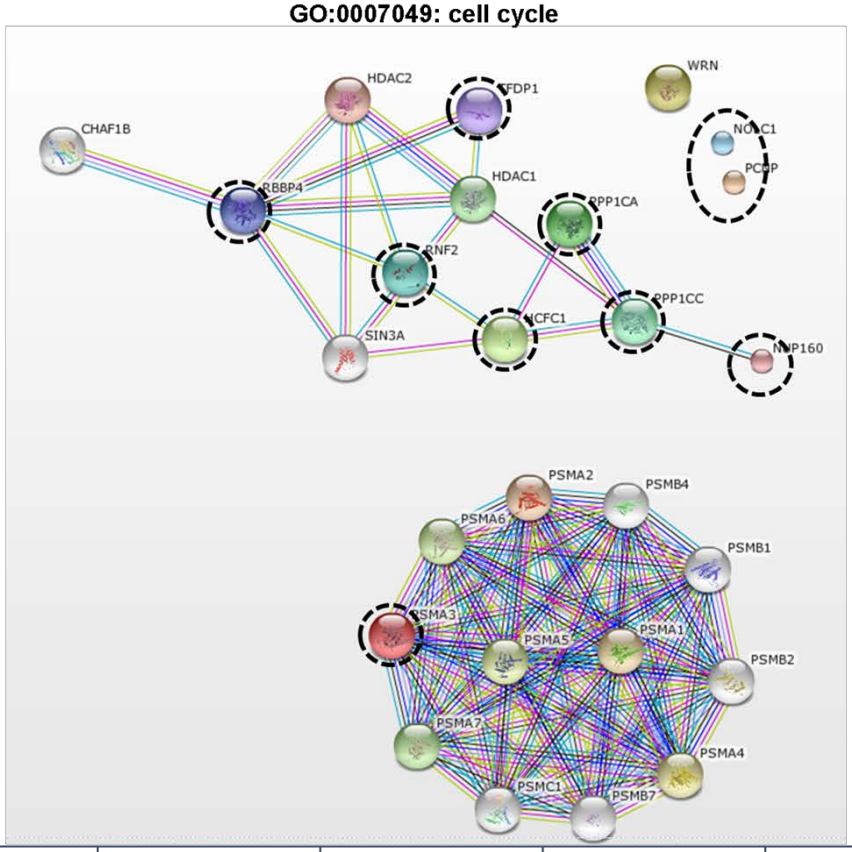

Protein Name	(+CPT) Total spec	(+CPT) SAINT score	(+DMSO) Total spec	(+DMSO) SAINT score
HCFC1	19	0.998	11	0.972
PCNP	28	0.988	19	0.766
RBBP4	7	0.952	20	0.122
NUP160	27	0.948	17	0
PSMA3	6	0.926	4	0.196
HDAC2	17	0.888	16	0.078
PSMA6	4	0.726	3	0.352
CHAF1B	4	0.724	2	0.212
PPP1CA	7	0.686	23	0.952
PSMA4	4	0.636	3	0.372
PSMA1	4	0.544	5	0.69
PSMA2	5	0.456	4	0.038
PSMB4	2	0.362	2	0.332
PSMA5	4	0.344	5	0.68
PSMB1	6	0.326	13	0.796
PSMB2	6	0.206	6	0.336
PSMB7	2	0.198	\N	\N
PSMA7	4	0.18	3	0.05
TFDP1	2	0.138	7	0.924
NOLC1	22	0.078	14	0.952
HDAC1	5	0	5	0
PPP1CC	20	0	61	1
PSMC1	15	0	8	0
RNF2	2	0	5	0.942
SIN3A	\N	\N	1	0

Figure 4.17: Protein network for proteins annotated to participate in cell cycle, as directly reported by STRING.

These protein networks were assembled from proteins that are shown in our identifications, and which have been previously annotated to the category of double-strand break repair. Included tables report on all supporting data from our experiments, including total spectral counts by treatment, and scores reported by the SAINT algorithm. Proteins that were identified with the stringent cutoff of SAINT score ≥0.9 are highlighted in the table are also circled in the network.

Section 4: Discussion

We examined the changes in protein complexes surrounding WRN protein in response to treatment with genotoxic agent CPT using a combination of AP and profiling MS. The experiment incorporated a control protein, which was isolated from isogenic cells using the same protocol as WRN, and the resulting datasets were compared for bait-specific enrichment using SAINT (54). The inclusion of a control protein that localizes to the same compartment is crucial. Nucleus is a compartment packed with proteins and nucleic acids that form extensive complexes, assemblies, and conduct a large number of biological processes in close proximity. The possibility of a transient interaction between two molecules increases substantially, and SAINT confirmed that enrichment score of even verified WRN-interacting proteins can fall below the threshold when proteins in question are of high abundance or amenable to MS detection.

SAINT returned a large number of identified proteins, with a small number being strongly enriched as WRN interactors. Among proteins that were not found to be enriched we found XRCC5 and MRE11, both of which have been shown to interact with WRN (25,119,136,167,168). Both of these proteins were detected with a large number of spectra, but they were also present in the control sample. Unless a cell line transfected with an empty vector is analyzed, it is impossible to know whether nLacZ or the epitope tag specifically interacts with

these proteins, or whether their abundance or favorable chemical properties facilitated detection without bait-specific enrichment. Like in many such analyses, we walk the fine line between specificity and sensitivity. During the AP step we chose the conditions that favor maintaining the integrity of protein complexes by limiting detergent and salt, yet allow us to remove transiently interacting proteins that do not participate in stable complexes during wash steps. During analysis by MS we optimized chromatography conditions to achieve maximum separation of the complex mixture of peptides, and allow identification of individual sequences. Finally, SAINT was used to determine whether spectral abundance for a particular peptide was significantly higher in experimental sample compared to the control, to determine the extent of bait-specific enrichment. The results of our analysis suggest that the stringent score cutoff has resulted in high selectivity of our results.

We investigated whether proteins that were found to be significantly enriched in WRN APs shared known biological functions or participated in specific biological processes using gene ontology (GO) annotation. Michael Riffle and Veronika Glukhova developed a robust new tool, CompGO, which streamlines the comparison by GO categories between samples, and identifies specific points or branches or divergence in GO terms. Importantly, the graphical representation shows a clear relationship between terms, allowing the inquirer to identify minute differences between samples. The categories of interest can be further explored by using the tabular format that includes all p-values for category assignment and the proteins that are included as evidence. The level of detail is adjusted by the operator by tuning the significance level of assignments.

Based on the results of our profiling analysis CompGO identified the nuanced differences in WRN-associated proteins in response to treatment with CPT. Gene ontology categories of

gene expression, chromatin binding, and cell cycle regulation as categories are significantly over-represented after CPT treatment.

Groups of proteins as linked by GO biological process were tested for previously reported interactions by STRING, a tool for exploring known protein networks. The results demonstrate that many of the proteins that were detected in our analysis are known to physically interact and perform biological functions that are related to the DNA damage response. We used the results of this analysis as a guide to validate our initial findings, and to explore the potential involvement of WRN in coordinating a number of protein complexes that are involved in chromatin remodeling, FACT, NuRD, and CAF1, as described in more detail in Chapter 5.

Notes to Chapter 4

Figure 4.6 was generated with the help from Alden Hackmann.

Michael Riffle executed CompGO.

All Supplementary data to Chapter 4 can be found in Appendix B, as noted.

Supplementary tables:

Supplementary Table 1,A: all nuclear proteins with SAINT score ≥0.9 in SH-WRN (+DMSO)

Supplementary Table 1,B: all nuclear proteins with SAINT score ≥0.9 in SH-WRN (+CPT)

Supplementary Figure B1: Full map of pFTSH-WRN plasmid

Supplementary Figure B2: complete GO_CC dendrogram (p-value cutoff 1E-2), as imported from CompGO. Input data is from **Supplementary Table 1A** as sample (1) and **Supplementary Table 1B** as sample (2).

Supplementary Figure B3: complete GO_BP dendrograms (p-value cutoff 1E-5), as imported from CompGO. Input data is from **Supplementary Table 1A** as sample (1) and **Supplementary Table 1B** as sample (2).

Supplementary Figure B4: all data as exported from MSstats on protein association dynamics between WRN and its potential interaction partners

Chapter 5 – Targeted proteomic analysis of WRN-interacting proteins as a function of time after CPT treatment.

Section 1: Introduction

To expand on the validation, and to interrogate further the list of putative WRN interacting proteins we describe in Chapter 4, we used Selected Reaction Monitoring (SRM), as described previously in Chapter 2 and published (170). This MS-based approach has been successfully used in a number of studies for identification of low-abundance proteins in subcellular isolates (171) and whole cell extracts (170). It has the potential to be a rapid, accurate, and quantitative approach. The development of methods can be labor-intensive, although with current advancements in software that aids in identification and refinement of SRM methods (79,172) and workflow approaches (80,170,171), SRM presents an attractive method for validation of a large number of putative interacting proteins for studies such as ours.

While immunoblotting is still the most widely used method of validation, due to its requirements for labor, expense, sometimes limited availability of immunoreagents, and varied sensitivity, most studies present validation of only a small number of putative interacting proteins. We used the results of our profiling study to identify a list of proteins with highest differential association with WRN in response to 1-hour treatment with Camptothecin, and to develop SRM methods for these high-value targets. We attempted to generate methods for nearly all proteins that were reported to us as significantly interacting by SAINT, successfully generated

methods for a large number of those, and then successfully demonstrated the enrichment of these proteins in our AP samples.

To aid in development of some SRM methods we used *in vitro* translation (IVT) to generate a number of nuclear proteins, and to then verify their presence in our AP samples with high accuracy as applied previously (171). Our methods are freely available via Panorama viewer (link provided in Notes to this Chapter), and are expected to be of great value for other researchers.

Using these methods we performed two large-scale targeted experiments. First, we screened independently prepared biological samples to validate our findings in profiling analysis, and to gain quantitative measure of differential protein association with WRN in response to 1-hour CPT treatment. These samples were prepared in biological triplicate, and then were run in analytical replicates to yield a very high quality dataset.

In the second experiment, we expanded on the time course of treatment, and asked whether the dynamics of association of these proteins with WRN change as a function of drug treatment length. We prepared an independent biological replicate, which included treatment with control DMSO, and CPT treatment at 1h, 6h, and 12h. We hypothesized that the analyte proteins could be clustered into distinct groups based on their time-dependent association with WRN. We also hypothesized that these clusters would reflect known patterns of recruitment of DDR participants to DNA lesions (173). We used clustering analysis to serve as a guide to view binding proteins not just as individual entities, but as concerted participants in distinct transactions within DNA damage repair, and serve as guide for stages in DDR at which WRN exerts its function.

Section 2: Experimental

Method development for SRM-based validation.

In vitro protein translation was used to generate purified protein standards for selected proteins. General protocol adapted from Stergachis et al (171), with the exception of updated in vitro translation kit, where we used the 1-Step Human Coupled IVT Kit (product 88882, Thermo Scientific).

To measure retention time reproducibility and to infer peak location between replicates, retention time standards were added. iRT-Kit solution was added at 1:100 dilution to all IVT standard proteins (Biognosys, Schlieren, Switzerland).

For full list of analyte proteins see Results. Sequences of proteins that were chosen for validation were extracted from UniProt. Sequences were imported into Skyline (available at skyline.maccosslab.org)(79). Proteins of interest were screened according to our method development pipeline as described in detail elsewhere (80,170).

Data Acquisition via LC-SRM.

Columns were prepared as described in previous section, and packed with 17 cm Jupiter Proteo reversed-phase chromatography material (Phenomonex, Torrance, CA). The peptides were trapped onto a 2.5 cm trap of ReproSil-Pur C18 AQ, 3 µm particle size (Dr. Maisch GmbH, Germany). Nanoflow liquid chromatography was performed using an Eksigent nanoLC-1D system (Dublin, CA). Samples were injected into a 5 μL loop using an autosampler, and washed directly onto the column. Solvents A and B for gradient elutions were water/acetonitrile (95%/5% v/v), and water/acetonitrile (20%/80% v/v), respectively. Both contained 0.1% formic acid. Solvent B was increased from 2% to 40% acetonitrile over 30 min, followed by an increase

to 60% over the subsequent 5 min and maintained for 5 min; a step to 95% for 1 min and maintained for 8 minutes; then a return to Solvent B at 2% for 21 min. The total gradient time was 70 min at a flow rate of 250 nL/min.

Eluting peptides were ionized via electrospray with the emitter held at 2.4 kV using a homebuilt ESI source, and directed into a Thermo Scientific TSQ Quantum Ultra Triple Quadrupole mass spectrometer. Transitions developed in Skyline were used to monitor precursor-fragment ion pairs defined in the corresponding section. Resolution in Q1 and Q3 was 0.7 in all experiments. Skyline was used to calculate peak areas by integrating total ion chromatograms. In order to normalize signal intensity, total peak areas for individual peptides from each target protein were divided by total peak areas for each internal control peptide. Differences in relative protein abundance were calculated by dividing the normalized peak areas of experimental samples by the analogous peak areas of control samples in the same experiment.

Data analysis using MSstats.

The MSstats software package (v. 2.1.3) (http://www.stat.purdue.edu/~ovitek/Software.html) (174) was used to analyze the results of the two large-scale experiments described in the introduction. The data from the first experiment comparing a control treatment DMSO to CPT treatment for 1 hour was processed to determine which proteins had significant changes in WRN-association in response to the CPT treatment. The data from the second experiment comparing a control treatment DMSO to CPT treatment at multiple time points (1h, 6h, 12h) was analyzed to visualize the changes in WRN-association relative to the control treatment DMSO of each protein as well as to determine which proteins/time-points had significant changes in WRN-association.

Experiment 1: DMSO vs. CPT treatment for 1 hour

Prior to processing the data in MSStats, the transitions measured were refined to only contain transitions that were measured for a given peptide in every analysis. This resulted in the removal of the transitions y7 and y5 (singly charged) for peptide VTLNTLQAWSK++ of CAF1B. Additionally, all of the normalized intensity values were multiplied by 10,000 to make sure that no intensities had a value below 1 as MSStats would not process values below 1 correctly (personal communication: Meena Choi). Certain proteins had only 2 biological replicates in the CPT1 treatment: BLM, NUCL, TRIM28, and H2AX. The data were analyzed using no normalization in MSStats (because normalization was already performed in Skyline). The scope of biological replication and technical replication were set to "restricted", and "expanded" respectively. Interference was not included as a parameter in the model as most transitions did not contain interference because they were manually refined. Transitions were not assumed to have constant variance.

Experiment 2: DMSO vs. CPT extended time course

MSStats was run by using two methods to handle changes in the peptides used to measure proteins throughout the course of the time-course experiment. One was using the default setting "noInteraction" which assumes that the peptides demonstrate no interference across runs. The other was to impute the missing data with the average minimum intensity across runs. Both methods returned similar results. The results from the "noInteraction" method are presented. Certain proteins were not measured at the 1 hour time point: BLM, H2AX, NUCL, and TRIM28. All other MSStats parameters were the same as in Experiment 1.

Full information on running these methods, including R scripts can be found in the supplement.

Section 3: Results

The scheme in Figure 5.1 shows that, again, isolated protein complexes containing the bait protein SH-WRN and its bound milieu, were subjected to standard proteomic preparation (as described in Figure 1.3) and subsequent interrogation by SRM. The relative quantitation of peptide signal derived from DMSO- and CPT-treated sample was analyzed using MSstats (174). Furthermore, an expanded analysis of samples treated with control DMSO and samples treated with CPT at 1, 6, and 12-hour time points yielded a high-quality data set that was visualized using a heatmap. Some interactions were further confirmed by Western blotting.

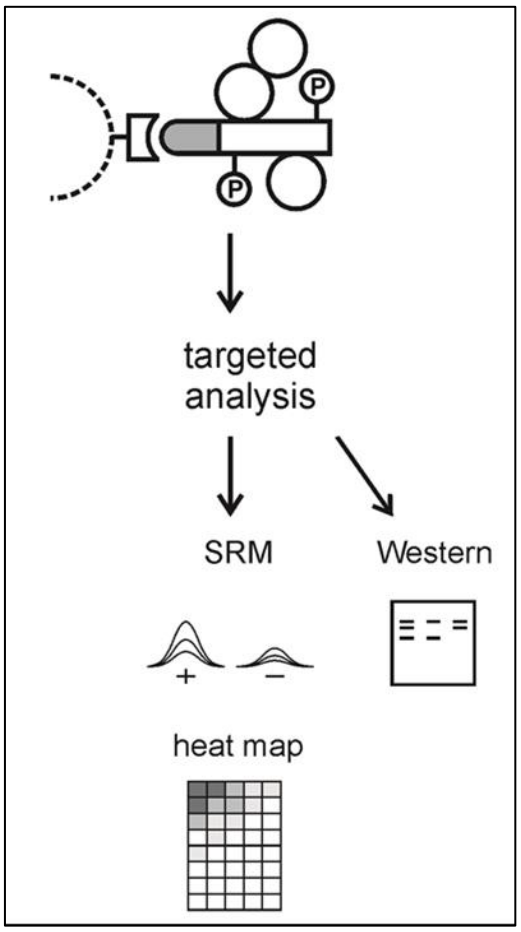

Figure 5.1: Isolation of the protein complex and subsequent steps in targeted analysis: validation of previously proposed interacting proteins, and targeted discovery of new interacting partners.

Table 5.1 lists proteins in tabular form, which we initially attempted to detect using SRM. These proteins were selected as targets for SRM based on initial results from profiling MS. As described previously (80,170), development of methods requires intensive refining and screening of many peptides. Due to constraints of our experiment and the low cellular abundance of many proteins, method development was initially carried out on whole cell extracts, followed by verification on AP samples. Scarcity of sample was the biggest factor preventing more rigorous method development.

In isolated cases, *in vitro* translation (IVT) was performed to generate protein standard with available cDNA sequences. As summarized in Figure 5.2, a number of proteins were successfully detected following IVT.

ATM	EPN1	HNRPC	MRE11	PHB	RBP56	TFDP1
AURKA	EXO1	HNRPR	MSH2	POLD1	RPA1	THOC2
BLM	F175B	HS74L	MTA1	POLD2	RGPA1	TOP1
CHAP1	FEN1	IMA4	MTA2	PP1RA	RIR2	TPIS
CHD3	FUBP1	KCMF1	NBN	PPIA	ROA1	TSR1
CHD4	FUBP2	KPYM	NFKBIE	PRKDC	RPA4	UBR4
CPSF7	H2A2A	LSM12	NOTC2	PSA3	RPB11	WRN
DDX3Y	H2A2B	MATR3	NU160	PTRF	RPC4	WRNIP1
DEK	H2AX	MBB1A	P53	PUF60	RPL3	XRCC3
DMRT3	H2B1L	MBD3	PARP1	RAD21	S10A8	XRCC5
DPY30	H2B2C	MDC1	PCBP2	Rad51	SKIV2	XRCC6
DX39A	HCFC1	MDN1	PCNA	RAD52	SMCE1	YBOX1
EDC4	HDAC1	MED4	PCNP	RALY	SP16H	ZCHC8
ENOA	HDAC2	MEIS1	PGAM2	RBBP4	TFAM	ZN326

Table 5.1: List of all proteins for which SRM methods were initially attempted. Orange shaded entries represent proteins that were successfully analyzed with SRM.

Methods were verified by repeated rounds of analysis using protein mixtures of different concentrations and isolation. Association with WRN was tested by normalization against the sum of peak areas from two peptides from WRN, **C**TETWSLNSLVK and LLSAVDILGEK, and one peptide from affinity tag SH, sequence AADITSLYK.

Results of SRM analyses are summarized in Figure 5.2. We have developed methods and determined change in association with bait WRN for a large number of previously proposed interacting proteins (25), and additionally detected a number of proteins that have not been previously reported (14). All RAW data and original Skyline files are available on Panorama .

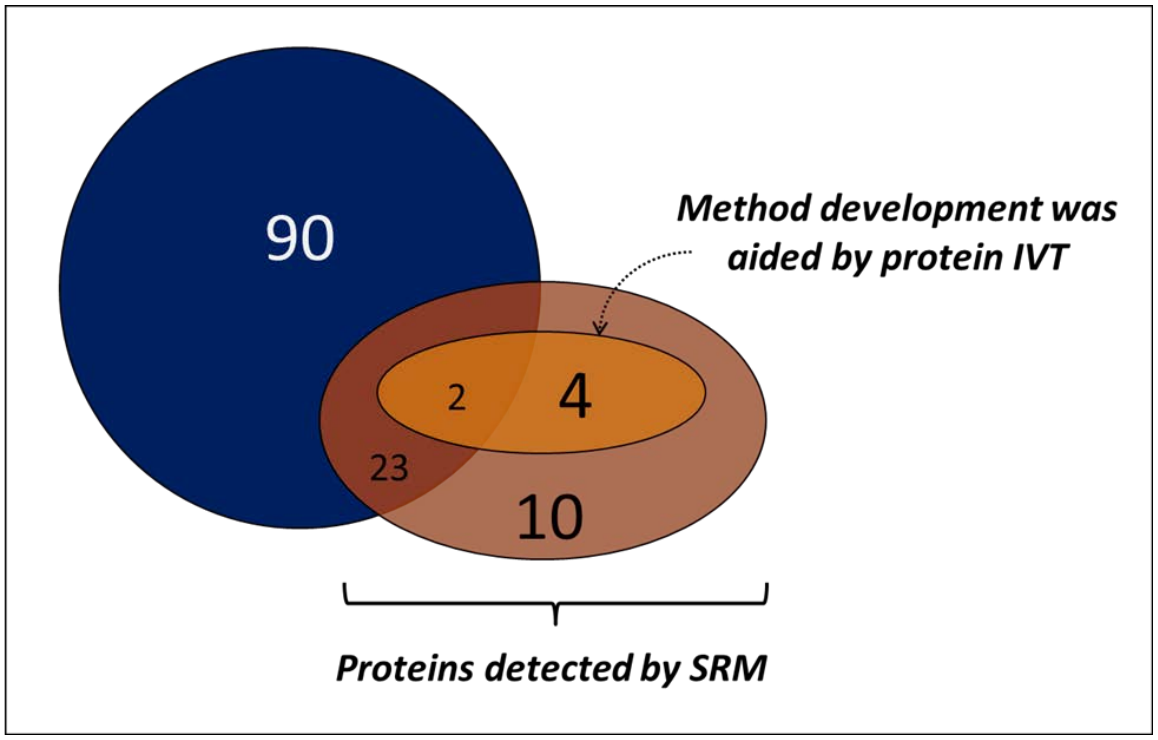

Figure 5.2: The extent of overlap in identification of WRN-associated proteins between our study and previous identifications. Previously identified proteins are shown in blue circle, while orange oval shows the number of proteins monitored in our analysis. Light-orange oval shows the proportion that was monitored using high-quality methods developed using *in vitro* protein translation.

Methods for 39 potential interacting proteins, as well as WRN and the affinity tag were developed in the course of this study. *In vitro* protein translation was used to rapidly generate material for high-confidence methods, where cDNA was available.

For quantitative comparison of proteins between different samples we used MSstats, a tool developed to analyze MS data in SRM applications such as ours. As described in more detail in Experimental section, MSstats combines data from peptides into proteins, takes into account biological and analytical replicates, and calculates p-value to determine whether run-to-run reproducibility accounted for the observed difference between treated and untreated samples. The significance analysis reflects the level of reproducibility in our study across three biological replicates, and summarizes our data. The assigned p-values are not used to make generalized statements about underlying reality, but are used to qualify the reproducibility in our experiments

based on a predefined null hypothesis.

Figure 5.3 demonstrates that of the 39 proteins analyzed by SRM in control vs. CPT-treated sample, two proteins showed no significant change, three proteins showed significant decrease, and 34 proteins showed a significant increase in association with WRN after treatment with CPT for 1 hour. Exact p-values were not calculated below 8.7E-19.

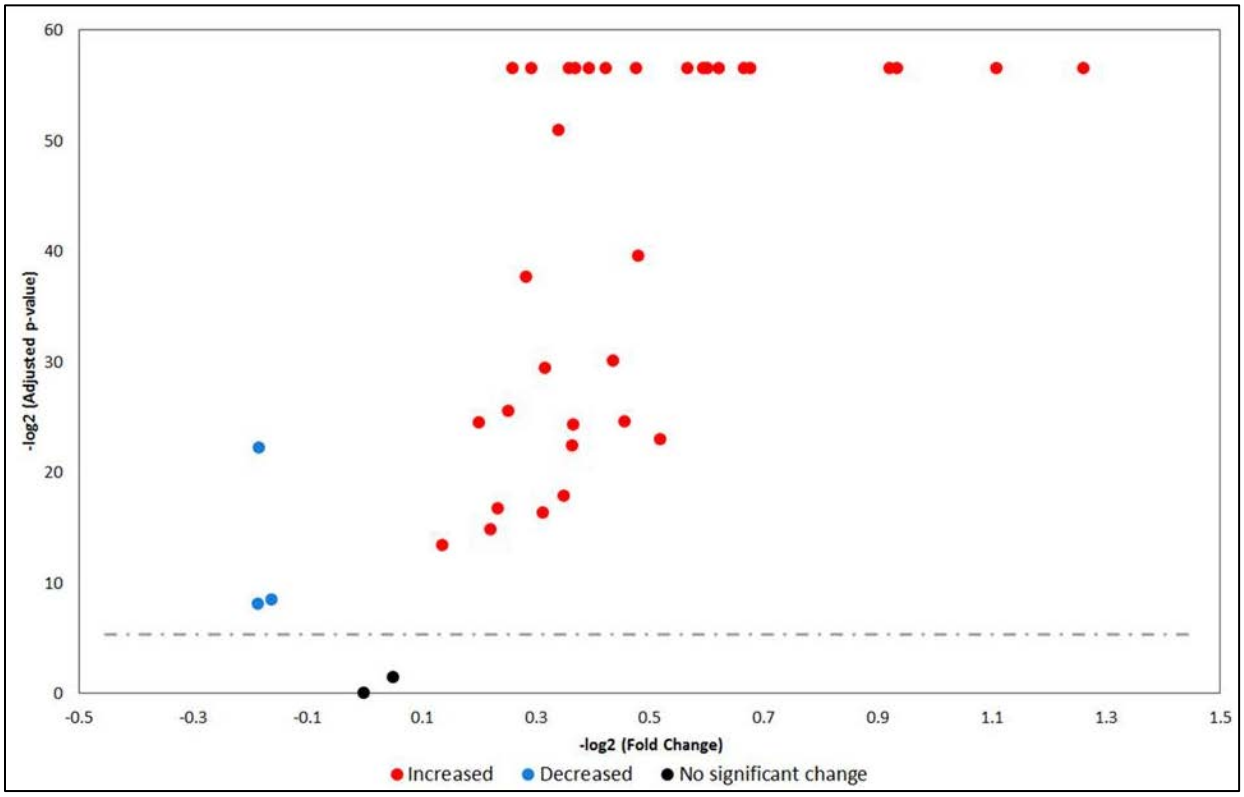

Figure 5.3: The volcano plot summarizing the changes in association of WRN with a number of its putative interacting partners in response to 1-hour treatment with CPT. Dashed line delineates p-value cutoff of 0.05.

Figure 5.4 explores in more detail the proteins that were found to be significantly changed in association with the WRN bait in response to drug treatment. We show that proteins range widely in their association, and add functional annotation based on GO. Interestingly, this

study showed that TOP1 is significantly decreased in association with WRN immediately following CPT treatment, which may be due to sequestration of this protein to DNA, and increasing its availability for protein-protein interactions. Proteins NBN and MRE11 are shown to increase very slightly in association with WRN immediately following CPT treatment (log_2 fold change 0.221 and 0.234, respectively), but this increase appears to be concerted, as expected for two proteins that act in a known complex. Same parallel trend is shown in increased association of XRCC5 and XRCC6 (log_2 fold change 0.316 and 0.259, respectively).

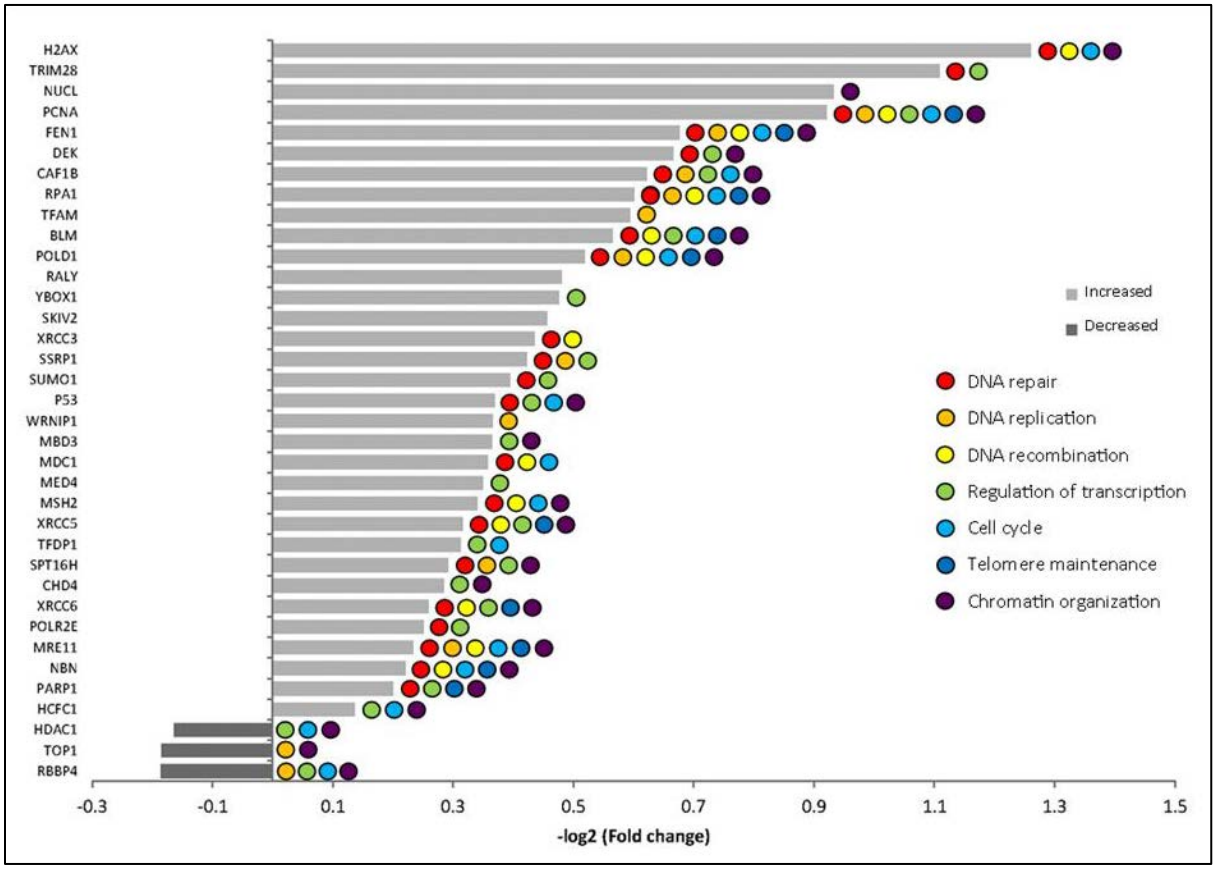

Figure 5.4: Bar graph expands on the proteins whose association with WRN was found to be significantly changed in response to CPT treatment in Fig 5.3.

The figure demonstrates the relative fold change in association with WRN, lists protein names along the y-axis, and identifies how the proteins were functionally annotated by gene ontology.

To look at trend in association rather than a snapshot of an isolated condition, we extended the time course of drug treatment to include CPT exposure for 6 hours and 12 hours in addition to the previously tested 1 hour time point. Peak areas for all measured peptides were compared to the control DMSO. For this analysis, an independent sample was prepared, and analyzed as previously described. For every measured peptide the peak area was normalized to the sum of two peptides from WRN and one peptide from the affinity tag SH. MSstats was used to combine signal intensity values for all peptides assigned to proteins, and to calculate fold change between each drug treatment time point and control treatment with DMSO. All fold change calculations are reported in Appendix C.

Proteins that showed significant change over control were plotted using Matrix2png (175). Standardization of the dataset was performed to approximate a Gaussian distribution with zero mean and unit variance. The data was transformed using a standard algorithm to center it by removing the mean value of each feature, then scaling it by dividing non-constant features by their standard deviation. The resulting heatmap was clustered by general trend of association, and presented in Figure 5.5.

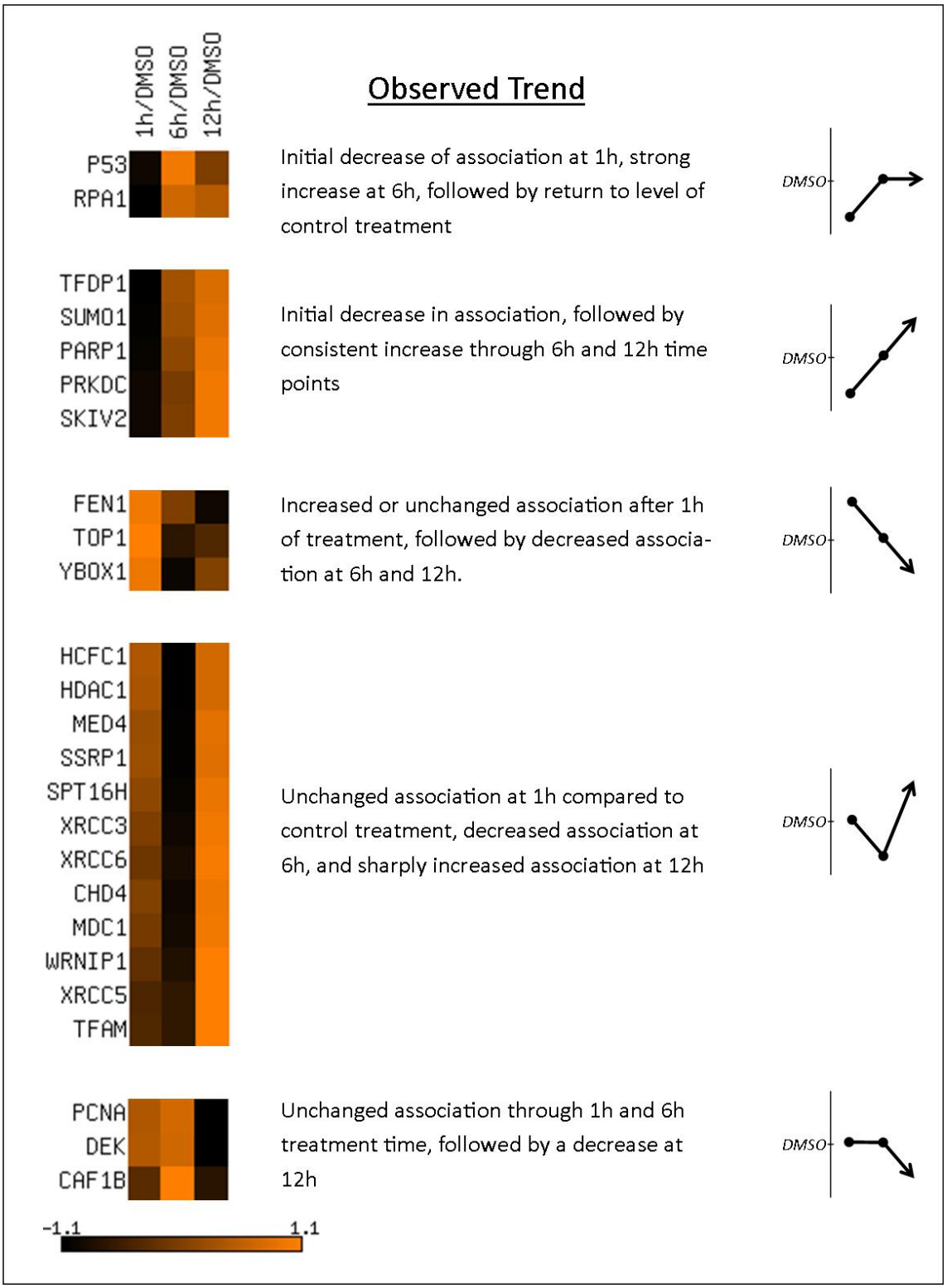

Figure 5.5: Fold changes, as calculated by MSstats for all WRN proteins that showed significant change in association with WRN at every measured time point. Trend in protein association relative to control as well as across the time points was considered when clustering.

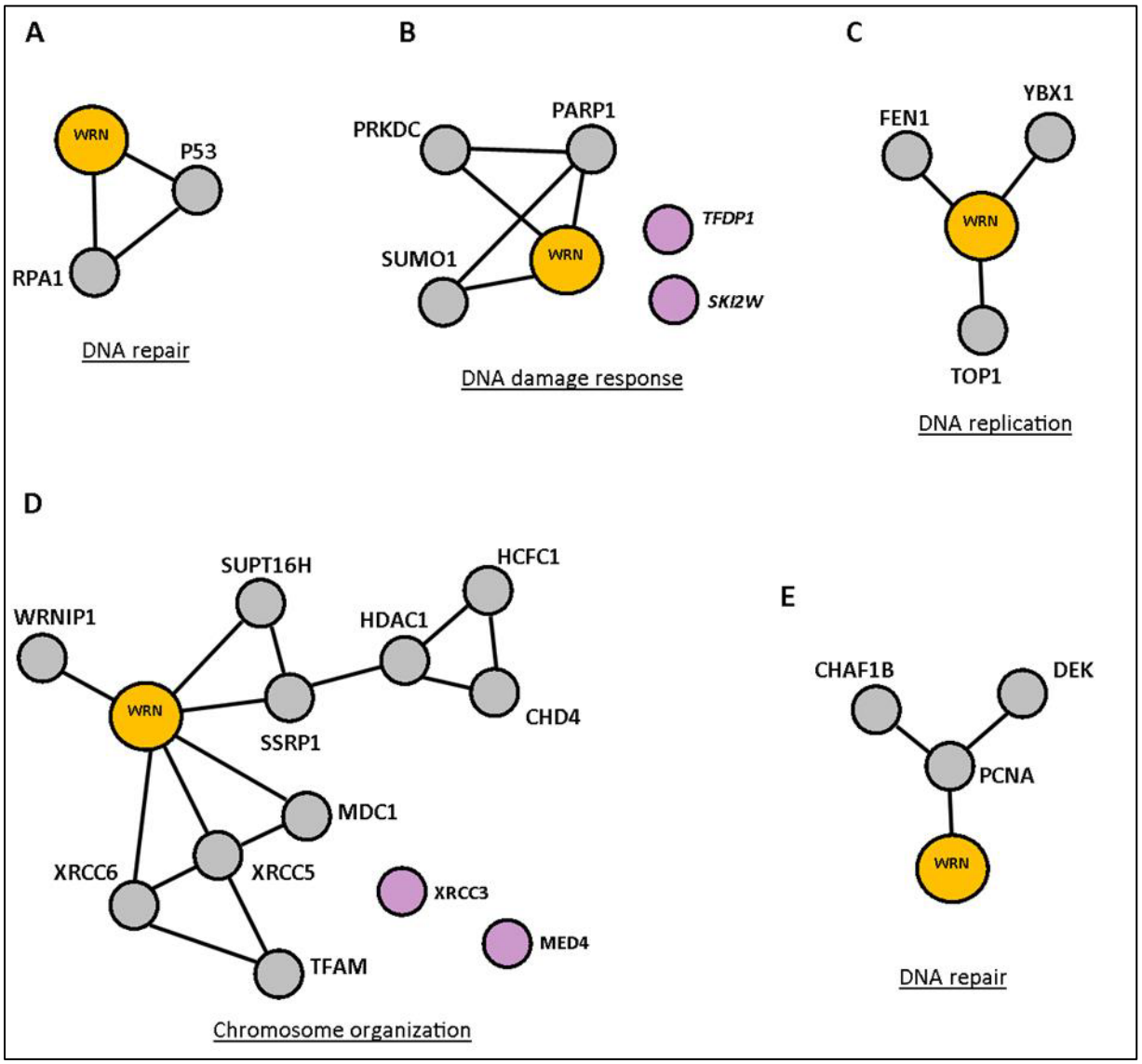

Figure 5.6: Proteins were clustered based on trend in association with WRN across three time points of treatment with CPT, 1h, 6h, and 12h, visualized using STRING, and redrawn for emphasis.

STRING as used to determine whether the proteins that cluster together based on their association, are known to interact physically among themselves. This figure demonstrates that proteins that were shown to follow similar trend are also independently verified to interact and show a very high degree of connectivity, suggesting that their association and dissociation from WRN could occur as a complex. STRING was further used to determine whether individual clusters show enrichment by GO, and predominant categories are listed. WRN is shaded in orange, all interacting proteins are shown in gray, and proteins that are not listed as interacting are shown in purple.

A closer look at subgroups within the list of proteins reveals that some of the proteins that are known to form complexes exhibit similar dynamics when binding to WRN. Figure 5.7 an in-depth analysis of previously reported WRN interaction partners, the Ku heterodimer proteins Ku70 (XRCC6) and Ku86 (also Ku80, XRCC5). Data was processed by Skyline and MSstats to first normalize peak areas for all measured peptides to the sum of three control peptides (WRN and SH-tag), then combine all normalized peptide peak areas into a single value for each protein, and then to compare each value to the normalized peak area from DMSO-treated control. Here we report the three ratios corresponding to fold change in $\log_2$ scale of protein association with WRN over the control at each treatment time point.

Analysis of the Ku complex shows that both proteins exhibit similar, but somewhat divergent, binding patterns (Figure 5.7). Although we detected both proteins with SRM, only XRCC6 was shown to be enriched in WRN AP-MS samples in profiling analysis. This may be a reflection of our study design, or a suggestion that WRN preferentially binds the 70 kDa subunit, which then recruits the 86 kDa subunit to the complex.

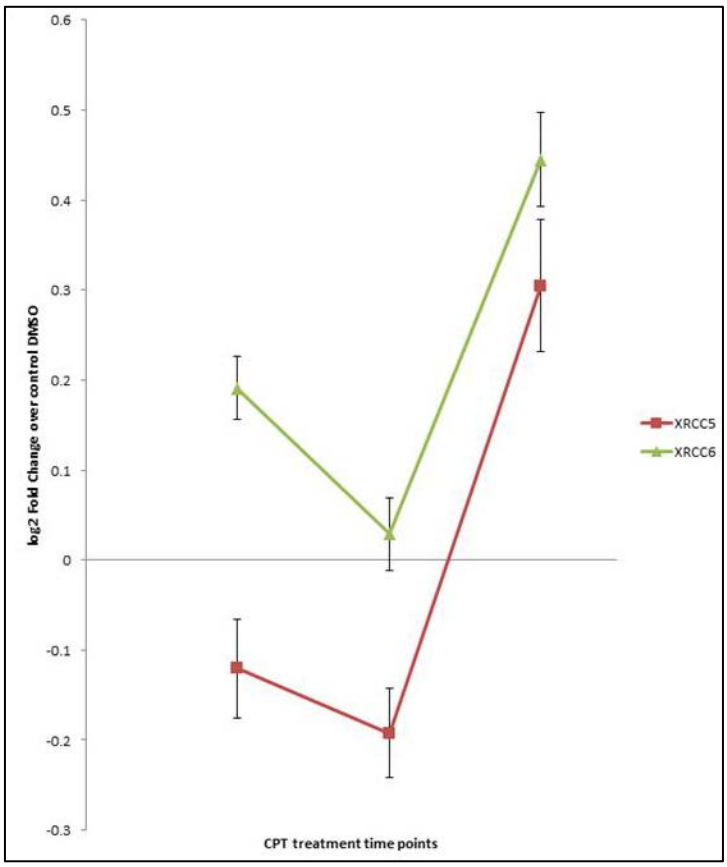

Figure 5.7: Members of the Ku heterodimer XRCC5 and XRCC6 exhibit similar binding dynamics to WRN as a function of treatment time point.

We then analyzed the pattern of association for members of three chromatin remodeling complexes detected in our analysis: NuRD, CAF1 and FACT. Figure 5.8 shows how four of five of the proteins that make up human NuRD (Nucleosome Remodeling and Deacetylation) complex exhibit parallel binding patterns to WRN. The figure shows that proteins, CHD4, MTA2, RBBP4, and HDAC1 exhibit very similar association dynamics, while MBD3 binding follows a very different pattern. The line is dashed for emphasis. The data is supported by monitoring of two high-quality peptides corresponding uniquely to MBD3, and shows that MBD increases in association with WRN at 1hour and 6 hour treatment time points, while the rest of

the complex appears to decrease in association at 6 h; however the measurement of MBD3 at 12 hour treatment time point was not determined to be significantly different from the control, with p-value 0.947, failing to reject the null hypothesis.

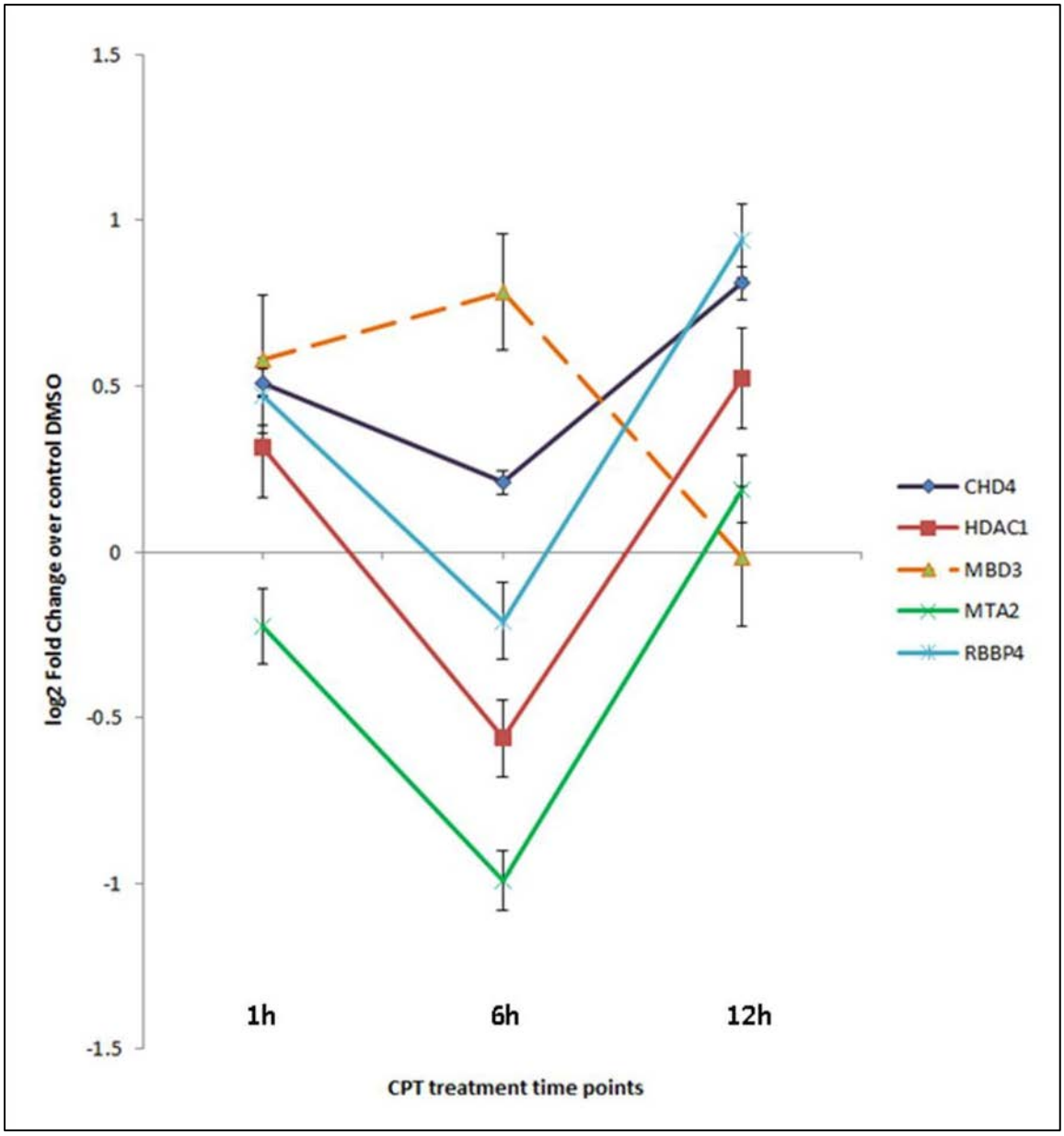

Figure 5.8: Four of five members of the NuRD complex exhibit similar binding dynamics to WRN as a function of treatment time point. Dashed line is used for emphasis of the divergent pattern.

Western blot data confirms the interaction between WRN, CHD4, and RBBP4 (Figure 5.9), and also exemplifies the limitations of western blotting for quantitative comparison of protein abundance. It is impossible to determine differences between bands in different samples due to restricted dynamic range, a problem that is easily addressed with SRM.

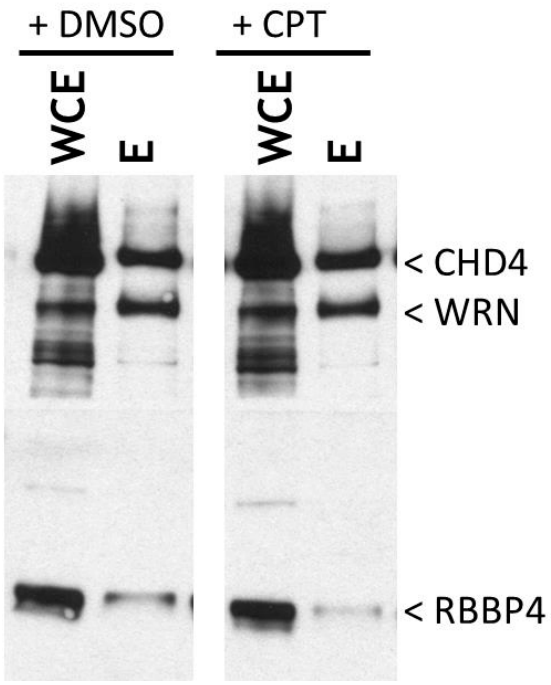

Figure 5.9: Western blot confirms interaction between WRN, CHD4 and RBBP4 in anti-SH-WRN affinity pulldown. Whole cell extract (WCE) and eluate (E) from samples treated with DMSO and CPT are shown.

Figure 5.10 compares the patterns of association of proteins CHD4, MDC1 and PARP1. CHD4 and MDC1 have been previously shown to act early in DDR, in parallel (176–179), and they show strikingly similar pattern of association with WRN as a function of treatment time. Protein PARP1 is an obligatory modifier of CHD4, and has also been shown to interact with WRN (119,136–138). The traces demonstrate that these proteins do not associate with WRN as a single complex.

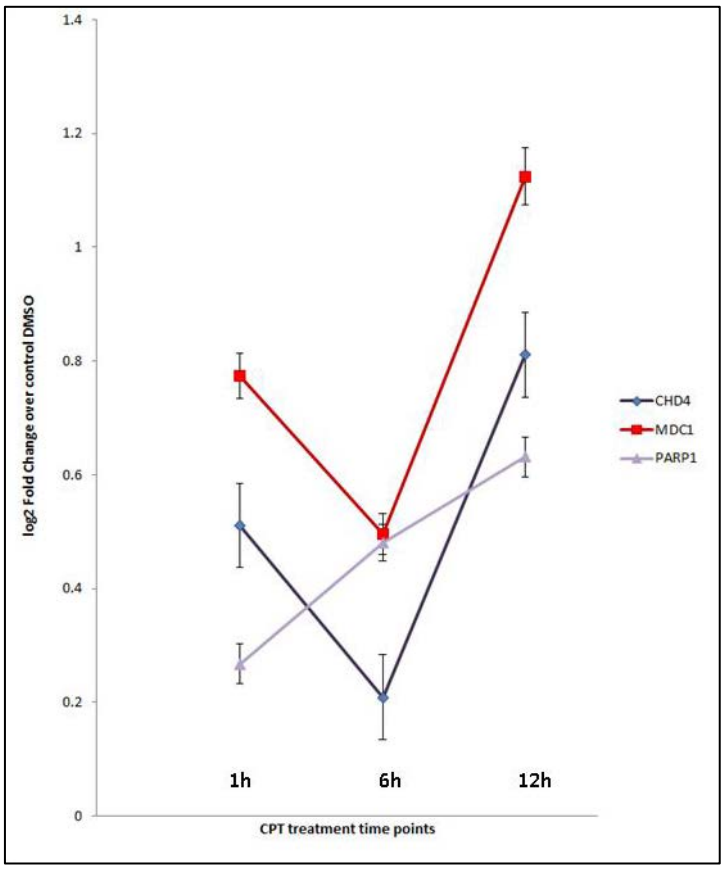

Figure 5.10: Catalytic core of the NuRD complex protein CHD4 and protein MDC1 exhibit nearly identical binding pattern to WRN.

We analyzed the association dynamics between WRN and two of the three members of the CAF1 complex, proteins CHAF1B (also CAF1B) and RBBP4. These proteins show different patterns of association, as demonstrated in Figure 5.11. This is particularly interesting because protein RBBP4 has been detected as an interaction partner of WRN, while also potentially interacting with members of the CAF1 and the NuRD complex. Its pattern of association agrees with patterns of almost all assayed members of the NuRD complex (Figure 5.8), suggesting perhaps that it forms preferential associations with some complexes and not others in the context

of WRN interactome. We further confirmed the interaction between WRN and CHAF1B by Western blot (Figure 5.12).

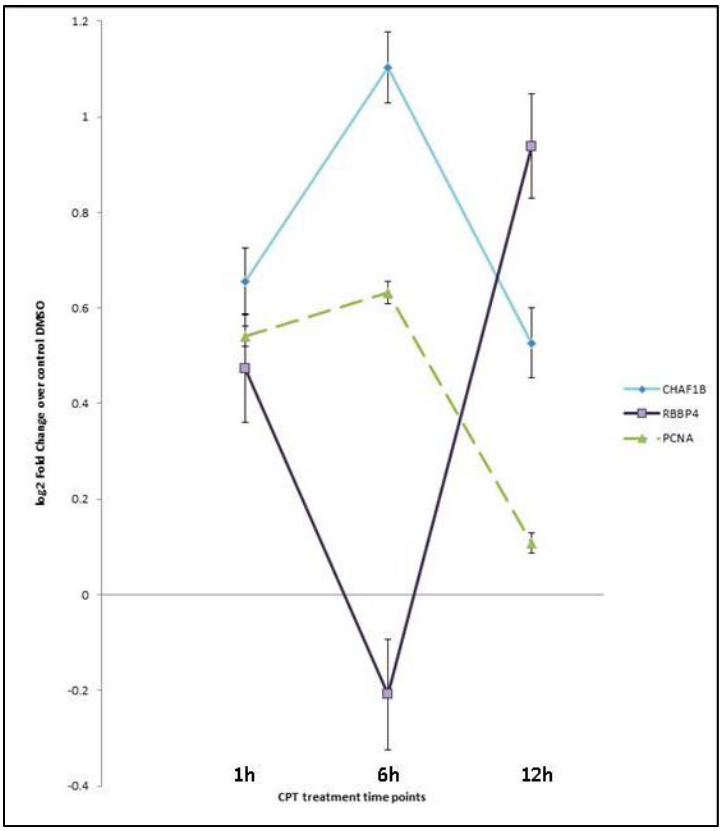

Figure 5.11: Members of the CAF1 complex CAF1B and RBBP4 exhibit divergent binding dynamics to WRN as a function of treatment time point, while functional interacting protein PCNA shows similar binding dynamics to CHAF1B. Dashed line is used for emphasis.

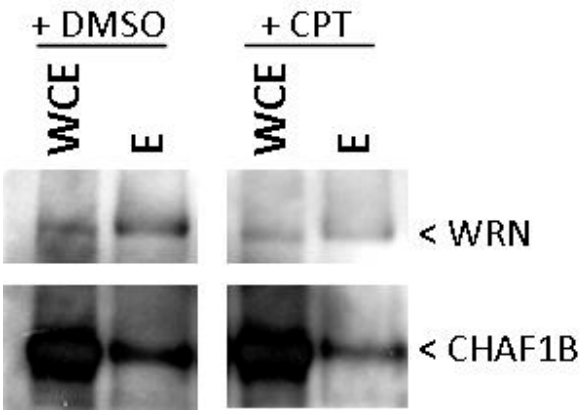

Figure 5.12: Western blot confirms interaction between WRN and CHAF1B in anti-SH-WRN affinity pulldown. Whole cell extract (WCE) and eluate (E) from samples treated with DMSO and CPT are shown.

Members of the FACT complex SSRP1 and SPT16H (also SUPT16 and SUPT16H) have been previously reported to interact with WRN, and we present the patterns of their association in Figure 5.13. These proteins have been very amenable to detection by MS, as demonstrated by both, results of the profiling analysis, and the SRM study. Despite confident identification and the prediction that these two proteins would show concerted behavior, figure 5.13 demonstrates that their association pattern differs in the context of interaction with WRN.

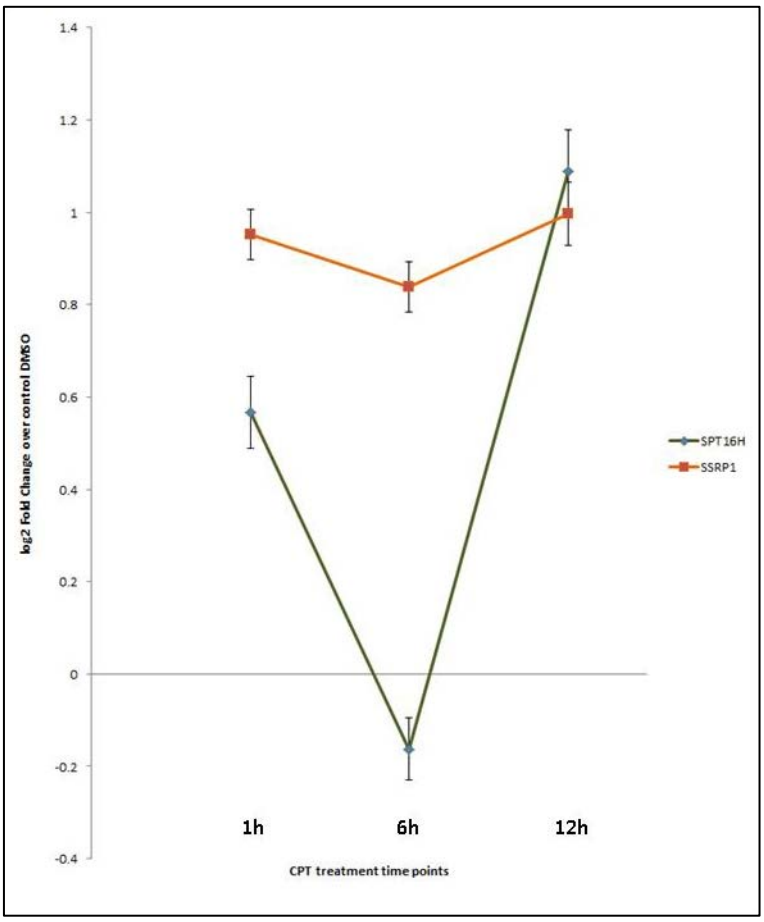

Figure 5.13: Members of the FACT complex SSRP1 and SPT16H exhibit divergent binding dynamics to WRN as a function of treatment time point.

Section 4: Discussion

Validation of protein-protein interaction studies is necessary as many sources of nonspecific interactions exist in AP experiments. For example, the resin of the beads and the epitope tag are common sources of false positive identification of interaction (180). To control for this nonspecific interactions, in parallel with anti-WRN APs, we performed analogous APs with the nuclear-localized control protein LacZ (nLacZ), thus controlling for nonspecific binding to resin and beads, as well as “sticky”, high-abundance proteins in the same subcellular

compartment. The MS examination was followed up with SAINT, which calculates a probability of a true interaction based on a probability distribution model. This approach carries a small probability of false positive, and a larger probability of false negative assignment of interactions (48), favoring specificity over sensitivity. Therefore, for follow-up studies, we partially relaxed the constraints of SAINT score when demonstrating the overlap between our findings and previously reported protein-protein interaction by functional cluster, as described in Chapter 4, and shown in Figures 4.12-4.16. Although assignment of the GO_BP category was made based on the most confidently identified and enriched proteins, other proteins identified in our analysis, but not confined to the SAINT score threshold, were included in protein networks. Initial restriction of the pool of potential interacting partners allowed us to minimize the false discovery rate and avoiding follow-up experiments on nonspecific interactors, while carrying the cost of missing out on true identifications. Subsequent relaxation of the constraints allowed us to focus on a limited number of interactors that did not meet the SAINT threshold despite having been previously suggested to physically associate with other identified interactors.

Examples of proteins that did not meet the initial SAINT threshold, but were identified in downstream validation studies include p53, MDC1, CHAF1B, DEK, YBX1, and XRCC5.

The targeted approach has allowed us to restrict the scope of our study and to selectively interrogate the differential association of WRN with a relatively few interacting proteins. The main challenges of this approach have included extensive method development, large-scale sample generation to measure all proteins, and the time requirement for running many replicate experiments. In turn, the successful method development has allowed us to rapidly screen a very large number of samples at cost of only the instrument running time, to enable multiplexing, and thus generate a large enough dataset of replicate experiments to use statistical approaches to

ascertain our findings. The focused analysis of a large set of WRN-interacting proteins has yielded quantitative information about changes in their association as a function of drug treatment at a number of time points.

Screening for 3 internal control peptides alongside experimental target proteins in every analysis allowed normalization of the signal across many replicates, and calculation of changes in relative association between the bait protein and its putative binding partners. Running each screen separately while normalizing against common standards has negated the need for labeling, and has enabled the comparison of multiple states. The power of this approach is reflected in the ability to track protein association as a function of time point in drug treatment. The results show that in our first study on short-term CPT treatment (1 hr), 34 of 39 of analyzed proteins increase in association with WRN in response to treatment, and 3 of the 39 decrease. We tested three independent biological replicates to ascertain that the differences are due to the biology, regardless of preparation. Although the magnitude of change detected in this method is small, the p-values associated with the changes in protein association warrant a second look at the data, and qualify our findings as significant in guiding future, more targeted research.

The results show that our targeted proteins formed clusters based on their similar patterns in association with WRN as a function of CPT treatment time point. Standardization of rows allowed us to emphasize similarities in trends between proteins. For example, members of the FACT (Facilitates Chromatin Transcription) complex SPT16H and SSRP1 are known to interact among themselves, and with WRN. Our first analysis of 1 hour treatment with CPT showed that these proteins increased in association with WRN to different extent ($\log_2$ fold change 0.292 for SPT16H and 0.422 for SSRP1). However, the trend analysis showed that they in fact exhibited a very similar pattern in association after treatment, and clustered in the same group.

Only proteins that showed significant difference in association with WRN at any time point over DMSO were plotted on the heat map. Therefore, if there was no significant change between any time point and control, that protein was omitted. This summary view was useful for assessing the general patterns, but a closer inspection of individual complexes revealed that even members of the same complex do not always bind to the same bait in concert.

The results in Figures 5.7-5.10 illustrate the differences and similarities in binding patterns of members of previously reported protein complexes. The Ku heterodimer, which consists of two polypeptides Ku70 (XRCC6) and Ku86 (also Ku80, XRCC5), binds to the ends of the DNA in the event of a double-strand break, and is required for the non-homologous end joining (NHEJ) pathway of DNA repair. Ku has been proposed to act as a scaffold for recruitment of other NHEJ participants, including PRKDC and PARP1 (181). In agreement with previous reports (see Table 4.1 and Supplementary Table 2, Appendix B and the references therein), we detected the interaction between WRN and the Ku heterodimer by all methods. After a slight initial increase in association immediately after treatment with CPT, we see a decrease, and then a sharp increase 12 hours after the start of treatment, as compared to control. A detailed analysis of binding to WRN shows a slightly divergent pattern between the two components of the heterodimer, which may be a reflection of either our study design, or a suggestion that WRN preferentially binds the 70 kDa subunit, which then recruits the 86 kDa subunit to the complex.

We then focused on the possibility of concerted recruitment and binding of WRN to members of three chromatin remodeling complexes, NuRD, CAF1, and FACT. All three of these complexes have been implicated in DDR, and their roles and specific functions are described in the following subsections. Our results not only suggest that WRN can bind to members of a single complex in concerted manner, but that it can show that interactions with other proteins

occur independently of each other.

Nucleosome Remodeling and Deacetylation (NuRD)

The NuRD complex has been described to function in transcriptional regulation and chromatin remodeling, and is highly conserved throughout animal and plant kingdoms. Here we discuss the evidence for interaction between WRN protein and members of the NuRD complex in context of our affinity purification data, and specifically focus on the importance of possible interaction between WRN and the catalytic core of NuRD, protein CHD4.

The NuRD complex (also Mi-2) is composed of seven protein members RBBP4 (RbAp48), RBBP7 (RbAp46), histone deacetylase proteins HDAC1 and HDAC2, chromodomain-helicase-DNA-binding protein CHD3/CHD4, metastasis-associated proteins MTA1/MTA 2, and MBD3/MBD2. The exact structure of the NuRD complex is somewhat modular, and presence of different components has been shown to affect its overall activity. Here we will focus on individual components that were identified in our analysis, proteins CHD4, RBBP4, MTA2, HDAC1, and MBD3. We initially found CHD4 and RBBP4 to be highly enriched in WRN samples treated with CPT for 1 hour, and we subsequently confirmed this interaction with SRM, western blotting, and reciprocal IPs using our SH-tagged proteins and untransfected HEK293T cells. Sequences for CHD4 and RBBP4 were generated by *in vitro* translation to aid in SRM method development, and retention time prediction.

The NuRD complex plays an important role in controlling chromatin superstructure by regulaing access to the genome, and it function is tied to transcription, chromatin assembly, cell cycle progression, DNA repair, oxidative stress response, and genomic stability (182–186).

The core catalytic subunit of NuRD is a ubiquitously expressed nuclear protein CHD4. It

has been found to promote DSB signaling and stimulate DDR, HR repair and p53-dependent pathways such as apoptosis and senescence (177,185,187,188).

CHD4 and NuRD components MTA2 and MBD3 rapidly localize to sites of DNA damage, and co-localize along γ-H2AX tracks and to IR-induced chromatin fractions(177,187,189,190). CHD4 knockdown cells showed increased levels of γ-H2AX at baseline, but no increase due to IR damage (177,185). WRN also co-localizes and associates with γ-H2AX, and its depletion results in elevated focus formation after HU-mediated arrest (78,128). DDR is a multistep process that involves early- and late-acting cofactors, which have been previously defined. Among the early responders is protein MDC1, which binds to γ-H2AX following initial signaling of the DSBs (176–179,187) . GFP-CHD4, GFP-MTA2, and GFP-MBD3 arrive at the DSB track as early as GFP-MDC1(177), classifying these components of the NuRD complex as early responders to DSBs. Despite the common early recruitment to DSB-flanking sites following initial γ-H2AX nucleation, binding of these mediators occurs in parallel. This was shown after depletion of CHD4 did not affect damage-dependent γ-H2AX formation or recruitment of MDC1(177). CHD4 was previously detected in an YFP-WRN AP-MS experiment, when chromatin was not disrupted with nuclease (111), and interaction of WRN with MDC1 was predicted, though not verified via biochemical approaches (131). We asked whether WRN exhibited different dynamics of association with CHD4 or MDC1 as a function of treatment time.

Figure 5.10 shows that the traces are nearly identical, raising the possibility that they either form a complex prior to binding WRN, or they bind WRN independently but at approximately the same time. It is also uncertain whether the rapid association of these proteins with WRN is due to active recruitment, or prior independent co-localization to DSB sites. The

resolution of our study is insufficient to differentiate between these possibilities, but a similar study with removal of each component or abrogation of binding should answer this question definitively.

CHD4 lacks a DNA-binding domain, recruitment of CHD4 to sites of DNA damage depends on PARP1 by modification with poly(ADP-ribose) chains (PAR chains), and inhibition of PARP was shown to abrogate CHD4 accumulation at sites of DNA damage (189,190). CHD4 has a major role as an HR regulator (188) and HR-deficient cancer cells have been shown to suffer from synthetic lethality when exposed to PARP inhibitors (191–193). In agreement with these previous studies, depletion of CHD4 imparts sensitivity to PARP inhibitors (188), as does depletion of WRN (194,195) . In cells, PARP activation and modification results in subsequent activation of repair factors such as ATM, promotion of HR and NHEJ, and ihbitition of TOP1 (185,190,196). PARP inhibitors have been shown to achieve additional sensitization when used in combination with methylating agents and TOP1 poisons (197,198) **.**

Figure 5.10 demonstrates that temporal association of PARP1 with WRN after treatment with CPT differs from association with CHD4, making it unlikely that these proteins maintain a single, stable complex during the entire course of drug treatment. As noted previously, at every time point we are looking at the total signal from all proteins, regardless of individual complexes in which they occur. While perfectly parallel traces may be suggestive of concerted association and dissociation of preys from bait, discordant patterns may be a result of a sum of complexes being assayed. Because PARP1 has a large number of interacting partners, its pool is likely split into multiple sub-complexes, each of which has the potential to exhibit its unique pattern of association with WRN.

Analyses of human cancers revealed that expression of *CHD4* was decreased in some

gastric and colorectal cancers (199), and that mutated *CHD4* was present in 17% of endometrial cancers analyzed (55). CHD4 is emerging as an interesting therapeutic target, and an important next step is to determine whether a double mutation or a disruption of interaction between WRN and CHD4 can produce a compounded effect on HR defect, and thus improving the efficacy of PARP inhibitors further, or opening doors to other combination therapy.

Other members of the NuRD complex, RBBP4, HDAC1, and MTA2 were shown to bind WRN in the manner similar to CHD4, and we hypothesize that their activity occurs in context of the NuRD complex.

WD40 repeat-containing proteins RBBP4 (RbAp48) was initially identified as interactor of the tumor suppressor retinoblastoma protein Rb(200), and is proposed to help regulate cell proliferation. Additionally, the decrease of this protein in hippocampus is proposed to be the main cause of memory loss in aging, supported in part by its depletion from both human and mouse brains in normal aging, and by ability to rescue the memory loss phenotype by knock-in (201). Cells depleted for RBBP4 show decreased histone deacetylase activity, probably due to its participation in NuRD and direct interaction with HDAC1/HDAC2 (202). Interaction between WRN and RBBP4 has not been previously reported, and warrants additional research. Cells of Hutchinson-Gilford progeria syndrome (HGPS) patients show significant depletion of RBBP4 (185).

MTA2, HDAC1 and HDAC2 were shown to promote NHEJ and HR (190,203,204). They physically localize to sites of DNA damage, but this localization was inhibited by knockdown of CHD4 in cells (190). HDAC inhibitors silence DNA repair pathways, inactivate non-histone proteins that are required for DNA stability, and induce reactive oxygen species and DNA double-strand breaks (203,205,206). WRN has been previously shown to cooperate with histone

deacetylase SIRT1, be required for SIRT1-mediated HR (207), but there are currently no other reports showing interaction between HDAC1 and WRN. Both HDAC1 and NuRD component MTA2 have been implicating in regulating p53 deacetylation and transcriptional activity (208). Similar to deficiency of CHD4, knockdown of MTA2 results in increased sensitivity to ionizing radiation (177), but expression levels of *HDAC1* and *MTA2* are unaffected by CHD4 knockdown (190). Overall, their activity appears to be in the context of the NuRD complex, and their DDR activity is governed by presence of CHD4 in cells.

MBD3 is a methyl-CpG-binding domain protein, and a direct interaction partner of MTA2 and HDAC1 within the NuRD complex. Knocking out MBD3 results in embryonic lethality (209), and depletion of MBD3 causes reprogramming of primed pluripotent epiblast stem cells to native pluripotency (210). Its functional contribution to NuRD complex may be helping organize potentially vulnerable eukaryotic sequences by depositing methylation marks (187,211). Based on our results, and the data presented in Figure 5.8, it is difficult to tell whether MBD3 participates in DDR separately from other NuRD components, whether it binds a fraction of the WRN pool independently, and if the distinct pattern of its interaction with WRN carries a functional consequence.

Chromatin Assembly Factor (CAF1)

Chromatin assembly factor I (CAF1) is a heterotrimer nuclear complex that consists of members p150 (CHAF1A), p60 (CHAF1B, CAF1B) and p48 (RBBP4, RbAp48). While we were able to develop methods for detection of CHAF1B and RBBP4, CHAF1A was refractory to SRM method development, and was not detected in the profiling study.

This complex mainly functions in the initial evens in DNA replication-associated chromatin assembly by depositing new histone H3/H4 tetramers onto replicating DNA (212). During replication, chromatin is rapidly made available by removal of parental nucleosomes in advance of the replication fork, and then re-packaged into chromatin behind the fork (213,214). CAF1 functions in depositing new nucleosomes at the replication fork (215,216), and in heterochromatin silencing during gene expression and in nucleosome assembly (217). It was also demonstrated that CHAF1A, but not CHAF1B is uniquely required for the progression of S phase in mouse cells (218). A similar defect in progression through the S-phase is also seen in fibroblasts and lymphoblastoid cells from WS patients (139,219) and in WRN-depleted normal primary fibroblasts (12). RNAi-mediated silencing of CHAF1B in proliferating cells is reported to result in accumulation of DNA DSBs, increased levels of γH2AX foci, 10-fold reduction of nucleosome assembly during DNA synthesis, and induction of apoptosis. Importantly, these cellular defects could be rescued by addition of recombinant CHAF1B (220).

Depletion studies of CAF1 in human cells have shown that it is required for progression through S-phase and successful replication-coupled chromatin assembly, and loss of CAF1 completely eliminated any replication-coupled chromatin assembly activity in cell extracts (221). Reduction of nucleosome assembly by CAF1 was shown to impair HR and NHEJ, and mutations in CAF1 cause hypersensitivity to a variety of DNA-damaging agents such as MMS and CPT (222,223). In quiescent human cells, DSBs induced by ionizing radiation (IR) or radiomimetic drugs cause recruitment of CAF1 and PCNA to damage sites, while depletion of CAF1 results in rapid DSB accumulation (224).

CAF1 subunit CHAF1A has been previously reported to interact with BLM (225), PCNA (226,227), and WRN (118). In fact, after treatment with Hydroxyurea, recruitment of CAF1

followed, and was dependent on the initial focus formation of WRN, which suggests a functional interaction between these proteins in the context of DNA damage (118). Figure 5.11 shows an increase in WRN-CHAF1B interaction shortly after CPT treatment, with a substantial increase 6 hours after treatment, when compared to control. The interaction then rapidly decreases at12 hours of CPT. This may suggest that a functional interaction between these proteins is in initial steps of DDR. In yeast depletion studies, histone chaperone Asf1 was found to physically interact with CAF1 subunit CHAF1B (228,229). A large study of double mutants in yeast showed that deletion of Asf1 and yeast homolog of WRN, Sgs1, causes synthetic lethality (230), raising the possibility of cooperation and acting in redundancy.

The results of our protein-protein interaction study indicate that WRN associates with CHAF1B and RBBP4, and this association is slightly elevated after treatment with CPT for 1 hour (Figure 5.4). The extended time course study showed that following this initial association, CHAF1B binding to WRN increases further, while RBBP4 association sharply decreases (Figure 5.11). CHAF1B was identified in the initial profiling analysis, and has been confirmed in an independent biological replicate via AP and subsequent analysis by SRM and Western blot. It is likely that this interaction is at least in part mediated by the shared association between these proteins and proliferating cell nuclear antigen (PCNA), which has been shown to associate with WRN in a similar pattern to CHAF1B (Figure 5.5), and confirmed again as shown in Figure 5.11. Both, physical and functional interaction between WRN and PCNA has been verified (141,142). Because a single site on PCNA can be occupied by a number of its interactors, it has been proposed that WRN competes for this interaction when the need for a reparative helicase arises. Once the repair at the stalled replication fork has been accomplished, replication factors such as FEN1 and LIG1 can displace it (142). It has been proposed that cooperation between

PCNA and CAF1 at sites of DNA damage may result in establishment of repressive chromatin structures, which temporarily suspend normal DNA transactions such as transcription and replication, and thus allowing the DDR to proceed. Our study shows a decreased association with CHAF1B and PCNA 12 hours after treatment with CPT, and at this point we see a sharp increase in association of WRN with a number of other DDR factors as shown in Figure 5.5.

Moggs JG et al (226) have found that DNA repair intermediates are able to trigger chromatin assembly prior to completion of repair, which in combination with findings by Jiao R et al (118) suggests that WRN may be recruited to sites of DNA double strand breaks, followed by CAF1 to help repress surrounding chromatin and amplify the signal of DNA damage up- and down-stream of the break site. Once replication forks resume, WRN is again required for the progression of replication (12,35).

Facilitates Chromatin Transcription (FACT) complex

An abundant nuclear complex that binds to nucleosomes and disrupts the interaction between H2A/H2B dimer and H3/H4 tertramer of the nucleosome, FACT belongs to a number of histone chaperones that ensures a timely reassembly of chromatin following DNA manipulation. It promotes the reestablishment of the nucleosome following the passage of RNA polymerase II as an H2A/H2B chaperone (231), and has been implicated in transcription elongation, DNA repair, and DNA replication (232). This complex was first discovered as a factor necessary for transcriptional elongation through chromatin (233), and unsurprisingly the eviction and replacement of histones by FACT is necessary for restart of arrested transcription following DNA damage (234).

FACT complex consists of members SPT16 (also SPT16H, SUPT16H, suppressor of Ty) and SSRP1 (structure specific recognition protein) in humans, both of which were found in our profiling data with high specificity, and their presence was verified using SRM in an independent biological replicates. Results of SRM study of association with WRN in response to CPT for 1 hour show that both proteins are slightly elevated in comparison to treatment with DMSO, but extended time course shows that association with these proteins at 6 hour time point is different (Figure 5.13), although both proteins were initially placed in the same cluster (Figure 5.5). Both subunits are necessary, but individually not sufficient for nucleosome assembly (231). Interaction between WRN, SPT16H and SMARCAL1 was previously reported (235). In human cells FACT localizes to replication origins and interacts with the MCM complex (236). WRN and SSRP1 physically interact with the Ku complex in the absence of DNase, co-localize to the nucleolus at steady state, and show diffuse nuclear staining after UV irradiation (237). Finally, interaction with both of these proteins has been previously reported using a profiling proteomic analysis of WRN interacting proteins (111).

Conditional knockout of the *SSRP1* gene in chicken DT 40 cells showed a growth defect, a delay in S-phase cell cycle progression, and slowed replication fork progression. Interestingly, the initiation of replication in these cells was not affected. SSRP1 depletion also did not affect nucleosome reassembly during DNA replication, in contrast with the significant reduction of nucleosome assembly seen with depletion of CAF1 subunit CHAF1A. Taken together, the data suggest that FACT plays a more significant role than CAF1 in maintaining replication progression, and this impairment was shown to be independent of transcription (238–240). WRN has also been shown to affect replication fork progression following HU-mediated replication fork stalling (12,35).

Functionally, FACT was previously reported to regulate response to cis-Pt with PRKDC, and RNA*i*-mediated depletion of SSRP1 causes cis-Pt sensitivity in human cells (241). Following treatment with HU, the over-expression of SSRP1 causes a decrease in HR events, while RNAi-mediated knockdown of SSRP1 causes an increase in such events (242). Depletion of SPT16H subunit alone resulted in hypersensitivity to UV, and depletion of both subunits produced no additive effect (234). Following damage by UV radiation, the exchange of H2A/H2B is accelerated, and is caused by SPT16H independent of SSRP1 (234). Two large-scale CPT sensitivity screens had found that FACT complex interacts with the MMS22L-NFKBIL2 complex and MCM complex in context of DNA damage by CPT (243,244). Neither of these proteins is found in our analysis, and conversely WRN was not detected in these large studies. Functionally, depletion of SSRP1 or SPT16H does not lead to increased γ-H2AX focus formation, while depletion of WRN causes a significant increase (78), as does depletion of MMS22L-NFKBIL2 in CPT sensitivity studies (243). Finally, depletion of either SPT16H or SSRP1 led to resistance to CPT (243).

Depletion of FACT complex has little effect on CHK1 phosphorylation (243), while knockdown of WRN expression abolished CHK1 phosphorylation in response to CPT, linking it to controlling the ATR-CHK1-mediated S-phase checkpoint in CPT-treated cells (112). It is possible that the interaction between WRN and FACT member SSRP1 attains a middle ground between promoting HR events and preventing error-prone HR.

Notes to Chapter 5

Figure 5.1 was generated with the help from Alden Hackmann.

All skyline files incorporating RAW data files are provided in Panorama:

http://proteome.gs.washington.edu/software/panorama/WRN_interactome_WRN-interacting_SRM.html

http://proteome.gs.washington.edu/software/panorama/WRN_interactome_IVT_standards.html

Chapter 6 - Proteomic data informs our understanding of WRN function and the origins of the Werner syndrome cellular and organismal phenotypes.

Section 1: We present preliminary data on analysis of phosphorylated proteins in the context of WRN interactome.

WRN has been previously shown to be extensively phosphorylated and regulated, and allows to localize either to nucleoli or nucleoplasm as a function of these phosphorylations (129,245,246). Here we present some preliminary data on the analysis of phosphopeptides isolated from WRN-enriched protein complexes. Analysis of phosphorylations was performed as two-step enrichment, as shown in Figure 6.1:

1) Cells stably expressing SH-WRN were treated either with DMSO or CPT for 6 hours. Whole WRN complex was first isolated via enrichment with its SH tag, as done in all other analyses, followed by proteolytic digestion and buffer exchange and described in Chapter 3.
2) This digest was then subjected to phosphopeptide enrichment by IMAC, as described previously (247).

This sequential analysis resulted in three samples that were all analyzed using the same method, instrument platform, and data processing: WRN complex as generated in step 1, above, phosphopeptide enriched sample and phosphopeptide depleted sample (flow-through). Due to sample scarcity, only a single replicate of samples was analyzed, making it impossible to assign significance to changes that occur between treatments. However, the data was collected on a

high-resolution LTQ-Orbitrap instrument. This enables analysis of MS1 data using Skyline, and carries the potential of comparing peak areas.

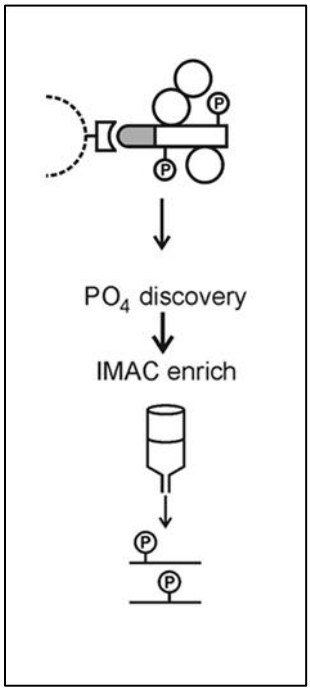

Figure 6.1: Isolation of the protein complex and subsequent phosphopeptide enrichment by IMAC.

The preliminary results of our study are very promising, as we identified a large number of WRN interacting proteins that appear to be differentially phosphorylated after treatment with CPT for 6 hours. All RAW data is available for further analysis. Here we present the results of phosphorylation on WRN as well as a few selected proteins that we consider to be targets for further analysis.

WRN protein was shown to be extensively phosphorylated in response to CPT treatment for 6 hours. Among modified sites we found PRKDC sites Ser 440 and Ser467 (245) and ATM-dependent sites Ser1058 and Ser1141 (129).

Phosphopeptide analysis identified 25 phosphorylation sites in response to CPT treatment, as detailed in Figures 6.2 and 6.3. Figure 6.2 shows previously sites, as reported on Phosphosite repository, and identifies sites that were found in our analysis in CPT-dependent manner.

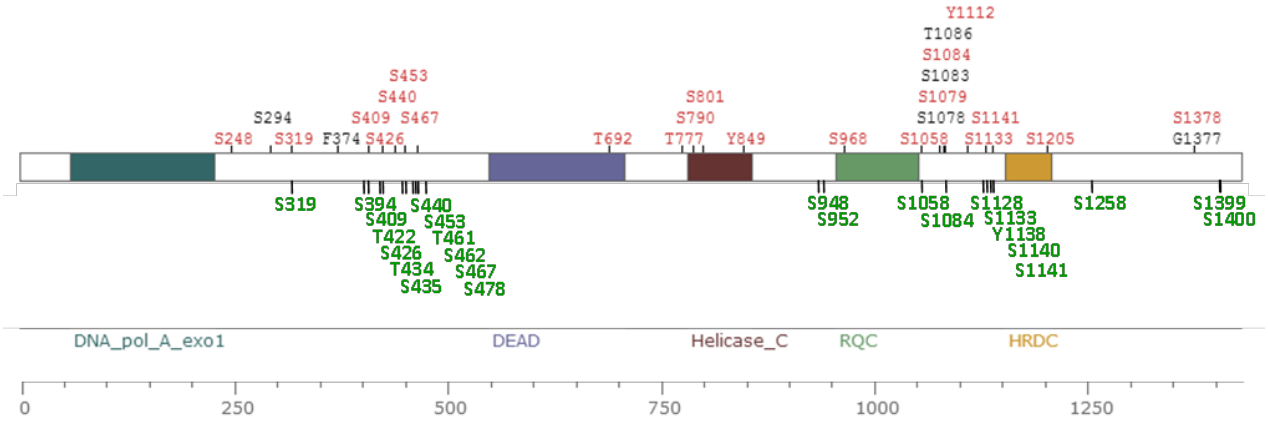

Figure 6.2: Full map of WRN protein with previously reported phosphosites, and CPT treatment-dependent phosphorylations detected in our analysis (listed below, in green).

				Spectral Count	
+DMSO	+CPT	Peptide Sequence	Charge	+DMSO	+CPT
	*	ACLM[147]SLDITEHELQILEQQS[167]QEEYLSDIAYK	3		1
*	*	SRLDHCYS[167]M[147]DDSEDTSWDFGPQAFK	3	2	3
	*	ACLM[147]S[167]LDITEHELQILEQQS[167]QEEYLSDIAYK	3		3
*	*	SKEEVGINTETSS[167]AER	2	1	1
	*	STEHLSPNDNENDTSYVIES[167]DEDLEMEMLK	3		1
	*	STEHLSPNDNENDT[181]SYVIES[167]DEDLEM[147]EM[147]LK	3		1
*	*	SIM[147]VQS[167]PEK	2	3	3
	*	HLS[167]PNDNENDTSYVIES[167]DEDLEMEM[147]LK	3		4
	*	HLSPNDNENDT[181]SYVIES[167]DEDLEMEMLK	3		2
*	*	HLS[167]PNDNENDTSYVIES[167]DEDLEM[147]EM[147]LK	3	3	12
	*	HLSPNDNENDT[181]SYVIES[167]DEDLEM[147]EM[147]LK	3		1
	*	TVSS[167]GTKEHCYNQVPVELSTEK	3		1
*	*	STEHLSPNDNENDTSYVIES[167]DEDLEMEM[147]LK	3	1	1
*	*	SIM[147]VQS[167]PEKAYSSSQPVISAQEQETQIVLYGK	3	2	3
	*	SIMVQS[167]PEKAYSSS[167]QPVISAQEQETQIVLYGK	3		1
	*	HLS[167]PNDNENDTSYVIES[167]DEDLEMEMLK	3		2
*		LDHCYS[167]M[147]DDSEDTSWDFGPQAFK	3	1	
	*	S[167]LENLNSGTVEPTHSK	2		1
	*	HLS[167]PNDNENDTSYVIES[167]DEDLEM[147]EMLK	3		6
	*	AYSSS[167]QPVISAQEQETQIVLYGK	3		2
	*	LDHCYSM[147]DDS[167]EDTSWDFGPQAFK	3		3
	*	SLENLNS[167]GTVEPTHSK	2		1
	*	LDHCYSMDDS[167]EDTSWDFGPQAFK	3		1
	*	ICTLSQS[167]M[147]AITYSLFQEK	3		1
	*	SLENLNS[167]GTVEPTHSK	3		1
	*	AYSSS[167]QPVISAQEQETQIVLYGK	2		1
	*	KSIM[147]VQS[167]PEK	2		1
	*	SIM[147]VQSPEKAY[243]SSS[167]QPVISAQEQETQIVLYGK	3		1
	*	KSIM[147]VQS[167]PEKAYSSSQPVISAQEQETQIVLYGK	3		1
	*	STEHLS[167]PNDNENDTSYVIES[167]DEDLEM[147]EM[147]LK	3		2
	*	M[147]IIGSTNIETELRPSNNLNLLS[167]FEDSTTGGVQQK	3		1
	*	AYSS[167]SQPVISAQEQETQIVLYGK	2		1
	*	SRLDHCYSM[147]DDS[167]EDTSWDFGPQAFK	3		8
	*	STEHLS[167]PNDNENDTSYVIES[167]DEDLEMEMLK	3		2
	*	SIM[147]VQS[167]PEKAYSSS[167]QPVISAQEQETQIVLYGK	3		3
	*	STEHLS[167]PNDNENDTSYVIES[167]DEDLEM[147]EMLK	3		1
	*	SIMVQS[167]PEK	2		1
*	*	SKEEVGINTETS[167]SAER	3	1	1
	*	HLSPNDNENDT[181]SYVIES[167]DEDLEM[147]EMLK	3		1
	*	S[167]IMVQSPEKAYSSS[167]QPVISAQEQETQIVLYGK	3		1
	*	SIMVQS[167]PEKAYSSSQPVISAQEQETQIVLYGK	3		1
	*	STEHLS[167]PNDNENDTSYVIESDEDLEM[147]EM[147]LK	3		1
	*	HLSPNDNENDTSYVIES[167]DEDLEM[147]EMLK	3		1
*	*	STEHLSPNDNENDTSYVIES[167]DEDLEM[147]EM[147]LK	3	4	4
	*	HLSPNDNENDTS[167]YVIESDEDLEM[147]EM[147]LK	3		1
	*	STEHLSPNDNENDTSYVIES[167]DEDLEM[147]EMLK	3		1
	*	HLSPNDNENDTSYVIES[167]DEDLEMEM[147]LK	3		1
	*	ANTES[167]QSLILQANEELCPK	2		1
	*	ST[181]EHLSPNDNENDTSYVIES[167]DEDLEM[147]EM[147]LK	3		2
*	*	HLSPNDNENDTSYVIES[167]DEDLEM[147]EM[147]LK	3	3	3
	*	ANTES[167]QSLILQANEELCPK	3		1
*		LLSAVDILGEK	2	1	
	*	STEHLS[167]PNDNENDTSYVIES[167]DEDLEMEM[147]LK	3		1
	*	ST[181]EHLSPNDNENDTSYVIES[167]DEDLEMEM[147]LK	3		1

Figure 6.3: Full results on WRN phosphorylations found in our analysis, peptide charge information and spectral counts, as reported by MSDaPl.

In addition to phosphorylations on WRN, we find phosphorylated sites on proteins CHD4, MDC1, TRIM28, and H2AX, as detailed below.

WRN

```
     1          11         21         31         41         51
     |          |          |          |          |          |
   1 MSEKKLETTA QQRKCPEWMN VQNKRCAVEE RKACVRKSVF EDDLPFLEFT GSIVYSYDAS  60
  61 DCSFLSEDIS MSLSDGDVVG FDMEWPPLYN RGKLGKVALI QLCVSESKCY LFHVSSMSVF 120
 121 PQGLKMLLEN KAVKKAGVGI EGDQWKLLRD FDIKLKNFVE LTDVANKKLK CTETWSLNSL 180
 181 VKHLLGKQLL KDKSIRCSNW SKFPLTEDQK LYAATDAYAG FIIYRNLEIL DDTVQRFAIN 240
 241 KEEEILLSDM NKQLTSISEE VMDLAKHLPH AFSKLENPRR VSILLKDISE NLYSLRRMII 300
 301 GSTNIETELR PSNNLNLLSF EDSTTGGVQQ KQIREHEVLI HVEDETWDPT LDHLAKHDGE 360
 361 DVLGNKVERK EDGFEDGVED NKLKENMERA CLMSLDITEH ELQILEQQSQ EEYLSDIAYK 420
 421 STEHLSPNDN ENDTSYVIES DEDLEMEMLK HLSPNDNEND TSYVIESDED LEMEMLKSLE 480
 481 NLNSGTVEPT HSKCLKMERN LGLPTKEEEE DDENEANEGE EDDDKDFLWP APNEEQVTCL 540
 541 KMYFGHSSFK PVQWKVIHSV LEERRDNVAV MATGYGKSLC FQYPPVYVGK IGLVISPLIS 600
 601 LMEDQVLQLK MSNIPACFLG SAQSENVLTD IKLGKYRIVY VTPEYCSGNM GLLQQLEADI 660
 661 GITLIAVDEA HCISEWGHDF RDSFRKLGSL KTALPMVPIV ALTATASSSI REDIVRCLNL 720
 721 RNPQITCTGF DRPNLYLEVR RKTGNILQDL QPFLVKTSSH WEFEGPTIIY CPSRKMTQQV 780
 781 TGELRKLNLS CGTYHAGMSF STRKDIHHRF VRDEIQCVIA TIAFGMGINK ADIRQVIHYG 840
 841 APKDMESYYQ EIGRAGRDGL QSSCHVLWAP ADINLNRHLL TEIRNEKFRL YKLKMMAKME 900
 901 KYLHSSRCRR QIILSHFEDK QVQKASLGIM GTEKCCDNCR SRLDHCYSMD DSEDTSWDFG 960
 961 PQAFKLLSAV DILGEKFGIG LPILFLRGSN SQRLADQYRR HSLFGTGKDQ TESWWKAFSR1020
1021 QLITEGFLVE VSRYNKFMKI CALTKKGRNW LHKANTESQS LILQANEELC PKKLLLPSSK1080
1081 TVSSGTKEHC YNQVPVELST EKKSNLEKLY SYKPCDKISS GSNISKKSIM VQSPEKAYSS1140
1141 SQPVISAQEQ ETQIVLYGKL VEARQKHANK MDVPPAILAT NKILVDMAKM RPTTVENVKR1200
1201 IDGVSEGKAA MLAPLLEVIK HFCQTNSVQT DLFSSTKPQE EQKTSLVAKN KICTLSQSMA1260
1261 ITYSLFQEKK MPLKSIAESR ILPLMTIGMH LSQAVKAGCP LDLERAGLTP EVQKIIADVI1320
1321 RNPPVNSDMS KISLIRMLVP ENIDTYLIHM AIEILKHGPD SGLQPSCDVN KRRCFPGSEE1380
1381 ICSSSKRSKE EVGINTETSS AERKRRLPVW FAKGSDTSKK LMDKTKRGGL FS
```

MDC1

```
   1          11         21         31         41         51
      |          |          |          |          |          |
    1 MEDTQAIDWD VEEEEETEQS SESLRCNVEP VGRLHIFSGA HGPEKDFPLH LGKNVVGRMP  60
   61 DCSVALPFPS ISKQHAEIEI LAWDKAPILR DCGSLNGTQI LRPPKVLSPG VSHRLRDQEL 120
  121 ILFADLLCQY HRLDVSLPFV SRGPLTVEET PRVQGETQPQ RLLLAEDSEE EVDFLSERRM 180
  181 VKKSRTTSSS VIVPESDEEG HSPVLGGLGP PFAFNLNSDT DVEEGQQPAT EEASSAARRG 240
  241 ATVEAKQSEA EVVTEIQLEK DQPLVKERDN DTKVKRGAGN GVVPAGVILE RSQPPGEDSD 300
  301 TDVDDDSRPP GRPAEVHLER AQPFGFIDSD TDAEEERIPA TPVVIPMKKR KIFHGVGTRG 360
  361 PGAPGLAHLQ ESQAGSDTDV EEGKAPQAVP LEKSQASMVI NSDTDDEEEV SAALTLAHLK 420
  421 ESQPAIWNRD AEEDMPQRVV LLQRSQTTTE RDSDTDVEEE ELPVENREAV LKDHTKIRAL 480
  481 VRAHSEKDQP PFGDSDDSVE ADKSSPGIHL ERSQASTTVD INTQVEKEVP PGSAIIHIKK 540
```

```
  541 HQVSVEGTNQ TDVKAVGGPA KLLVVSLEEA WPLHGDCETD AEEGTSLTAS VVADVRKSQL
600
  601 PAEGDAGAEW AAAVLKQERA HEVGAQGGPP VAQVEQDLPI SRENLTDLVV DTDTLGESTQ 660
  661 PQREGAQVPT GREREQHVGG TKDSEDNYGD SEDLDLQATQ CFLENQGLEA VQSMEDEPTQ 720
  721 AFMLTPPQEL GPSHCSFQTT GTLDEPWEVL ATQPFCLRES EDSETQPFDT HLEAYGPCLS 780
  781 PPRAIPGDQH PESPVHTEPM GIQGRGRQTV DKVMGIPKET AERVGPERGP LERETEKLLP 840
  841 ERQTDVTGEE ELTKGKQDRE QKQLLARDTQ RQESDKNGES ASPERDRESL KVEIETSEEI 900
  901 QEKQVQKQTL PSKAFEREVE RPVANRECDP AELEEKVPKV ILERDTQRGE PEGGSQDQKG 960
  961 QASSPTPEPG VGAGDLPGPT SAPVPSGSQS GGRGSPVSPR RHQKGLLNCK MPPAEKASRI1020
 1021 RAAEKVSRGD QESPDACLPP TVPEAPAPPQ KPLNSQSQKH LAPPPLLSPL LPSIKPTVRK1080
 1081 TRQDGSQEAP EAPLSSELEP FHPKPKIRTR KSSRMTPFPA TSAAPKLEPS TSTDQPVTPE1140
 1141 PTSQATRGRT NRSSVKTPET VVPTAPELQP STSTDQPVTP EPTSQATRGR TDRSSVKTPE1200
 1201 TVVPTAPELQ ASASTDQPVT SEPTSRTTRG RKNRSSVKTP ETVVPAAPAL QPSTSTDQPV1260
 1261 TPEPTSRATR GRTNRSSVKT PESIVPIAPE LQPSTSRNQL VTPEPTSRAT RCRTNRSSVK1320
 1321 TPEPVVPTAP EPHPTTSTDQ PVTPKLTSRA TRRKTNRSSV KTPKPVEPAA SDLEPFTPTD1380
 1381 QSVTPEAIAQ GGQSKTLRSS TVRAMPVPTT PEFQSPVTTD QPISPEPITQ PSCIKRQRAA1440
 1441 GNPGSLAAPI DHKPCSAPLE PKSQASRNQR WGAVRAAESL TAIPEPASPQ LLETPIHASQ1500
 1501 IQKVEPAGRS RFTPELQPKA SQSRKRSLAT MDSPPHQKQP QRGEVSQKTV IIKEEEEDTA1560
 1561 EKPGKEEDVV TPKPGKRKRD QAEEEPNRIP SRSLRRTKLN QESTAPKVLF TGVVDARGER1620
 1621 AVLALGGSLA GSAAEASHLV TDRIRRTVKF LCALGRGIPI LSLDWLHQSR KAGFFLPPDE1680
 1681 YVVTDPEQEK NFGFSLQDAL SRARERRLLE GYEIYVTPGV QPPPPQMGEI ISCCGGTYLP1740
 1741 SMPRSYKPQR VVITCPQDFP HCSIPLRVGL PLLSPEFLLT GVLKQEAKPE AFVLSPLEMS1800
 1801 ST
```

TRIM28

```
   1          11          21          31          41          51
      |           |           |           |           |           |
    1 MAASAAAASA AAASAASGSP GPGEGSAGGE KRSTAPSAAA SASASAAASS PAGGGAEALE  60
   61 LLEHCGVCRE RLRPEREPRL LPCLHSACSA CLGPAAPAAA NSSGDGGAAG DGTVVDCPVC 120
  121 KQQCFSKDIV ENYFMRDSGS KAATDAQDAN QCCTSCEDNA PATSYCVECS EPLCETCVEA 180
  181 HQRVKYTKDH TVRSTGPAKS RDGERTVYCN VHKHEPLVLF CESCDTLTCR DCQLNAHKDH 240
  241 QYQFLEDAVR NQRKLLASLV KRLGDKHATL QKSTKEVRSS IRQVSDVQKR VQVDVKMAIL 300
  301 QIMKELNKRG RVLVNDAQKV TEGQQERLER QHWTMTKIQK HQEHILRFAS WALESDNNTA 360
  361 LLLSKKLIYF QLHRALKMIV DPVEPHGEMK FQWDLNAWTK SAEAFGKIVA ERPGTNSTGP 420
  421 APMAPPRAPG PLSKQGSGSS QPMEVQEGYG FGSGDDPYSS AEPHVSGVKR SRSGEGEVSG 480
  481 LMRKVPRVSL ERLDLDLTAD SQPPVFKVFP GSTTEDYNLI VIERGAAAAA TGQPGTAPAG 540
  541 TPGAPPLAGM AIVKEEETEA AIGAPPTATE GPETKPVLMA LAEGPGAEGP RLASPSGSTS 600
  601 SGLEVVAPEG TSAPGGGPGT LDDSATICRV CQKPGDLVMC NQCEFCFHLD CHLPALQDVP 660
  661 GEEWSCSLCH VLPDLKEEDG SLSLDGADST GVVAKLSPAN QRKCERVLLA LFCHEPCRPL 720
  721 HQLATDSTFS LDQPGGTLDL TLIRARLQEK LSPPYSSPQE FAQDVGRMFK QFNKLTEDKA 780
  781 DVQSIIGLQR FFETRMNEAF GDTKFSAVLV EPPPMSLPGA GLSSQELSGG PGDGP
```

CHD4

```
   1          11          21          31          41          51
      |           |           |           |           |           |
    1 MASGLGSPSP CSAGSEEEDM DALLNNSLPP PHPENEEDPE EDLSETETPK LKKKKKPKKP  60
   61 RDPKIPKSKR QKKERMLLCR QLGDSSGEGP EFVEEEEEVA LRSDSEGSDY TPGKKKKKKL 120
  121 GPKKEKKSKS KRKEEEEEED DDDDSKEPKS SAQLLEDWGM EDIDHVFSEE DYRTLTNYKA 180
  181 FSQFVRPLIA AKNPKIAVSK MMMVLGAKWR EFSTNNPFKG SSGASVAAAA AAAVAVVESM 240
  241 VTATEVAPPP PPVEVPIRKA KTKEGKGPNA RRKPKGSPRV PDAKKPKPKK VAPLKIKLGG 300
  301 FGSKRKRSSS EDDDLDVESD FDDASINSYS VSDGSTSRSS RSRKKLRTTK KKKKGEEEVT 360
  361 AVDGYETDHQ DYCEVCQQGG EIILCDTCPR AYHMVCLDPD MEKAPEGKWS CPHCEKEGIQ 420
  421 WEAKEDNSEG EEILEEVGGD LEEEDDHHME FCRVCKDGGE LLCCDTCPSS YHIHCLNPPL 480
```

```
 481 PEIPNGEWLC PRCTCPALKG KVQKILIWKW GQPPSPTPVP RPPDADPNTP SPKPLEGRPE540
 541 RQFFVKWQGM SYWHCSWVSE LQLELHCQVM FRNYQRKNDM DEPPSGDFGG DEEKSRKRKN 600
 601 KDPKFAEMEE RFYRYGIKPE WMMIHRILNH SVDKKGHVHY LIKWRDLPYD QASWESEDVE 660
 661 IQDYDLFKQS YWNHRELMRG EEGRPGKKLK KVKLRKLERP PETPTVDPTV KYERQPEYLD 720
 721 ATGGTLHPYQ MEGLNWLRFS WAQGTDTILA DEMGLGKTVQ TAVFLYSLYK EGHSKGPFLV 780
 781 SAPLSTIINW EREFEMWAPD MYVVTYVGDK DSRAIIRENE FSFEDNAIRG GKKASRMKKE 840
 841 ASVKFHVLLT SYELITIDMA ILGSIDWACL IVDEAHRLKN NQSKFFRVLN GYSLQHKLLL 900
 901 TGTPLQNNLE ELFHLLNFLT PERFHNLEGF LEEFADIAKE DQIKKLHDML GPHMLRRLKA 960
 961 DVFKNMPSKT ELIVRVELSP MQKKYYKYIL TRNFEALNAR GGGNQVSLLN VVMDLKKCCN1020
1021 HPYLFPVAAM EAPKMPNGMY DGSALIRASG KLLLLQKMLK NLKEGGHRVL IFSQMTKMLD1080
1081 LLEDFLEHEG YKYERIDGGI TGNMRQEAID RFNAPGAQQF CFLLSTRAGG LGINLATADT1140
1141 VIIYDSDWNP HNDIQAFSRA HRIGQNKKVM IYRFVTRASV EERITQVAKK KMMLTHLVVR1200
1201 PGLGSKTGSM SKQELDDILK FGTEELFKDE ATDGGGDNKE GEDSSVIHYD DKAIERLLDR1260
1261 NQDETEDTEL QGMNEYLSSF KVAQYVVREE EMGEEEEVER EIIKQEESVD PDYWEKLLRH1320
1321 HYEQQQEDLA RNLGKGKRIR KQVNYNDGSQ EDRDWQDDQS DNQSDYSVAS EEGDEDFDER1380
1381 SEAPRRPSRK GLRNDKDKPL PPLLARVGGN IEVLGFNARQ RKAFLNAIMR YGMPPQDAFT1440
1441 TQWLVRDLRG KSEKEFKAYV SLFMRHLCEP GADGAETFAD GVPREGLSRQ HVLTRIGVMS1500
1501 LIRKKVQEFE HVNGRWSMPE LAEVEENKKM SQPGSPSPKT PTPSTPGDTQ PNTPAPVPPA1560
1561 EDGIKIEENS LKEEESIEGE KEVKSTAPET AIECTQAPAP ASEDEKVVVE PPEGEEKVEK1620
1621 AEVKERTEEP METEPKGAAD VEKVEEKSAI DLTPIVVEDK EEKKEEEEKK EVMLQNGETP1680
1681 KDLNDEKQKK NIKQRFMFNI ADGGFTELHS LWQNEERAAT VTKKTYEIWH RRHDYWLLAG1740
1741 IINHGYARWQ DIQNDPRYAI LNEPFKGEMN RGNFLEIKNK FLARRFKLLE QALVIEEQLR1800
1801 RAAYLNMSED PSHPSMALNT RFAEVECLAE SHQHLSKESM AGNKPANAVL HKVLKQLEEL1860
1861 LSDMKADVTR LPATIARIPP VAVRLQMSER NILSRLANRA PEPTPQQVAQ QQ
```

H2AX

```
   1          11         21         31         41         51
   |          |          |          |          |          |
   1 MSGRGKTGGK ARAKAKSRSS RAGLQFPVGR VHRLLRKGHY AERVGAGAPV YLAAVLEYLT  60
  61 AEILELAGNA ARDNKKTRII PRHLQLAIRN DEELNKLLGG VTIAQGGVLP NIQAVLLPKK 120
 121 TSATVGPKAP SGGKKATQAS QEY
```

This data is available for viewing in MSDaPl, with all RAW data currently stored in Chorus project (https://chorusproject.org/anonymous/download/experiment/6bd232af8b694c3083e2c2abf4f462b5), and searched data is available on MSDaPl, project 2005, Experiment 3028.

The coordinate analysis of damage-specific phosphorylation sites is an important component of these analyses. A key goal in the future is to describe the interplay between specific post-translational modifications (PTMs) and specific WRN protein interactions in

response to DNA damage. Such a study will require dynamic, simultaneous analysis of both PTMs and interactors. Here we provide a large set of preliminary data set of WRN-interacting proteins that are phosphorylated in response to DNA damage with CPT. Physiological relevance of each phosphorylation can be validated by shRNA-mediated depletion, reciprocal-tag purifications and the use of domain mutant alleles.

Section 2: We summarize the above results chapters, demonstrating the breadth of information gained from both profiling and targeted analyses of WRN interacting proteins.

In our extensive study we interrogated the WRN protein interactome by MS. We initially performed a large-scale profiling analysis using an ion trap instrument to determine with proteins are bound to WRN, and which are selectively enriched in WRN-containing samples compared to a control study. This approach is valuable in its unbiased determination of protein content, and this type of study is often conducted as an initial step in generating future hypothesis to be tested by orthologous methods. Our use of the control protein SH-nLacZ makes our study of WRN interactome unique, and our stringent quality cutoff when performing the enrichment analysis with SAINT was aimed at selecting the protein targets that were most highly enriched in WRN-containing samples.

Our profiling experiment and enrichment analysis agreed with some of the previous reports, confirming the interaction with XRCC6, PRKDC, and histone H2AX (full results are presented in Table 4.2). We also confirm the interaction of WRN with a number of interacting

proteins, which were previously reported based on either a single analysis or data of intermediate quality, such as CHD4, MDC1, and TRIM28. Finally, we also identified many completely new interacting proteins, including CDCA2, TFDP1, and RBBP4, and MBD3.

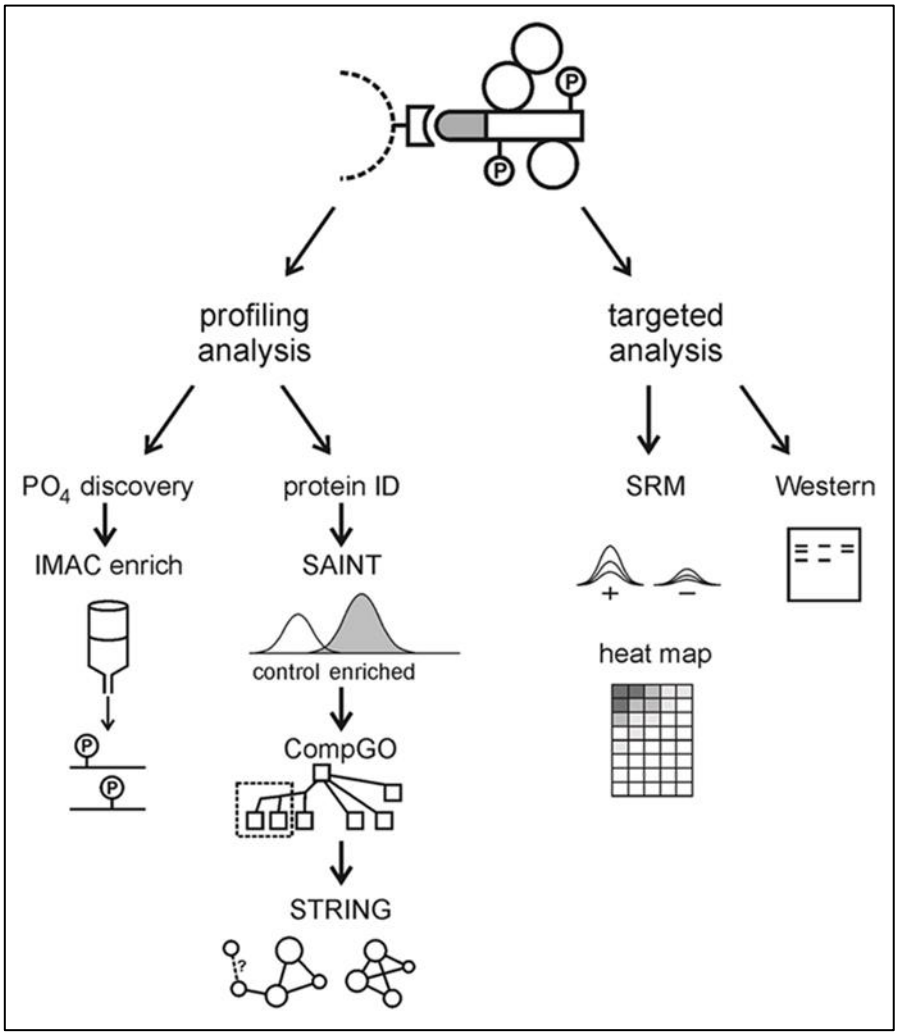

Figure 6.4: Summary of all analyses performed in this project. Profiling analysis of WRN protein complexes and additional enrichment of phosphopeptides resulted in a list of WRN-interacting proteins with and without DNA damage, as well as WRN-interacting proteins that were phosphorylated in response to DNA damage by CPT. Additional study targeted proteins of interest for analysis by SRM for analysis of enrichment in WRN interaction partners in response to CPT.

The results of our profiling study were used to select a number of proteins for validation of interaction and for further investigation. Subsequent studies were performed

using SRM, a method for targeted MS, which is highly specific and quantitative. Previous studies have suggested that WRN can be a participant in DDR, can be a scaffold that aids in assembly of repair factors, or can be both. Our analysis is descriptive and lacks resolution on its own to determine whether a functional consequence is seen when recruitment is disrupted. However, it is an excellent approach for describing with high confidence

We not only repeated our initial analysis for comparison of WRN interaction networks between control and 1-hour treatment with CPT, but also extended the time course of treatment to later stages of 6 and 12 hours, to generate a qualitative description of dynamics of protein association with WRN. This analysis was aimed at testing two hypotheses:

1) Proteins that are known to participate in protein complexes will associate or dissociate from their common target (WRN) in concert. For example, DNA end-binding proteins Ku70/86 are likely to have parallel increase or decrease in binding to WRN.
2) Proteins that may not necessarily bind to each other, but which are known to participate in distinct time points of DNA damage response and play specific roles (sensors, signal transducers, mediators, or repair proteins), may associate with WRN in concert due to their time-dependent recruitment to DNA lesions.

To test the first hypothesis, we asked whether the proteins that clustered into similar patterns of association with WRN (Figure 5.5) have been previously shown to interact (Figure 5.6). We have to be careful to draw too many conclusions, as our initial input was derived from proteins that were shown to interact (Figures 4.12-4.16), but overall we can state that we observe a certain level of connectivity between members of the same cluster, which raises the

possibility that many of them may interact with WRN in concerted manner. A few of the analyzed proteins are known to form stable complexes, such as the Ku heterodimer XRCC5/XRCC6, and members of the NuRD complex, and indeed these proteins show similar patterns of association with WRN as a function of time, as shown in Figures 5.7 and 5.8, respectively, and discussed at length in Chapter 5, Discussion. Interestingly, NuRD component MBD3 shows a deviant pattern from the rest of the members of the NuRD complex, which warrants further examination.

To test the second hypothesis we refer to the previous reports describing DDR, and participation of a number of protein factors as sensors, mediators and effectors (173,178,248,249). Proteins RPA1, γ-H2AX and the MRN complex are some of the the earliest responders to DSBs. Our analysis shows limited association of WRN with MRE11 and NBN as a function of time, and a strong increase of association with RPA1 and H2AX. Our analysis for phosphopeptide enrichment has also detected γ-H2AX peptide containing the key Ser139 phosphorylation in WRN AP sample that was treated with CPT for 6 hours. We can therefore state that WRN physically interacts with proteins involved in earliest stage of DDR, but these data are insufficient to determine whether WRN plays a functional role here. Abrogation of interaction with any of these proteins should help determine whether the interaction itself is important for proper resolution of the DNA damage.

It is known that WRN is a phosphorylation target of DDR transducers ATM, ATR and PRKDC (129,245), and we detect a strong interaction between WRN and PRKDC as a function of time. A recent report identified Ser440 and Ser467 as phosphorylation targets of PRKDC, and as important players in DDR to etoposide treatment (245). Our phosphopeptide analysis identifies WRN phosphorylation on both of these sites with high confidence. Although

we did not detect ATM or ATR in our analysis, the phosphopeptide analysis detected CPT-dependent phosphorylation on ATM sites Ser1058 and Ser1141, among others. This data is discussed in Section 1 of Chapter 6.

The mediators of DDR include proteins TP53BP1, BRCA1, and MDC1. Interaction between WRN and MDC1 was previously predicted after analysis of phosphopeptide affinity by tandem BRCT domains on MDC1 (131), but a direct physical interaction has not been previously reported. We detected MDC1 in our profiling analysis strongly enriched in CPT-treated sample over nLacZ control (SAINT score 0.864) although it fell just under our SAINT score cut-off of 0.9. Based on our selection of targets for SRM analysis using CompGO and STRING (detailed in Chapter 4) we developed the method for SRM validation. We showed the pattern of interaction between WRN and MDC1, and we detected a number of phosphorylated MDC1 peptides in our phosphopeptide analysis. NuRD components CHD4, MTA2 and MBD3 were recently shown to localize to DSBs as early as MDC1, suggesting that they may also act early in DDR (177). In agreement with this data, we also see association of WRN with these proteins. Interaction with CHD4 was previously detected in a MS screen (111), while interaction with other components of the NuRD has not been reported. Pattern of association of WRN with MDC1, CHD4, RBBP4 and MTA2 is nearly parallel, while MBD3 is very different (Figures 5.8 and 5.10). We conclude that WRN preferentially associates with DDR mediators MDC1, CHD4, RBBP4 and MTA2 as part of an early response to DSBs. The association is elevated over control treatment 1 hour after exposure to CPT, then decreased at 6 hours after treatment, and a strongly increased after 12 hours (Figures 5.8 and 5.10) .

Phosphorylated peptides from both, MDC1 and H2AX are found in our phosphopeptide enrichment analysis. While γ-H2AX is not thought to have a direct impact on nucleosome

spacing, it serves as the nucleating factor for propagation of chromatin alteration in areas flanking DSBs. Identification of phosphorylated peptides from these proteins, which are known to physically interact in response to DNA damage, is intriguing, and warrants further research.

It was recently shown that rate of repair of DSBs correlates to complexity of the chromatin in which they occur. More specifically, heterochromatic regions are associated with slower rates of DSB repair, than euchromatic ones, and ATM is required for repair with heterochromatin (173,250). Protein TRIM28 (also KAP-1, TIF1β, KRIP1) is a transcriptional repressor and an ATM target. It was recently shown that phosphorylation at Ser473 is essential for its function in DNA repair and apoptosis (251), and phosphorylation at Ser824 is essential for its role in chromatin condensation, DNA repair, and regulation of gene expression (252,253). We detect phosphorylation of both of these sites in WRN-associated sample in response to CPT treatment for 6 hours.TRIM28 was recently found to be the key regulator of chromatin structure responsible for generation and maintenance of PML (promyelocytic leukemia) nuclear bodies. Depletion of TRIM28 resulted in reduction of chromatin density, and reduced generation of PML nuclear bodies in response to etoposide treatment (254). TRIM28 was been previously shown to intact with WRNIP1 (255), but not WRN. We detected TRIM28 with a high number of spectral counts, but no enrichment over control nLacZ in our profiling analysis. This may be due to its high abundance. Further validation with SRM showed a large increase in its association with WRN following treatment with CPT for 1 hour (Figure 5.4). Unfortunately, we lack data for description of its association with WRN over the extended course of treatment with CPT. Its role in response to DNA damage by TOP1 poisons and association with γ-H2AX makes it an important target for future research.

The importance of WRN lies not only in the organismal manifestation of its absence, and resulting progeria, but also in its role in cancer. Epigenetic inactivation by methylation of CpG islands in the WRN gene promoter was found in epithelial and mesenchymal cancers, and specific WRN SNPs have been correlated with breast cancer incidence (256–258). Loss of WRN is likely to sensitize cancer cells to chemotherapeutic intervention, and screening for other sensitizing mutations will have a valuable impact on future therapies.

Section 3: We identify the next steps in this research, focusing on proteins of highest interest

We identify WRN-interacting proteins, which may collaborate with WRN in DNA damage response and resolution of damage by CPT, and newly identify a subset of proteins that control chromatin architecture. Many of these proteins work by regulating chromatin compaction and maintaining heterchromatic regions. Double depletion of WRN and any of these proteins, followed by treatment with drugs that affect DNA architecture could reveal cooperation and synthetic lethality. Genotoxic agents such as *cis*-Pt, CPT, and HDAC inhibitors appear the most promising agents for challenge experiments. We used SRM and replicate analysis as an orthogonal method of determining whether interactions proposed in the DDA analysis are real, and can be detected repeatedly, with different methods.We have completed the task of presenting a descriptive proteomic dataset of WRN interacting proteins, and our data can be used to generate hypotheses for further studies using proteomic or genetic approaches, as described in more detail further in this section.

Profiling analysis of cells grown in a dish represents an average of all the cells, and all activities that this population is involved in. The multitude of functions that WRN appears to perform in cells strongly suggests that it is recruited to multiple complexes depending on the function that it is required. If indeed this protein occurs in different complexes, at any time when an analysis is performed, we will detect the interacting proteins that occur in the majority of the complexes because they will be detected foremost by the mass spectrometer. Even if the proteins participating in the minority of the complexes are detected, they will be detected at lower overall intensity, with fewer peptides, and will be less likely to get fragmented for sequencing and identification. For this reason, analysis of individual complexes would provide a more accurate description of individual functions performed by WRN. Separation of chromatin-bound versus free complexes and analysis of different molecular complexes by size-based fractionation would increase resolution of individual WRN complexes.

MDC1.

In response to DSB formation, kinase ATM phosphorylates histone H2AX at Ser139 (detected in our phosphopeptide enrichment analysis after treatment with CPT), and this phosphorylation recruits MDC1 to the damaged DNA. Both HR and NHEJ repair pathways require initial recruitment of MDC1 to DSBs (259). MDC1 directly binds to γ-H2AX via BRCT domain, and is also a target of ATM (178,179). MDC1 is then phosphorylated, and serves as a platform for recruitment of a number of downstream effectors. We show that interaction between WRN and MDC1 is detected by SRM, and changes as a function of treatment with CPT, but no other evidence of a direct interaction between these proteins has been previously reported.

- Validate WRN-MDC1 interaction by western blotting and anti-MDC1 immunoprecipitation. I attempted a number of western blots using an anti-MDC1 antibody (Millipore, clone P2B11, cat. # 05-1572), but was not able to detect it in whole cell extracts or anti-WRN AP samples. A different antibody may work better.

WRN protein was predicted to have affinity for the BRCT domain (131). The WRN peptide that was predicted to have the affinity for MDC1, EFTG**S**IVYSY [48,57], maps to WRN exonuclease domain, which spans amino acids 38-236. Monnat lab has previously generated a number of domain-deleted cell lines in the si-resistant SH-tag vector (Tang W, Hoang S, Lauper J, unpublished data), which should be used to test whether deletion of this domain abrogates interaction with MDC1. Preliminary analysis for localization of domain-deleted mutants reveals that ExoΔ SH-WRN localizes in a focal, sub-nuclear pattern as WRN (See Figure 6.5). Whether it relocalizes in response to DNA damage is yet to be determined.

- ExoΔ SH-WRN should be used to determine whether WRN-MDC1 interaction is abrogated by deletion of the WRN Exonuclease domain, as predicted by Rodriguez et al.

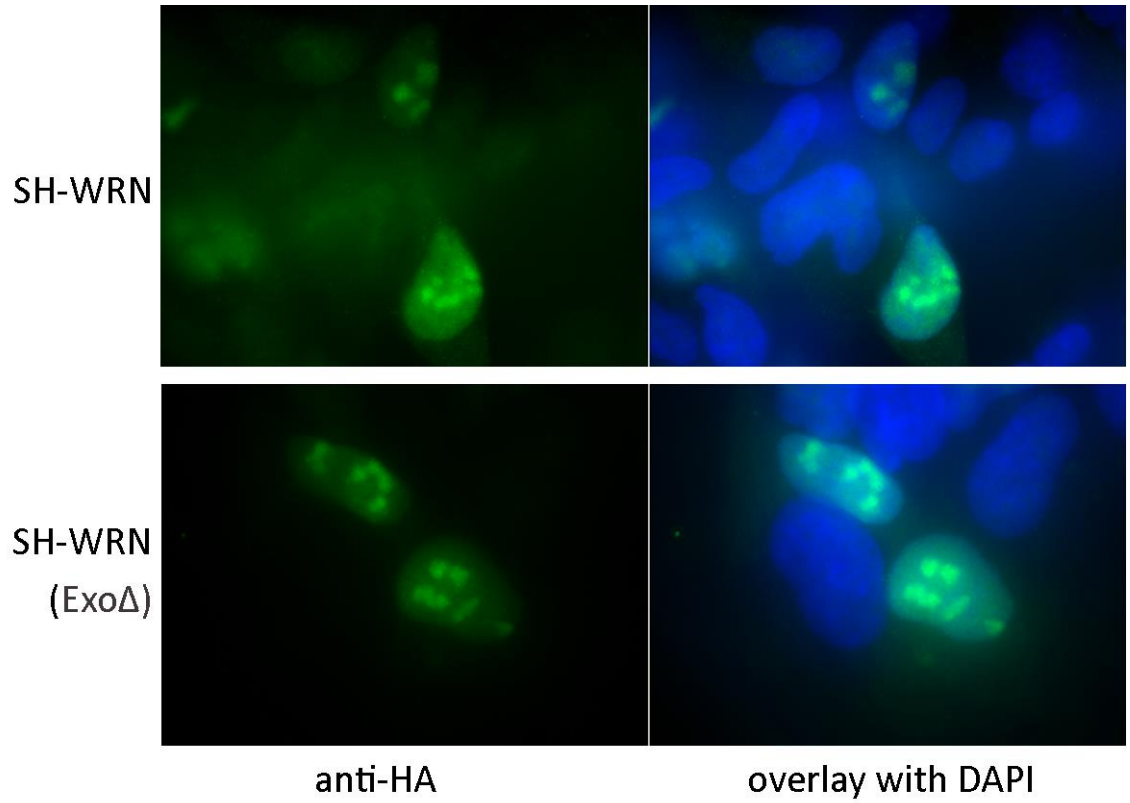

Figure 6.5: Preliminary results of localization analysis of domain-deleted WRN cells. Figure shows that SH-tagged ExoΔ **WRN protein localizes to subnuclear foci identically to SH-tagged wild type WRN.**

Phosphorylation by ATM regulates DDR activity of both, WRN and MDC1 (129,178,179,260). Monnat lab has previously generated a number of cells lines with abolishing or phosphomimetic mutations in ATM- and ATR-phosphorylatable sites in the si-resistant SH-tag vector (Tang W, Hoang S, Lauper J, unpublished data), which should be used to test whether phosphorylation of WRN at ATM sites has an effect on its interaction interaction with MDC1. Although these sites are not at the predicted interaction domain with MDC1, they may help establish a functional link between these proteins, or answer the question of whether phosphorylation of both is necessary for effective DSB repair.

- Use ATM phosphosite mutants (phospho-null and phospho-mimetic) to determine whether phosphorylation of WRN by ATM is necessary for interaction with MDC1.

Cells deficient in DNA DSB repair by HR tend to be highly sensitive to chemical inhibitors of PARP (191–193,261,262). Cells depleted of WRN are sensitive to PARP inhibitors (194,195), and depletion of MDC1 demethylating enzyme JMJD1C results in acquired resistance to PARP inhibitors (263). This resistance has a direct clinical implication – a screen of 58 invasive human breast carcinomas determined a loss of JMJD1C in 26% of cases (263).

- Use cells double-depleted of MDC1 and WRN to test sensitivity to PARP inhibitors. Extent of sensitivity will help determine whether these proteins act synergistically, or if one of them is more dominant in determining the outcome of exposure.

TRIM28.

Protein TRIM28 acts in DDR by enacting chromatin condensation and regulating gene expression and apoptosis (251–253). Phosphorylation of this protein by kinases ATM and ATR is essential for its function, and two phosphorylation sites have been identified: Ser473 and Ser824. We have determined that TRIM28 increases in association with WRN after 1 hour treatment with CPT, and the extent of this association is higher than all other protein assayed, except H2AX (Figure 5.4). Unfortunately, we lack interaction data on the extended time course of CPT exposure. In a single experiment we measured the association of WRN with TRIM28 after 6 and 12 hours of CPT treatment, and the trend shows a decrease. It is possible that the binding between these proteins initially increases after drug treatment, and then decreases over time.

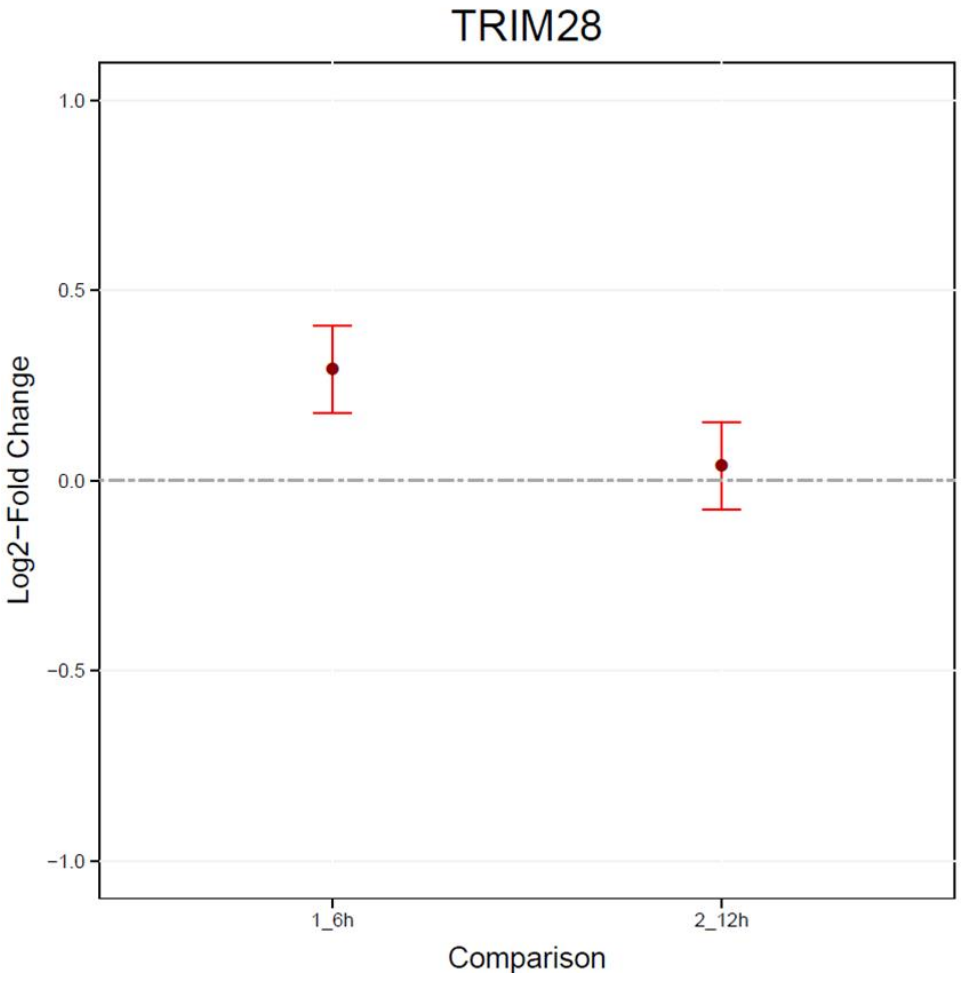

Figure 6.6: MSstats results of change in association between WRN and TRIM28 as a function of treatment with CPT. Values correspond to ratios between peak areas detected for protein TRIM28 at 6 and 12 hours after CPT application compared to peak area for protein after treatment with DMSO.

- Time course of association should be tested either by SRM (methods available), or by immunologic approach. TRIM28 was previously shown to intact with WRNIP1 (255), but not WRN. Therefore, simultaneous detection of WRNIP should be sought.
- Detection between these proteins has not been previously reported. Further determination of interaction site can be done by AP experiments using WRN domain deletion mutants.

Endogenous WRN localizes to nucleoli and nuclear PML bodies (143,264), and TRIM28 is a key regulator of chromatin structure responsible for generation and maintenance of PML bodies. Depletion of TRIM28 resulted in reduction of chromatin density and reduced generation of PML nuclear bodies in response to etoposide treatment (254).

- Immunofluorescence experiment to check co-localization of these proteins after treatment with CPT or etoposide should be performed. IF can be used to determine whether depletion of TRIM28 affects its localization to PML bodies.

CHD4.

CHD4 is the catalytic core of the NuRD complex, which functions in transcriptional regulation and chromatin remodeling. Depletion of CHD4 causes defective HR and mitotic progression, and imparts sensitivity to PARP inhibitors (188–190), and WRN-depleted cells have also shown this sensitivity (194,195).

- Use cells double-depleted of CHD4 and WRN to test sensitivity to PARP inhibitors and synthetic lethality. Extent of sensitivity will help determine whether these proteins act synergistically, or if one of them is more dominant in determining the outcome of exposure.
- PARP inhibitors have been shown to achieve additional sensitization when used in combination with methylating agents and TOP1 poisons (197,198). Cells depleted of CHD4 and WRN together should be exposed to camptothecin to determine whether sensitivity is increased in case of double depletion.

Endogenous WRN localizes to nucleoli and nuclear PML bodies (143,264), CHD4 and MBD3 localize in nucleoli, and CHD4 specifically associates with rDNA (265). Although CHD4 rapidly binds γ-H2AX following exposure to IR (177,266), it has not been shown whether induction of damage causes relocalization of CHD4 to nucleoplasm in a manner reminiscent of WRN.

- Immunofluorescence experiment to check co-localization of these proteins after treatment with CPT or etoposide should be performed. IF can be used to determine whether depletion of CHD4 affects localization of WRN and vice versa.

Notes to Chapter 6

Figures 6.1 and 6.4 were generated with the help from Alden Hackmann.

Jarrett Egertson executed MSstats in command line.

Danielle Swaney performed IMAC enrichment of phosphorylated peptides and collected MS data on enriched samples.

List of References

1. Goto M. Hierarchical deterioration of body systems in Werner's syndrome: implications for normal ageing. Mech Ageing Dev. 1997;98(3):239–54.

2. Lauper JM, Krause A, Vaughan TL, Monnat RJ. Spectrum and Risk of Neoplasia in Werner Syndrome: A Systematic Review. Burk RD, editor. PLoS ONE. 2013 Apr 1;8(4):e59709.

3. Moser MJ, Bigbee WL, Grant SG, Emond MJ, Langlois RG, Jensen RH, et al. Genetic instability and hematologic disease risk in Werner syndrome patients and heterozygotes. Cancer Res. 2000;60(9):2492–6.

4. Brosh RM, Bohr VA. Roles of the Werner syndrome protein in pathways required for maintenance of genome stability. Exp Gerontol. 2002;37(4):491–506.

5. Perry JJP, Yannone SM, Holden LG, Hitomi C, Asaithamby A, Han S, et al. WRN exonuclease structure and molecular mechanism imply an editing role in DNA end processing. Nat Struct 38 Mol Biol. 2006 Apr 23;13(5):414–22.

6. Shen J-C, Loeb LA. The Werner syndrome gene: the molecular basis of RecQ helicase-deficiency diseases. Trends Genet. 2000;16(5):213–20.

7. Saintigny Y, Makienko K, Swanson C, Emond MJ, Monnat RJ. Homologous Recombination Resolution Defect in Werner Syndrome. Mol Cell Biol. 2002 Oct 15;22(20):6971–8.

8. Yu CE, Oshima J, Fu YH, Wijsman EM, Hisama F, Alisch R, et al. Positional cloning of the Werner's syndrome gene. Science. 1996 Apr 12;272(5259):258–62.

9. Hickson ID. RecQ helicases: caretakers of the genome. Nat Rev Cancer. 2003 Mar;3(3):169–78.

10. Puranam KL, Blackshear PJ. Cloning and characterization of RECQL, a potential human homologue of the Escherichia coli DNA helicase RecQ. J Biol Chem. 1994 Nov 25;269(47):29838–45.

11. Johnson DS, Bai L, Smith BY, Patel SS, Wang MD. Single-molecule studies reveal dynamics of DNA unwinding by the ring-shaped T7 helicase. Cell. 2007 Jun 29;129(7):1299–309.

12. Sidorova JM, Li N, Folch A, Monnat RJ Jr. The RecQ helicase WRN is required for normal replication fork progression after DNA damage or replication fork arrest. Cell Cycle Georget Tex. 2008 Mar 15;7(6):796–807.

13. Davies SL, North PS, Hickson ID. Role for BLM in replication-fork restart and suppression of origin firing after replicative stress. Nat Struct Mol Biol. 2007 Jul;14(7):677–9.

14. Bernstein DA, Keck JL. Domain mapping of Escherichia coli RecQ defines the roles of conserved N- and C-terminal regions in the RecQ family. Nucleic Acids Res. 2003 Jun 1;31(11):2778–85.

15. Von Kobbe C, Bohr VA. A nucleolar targeting sequence in the Werner syndrome protein resides within residues 949-1092. J Cell Sci. 2002 Oct 15;115(Pt 20):3901–7.

16. Morozov V, Mushegian AR, Koonin EV, Bork P. A putative nucleic acid-binding domain in Bloom's and Werner's syndrome helicases. Trends Biochem Sci. 1997 Nov;22(11):417–8.

17. Liu Z, Macias MJ, Bottomley MJ, Stier G, Linge JP, Nilges M, et al. The three-dimensional structure of the HRDC domain and implications for the Werner and Bloom syndrome proteins. Struct Lond Engl 1993. 1999 Dec 15;7(12):1557–66.

18. Liu JL, Rigolet P, Dou S-X, Wang P-Y, Xi XG. The zinc finger motif of Escherichia coli RecQ is implicated in both DNA binding and protein folding. J Biol Chem. 2004 Oct 8;279(41):42794–802.

19. Choi JM, Kang SY, Bae WJ, Jin KS, Ree M, Cho Y. Probing the roles of active site residues in the 3'-5' exonuclease of the Werner syndrome protein. J Biol Chem. 2007 Mar 30;282(13):9941–51.

20. Huang S, Beresten S, Li B, Oshima J, Ellis NA, Campisi J. Characterization of the human and mouse WRN 3'-->5' exonuclease. Nucleic Acids Res. 2000 Jun 15;28(12):2396–405.

21. Compton SA, Tolun G, Kamath-Loeb AS, Loeb LA, Griffith JD. The Werner syndrome protein binds replication fork and holliday junction DNAs as an oligomer. J Biol Chem. 2008 Sep 5;283(36):24478–83.

22. Lees-Miller SP, Meek K. Repair of DNA double strand breaks by non-homologous end joining. Biochimie. 2003 Nov;85(11):1161–73.

23. Smith GC, Divecha N, Lakin ND, Jackson SP. DNA-dependent protein kinase and related proteins. Biochem Soc Symp. 1999;64:91–104.

24. Chen L, Huang S, Lee L, Davalos A, Schiestl RH, Campisi J, et al. WRN, the protein deficient in Werner syndrome, plays a critical structural role in optimizing DNA repair. Aging Cell. 2003 Aug;2(4):191–9.

25. Cooper MP, Machwe A, Orren DK, Brosh RM, Ramsden D, Bohr VA. Ku complex interacts with and stimulates the Werner protein. Genes Dev. 2000 Apr 15;14(8):907–12.

26. Aggarwal M, Banerjee T, Sommers JA, Iannascoli C, Pichierri P, Shoemaker RH, et al. Werner syndrome helicase has a critical role in DNA damage responses in the absence of a functional fanconi anemia pathway. Cancer Res. 2013 Sep 1;73(17):5497–507.

27. Cheng W-H, Kusumoto R, Opresko PL, Sui X, Huang S, Nicolette ML, et al. Collaboration of Werner syndrome protein and BRCA1 in cellular responses to DNA interstrand cross-links. Nucleic Acids Res. 2006;34(9):2751–60.

28. Prince PR, Emond MJ, Monnat RJ Jr. Loss of Werner syndrome protein function promotes aberrant mitotic recombination. Genes Dev. 2001 Apr 15;15(8):933–8.

29. Swanson C, Saintigny Y, Emond MJ, Monnat RJ Jr. The Werner syndrome protein has separable recombination and survival functions. DNA Repair. 2004 May 4;3(5):475–82.

30. Poot M, Gollahon KA, Emond MJ, Silber JR, Rabinovitch PS. Werner syndrome diploid fibroblasts are sensitive to 4-nitroquinoline-N-oxide and 8-methoxypsoralen: implications for the disease phenotype. FASEB J [Internet]. 2002 Mar 12 [cited 2014 Feb 26]; Available from: http://www.fasebj.org/content/early/2002/05/02/fj.01-0906fje

31. Poot M, Yom JS, Whang SH, Kato JT, Gollahon KA, Rabinovitch PS. Werner syndrome cells are sensitive to DNA cross-linking drugs. FASEB J [Internet]. 2001 Mar 5 [cited 2014 Feb 26]; Available from: http://www.fasebj.org/content/early/2001/05/02/fj.00-0611fje

32. Pichierri P, Franchitto A, Mosesso P, Palitti F. Werner's syndrome cell lines are hypersensitive to camptothecin-induced chromosomal damage. Mutat Res. 2000 Nov 30;456(1-2):45–57.

33. Poot M, Gollahon KA, Rabinovitch PS. Werner syndrome lymphoblastoid cells are sensitive to camptothecin-induced apoptosis in S-phase. Hum Genet. 1999 Jan;104(1):10–4.

34. Petermann E, Helleday T. Pathways of mammalian replication fork restart. Nat Rev Mol Cell Biol. 2010 Oct;11(10):683–7.

35. Sidorova JM, Kehrli K, Mao F, Monnat R Jr. Distinct functions of human RECQ helicases WRN and BLM in replication fork recovery and progression after hydroxyurea-induced stalling. DNA Repair. 2013 Feb 1;12(2):128–39.

36. Chakraverty RK, Hickson ID. Defending genome integrity during DNA replication: a proposed role for RecQ family helicases. BioEssays News Rev Mol Cell Dev Biol. 1999 Apr;21(4):286–94.

37. Fenn JB, Mann M, Meng CK, Wong SF, Whitehouse CM. Electrospray ionization for mass spectrometry of large biomolecules. Science. 1989 Oct 6;246(4926):64–71.

38. Karas M, Bachmann D, Hillenkamp F. Influence of the wavelength in high-irradiance ultraviolet laser desorption mass spectrometry of organic molecules. Anal Chem. 1985 Dec 1;57(14):2935–9.

39. Karas M, Bachmann D, Bahr U, Hillenkamp F. Matrix-assisted ultraviolet laser desorption of non-volatile compounds. Int J Mass Spectrom Ion Process. 1987 Sep 24;78:53–68.

40. Sheng S, Skalnikova H, Meng A, Tra J, Fu Q, Everett A, et al. Intact protein separation by one- and two-dimensional liquid chromatography for the comparative proteomic separation of partitioned serum or plasma. Methods Mol Biol Clifton NJ. 2011;728:29–46.

41. Imoto T, Yamada H. Peptide separation by reversed-phase high-performance liquid chromatography. Mol Cell Biochem. 1983;51(2):111–21.

42. Wysocki VH, Resing KA, Zhang Q, Cheng G. Mass spectrometry of peptides and proteins. Methods San Diego Calif. 2005 Mar;35(3):211–22.

43. Delahunty CM, Yates JR 3rd. MudPIT: multidimensional protein identification technology. BioTechniques. 2007 Nov;43(5):563, 565, 567 passim.

44. Link AJ, Eng J, Schieltz DM, Carmack E, Mize GJ, Morris DR, et al. Direct analysis of protein complexes using mass spectrometry. Nat Biotechnol. 1999 Jul;17(7):676–82.

45. Wang H, Clouthier SG, Galchev V, Misek DE, Duffner U, Min C-K, et al. Intact-protein-based high-resolution three-dimensional quantitative analysis system for proteome profiling of biological fluids. Mol Cell Proteomics MCP. 2005 May;4(5):618–25.

46. Eng JK, McCormack AL, Yates JR. An approach to correlate tandem mass spectral data of peptides with amino acid sequences in a protein database. J Am Soc Mass Spectrom. 1994 Nov;5(11):976–89.

47. Dunham WH, Mullin M, Gingras A-C. Affinity-purification coupled to mass spectrometry: basic principles and strategies. Proteomics. 2012 May;12(10):1576–90.

48. Miteva YV, Budayeva HG, Cristea IM. Proteomics-Based Methods for Discovery, Quantification, and Validation of Protein–Protein Interactions. Anal Chem. 2013 Jan 15;85(2):749–68.

49. Angers S, Li T, Yi X, MacCoss MJ, Moon RT, Zheng N. Molecular architecture and assembly of the DDB1-CUL4A ubiquitin ligase machinery. Nature. 2006 Oct 5;443(7111):590–3.

50. Angers S, Thorpe CJ, Biechele TL, Goldenberg SJ, Zheng N, MacCoss MJ, et al. The KLHL12-Cullin-3 ubiquitin ligase negatively regulates the Wnt-beta-catenin pathway by targeting Dishevelled for degradation. Nat Cell Biol. 2006 Apr;8(4):348–57.

51. Wepf A, Glatter T, Schmidt A, Aebersold R, Gstaiger M. Quantitative interaction proteomics using mass spectrometry. Nat Methods. 2009 Mar;6(3):203–5.

52. Gavin A-C, Bösche M, Krause R, Grandi P, Marzioch M, Bauer A, et al. Functional organization of the yeast proteome by systematic analysis of protein complexes. Nature. 2002 Jan 10;415(6868):141–7.

53. Puig O, Caspary F, Rigaut G, Rutz B, Bouveret E, Bragado-Nilsson E, et al. The tandem affinity purification (TAP) method: a general procedure of protein complex purification. Methods San Diego Calif. 2001 Jul;24(3):218–29.

54. Choi H, Larsen B, Lin Z-Y, Breitkreutz A, Mellacheruvu D, Fermin D, et al. SAINT: probabilistic scoring of affinity purification-mass spectrometry data. Nat Methods. 2011 Jan;8(1):70–3.

55. Le Gallo M, O'Hara AJ, Rudd ML, Urick ME, Hansen NF, O'Neil NJ, et al. Exome sequencing of serous endometrial tumors identifies recurrent somatic mutations in chromatin-remodeling and ubiquitin ligase complex genes. Nat Genet. 2012 Dec;44(12):1310–5.

56. Hansen M, Ao-Lin Hsu, Dillin A, Kenyon C, Kim S. New Genes Tied to Endocrine, Metabolic, and Dietary Regulation of Lifespan from a Caenorhabditis elegans Genomic RNAi Screen. PLoS Genet. 2005 Jul;1(1):119–28.

57. Lord CJ, Martin SA, Ashworth A. RNA interference screening demystified. J Clin Pathol. 2009 Mar;62(3):195–200.

58. Mohr S, Bakal C, Perrimon N. Genomic screening with RNAi: results and challenges. Annu Rev Biochem. 2010;79:37–64.

59. Mullenders J, Bernards R. Loss-of-function genetic screens as a tool to improve the diagnosis and treatment of cancer. Oncogene. 2009 Dec 17;28(50):4409–20.

60. Echeverri CJ, Beachy PA, Baum B, Boutros M, Buchholz F, Chanda SK, et al. Minimizing the risk of reporting false positives in large-scale RNAi screens. Nat Methods. 2006 Oct;3(10):777–9.

61. Williams DK, Muddiman DC. Absolute quantification of C-reactive protein in human plasma derived from patients with epithelial ovarian cancer utilizing protein cleavage isotope dilution mass spectrometry. J Proteome Res. 2009 Feb;8(2):1085–90.

62. Anderson L, Hunter CL. Quantitative mass spectrometric multiple reaction monitoring assays for major plasma proteins. Mol Cell Proteomics MCP. 2006 Apr;5(4):573–88.

63. Picotti P, Aebersold R, Domon B. The implications of proteolytic background for shotgun proteomics. Mol Cell Proteomics MCP. 2007 Sep;6(9):1589–98.

64. Picotti P, Bodenmiller B, Mueller LN, Domon B, Aebersold R. Full dynamic range proteome analysis of S. cerevisiae by targeted proteomics. Cell. 2009 Aug 21;138(4):795–806.

65. Stahl-Zeng J, Lange V, Ossola R, Eckhardt K, Krek W, Aebersold R, et al. High sensitivity detection of plasma proteins by multiple reaction monitoring of N-glycosites. Mol Cell Proteomics MCP. 2007 Oct;6(10):1809–17.

66. Domon B, Aebersold R. Options and considerations when selecting a quantitative proteomics strategy. Nat Biotechnol. 2010 Jul;28(7):710–21.

67. Collavin L, Lunardi A, Del Sal G. p53-family proteins and their regulators: hubs and spokes in tumor suppression. Cell Death Differ. 2010 Jun;17(6):901–11.

68. Hollstein M, Hainaut P. Massively regulated genes: the example of TP53. J Pathol. 2010 Jan;220(2):164–73.

69. Chen PS, Stumm-Zollinger E, Aigaki T, Balmer J, Bienz M, Böhlen P. A male accessory gland peptide that regulates reproductive behavior of female D. melanogaster. Cell. 1988 Jul 29;54(3):291–8.

70. Wagstaff BJ, Begun DJ. Comparative genomics of accessory gland protein genes in Drosophila melanogaster and D. pseudoobscura. Mol Biol Evol. 2005 Apr;22(4):818–32.

71. Peng J, Chen S, Büsser S, Liu H, Honegger T, Kubli E. Gradual release of sperm bound sex-peptide controls female postmating behavior in Drosophila. Curr Biol CB. 2005 Feb 8;15(3):207–13.

72. Monnat RJ Jr, Saintigny Y. Werner syndrome protein--unwinding function to explain disease. Sci Aging Knowl Environ SAGE KE. 2004 Mar 31;2004(13):re3.

73. Moser MJ, Kamath-Loeb AS, Jacob JE, Bennett SE, Oshima J, Monnat RJ Jr. WRN helicase expression in Werner syndrome cell lines. Nucleic Acids Res. 2000 Jan 15;28(2):648–54.

74. Beck M, Schmidt A, Malmstroem J, Claassen M, Ori A, Szymborska A, et al. The quantitative proteome of a human cell line. Mol Syst Biol. 2011;7:549.

75. Dietzl G, Chen D, Schnorrer F, Su K-C, Barinova Y, Fellner M, et al. A genome-wide transgenic RNAi library for conditional gene inactivation in Drosophila. Nature. 2007 Jul 12;448(7150):151–6.

76. Ram KR, Wolfner MF. Sustained post-mating response in Drosophila melanogaster requires multiple seminal fluid proteins. PLoS Genet. 2007 Dec;3(12):e238.

77. Findlay GD, Yi X, Maccoss MJ, Swanson WJ. Proteomics reveals novel Drosophila seminal fluid proteins transferred at mating. PLoS Biol. 2008 Jul 29;6(7):e178.

78. Mao FJ, Sidorova JM, Lauper JM, Emond MJ, Monnat RJ. The Human WRN and BLM RecQ Helicases Differentially Regulate Cell Proliferation and Survival after Chemotherapeutic DNA Damage. Cancer Res. 2010 Aug 15;70(16):6548–55.

79. MacLean B, Tomazela DM, Shulman N, Chambers M, Finney GL, Frewen B, et al. Skyline: an open source document editor for creating and analyzing targeted proteomics experiments. Bioinforma Oxf Engl. 2010 Apr 1;26(7):966–8.

80. Bereman MS, MacLean B, Tomazela DM, Liebler DC, MacCoss MJ. The development of selected reaction monitoring methods for targeted proteomics via empirical refinement. Proteomics. 2012 Apr;12(8):1134–41.

81. Stein S, Rudnick P. NIST Peptide Tandem Mass Spectral Libraries. Human Peptide Mass Spectral Reference Data, H. sapiens, ion trap, Official Build Date: Feb. 4, 2009. Gathersburg, MD 20899: National Institute of Standards and Technology; 2009.

82. Aagaard JE, Yi X, MacCoss MJ, Swanson WJ. Rapidly evolving zona pellucida domain proteins are a major component of the vitelline envelope of abalone eggs. Proc Natl Acad Sci U S A. 2006 Nov 14;103(46):17302–7.

83. Ram KR, Wolfner MF. A network of interactions among seminal proteins underlies the long-term postmating response in Drosophila. Proc Natl Acad Sci U S A. 2009 Sep 8;106(36):15384–9.

84. Hoofnagle AN, Becker JO, Oda MN, Cavigiolio G, Mayer P, Vaisar T. Multiple-reaction monitoring-mass spectrometric assays can accurately measure the relative protein abundance in complex mixtures. Clin Chem. 2012 Apr;58(4):777–81.

85. Brönstrup M. Absolute quantification strategies in proteomics based on mass spectrometry. Expert Rev Proteomics. 2004 Dec;1(4):503–12.

86. Monnat RJ. Human RECQ helicases: Roles in DNA metabolism, mutagenesis and cancer biology. Semin Cancer Biol. 2010 Oct;20(5):329–39.

87. Gray MD, Shen JC, Kamath-Loeb AS, Blank A, Sopher BL, Martin GM, et al. The Werner syndrome protein is a DNA helicase. Nat Genet. 1997 Sep;17(1):100–3.

88. Bukowy Z, Harrigan JA, Ramsden DA, Tudek B, Bohr VA, Stevnsner T. WRN Exonuclease activity is blocked by specific oxidatively induced base lesions positioned in either DNA strand. Nucleic Acids Res. 2008 Sep;36(15):4975–87.

89. Oikawa S, Hirosawa I, Hirakawa K, Kawanishi S. Site specificity and mechanism of oxidative DNA damage induced by carcinogenic catechol. Carcinogenesis. 2001 Aug;22(8):1239–45.

90. Oikawa S, Hiraku Y, Fujiwara T, Saito I, Kawanishi S. Site-specific hydroxylation at polyguanosine in double-stranded DNA by nickel(II) in the presence of SH compounds:

comparison with singlet oxygen-induced DNA damage. Chem Res Toxicol. 2002 Aug;15(8):1017–22.

91. Bartkova J, Horejsí Z, Koed K, Krämer A, Tort F, Zieger K, et al. DNA damage response as a candidate anti-cancer barrier in early human tumorigenesis. Nature. 2005 Apr 14;434(7035):864–70.

92. Downs JA, Nussenzweig MC, Nussenzweig A. Chromatin dynamics and the preservation of genetic information. Nature. 2007 Jun 21;447(7147):951–8.

93. Jasin M. Homologous repair of DNA damage and tumorigenesis: the BRCA connection. Oncogene. 2002 Dec 16;21(58):8981–93.

94. Pommier Y. Topoisomerase I inhibitors: camptothecins and beyond. Nat Rev Cancer. 2006 Oct;6(10):789–802.

95. Pommier Y. DNA topoisomerase I inhibitors: chemistry, biology, and interfacial inhibition. Chem Rev. 2009 Jul;109(7):2894–902.

96. Käll L, Canterbury JD, Weston J, Noble WS, MacCoss MJ. Semi-supervised learning for peptide identification from shotgun proteomics datasets. Nat Methods. 2007 Nov;4(11):923–5.

97. Zhang B, Chambers MC, Tabb DL. Proteomic parsimony through bipartite graph analysis improves accuracy and transparency. J Proteome Res. 2007 Sep;6(9):3549–57.

98. Sharma V, Eng JK, Maccoss MJ, Riffle M. A mass spectrometry proteomics data management platform. Mol Cell Proteomics MCP. 2012 Sep;11(9):824–31.

99. Griss J, Foster JM, Hermjakob H, Vizcaíno JA. PRIDE Cluster: building a consensus of proteomics data. Nat Methods. 2013 Feb;10(2):95–6.

100. Breitkreutz A, Choi H, Sharom JR, Boucher L, Neduva V, Larsen B, et al. A Global Protein Kinase and Phosphatase Interaction Network in Yeast. Science. 2010 May 20;328(5981):1043–6.

101. Skarra DV, Goudreault M, Choi H, Mullin M, Nesvizhskii AI, Gingras A-C, et al. Label-free quantitative proteomics and SAINT analysis enable interactome mapping for the human Ser/Thr protein phosphatase 5. Proteomics. 2011 Apr;11(8):1508–16.

102. Mellacheruvu D, Wright Z, Couzens AL, Lambert J-P, St-Denis NA, Li T, et al. The CRAPome: a contaminant repository for affinity purification-mass spectrometry data. Nat Methods. 2013 Aug;10(8):730–6.

103. Riffle M, Malmström L, Davis TN. The Yeast Resource Center Public Data Repository. Nucleic Acids Res. 2005 Jan 1;33(Database issue):D378–382.

104. Franceschini A, Szklarczyk D, Frankild S, Kuhn M, Simonovic M, Roth A, et al. STRING v9.1: protein-protein interaction networks, with increased coverage and integration. Nucleic Acids Res. 2013 Jan;41(Database issue):D808–815.

105. Gray MD, Wang L, Youssoufian H, Martin GM, Oshima J. Werner helicase is localized to transcriptionally active nucleoli of cycling cells. Exp Cell Res. 1998 Aug 1;242(2):487–94.

106. Sakamoto S, Nishikawa K, Heo SJ, Goto M, Furuichi Y, Shimamoto A. Werner helicase relocates into nuclear foci in response to DNA damaging agents and co-localizes with RPA and Rad51. Genes Cells Devoted Mol Cell Mech. 2001 May;6(5):421–30.

107. Slupianek A, Poplawski T, Jozwiakowski SK, Cramer K, Pytel D, Stoczynska E, et al. BCR/ABL stimulates WRN to promote survival and genomic instability. Cancer Res. 2011 Feb 1;71(3):842–51.

108. Cheng W-H, von Kobbe C, Opresko PL, Fields KM, Ren J, Kufe D, et al. Werner syndrome protein phosphorylation by abl tyrosine kinase regulates its activity and distribution. Mol Cell Biol. 2003 Sep;23(18):6385–95.

109. Otterlei M, Bruheim P, Ahn B, Bussen W, Karmakar P, Baynton K, et al. Werner syndrome protein participates in a complex with RAD51, RAD54, RAD54B and ATR in response to ICL-induced replication arrest. J Cell Sci. 2006 Dec 15;119(Pt 24):5137–46.

110. Kim ST, Lim DS, Canman CE, Kastan MB. Substrate specificities and identification of putative substrates of ATM kinase family members. J Biol Chem. 1999 Dec 31;274(53):37538–43.

111. Lachapelle S, Gagné J-P, Garand C, Desbiens M, Coulombe Y, Bohr VA, et al. Proteome-wide identification of WRN-interacting proteins in untreated and nuclease-treated samples. J Proteome Res. 2011;10(3):1216–27.

112. Patro BS, Frohlich R, Bohr VA, Stevnsner T. WRN helicase regulates the ATR-CHK1-induced S-phase checkpoint pathway in response to topoisomerase-I-DNA covalent complexes. J Cell Sci. 2011 Dec 8;124(23):3967–79.

113. Von Kobbe C, Karmakar P, Dawut L, Opresko P, Zeng X, Brosh RM Jr, et al. Colocalization, physical, and functional interaction between Werner and Bloom syndrome proteins. J Biol Chem. 2002 Jun 14;277(24):22035–44.

114. Wu X, Ranganathan V, Weisman DS, Heine WF, Ciccone DN, O'Neill TB, et al. ATM phosphorylation of Nijmegen breakage syndrome protein is required in a DNA damage response. Nature. 2000 May 25;405(6785):477–82.

115. Zhang N, Kaur R, Lu X, Shen X, Li L, Legerski RJ. The Pso4 mRNA splicing and DNA repair complex interacts with WRN for processing of DNA interstrand cross-links. J Biol Chem. 2005 Dec 9;280(49):40559–67.

116. Woods YL, Xirodimas DP, Prescott AR, Sparks A, Lane DP, Saville MK. p14 Arf promotes small ubiquitin-like modifier conjugation of Werners helicase. J Biol Chem. 2004 Nov 26;279(48):50157–66.

117. Jiao R, Harrigan JA, Shevelev I, Dietschy T, Selak N, Indig FE, et al. The Werner syndrome protein is required for recruitment of chromatin assembly factor 1 following DNA damage. Oncogene. 2006;26(26):3811–22.

118. Jiao R, Harrigan JA, Shevelev I, Dietschy T, Selak N, Indig FE, et al. The Werner syndrome protein is required for recruitment of chromatin assembly factor 1 following DNA damage. Oncogene. 2007 May 31;26(26):3811–22.

119. Sand-Dejmek J, Adelmant G, Sobhian B, Calkins AS, Marto J, Iglehart DJ, et al. Concordant and opposite roles of DNA-PK and the “facilitator of chromatin transcription”(FACT) in DNA repair, apoptosis and necrosis after cisplatin. Mol Cancer. 2011;10:74.

120. Zhang S, Hemmerich P, Grosse F. Werner syndrome helicase (WRN), nuclear DNA helicase II (NDH II) and histone gammaH2AX are localized to the centrosome. Cell Biol Int. 2007 Oct;31(10):1109–21.

121. Friedemann J, Grosse F, Zhang S. Nuclear DNA helicase II (RNA helicase A) interacts with Werner syndrome helicase and stimulates its exonuclease activity. J Biol Chem. 2005 Sep 2;280(35):31303–13.

122. Aggarwal M, Sommers JA, Morris C, Brosh RM Jr. Delineation of WRN helicase function with EXO1 in the replicational stress response. DNA Repair. 2010 Jul 1;9(7):765–76.

123. Sharma S, Sommers JA, Wu L, Bohr VA, Hickson ID, Brosh RM Jr. Stimulation of flap endonuclease-1 by the Bloom’s syndrome protein. J Biol Chem. 2004 Mar 12;279(11):9847–56.

124. Brosh RM Jr, von Kobbe C, Sommers JA, Karmakar P, Opresko PL, Piotrowski J, et al. Werner syndrome protein interacts with human flap endonuclease 1 and stimulates its cleavage activity. EMBO J. 2001 Oct 15;20(20):5791–801.

125. Sharma S, Otterlei M, Sommers JA, Driscoll HC, Dianov GL, Kao H-I, et al. WRN helicase and FEN-1 form a complex upon replication arrest and together process branchmigrating DNA structures associated with the replication fork. Mol Biol Cell. 2004 Feb;15(2):734–50.

126. Sharma S, Sommers JA, Gary RK, Friedrich-Heineken E, Hübscher U, Brosh RM. The interaction site of Flap Endonuclease-1 with WRN helicase suggests a coordination of WRN and PCNA. Nucleic Acids Res. 2005 Jan 1;33(21):6769–81.

127. Tronnersjö S, Hanefalk C, Balciunas D, Hu G-Z, Nordberg N, Murén E, et al. The jmjN and jmjC domains of the yeast zinc finger protein Gis1 interact with 19 proteins involved in transcription, sumoylation and DNA repair. Mol Genet Genomics MGG. 2007 Jan;277(1):57–70.

128. Cheng W-H, Sakamoto S, Fox JT, Komatsu K, Carney J, Bohr VA. Werner syndrome protein associates with gamma H2AX in a manner that depends upon Nbs1. FEBS Lett. 2005 Feb 28;579(6):1350–6.

129. Ammazzalorso F, Pirzio LM, Bignami M, Franchitto A, Pichierri P. ATR and ATM differently regulate WRN to prevent DSBs at stalled replication forks and promote replication fork recovery. EMBO J. 2010 Sep 15;29(18):3156–69.

130. Fritsch O, Burkhalter MD, Kais S, Sogo JM, Schär P. DNA ligase 4 stabilizes the ribosomal DNA array upon fork collapse at the replication fork barrier. DNA Repair. 2010 Aug 5;9(8):879–88.

131. Rodriguez M, Yu X, Chen J, Songyang Z. Phosphopeptide binding specificities of BRCA1 COOH-terminal (BRCT) domains. J Biol Chem. 2003 Dec 26;278(52):52914–8.

132. Cheng W-H, von Kobbe C, Opresko PL, Arthur LM, Komatsu K, Seidman MM, et al. Linkage between Werner syndrome protein and the Mre11 complex via Nbs1. J Biol Chem. 2004 May 14;279(20):21169–76.

133. Franchitto A, Pichierri P. Werner syndrome protein and the MRE11 complex are involved in a common pathway of replication fork recovery. Cell Cycle Georget Tex. 2004 Oct;3(10):1331–9.

134. Kobayashi J, Okui M, Asaithamby A, Burma S, Chen BPC, Tanimoto K, et al. WRN participates in translesion synthesis pathway through interaction with NBS1. Mech Ageing Dev. 2010 Jun;131(6):436–44.

135. Popuri V, Croteau DL, Bohr VA. Substrate specific stimulation of NEIL1 by WRN but not the other human RecQ helicases. DNA Repair. 2010 Jun 4;9(6):636–42.

136. Li B, Navarro S, Kasahara N, Comai L. Identification and Biochemical Characterization of a Werner's Syndrome Protein Complex with Ku70/80 and Poly(ADP-ribose) Polymerase-1. J Biol Chem. 2004 Apr 2;279(14):13659–67.

137. Li, Comai. Functional interaction between Ku and the werner syndrome protein in DNA end processing. J Biol Chem. 2000 Dec 15;275(50):39800.

138. Adelfalk C, Kontou M, Hirsch-Kauffmann M, Schweiger M. Physical and functional interaction of the Werner syndrome protein with poly-ADP ribosyl transferase. FEBS Lett. 2003 Nov 6;554(1-2):55–8.

139. Rodríguez-López AM, Jackson DA, Iborra F, Cox LS. Asymmetry of DNA replication fork progression in Werner's syndrome. Aging Cell. 2002 Oct;1(1):30–9.

140. Baynton K, Otterlei M, Bjørås M, von Kobbe C, Bohr VA, Seeberg E. WRN interacts physically and functionally with the recombination mediator protein RAD52. J Biol Chem. 2003 Sep 19;278(38):36476–86.

141. Lebel M, Spillare EA, Harris CC, Leder P. The Werner syndrome gene product co-purifies with the DNA replication complex and interacts with PCNA and topoisomerase I. J Biol Chem. 1999 Dec 31;274(53):37795–9.

142. Rodríguez-López AM, Jackson DA, Nehlin JO, Iborra F, Warren AV, Cox LS. Characterisation of the interaction between WRN, the helicase/exonuclease defective in progeroid Werner's syndrome, and an essential replication factor, PCNA. Mech Ageing Dev. 2003 Feb;124(2):167–74.

143. Liu J, Song Y, Qian J, Liu B, Dong Y, Tian B, et al. Promyelocytic leukemia protein interacts with werner syndrome helicase and regulates double-strand break repair in γ-irradiation-induced DNA damage responses. Biochem Biokhimiia. 2011 May;76(5):550–4.

144. Harrigan JA, Wilson DM 3rd, Prasad R, Opresko PL, Beck G, May A, et al. The Werner syndrome protein operates in base excision repair and cooperates with DNA polymerase beta. Nucleic Acids Res. 2006;34(2):745–54.

145. Szekely AM, Chen YH, Zhang C, Oshima J, Weissman SM. Werner protein recruits DNA polymerase delta to the nucleolus. Proc Natl Acad Sci U S A. 2000 Oct 10;97(21):11365–70.

146. Shiratori M, Suzuki T, Itoh C, Goto M, Furuichi Y, Matsumoto T. WRN helicase accelerates the transcription of ribosomal RNA as a component of an RNA polymerase I-associated complex. Oncogene. 2002 Apr 11;21(16):2447–54.

147. Takahashi K, Imano R, Kibe T, Seimiya H, Muramatsu Y, Kawabata N, et al. Fission yeast Pot1 and RecQ helicase are required for efficient chromosome segregation. Mol Cell Biol. 2011 Feb;31(3):495–506.

148. Karmakar P, Piotrowski J, Brosh RM Jr, Sommers JA, Miller SPL, Cheng W-H, et al. Werner protein is a target of DNA-dependent protein kinase in vivo and in vitro, and its catalytic activities are regulated by phosphorylation. J Biol Chem. 2002 May 24;277(21):18291–302.

149. Aygün O, Svejstrup J, Liu Y. A RECQ5-RNA polymerase II association identified by targeted proteomic analysis of human chromatin. Proc Natl Acad Sci U S A. 2008 Jun 24;105(25):8580–4.

150. Sharma S, Stumpo DJ, Balajee AS, Bock CB, Lansdorp PM, Brosh RM, et al. RECQL, a Member of the RecQ Family of DNA Helicases, Suppresses Chromosomal Instability. Mol Cell Biol. 2007 Mar;27(5):1784–94.

151. Sommers JA, Sharma S, Doherty KM, Karmakar P, Yang Q, Kenny MK, et al. p53 modulates RPA-dependent and RPA-independent WRN helicase activity. Cancer Res. 2005 Feb 15;65(4):1223–33.

152. Brosh RM Jr, Orren DK, Nehlin JO, Ravn PH, Kenny MK, Machwe A, et al. Functional and physical interaction between WRN helicase and human replication protein A. J Biol Chem. 1999 Jun 25;274(26):18341–50.

153. Doherty KM, Sommers JA, Gray MD, Lee JW, von Kobbe C, Thoma NH, et al. Physical and functional mapping of the replication protein a interaction domain of the werner and bloom syndrome helicases. J Biol Chem. 2005 Aug 19;280(33):29494–505.

154. Li K, Casta A, Wang R, Lozada E, Fan W, Kane S, et al. Regulation of WRN protein cellular localization and enzymatic activities by SIRT1-mediated deacetylation. J Biol Chem. 2008 Mar 21;283(12):7590–8.

155. Matafora V, D'Amato A, Mori S, Blasi F, Bachi A. Proteomics analysis of nucleolar SUMO-1 target proteins upon proteasome inhibition. Mol Cell Proteomics MCP. 2009 Oct;8(10):2243–55.

156. Golebiowski F, Matic I, Tatham MH, Cole C, Yin Y, Nakamura A, et al. System-wide changes to SUMO modifications in response to heat shock. Sci Signal. 2009;2(72):ra24.

157. Brosh RM Jr, Karmakar P, Sommers JA, Yang Q, Wang XW, Spillare EA, et al. p53 Modulates the exonuclease activity of Werner syndrome protein. J Biol Chem. 2001 Sep 14;276(37):35093–102.

158. Yang Q, Zhang R, Wang XW, Spillare EA, Linke SP, Subramanian D, et al. The processing of Holliday junctions by BLM and WRN helicases is regulated by p53. J Biol Chem. 2002 Aug 30;277(35):31980–7.

159. Wang XW, Tseng A, Ellis NA, Spillare EA, Linke SP, Robles AI, et al. Functional interaction of p53 and BLM DNA helicase in apoptosis. J Biol Chem. 2001 Aug 31;276(35):32948–55.

160. Opresko PL, von Kobbe C, Laine J-P, Harrigan J, Hickson ID, Bohr VA. Telomere-binding protein TRF2 binds to and stimulates the Werner and Bloom syndrome helicases. J Biol Chem. 2002 Oct 25;277(43):41110–9.

161. Li B, Jog SP, Reddy S, Comai L. WRN controls formation of extrachromosomal telomeric circles and is required for TRF2DeltaB-mediated telomere shortening. Mol Cell Biol. 2008 Mar;28(6):1892–904.

162. Danielsen JMR, Sylvestersen KB, Bekker-Jensen S, Szklarczyk D, Poulsen JW, Horn H, et al. Mass spectrometric analysis of lysine ubiquitylation reveals promiscuity at site level. Mol Cell Proteomics MCP. 2011 Mar;10(3):M110.003590.

163. Kawabe Y, Seki M, Seki T, Wang WS, Imamura O, Furuichi Y, et al. Covalent modification of the Werner's syndrome gene product with the ubiquitin-related protein, SUMO-1. J Biol Chem. 2000 Jul 14;275(28):20963–6.

164. Partridge JJ, Lopreiato JO Jr, Latterich M, Indig FE. DNA damage modulates nucleolar interaction of the Werner protein with the AAA ATPase p97/VCP. Mol Biol Cell. 2003 Oct;14(10):4221–9.

165. Sowa ME, Bennett EJ, Gygi SP, Harper JW. Defining the human deubiquitinating enzyme interaction landscape. Cell. 2009 Jul 23;138(2):389–403.

166. Kawabe Yi, Branzei D, Hayashi T, Suzuki H, Masuko T, Onoda F, et al. A novel protein interacts with the Werner's syndrome gene product physically and functionally. J Biol Chem. 2001 Jun 8;276(23):20364–9.

167. Orren DK, Machwe A, Karmakar P, Piotrowski J, Cooper MP, Bohr VA. A functional interaction of Ku with Werner exonuclease facilitates digestion of damaged DNA. Nucleic Acids Res. 2001 May 1;29(9):1926–34.

168. Karmakar P, Snowden CM, Ramsden DA, Bohr VA. Ku heterodimer binds to both ends of the Werner protein and functional interaction occurs at the Werner N-terminus. Nucleic Acids Res. 2002 Aug 15;30(16):3583–91.

169. Guay D, Gaudreault I, Massip L, Lebel M. Formation of a nuclear complex containing the p53 tumor suppressor, YB-1, and the Werner syndrome gene product in cells treated with UV light. Int J Biochem Cell Biol. 2006 Jan;38(8):1300–13.

170. Glukhova VA, Tomazela DM, Findlay GD, Monnat RJ, MacCoss MJ. Rapid Assessment of RNAi-mediated Protein Depletion by Selected Reaction Monitoring Mass Spectrometry. J Proteome Res. 2013 Jul 5;12(7):3246–54.

171. Stergachis AB, MacLean B, Lee K, Stamatoyannopoulos JA, MacCoss MJ. Rapid empirical discovery of optimal peptides for targeted proteomics. Nat Methods. 2011 Dec;8(12):1041–3.

172. Reiter L, Rinner O, Picotti P, Hüttenhain R, Beck M, Brusniak M-Y, et al. mProphet: automated data processing and statistical validation for large-scale SRM experiments. Nat Methods. 2011 May;8(5):430–5.

173. Sulli G, Di Micco R, d' Adda di Fagagna F. Crosstalk between chromatin state and DNA damage response in cellular senescence and cancer. Nat Rev Cancer. 2012 Oct;12(10):709–20.

174. Chang C-Y, Picotti P, Hüttenhain R, Heinzelmann-Schwarz V, Jovanovic M, Aebersold R, et al. Protein Significance Analysis in Selected Reaction Monitoring (SRM) Measurements. Mol Cell Proteomics. 2012 Apr 1;11(4):M111.014662.

175. Pavlidis P, Noble WS. Matrix2png: a utility for visualizing matrix data. Bioinforma Oxf Engl. 2003 Jan 22;19(2):295–6.

176. Mailand N, Bekker-Jensen S, Faustrup H, Melander F, Bartek J, Lukas C, et al. RNF8 Ubiquitylates Histones at DNA Double-Strand Breaks and Promotes Assembly of Repair Proteins. Cell. 2007 Nov 30;131(5):887–900.

177. Smeenk G, Wiegant WW, Vrolijk H, Solari AP, Pastink A, Attikum H van. The NuRD chromatin–remodeling complex regulates signaling and repair of DNA damage. J Cell Biol. 2010 Sep 6;190(5):741–9.

178. Stewart GS, Wang B, Bignell CR, Taylor AMR, Elledge SJ. MDC1 is a mediator of the mammalian DNA damage checkpoint. Nature. 2003 Feb 27;421(6926):961–6.

179. Stucki M, Clapperton JA, Mohammad D, Yaffe MB, Smerdon SJ, Jackson SP. MDC1 Directly Binds Phosphorylated Histone H2AX to Regulate Cellular Responses to DNA Double-Strand Breaks. Cell. 2005 Dec 29;123(7):1213–26.

180. Trinkle-Mulcahy L. Resolving protein interactions and complexes by affinity purification followed by label-based quantitative mass spectrometry. Proteomics. 2012 May;12(10):1623–38.

181. Downs JA, Jackson SP. A means to a DNA end: the many roles of Ku. Nat Rev Mol Cell Biol. 2004 May;5(5):367–78.

182. Lai AY, Wade PA. Cancer biology and NuRD: a multifaceted chromatin remodelling complex. Nat Rev Cancer. 2011 Aug;11(8):588–96.

183. Nair SS, Li D-Q, Kumar R. A Core Chromatin Remodeling Factor Instructs Global Chromatin Signaling through Multivalent Reading of Nucleosome Codes. Mol Cell. 2013 Feb 21;49(4):704–18.

184. O'Shaughnessy A, Hendrich B. CHD4 in the DNA-damage response and cell cycle progression: not so NuRDy now. Biochem Soc Trans. 2013 Jun 1;41(Pt 3):777–82.

185. Pegoraro G, Kubben N, Wickert U, Göhler H, Hoffmann K, Misteli T. Ageing-related chromatin defects through loss of the NURD complex. Nat Cell Biol. 2009 Sep 6;11(10):1261–7.

186. Stanley FKT, Moore S, Goodarzi AA. CHD chromatin remodelling enzymes and the DNA damage response. Mutat Res. 2013 Oct;750(1-2):31–44.

187. Larsen DH, Poinsignon C, Gudjonsson T, Dinant C, Payne MR, Hari FJ, et al. The chromatin-remodeling factor CHD4 coordinates signaling and repair after DNA damage. J Cell Biol. 2010 Sep 6;190(5):731–40.

188. Pan M-R, Hsieh H-J, Dai H, Hung W-C, Li K, Peng G, et al. Chromodomain Helicase DNA-binding Protein 4 (CHD4) Regulates Homologous Recombination DNA Repair, and Its Deficiency Sensitizes Cells to Poly(ADP-ribose) Polymerase (PARP) Inhibitor Treatment. J Biol Chem. 2012 Jan 4;287(9):6764–72.

189. Chou DM, Adamson B, Dephoure NE, Tan X, Nottke AC, Hurov KE, et al. A chromatin localization screen reveals poly (ADP ribose)-regulated recruitment of the repressive polycomb and NuRD complexes to sites of DNA damage. Proc Natl Acad Sci. 2010 Oct 11;201012946.

190. Polo SE, Kaidi A, Baskcomb L, Galanty Y, Jackson SP. Regulation of DNA-damage responses and cell-cycle progression by the chromatin remodelling factor CHD4. EMBO J. 2010 Sep 15;29(18):3130–9.

191. Fong PC, Boss DS, Yap TA, Tutt A, Wu P, Mergui-Roelvink M, et al. Inhibition of poly(ADP-ribose) polymerase in tumors from BRCA mutation carriers. N Engl J Med. 2009 Jul 9;361(2):123–34.

192. Audeh MW, Carmichael J, Penson RT, Friedlander M, Powell B, Bell-McGuinn KM, et al. Oral poly(ADP-ribose) polymerase inhibitor olaparib in patients with BRCA1 or BRCA2 mutations and recurrent ovarian cancer: a proof-of-concept trial. The Lancet. 2010 Jul 30;376(9737):245–51.

193. Tutt A, Robson M, Garber JE, Domchek SM, Audeh MW, Weitzel JN, et al. Oral poly(ADP-ribose) polymerase inhibitor olaparib in patients with BRCA1 or BRCA2 mutations and advanced breast cancer: a proof-of-concept trial. The Lancet. 2010 Jul 30;376(9737):235–44.

194. Aggarwal M, Sommers JA, Shoemaker RH, Brosh RM. Inhibition of helicase activity by a small molecule impairs Werner syndrome helicase (WRN) function in the cellular response to DNA damage or replication stress. Proc Natl Acad Sci. 2011 Jan 10;201006423.

195. Kobbe C von, Harrigan JA, Schreiber V, Stiegler P, Piotrowski J, Dawut L, et al. Poly(ADP-ribose) polymerase 1 regulates both the exonuclease and helicase activities of the Werner syndrome protein. Nucleic Acids Res. 2004 Jan 1;32(13):4003–14.

196. Rouleau M, Patel A, Hendzel MJ, Kaufmann SH, Poirier GG. PARP inhibition: PARP1 and beyond. Nat Rev Cancer. 2010 Apr;10(4):293–301.

197. Ratnam K, Low JA. Current development of clinical inhibitors of poly(ADP-ribose) polymerase in oncology. Clin Cancer Res Off J Am Assoc Cancer Res. 2007 Mar 1;13(5):1383–8.

198. Zaremba T, Curtin NJ. PARP inhibitor development for systemic cancer targeting. Anticancer Agents Med Chem. 2007 Sep;7(5):515–23.

199. Kim MS, Chung NG, Kang MR, Yoo NJ, Lee SH. Genetic and expressional alterations of CHD genes in gastric and colorectal cancers. Histopathology. 2011 Apr;58(5):660–8.

200. Qian Y-W, Wang Y-CJ, Hollingsworth RE, Jones D, Ling N, Lee EY-HP. A retinoblastoma-binding protein related to a negative regulator of Ras in yeast. Nature. 1993 Aug 12;364(6438):648–52.

201. Pavlopoulos E, Jones S, Kosmidis S, Close M, Kim C, Kovalerchik O, et al. Molecular Mechanism for Age-Related Memory Loss: The Histone-Binding Protein RbAp48. Sci Transl Med. 2013 Aug 28;5(200):200ra115–200ra115.

202. Nicolas E, Morales V, Magnaghi-Jaulin L, Harel-Bellan A, Richard-Foy H, Trouche D. RbAp48 Belongs to the Histone Deacetylase Complex That Associates with the Retinoblastoma Protein. J Biol Chem. 2000 Mar 31;275(13):9797–804.

203. Kachhap SK, Rosmus N, Collis SJ, Kortenhorst MSQ, Wissing MD, Hedayati M, et al. Downregulation of homologous recombination DNA repair genes by HDAC inhibition in prostate cancer is mediated through the E2F1 transcription factor. PloS One. 2010;5(6):e11208.

204. Miller KM, Tjeertes JV, Coates J, Legube G, Polo SE, Britton S, et al. Human HDAC1 and HDAC2 function in the DNA-damage response to promote DNA nonhomologous end-joining. Nat Struct Mol Biol. 2010 Sep;17(99):1144–51.

205. Jang ER, Choi JD, Park MA, Jeong G, Cho H, Lee J-S. ATM modulates transcription in response to histone deacetylase inhibition as part of its DNA damage response. Exp Mol Med. 2010 Mar 31;42(3):195–204.

206. Rajendran P, Ho E, Williams DE, Dashwood RH. Dietary phytochemicals, HDAC inhibition, and DNA damage/repair defects in cancer cells. Clin Epigenetics. 2011 Oct 26;3(1):4.

207. Uhl M, Csernok A, Aydin S, Kreienberg R, Wiesmüller L, Gatz SA. Role of SIRT1 in homologous recombination. DNA Repair. 2010 Apr 4;9(4):383–93.

208. Luo J, Su F, Chen D, Shiloh A, Gu W. Deacetylation of p53 modulates its effect on cell growth and apoptosis. Nature. 2000 Nov 16;408(6810):377–81.

209. Hendrich B, Guy J, Ramsahoye B, Wilson VA, Bird A. Closely related proteins MBD2 and MBD3 play distinctive but interacting roles in mouse development. Genes Dev. 2001 Mar 15;15(6):710–23.

210. Rais Y, Zviran A, Geula S, Gafni O, Chomsky E, Viukov S, et al. Deterministic direct reprogramming of somatic cells to pluripotency. Nature. 2013 Oct 3;502(7469):65–70.

211. Peng JC, Karpen GH. Heterochromatic Genome Stability Requires Regulators of Histone H3 K9 Methylation. PLoS Genet. 2009 Mar 27;5(3):e1000435.

212. Smith S, Stillman B. Stepwise assembly of chromatin during DNA replication in vitro. EMBO J. 1991 Apr;10(4):971–80.

213. Jackson V. In vivo studies on the dynamics of histone-DNA interaction: evidence for nucleosome dissolution during replication and transcription and a low level of dissolution independent of both. Biochemistry (Mosc). 1990 Jan 23;29(3):719–31.

214. Lucchini R, Wellinger RE, Sogo JM. Nucleosome positioning at the replication fork. EMBO J. 2001 Dec 17;20(24):7294–302.

215. Smith S, Stillman B. Purification and characterization of CAF-I, a human cell factor required for chromatin assembly during DNA replication in vitro. Cell. 1989 Jul 14;58(1):15–25.

216. Verreault A. De novo nucleosome assembly: new pieces in an old puzzle. Genes Dev. 2000 Jun 15;14(12):1430–8.

217. Verreault A, Kaufman PD, Kobayashi R, Stillman B. Nucleosome assembly by a complex of CAF-1 and acetylated histones H3/H4. Cell. 1996 Oct 4;87(1):95–104.

218. Quivy J-P, Gérard A, Cook AJL, Roche D, Almouzni G. The HP1-p150/CAF-1 interaction is required for pericentric heterochromatin replication and S-phase progression in mouse cells. Nat Struct Mol Biol. 2008 Sep;15(9):972–9.

219. Poot M, Hoehn H, Rünger TM, Martin GM. Impaired S-phase transit of Werner syndrome cells expressed in lymphoblastoid cell lines. Exp Cell Res. 1992 Oct;202(2):267–73.

220. Nabatiyan A, Krude T. Silencing of chromatin assembly factor 1 in human cells leads to cell death and loss of chromatin assembly during DNA synthesis. Mol Cell Biol. 2004 Apr;24(7):2853–62.

221. Hoek M, Stillman B. Chromatin assembly factor 1 is essential and couples chromatin assembly to DNA replication in vivo. Proc Natl Acad Sci U S A. 2003 Oct 14;100(21):12183–8.

222. Lewis LK, Karthikeyan G, Cassiano J, Resnick MA. Reduction of nucleosome assembly during new DNA synthesis impairs both major pathways of double-strand break repair. Nucleic Acids Res. 2005;33(15):4928–39.

223. Linger J, Tyler JK. The yeast histone chaperone chromatin assembly factor 1 protects against double-strand DNA-damaging agents. Genetics. 2005 Dec;171(4):1513–22.

224. Nabatiyan A, Szüts D, Krude T. Induction of CAF-1 expression in response to DNA strand breaks in quiescent human cells. Mol Cell Biol. 2006 Mar;26(5):1839–49.

225. Jiao R, Bachrati CZ, Pedrazzi G, Kuster P, Petkovic M, Li J-L, et al. Physical and functional interaction between the Bloom's syndrome gene product and the largest subunit of chromatin assembly factor 1. Mol Cell Biol. 2004 Jun;24(11):4710–9.

226. Moggs JG, Grandi P, Quivy JP, Jónsson ZO, Hübscher U, Becker PB, et al. A CAF-1-PCNA-mediated chromatin assembly pathway triggered by sensing DNA damage. Mol Cell Biol. 2000 Feb;20(4):1206–18.

227. Shibahara K, Stillman B. Replication-dependent marking of DNA by PCNA facilitates CAF-1-coupled inheritance of chromatin. Cell. 1999 Feb 19;96(4):575–85.

228. Mello JA, Silljé HHW, Roche DMJ, Kirschner DB, Nigg EA, Almouzni G. Human Asf1 and CAF-1 interact and synergize in a repair-coupled nucleosome assembly pathway. EMBO Rep. 2002 Apr;3(4):329–34.

229. Tang Y, Poustovoitov MV, Zhao K, Garfinkel M, Canutescu A, Dunbrack R, et al. Structure of a human ASF1a-HIRA complex and insights into specificity of histone chaperone complex assembly. Nat Struct Mol Biol. 2006 Oct;13(10):921–9.

230. Tong AH, Evangelista M, Parsons AB, Xu H, Bader GD, Pagé N, et al. Systematic genetic analysis with ordered arrays of yeast deletion mutants. Science. 2001 Dec 14;294(5550):2364–8.

231. Belotserkovskaya R, Oh S, Bondarenko VA, Orphanides G, Studitsky VM, Reinberg D. FACT facilitates transcription-dependent nucleosome alteration. Science. 2003 Aug 22;301(5636):1090–3.

232. Winkler DD, Luger K. The histone chaperone FACT: structural insights and mechanisms for nucleosome reorganization. J Biol Chem. 2011 May 27;286(21):18369–74.

233. Orphanides G, LeRoy G, Chang CH, Luse DS, Reinberg D. FACT, a factor that facilitates transcript elongation through nucleosomes. Cell. 1998 Jan 9;92(1):105–16.

234. Dinant C, Ampatziadis-Michailidis G, Lans H, Tresini M, Lagarou A, Grosbart M, et al. Enhanced chromatin dynamics by FACT promotes transcriptional restart after UV-induced DNA damage. Mol Cell. 2013 Aug 22;51(4):469–79.

235. Bétous R, Glick GG, Zhao R, Cortez D. Identification and characterization of SMARCAL1 protein complexes. PloS One. 2013;8(5):e63149.

236. Tan BC-M, Chien C-T, Hirose S, Lee S-C. Functional cooperation between FACT and MCM helicase facilitates initiation of chromatin DNA replication. EMBO J. 2006 Sep 6;25(17):3975–85.

237. Adelmant G, Calkins AS, Garg BK, Card JD, Askenazi M, Miron A, et al. DNA ends alter the molecular composition and localization of Ku multicomponent complexes. Mol Cell Proteomics MCP. 2012 Aug;11(8):411–21.

238. Abe T, Sugimura K, Hosono Y, Takami Y, Akita M, Yoshimura A, et al. The histone chaperone facilitates chromatin transcription (FACT) protein maintains normal replication fork rates. J Biol Chem. 2011 Sep 2;286(35):30504–12.

239. Okuhara K, Ohta K, Seo H, Shioda M, Yamada T, Tanaka Y, et al. A DNA unwinding factor involved in DNA replication in cell-free extracts of Xenopus eggs. Curr Biol CB. 1999 Apr 8;9(7):341–50.

240. Takami Y, Ono T, Fukagawa T, Shibahara K, Nakayama T. Essential role of chromatin assembly factor-1-mediated rapid nucleosome assembly for DNA replication and cell division in vertebrate cells. Mol Biol Cell. 2007 Jan;18(1):129–41.

241. Dejmek J, Iglehart JD, Lazaro J-B. DNA-dependent protein kinase (DNA-PK)–dependent cisplatin-induced loss of nucleolar facilitator of chromatin transcription (FACT) and regulation of cisplatin sensitivity by DNA-PK and FACT. Mol Cancer Res. 2009;7(4):581–91.

242. Kumari A, Mazina OM, Shinde U, Mazin AV, Lu H. A role for SSRP1 in recombination-mediated DNA damage response. J Cell Biochem. 2009 Jul 28;108(2):508–18.

243. O'Connell BC, Adamson B, Lydeard JR, Sowa ME, Ciccia A, Bredemeyer AL, et al. A Genome-wide Camptothecin Sensitivity Screen Identifies a Mammalian MMS22L-NFKBIL2 Complex Required for Genomic Stability. Mol Cell. 2010 Nov;40(4):645–57.

244. Piwko W, Olma MH, Held M, Bianco JN, Pedrioli PGA, Hofmann K, et al. RNAi-based screening identifies the Mms22L-Nfkbil2 complex as a novel regulator of DNA replication in human cells. EMBO J. 2010 Dec 15;29(24):4210–22.

245. Kusumoto-Matsuo R, Ghosh D, Karmakar P, May A, Ramsden D, Bohr VA. Serines 440 and 467 in the Werner syndrome protein are phosphorylated by DNA-PK and affects its dynamics in response to DNA double strand breaks. Aging. 2014 Jan 14;

246. Perry JJP, Asaithamby A, Barnebey A, Kiamanesch F, Chen DJ, Han S, et al. Identification of a coiled coil in werner syndrome protein that facilitates multimerization and promotes exonuclease processivity. J Biol Chem. 2010 Aug 13;285(33):25699–707.

247. Swaney DL, Beltrao P, Starita L, Guo A, Rush J, Fields S, et al. Global analysis of phosphorylation and ubiquitylation cross-talk in protein degradation. Nat Methods. 2013 Jul;10(7):676–82.

248. Ciccia A, Elledge SJ. The DNA Damage Response: Making It Safe to Play with Knives. Mol Cell. 2010 Oct 22;40(2):179–204.

249. Polo SE, Jackson SP. Dynamics of DNA damage response proteins at DNA breaks: a focus on protein modifications. Genes Dev. 2011 Mar 1;25(5):409–33.

250. Goodarzi AA, Noon AT, Deckbar D, Ziv Y, Shiloh Y, Löbrich M, et al. ATM signaling facilitates repair of DNA double-strand breaks associated with heterochromatin. Mol Cell. 2008 Jul 25;31(2):167–77.

251. Hu C, Zhang S, Gao X, Gao X, Xu X, Lv Y, et al. Roles of the KRAB-associated co-repressor KAP1 S473 phosphorylation in DNA damage response. J Biol Chem. 2012 Apr 11;jbc.M111.313262.

252. Ziv Y, Bielopolski D, Galanty Y, Lukas C, Taya Y, Schultz DC, et al. Chromatin relaxation in response to DNA double-strand breaks is modulated by a novel ATM- and KAP-1 dependent pathway. Nat Cell Biol. 2006 Aug;8(8):870–6.

253. White D, Rafalska-Metcalf IU, Ivanov AV, Corsinotti A, Peng H, Lee S-C, et al. The ATM substrate KAP1 controls DNA repair in heterochromatin: regulation by HP1 proteins and serine 473/824 phosphorylation. Mol Cancer Res MCR. 2012 Mar;10(3):401–14.

254. Kepkay R, Attwood KM, Ziv Y, Shiloh Y, Dellaire G. KAP1 depletion increases PML nuclear body number in concert with ultrastructural changes in chromatin. Cell Cycle Georget Tex. 2011 Jan 15;10(2):308–22.

255. Kristensen AR, Gsponer J, Foster LJ. A high-throughput approach for measuring temporal changes in the interactome. Nat Methods. 2012 Sep;9(9):907–9.

256. Ding S, Yu J-C, Chen S-T, Hsu G-C, Shen C-Y. Genetic variation in the premature aging gene WRN: a case-control study on breast cancer susceptibility. Cancer Epidemiol Biomark Prev Publ Am Assoc Cancer Res Cosponsored Am Soc Prev Oncol. 2007 Feb;16(2):263–9.

257. Lao VV, Welcsh P, Luo Y, Carter KT, Dzieciatkowski S, Dintzis S, et al. Altered RECQ Helicase Expression in Sporadic Primary Colorectal Cancers. Transl Oncol. 2013 Aug;6(4):458–69.

258. Agrelo R, Cheng W-H, Setien F, Ropero S, Espada J, Fraga MF, et al. Epigenetic inactivation of the premature aging Werner syndrome gene in human cancer. Proc Natl Acad Sci U S A. 2006 Jun 6;103(23):8822–7.

259. Luijsterburg MS, van Attikum H. Close encounters of the RNF8th kind: when chromatin meets DNA repair. Curr Opin Cell Biol. 2012 Jun;24(3):439–47.

260. Spycher C, Miller ES, Townsend K, Pavic L, Morrice NA, Janscak P, et al. Constitutive phosphorylation of MDC1 physically links the MRE11–RAD50–NBS1 complex to damaged chromatin. J Cell Biol. 2008 Apr 21;181(2):227–40.

261. Bryant HE, Schultz N, Thomas HD, Parker KM, Flower D, Lopez E, et al. Specific killing of BRCA2-deficient tumours with inhibitors of poly(ADP-ribose) polymerase. Nature. 2005 Apr 14;434(7035):913–7.

262. McCabe N, Turner NC, Lord CJ, Kluzek K, Bialkowska A, Swift S, et al. Deficiency in the repair of DNA damage by homologous recombination and sensitivity to poly(ADP-ribose) polymerase inhibition. Cancer Res. 2006 Aug 15;66(16):8109–15.

263. Watanabe S, Watanabe K, Akimov V, Bartkova J, Blagoev B, Lukas J, et al. JMJD1C demethylates MDC1 to regulate the RNF8 and BRCA1–mediated chromatin response to DNA breaks. Nat Struct Mol Biol. 2013 Dec;20(12):1425–33.

264. Vaitiekunaite R, Butkiewicz D, Krześniak M, Przybyłek M, Gryc A, Snietura M, et al. Expression and localization of Werner syndrome protein is modulated by SIRT1 and PML. Mech Ageing Dev. 2007 Dec;128(11-12):650–61.

265. Xie W, Ling T, Zhou Y, Feng W, Zhu Q, Stunnenberg HG, et al. The chromatin remodeling complex NuRD establishes the poised state of rRNA genes characterized by bivalent histone modifications and altered nucleosome positions. Proc Natl Acad Sci. 2012 May 22;109(21):8161–6.

266. Larsen DH, Poinsignon C, Gudjonsson T, Dinant C, Payne MR, Hari FJ, et al. The chromatin-remodeling factor CHD4 coordinates signaling and repair after DNA damage. J Cell Biol. 2010 Sep 6;190(5):731–40.

Appendix A: Supplementary data from Chapter 2.

Contained here are all Supplementary Figures as listed in Results section of Chapter 2.

Supplementary figure 1

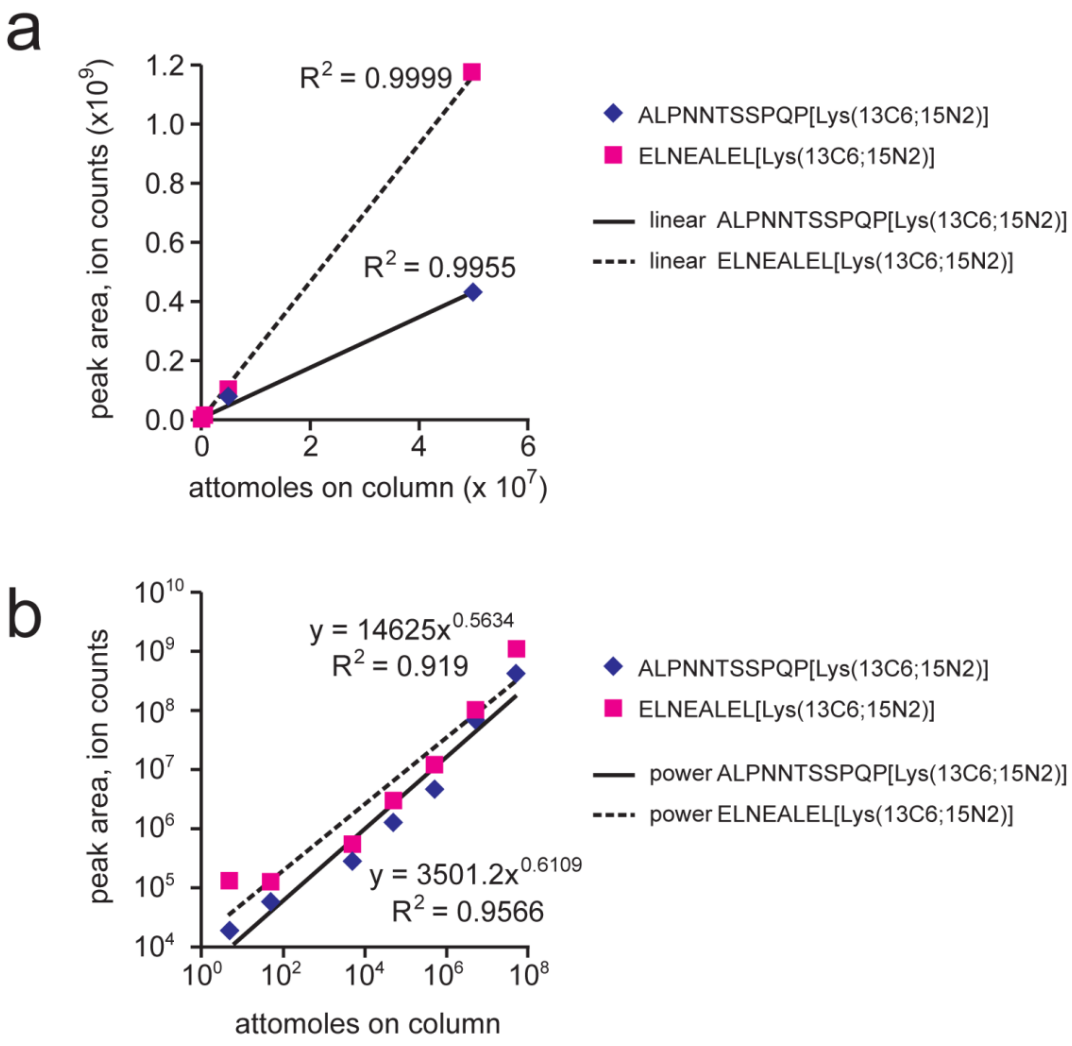

Supplementary figure 1

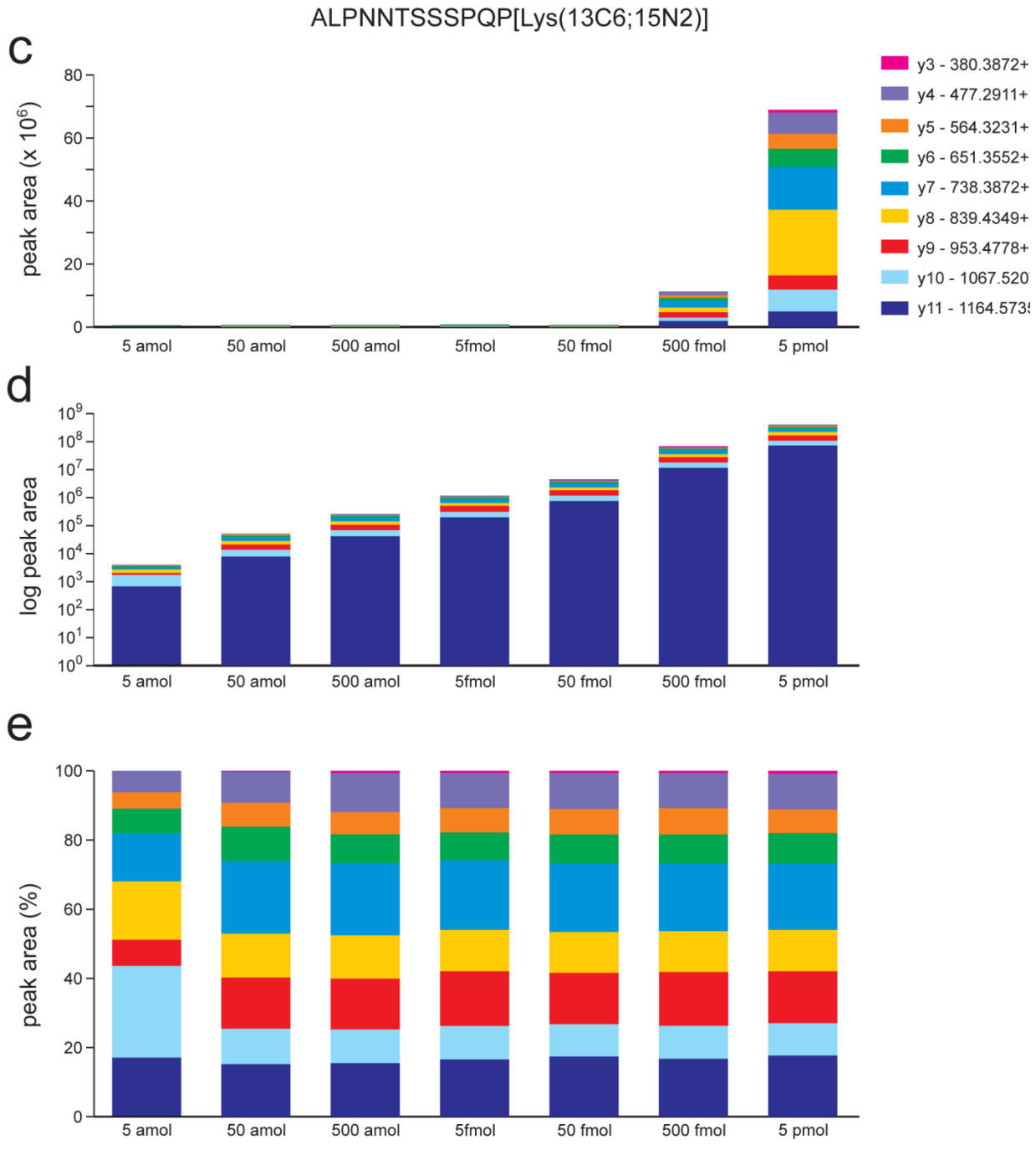

Supplementary figure 1

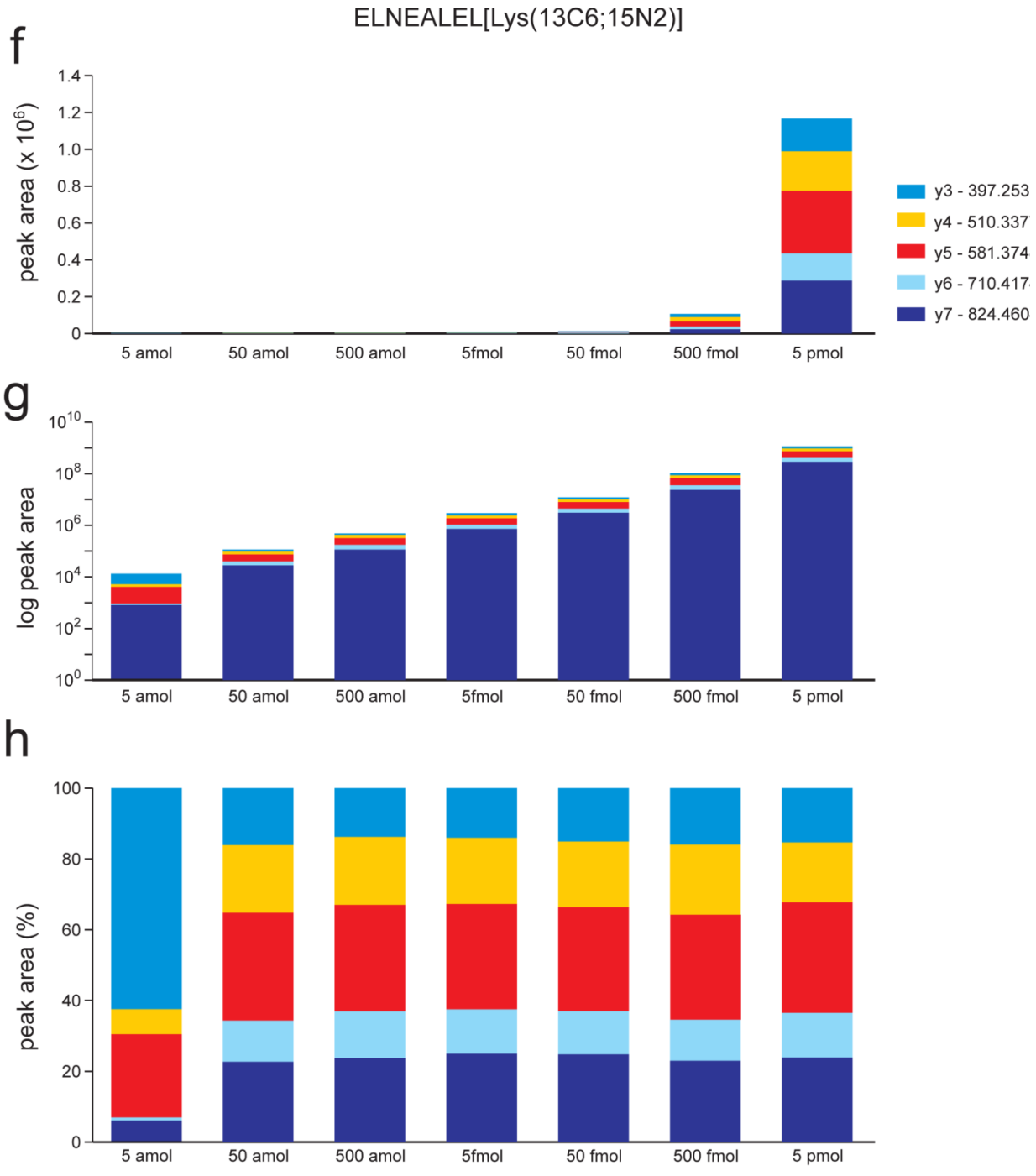

Supplementary Figure A.1: Limit of quantitation (LOQ) and limit of detection (LOD) were determined for SIL peptides in buffer solution. Presented in this figure are the regression analysis to demonstrate linearity of peak areas in response to increasing amount of spiked-in protein, and peak areas as extracted by Skyline software, mapped in absolute amount, on logarithmic scale, and normalized to total intensity. The normalized intensities most accurately reflect relative ion fragment ratios regardless of absolute amount.
Linear regression analysis of both SIL peptides shows a linear response over 6 orders of magnitude (**a**), while power regression of log-transformed data shows linear response over 4 orders of magnitude (**b**).
Absolute (**c**), log-transformed (**d**), and normalized (**e**) peak areas and contributing ion ratios from TP53 peptide ALPNNSSSPQPK are graphed from 5 amol to 5 pmol amounts spiked into ammonium bicarbonate buffer. Same peak area measurements are demonstrated for TP53 peptide ELNEALELK respectively in panels (**f**), (**g**), and (**h**).

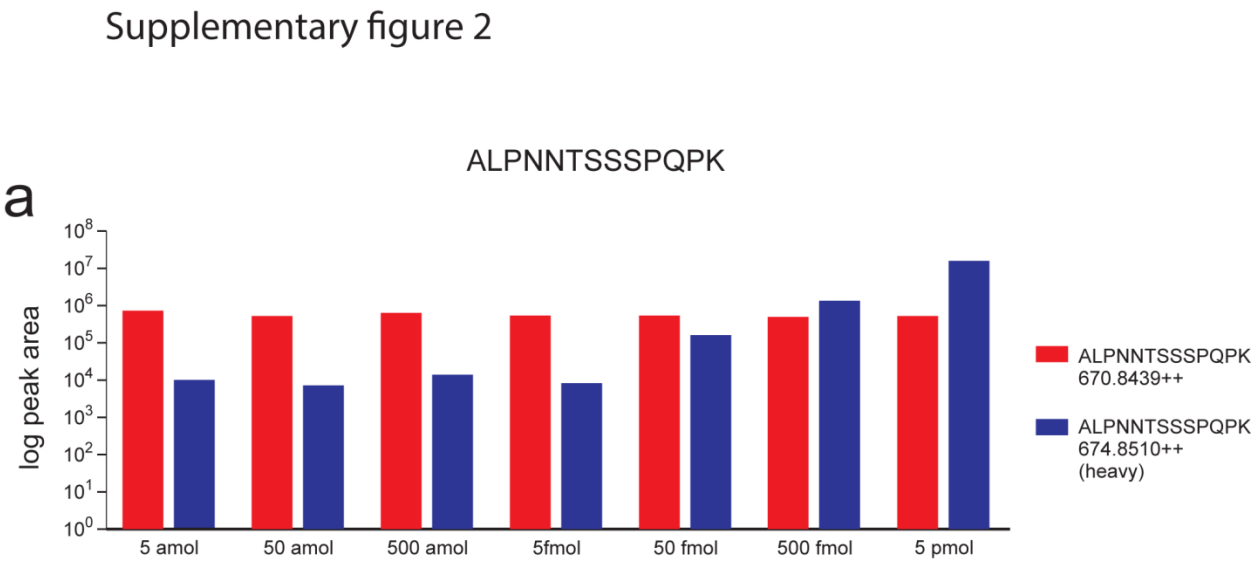

Supplementary figure 2

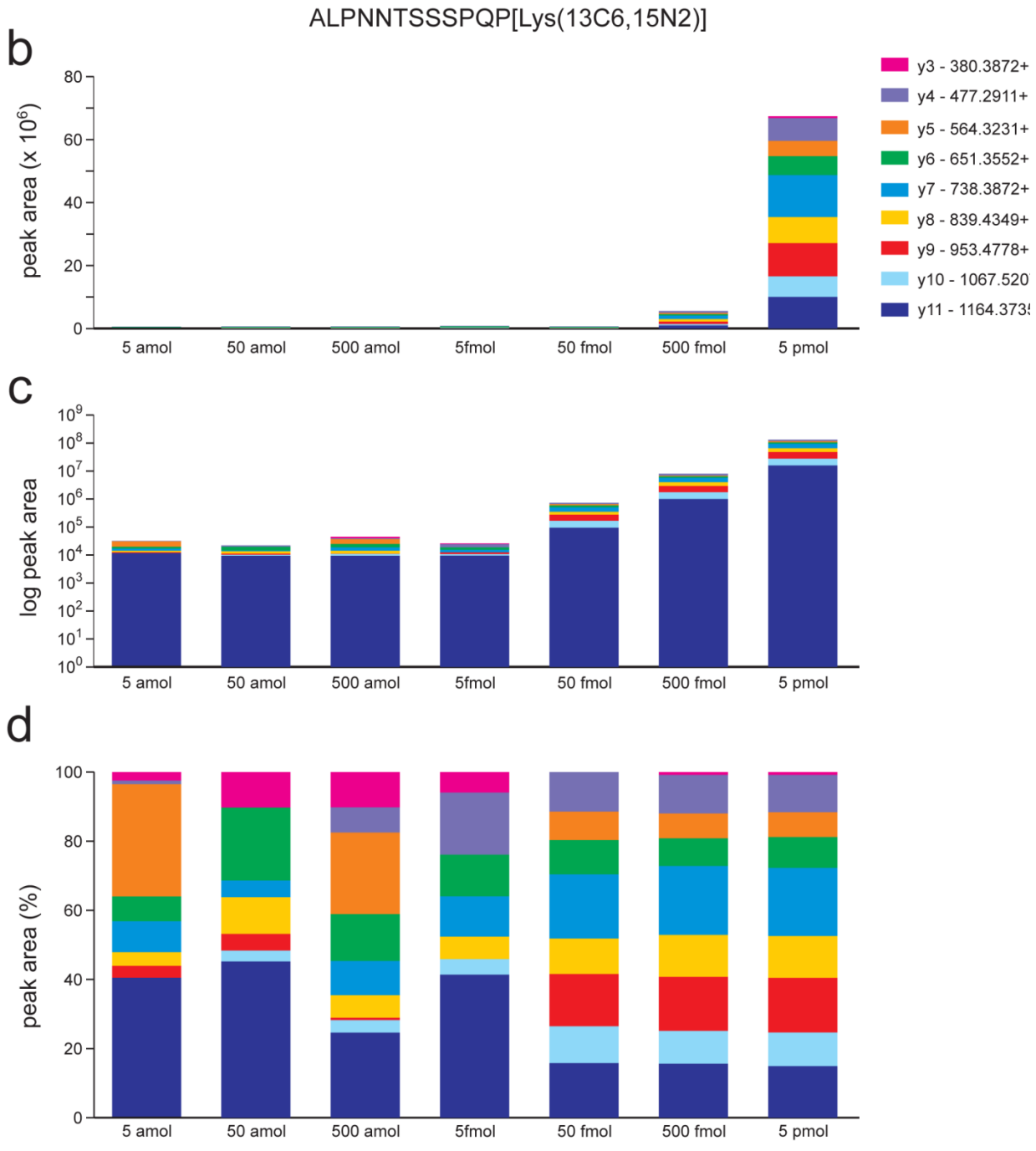

Supplementary figure 2

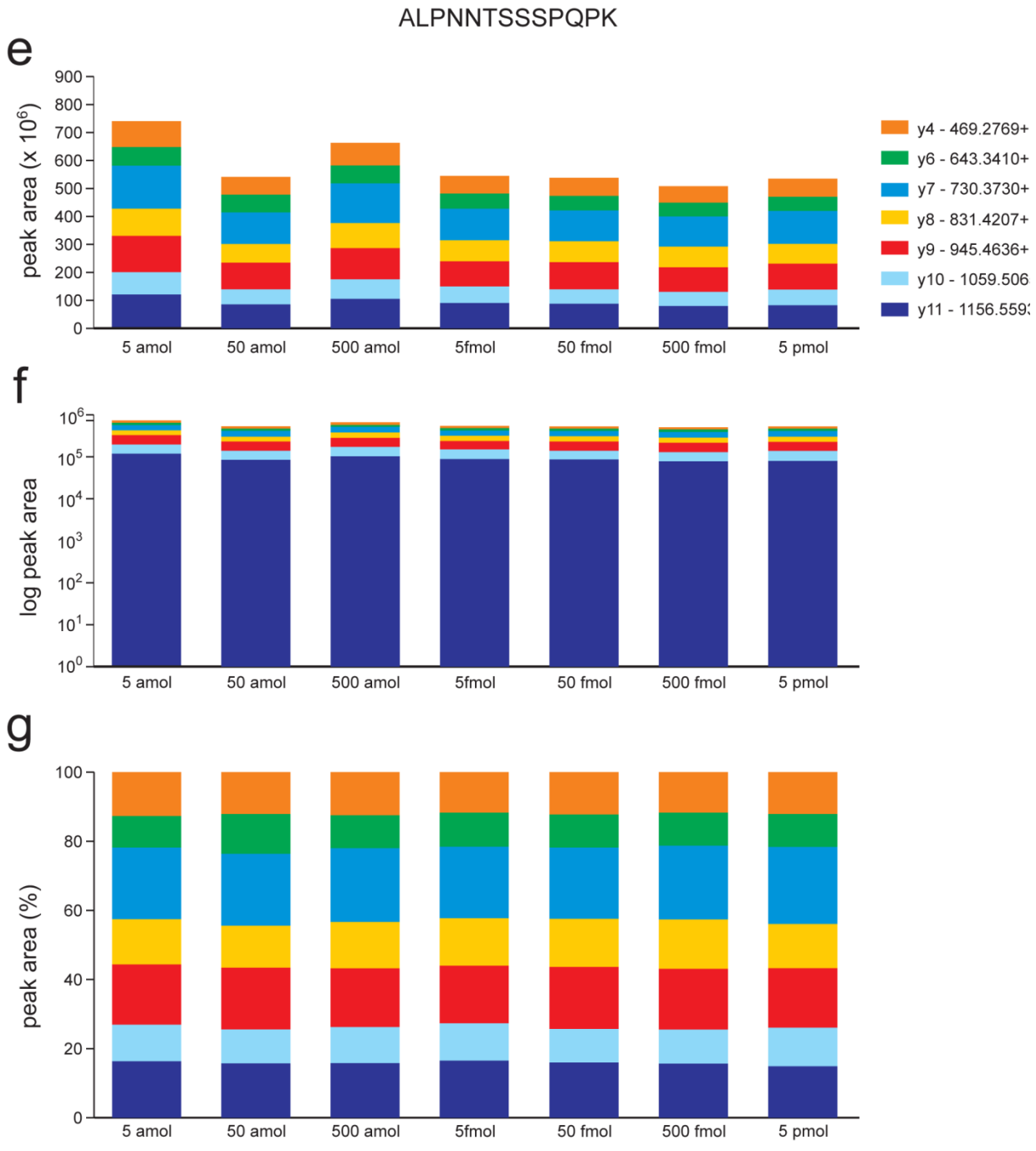

Supplementary figure 2

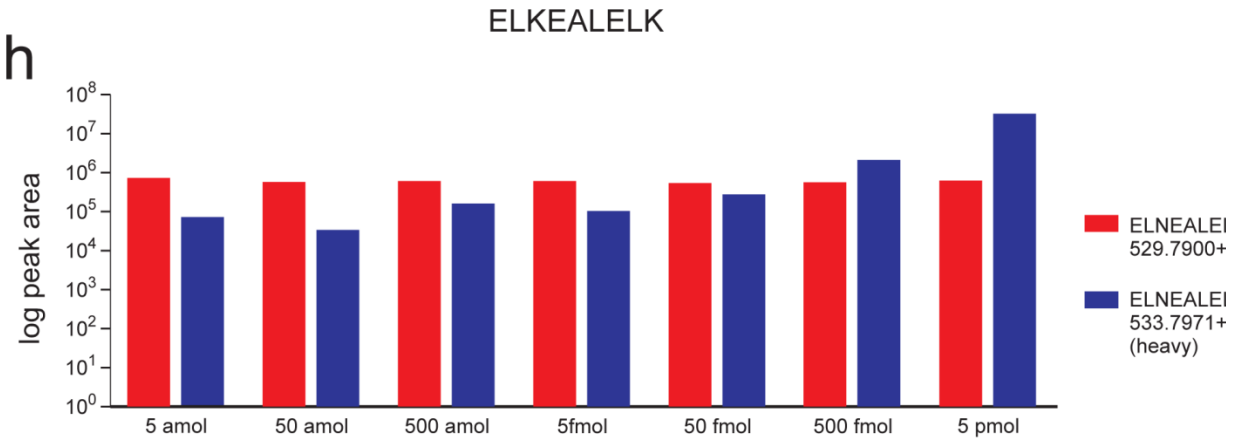

Supplementary figure 2

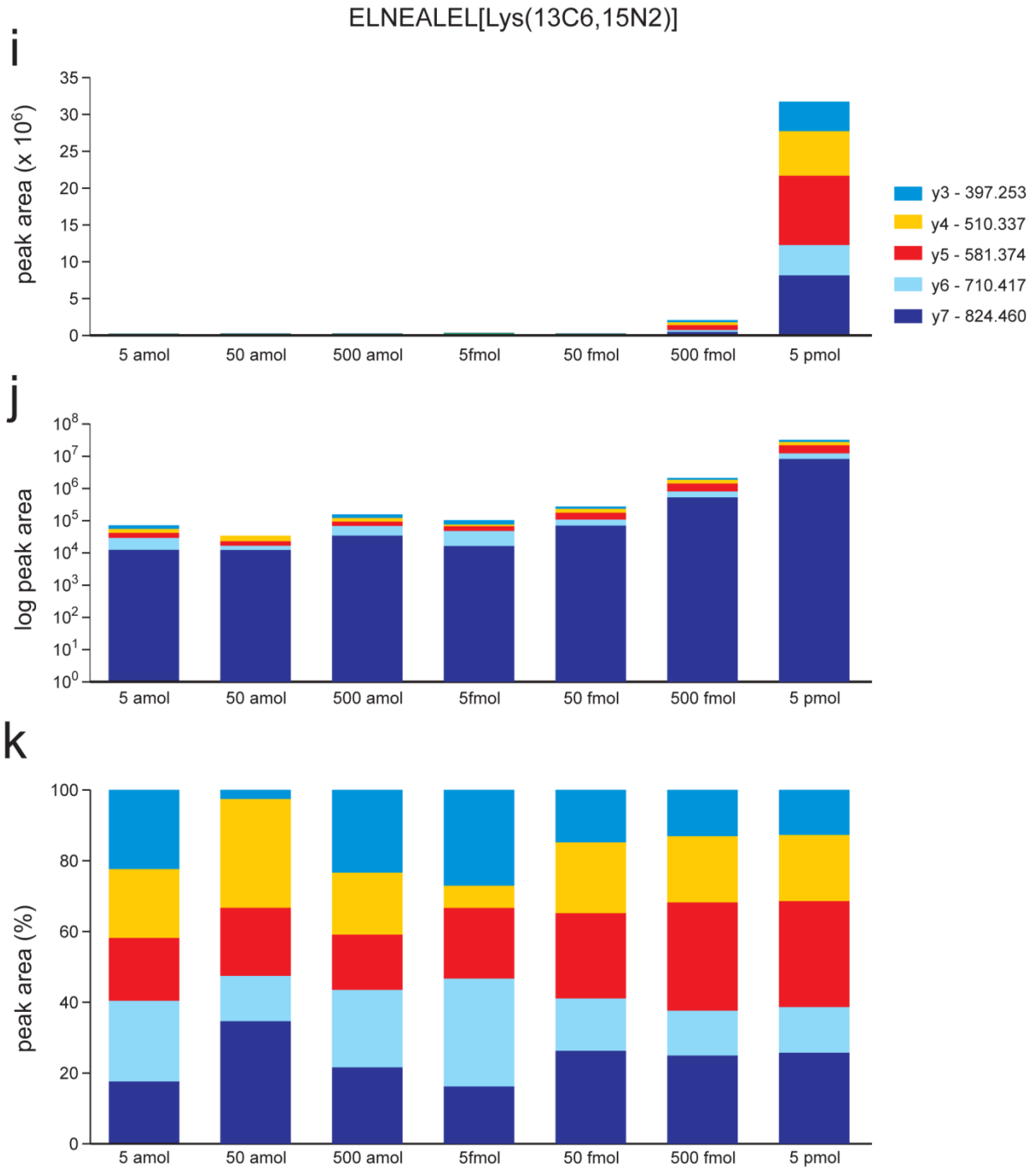

Supplementary figure 2

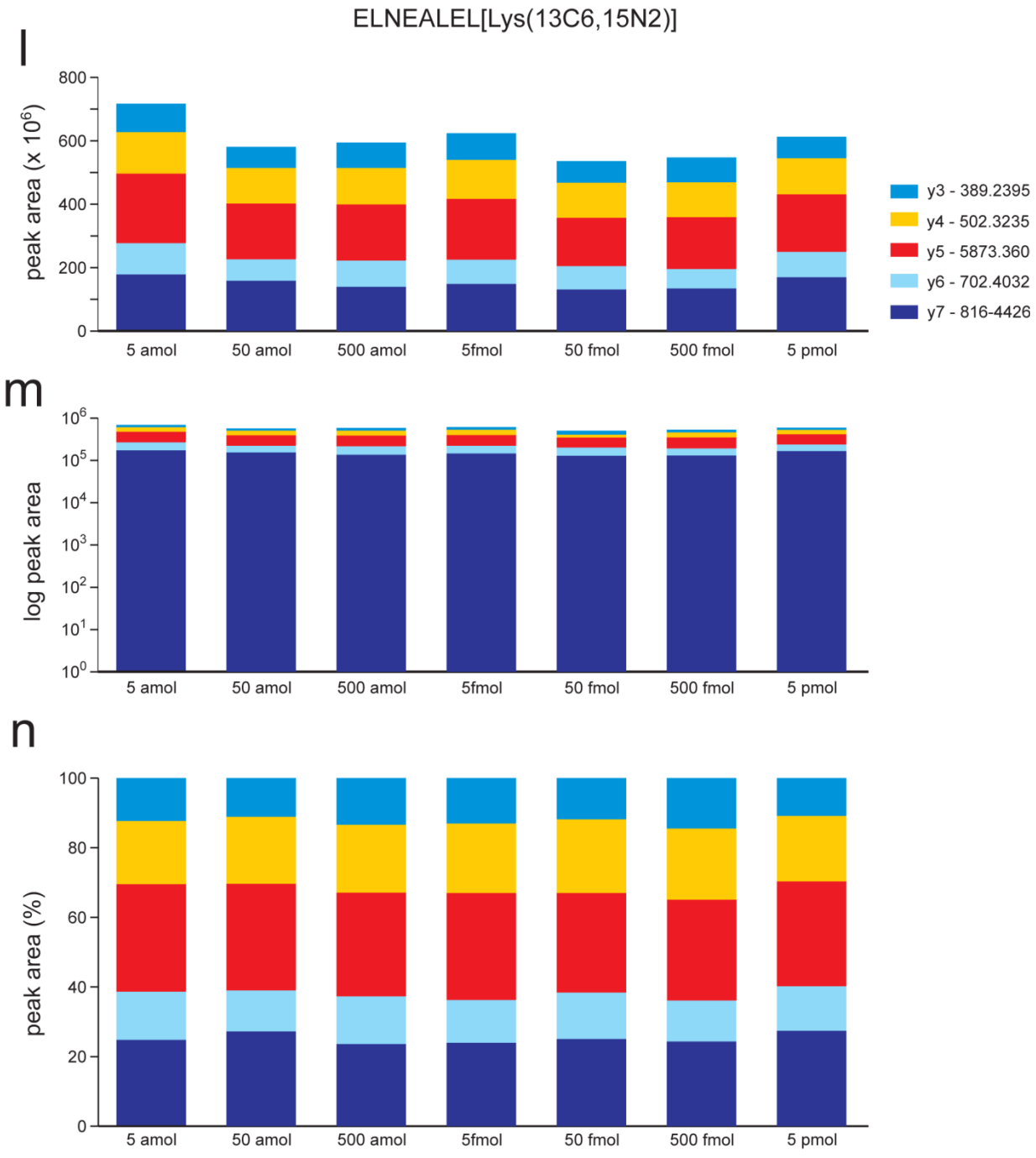

Supplementary Figure A.2: Limit of quantitation (LOQ) and limit of detection (LOD) were determined for SIL peptides within a complex background of whole cell extract (WCE) using TP53 peptides ALPNNSSSPQPK and ELNEALELK. Panel (**a**) shows relative peak area ratios of an

endogenous TP53 peptide ALPNNSSSPQPK extracted from WCE and peak areas for its heavy cognate ALPNNTSSSPQP[Lys(13C6; 15N2)], which was added in indicated amounts. Panels (**b**), (**c**), and (**d**) show absolute, log-transformed, and normalized peak area intensities and ion fragment ratios for the heavy peptide. Panels (**e**), (**f**), and (**g**) show absolute, log-transformed, and normalized peak area intensities and ion fragment ratios for the endogenous peptide.
Panel (**h**) shows relative peak area ratios of the endogenous peptide ELNEALELK found in WCE and peak areas for its heavy cognate ELNEALEL[Lys(13C6; 15N2)], which was added in indicated amounts. Panels (**i**), (**j**), and (**k**) show absolute, log-transformed, and normalized peak area intensities and ion fragment ratios for the heavy peptide. Panels (**l**), (**m**), and (**n**) show absolute, log-transformed, and normalized peak area intensities and ion fragment ratios for the endogenous peptide.

Supplementary figure 3

a

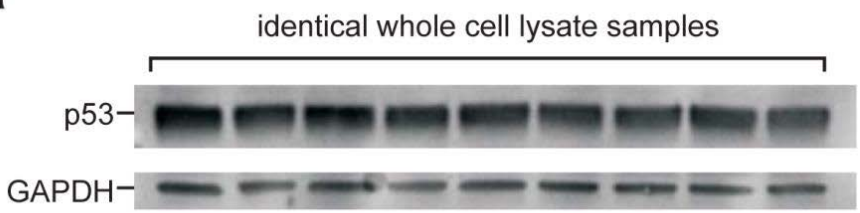

b

Western blot	CV (%)	SRM peptide	CV (%)
TP53	16.9	ALPNNTSSSPQPK	16.8
		ELNEALELK	12.3
GAPDH	38.2	IISNASCTTNCLAPLAK	8.7
		VPTANVSVVDLTCR	5.4

Supplementary Figure A.3: Replicate analysis to determine the coefficient of variation (CV) for protein detection by Western blot or SRM. (**a**) Aliquots of 50 μg of total protein from human embryonic kidney (HEK-293T) cells were loaded in replicate lanes prior to electrophoresis and Western blot detection with anti-TP53 and anti-GAPDH antibodies (see Methods). In parallel, 6 technical replicates of trypsin-digested whole cell lysate from HEK-293T cells were analyzed by SRM as illustrated in **Figure 2** to detect and quantify TP53 and GAPDH. (**b**) CV values were determined for Western blot analyses by quantifying band intensities using Image Quant software, and by peak areas as determined by Skyline for SRM analyses.

Supplementary figure 4

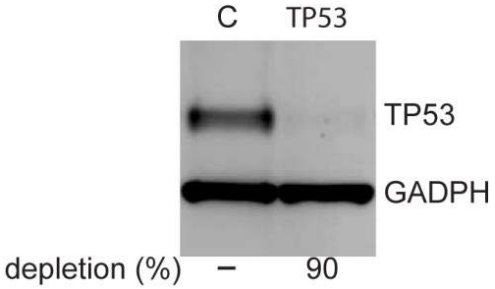

Supplementary Figure A.4: Western blot verification of TP53 depletion from human cells, prior to adding SIL peptides to samples. Cells were transfected with *TP53*-specific or control (C) siRNAs prior to preparing whole cell extracts. TP53 and GAPDH were detected by Western blot analysis. Band intensities for TP53 versus GAPDH were normalized against the blot background, then used to estimate percent TP53 depletion as a function of siRNA dose (**a**).

Supplementary figure 5

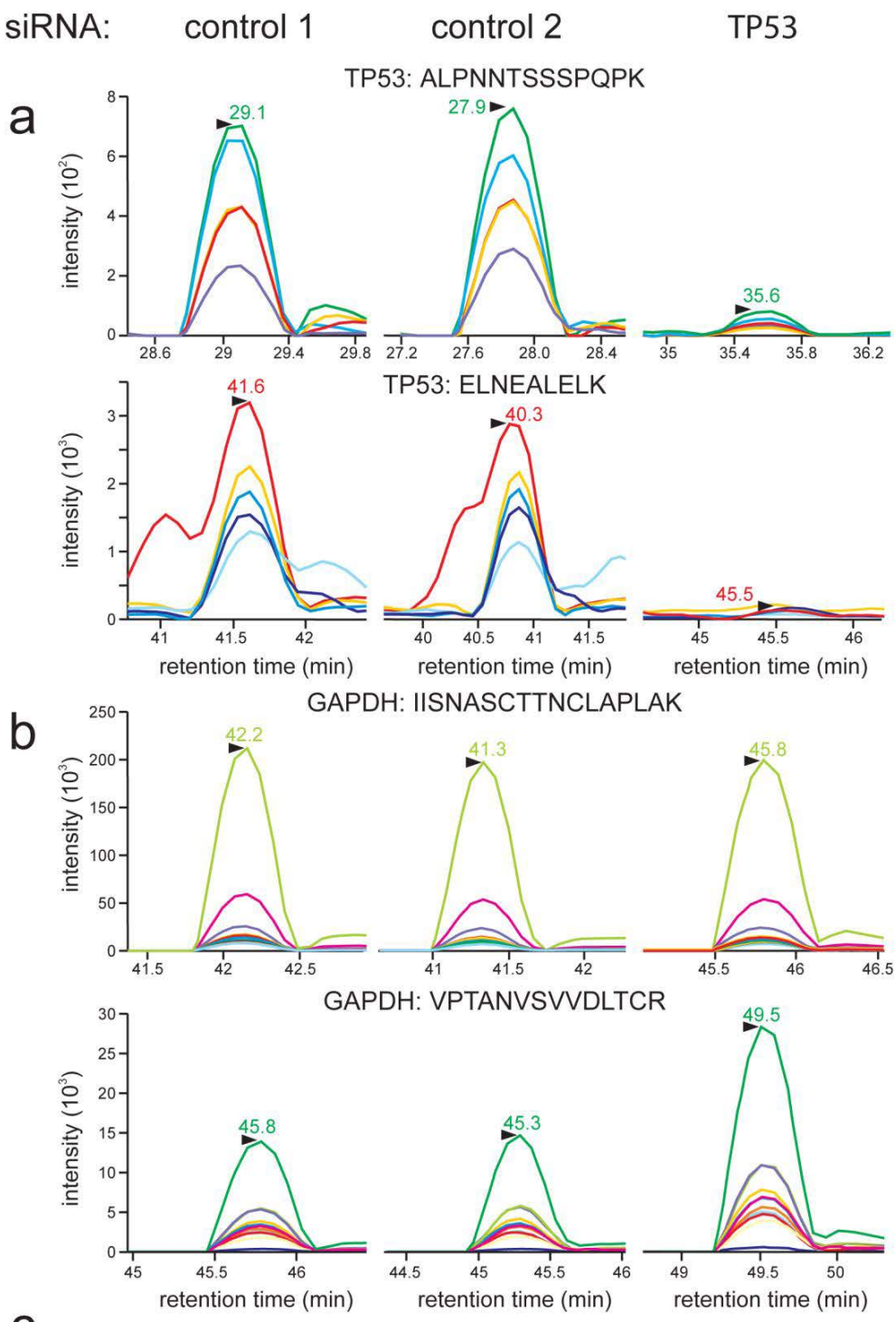

TP53 peptide	/	control peptide	TP53 depletion (%) control 1	control 2
ALPNNTSSSPQPK	/	ALPNNTSSSPQPK	86	89
ALPNNTSSSPQPK	/	IISNASCTTNCLAPLAK	92	94
ALPNNTSSSPQPK	/	VPTANVSVVDLTCR	97	97
ELNEALELK	/	ELNEALELK	88	90
ELNEALELK	/	IISNASCTTNCLAPLAK	95	96
ELNEALELK	/	VPTANVSVVDLTCR	98	98

Supplementary Figure A.5: Second set of RNAi-mediated TP53 depletions was quantified by Selected Reaction Monitoring (SRM) mass spectrometry. SIL peptides ALPNNTSSSPQP[Lys(13C6; 15N2)] and ELNEALEL[Lys(13C6; 15N2)] were added to the WCE for normalization. The chromatograms show sets of transitions for specific peptides derived from target protein TP53 (**a**) or loading control GAPDH (**b**) in human cell RNAi depletion experiments. Samples were treated with a control RNAi and analyzed in duplicate (control 1 and control 2) or with a *TP53*-specific siRNA prior to SRM analysis. Specific peptides detected and quantified from TP53 were ALPNNTSSSPQPK and ELNEALELK, and from GAPDH VPTANVSVVDLTCR and IISNASCTTNCLAPLAK. Panel (**c**) shows quantitation of depletion determined from SRM data, as peak intensities from TP53 peptides ALPNNTSSSPQPK and ELNEALELK were normalized against corresponding SIL peptides, and two GAPDH peptides IISNASCTTNCLAPLAK and VPTANVSVVDLTCR against two analytical replicates of control sample.

Supplementary figure 6

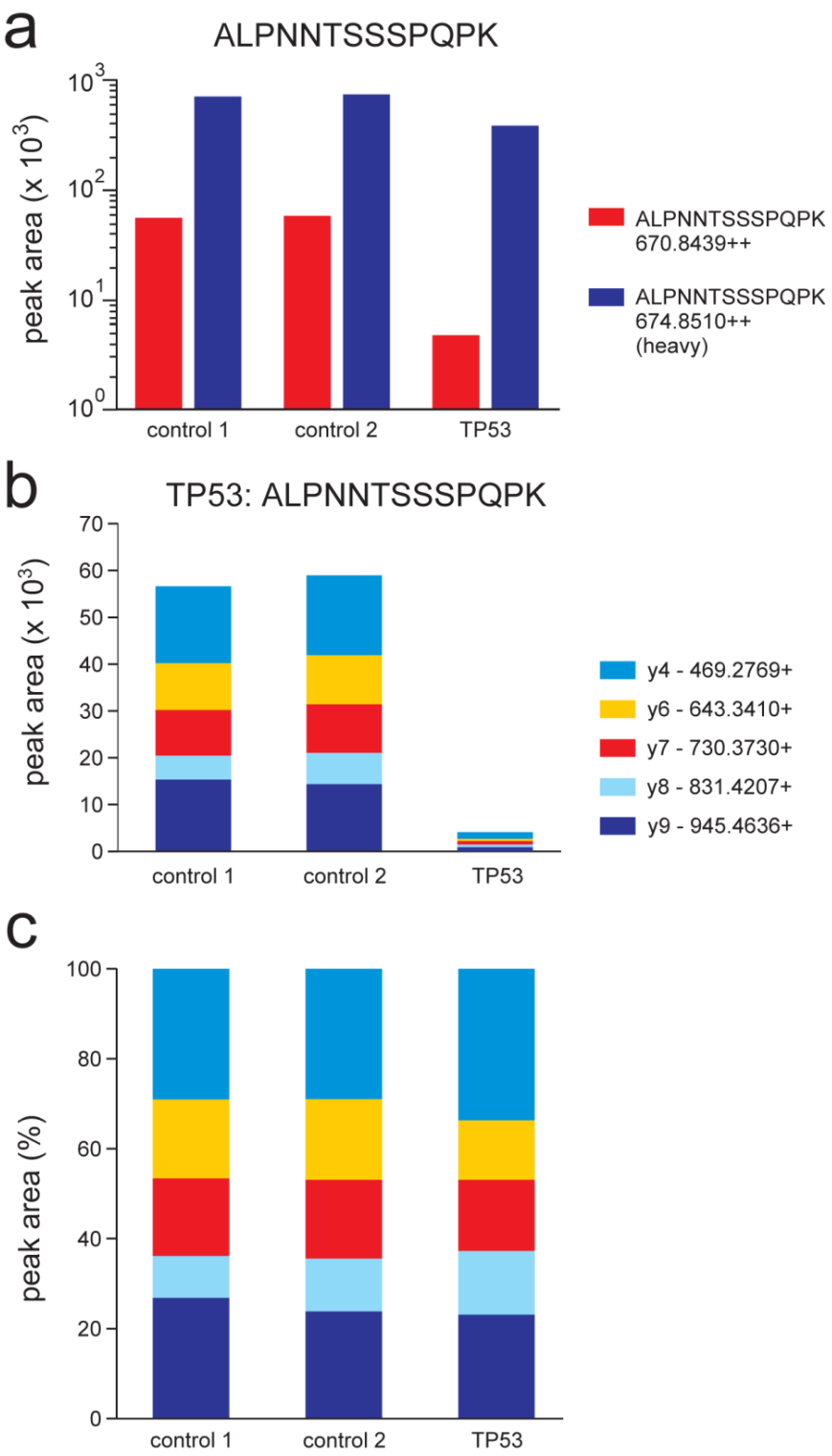

Supplementary figure 6

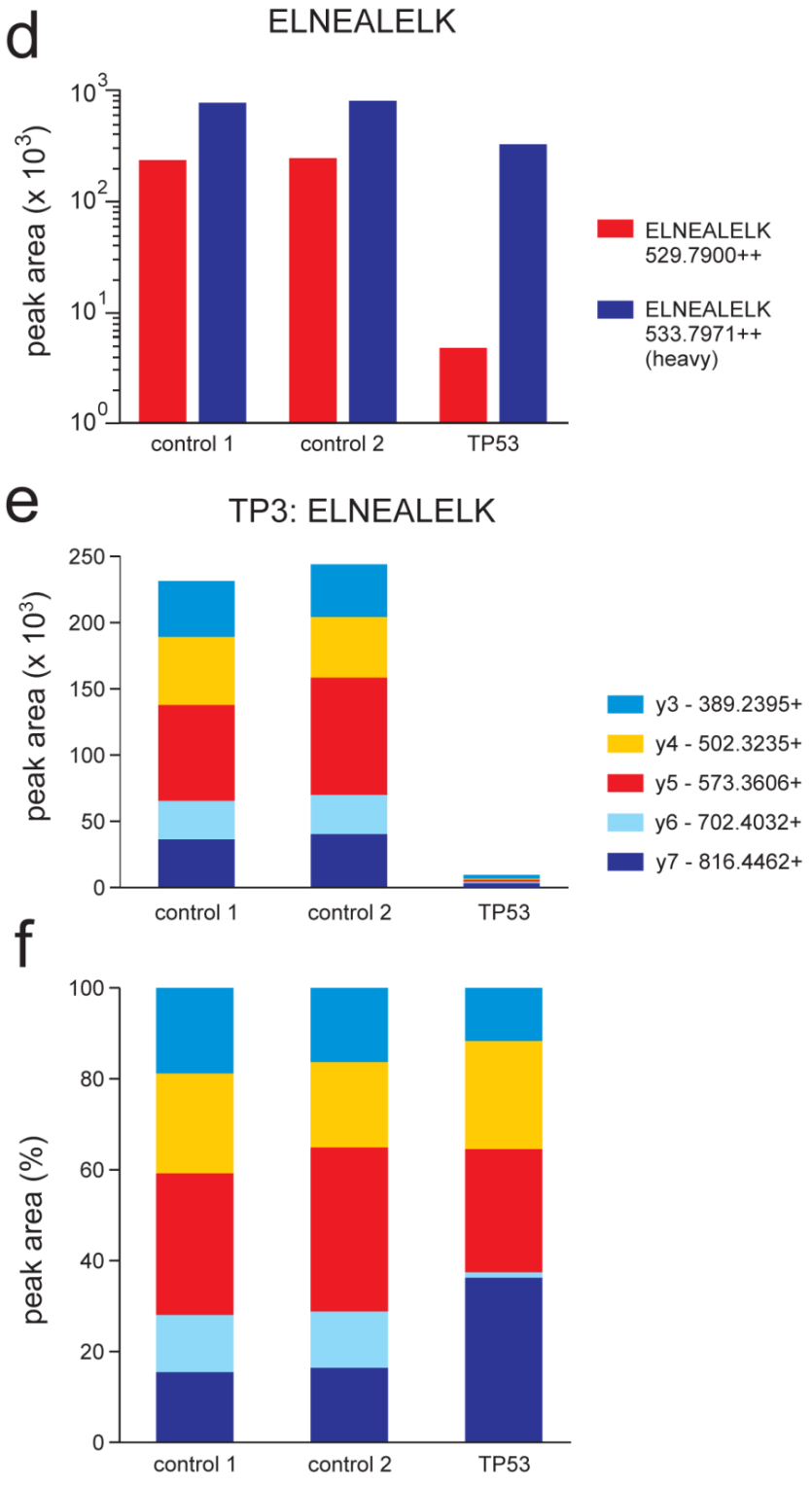

Supplementary figure 6

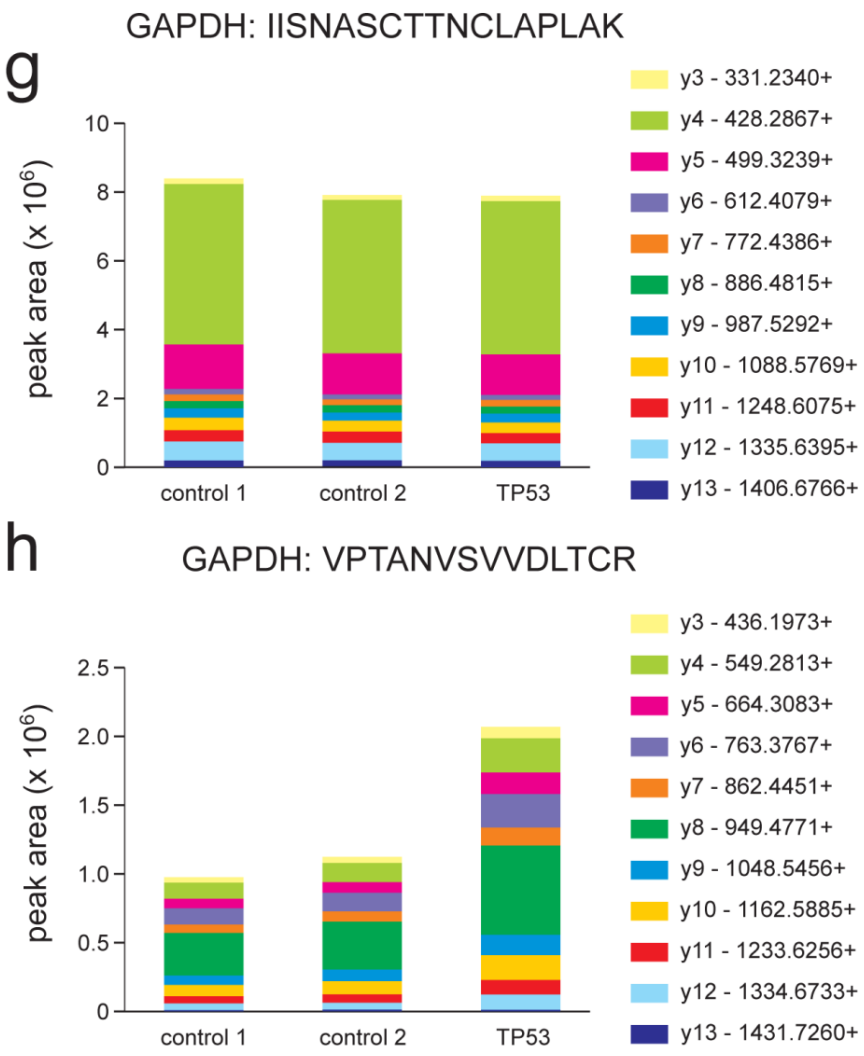

Supplementary Figure A.6: Target protein-specific ion ratios are maintained in samples having different protein abundances in samples where SIL were added. Two analytical replicates of control (without knockdown) lysate were run, followed by knockdown sample. Signal from spiked-in heavy peptides remained relatively even in samples with and without knockdown of endogenous protein, as detected for both analyzed TP53 peptides, ALPNNSSSPQPK (**a**) and ELNEALELK (**d**). Absolute (**b**) and normalized (**c**) ion ratios from TP53 peptide ALPNNSSSPQPK are shown for samples having substantially different amounts of endogenous TP53 protein. Panels (**e**) and (**f**) show ion ratios for TP53 peptide ELNEALELK, (**g**) and (**h**) show ion ratios for GAPDH peptides IISNASCTTNCLAPLAK and VPTANVSVVDLTCR, respectively.

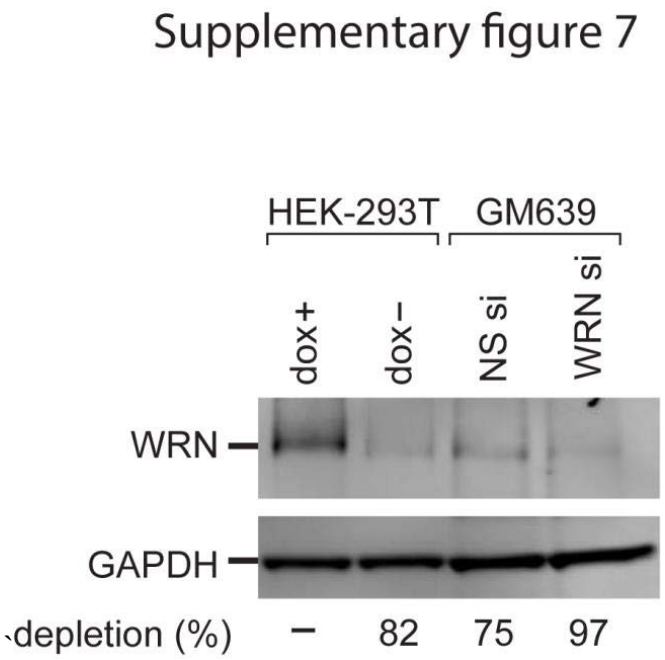

Supplementary Figure A.7: Western blot verification of WRN protein induction and depletion from human cells. Sample nomenclature is explained in legend for **Supplementary Figure A.8**.

Supplementary figure 8

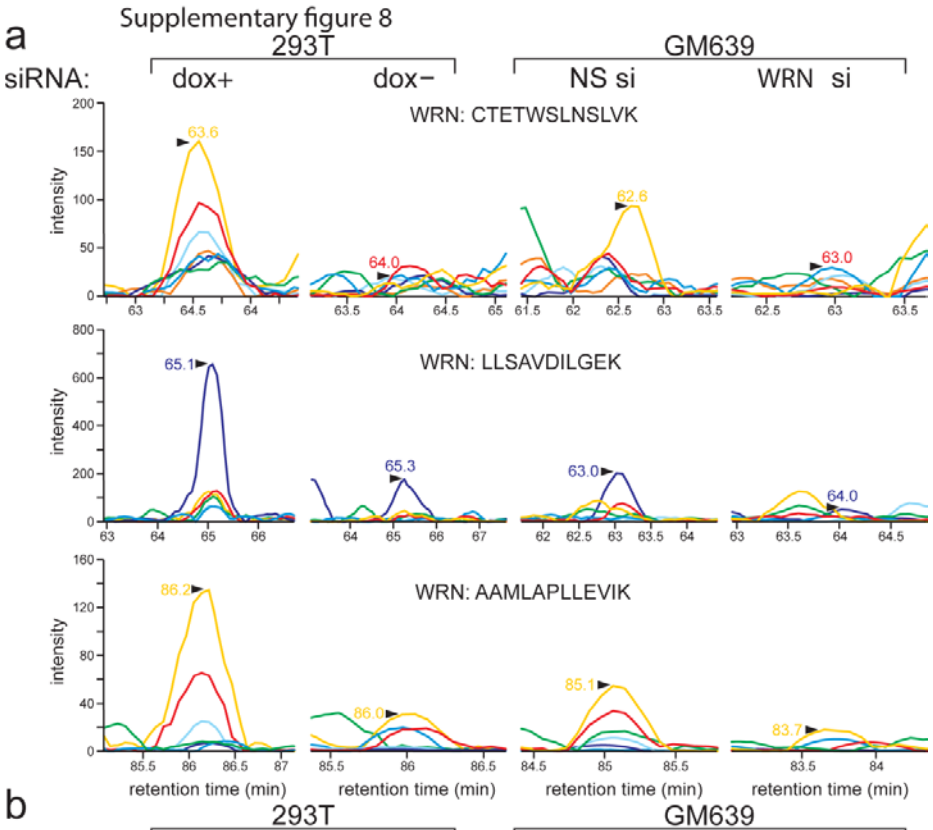

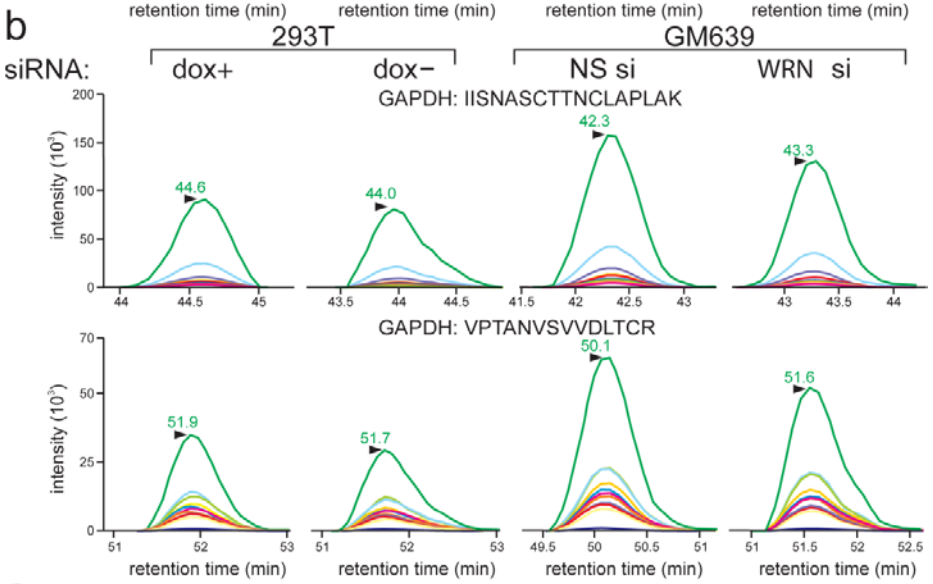

c

WRN peptide	/	control peptide	WRN depletion (%) normalized to dox+ dox−	NS si	WRN si
CTETWSLNSLVK	/	IISNASCTTNCLAPLAK	74.1	78.1	90.5
CTETWSLNSLVK	/	VPTANVSVVDLTCR	69.7	69.2	87.3
LLSAVDILGEK	/	IISNASCTTNCLAPLAK	72.2	84.2	95.5
LLSAVDILGEK	/	VPTANVSVVDLTCR	67.4	77.8	94.0
AAMLAPLLEVIK	/	IISNASCTTNCLAPLAK	83.4	84.8	94.5
AAMLAPLLEVIK	/	VPTANVSVVDLTCR	80.5	78.6	92.6

	dot products between experimental data and NIST spectral library dox+	dox−	NS si	WRN si
CTETWSLNSLVK	1.00	0.97	0.99	0.88
LLSAVDILGEK	1.00	0.98	0.97	0.94
AAMLAPLLEVIK	0.99	0.88	0.95	0.85
IISNASCTTNCLAPLAK	0.91	0.91	0.91	0.91
VPTANVSVVDLTCR	0.90	0.90	0.90	0.90

Supplementary Figure A.8: RNAi-mediated WRN protein depletion quantified by SRM. Specific peptides detected and quantified from WRN were CTETWSLNSLVK, LLSAVDILGEK, and AAMLAPLLEVIK. Their signal intensity was normalized against GAPDH peptides VPTANVSVVDLTCR and IISNASCTTNCLAPLAK. The chromatograms show sets of transitions for three peptides derived from target protein WRN (**a**) or loading control GAPDH (**b**) in human cell induction and RNAi depletion experiments. Tet-inducible Flp-In T-REx-293 cells were treated with doxycycline to induce increased expression of WRN in "dox+" samples, and were left uninduced for measurement of baseline expression in "dox-" samples. Human GM639 cells were treated with nonspecific RNAi ("NS si") or a *WRN*-specific siRNA ("*WRN* si") prior to SRM analysis. (**c**) TP53 depletion was quantified from individual peak area ratios determined for all measured peptides and normalized against an internal standard GAPDH as described in Methods. Dot products were calculated by Skyline to characterize the agreement between ion fragment ratios in our experimental data and NIST spectral library for each measured peptide.

Supplementary figure 9

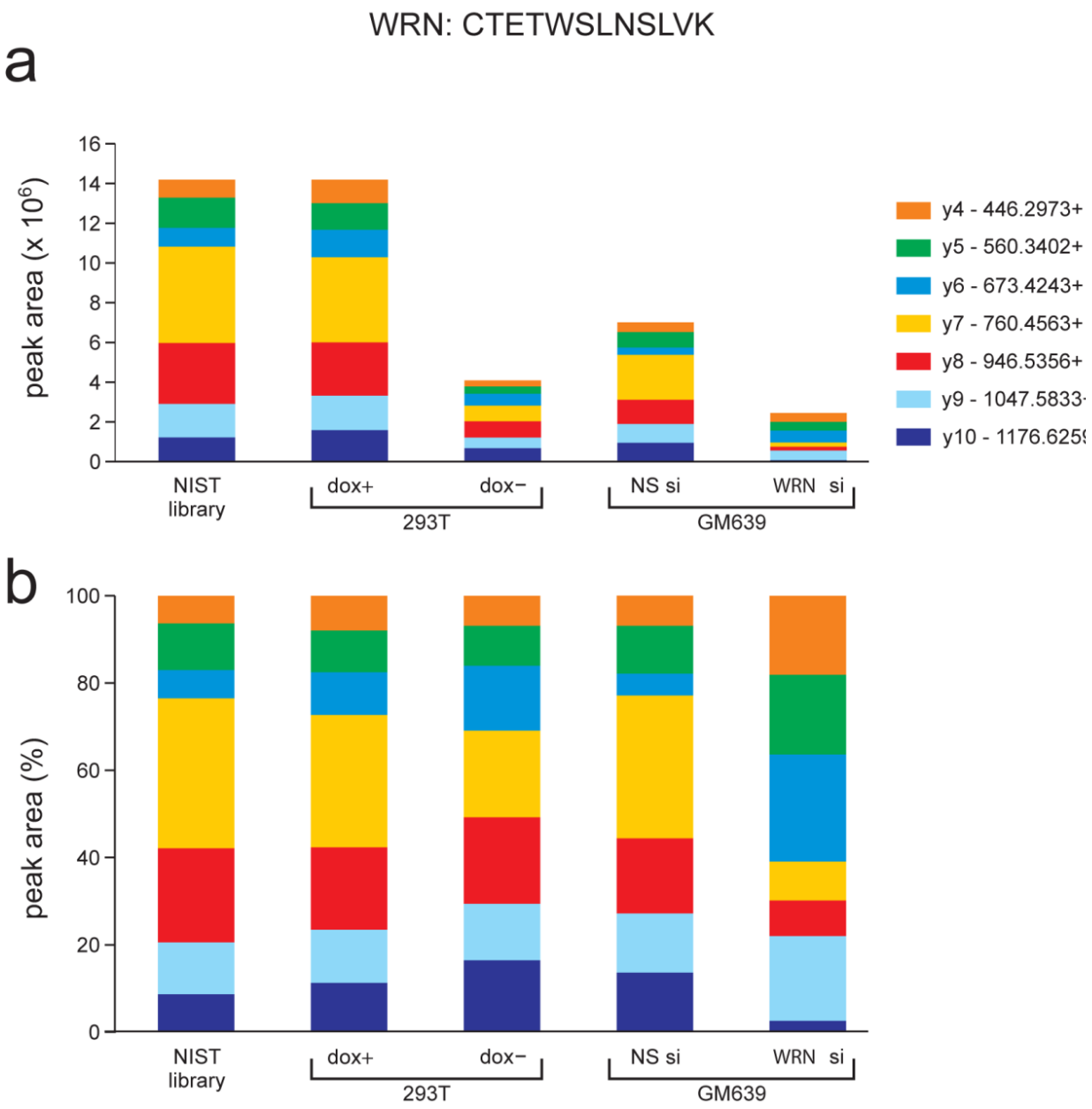

Supplementary figure 9

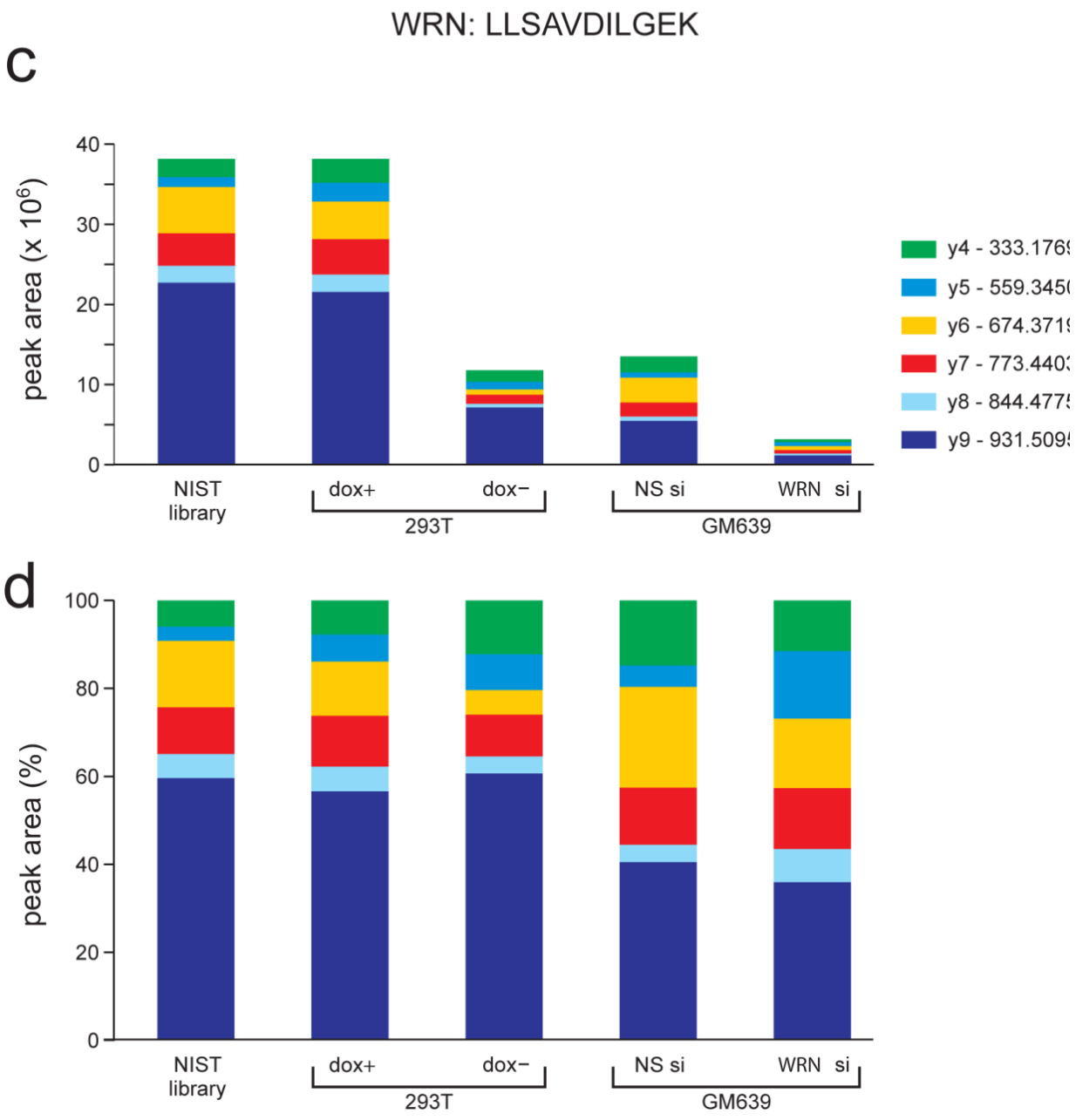

Supplementary figure 9

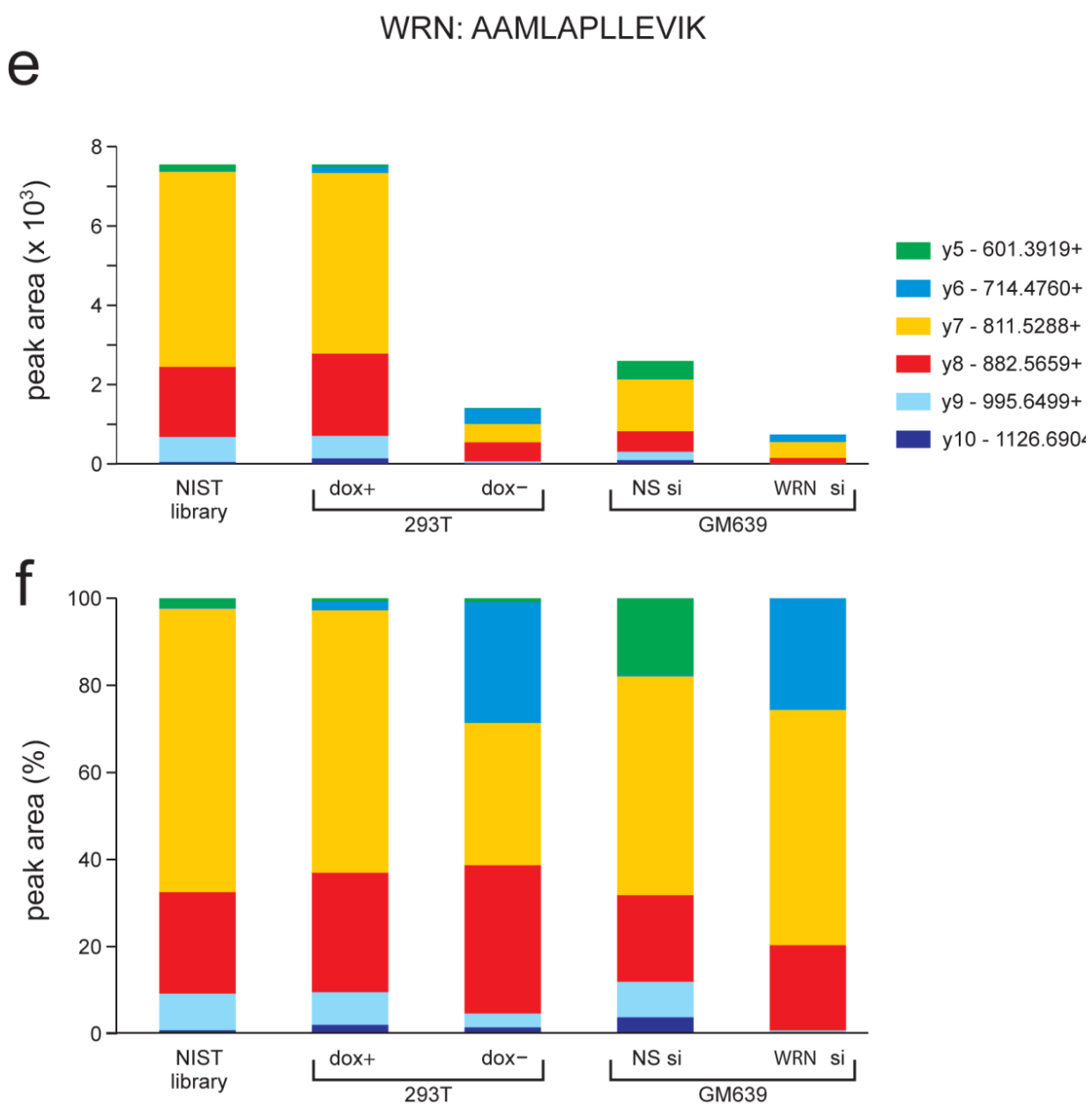

Supplementary figure 9

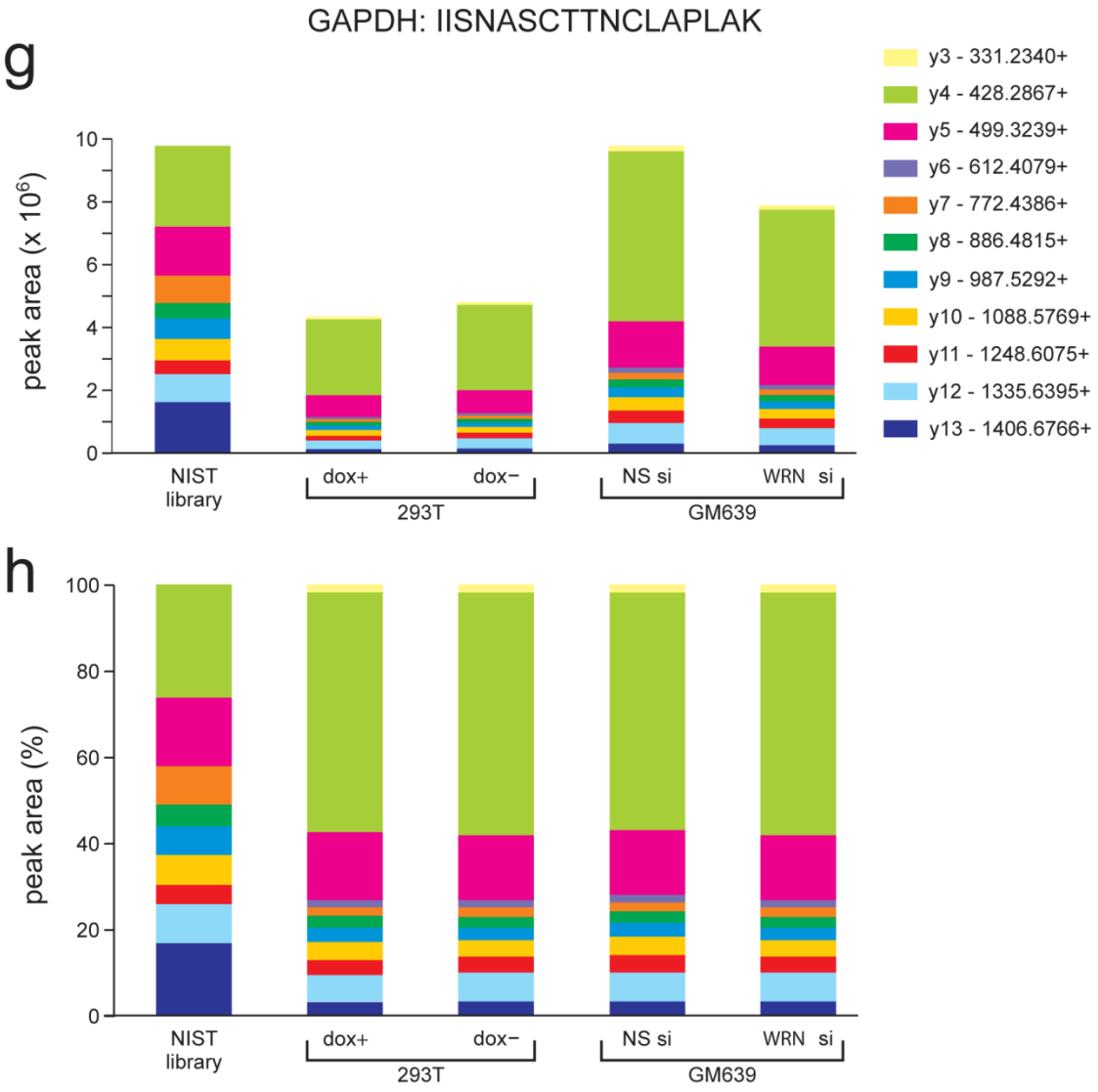

Supplementary figure 9

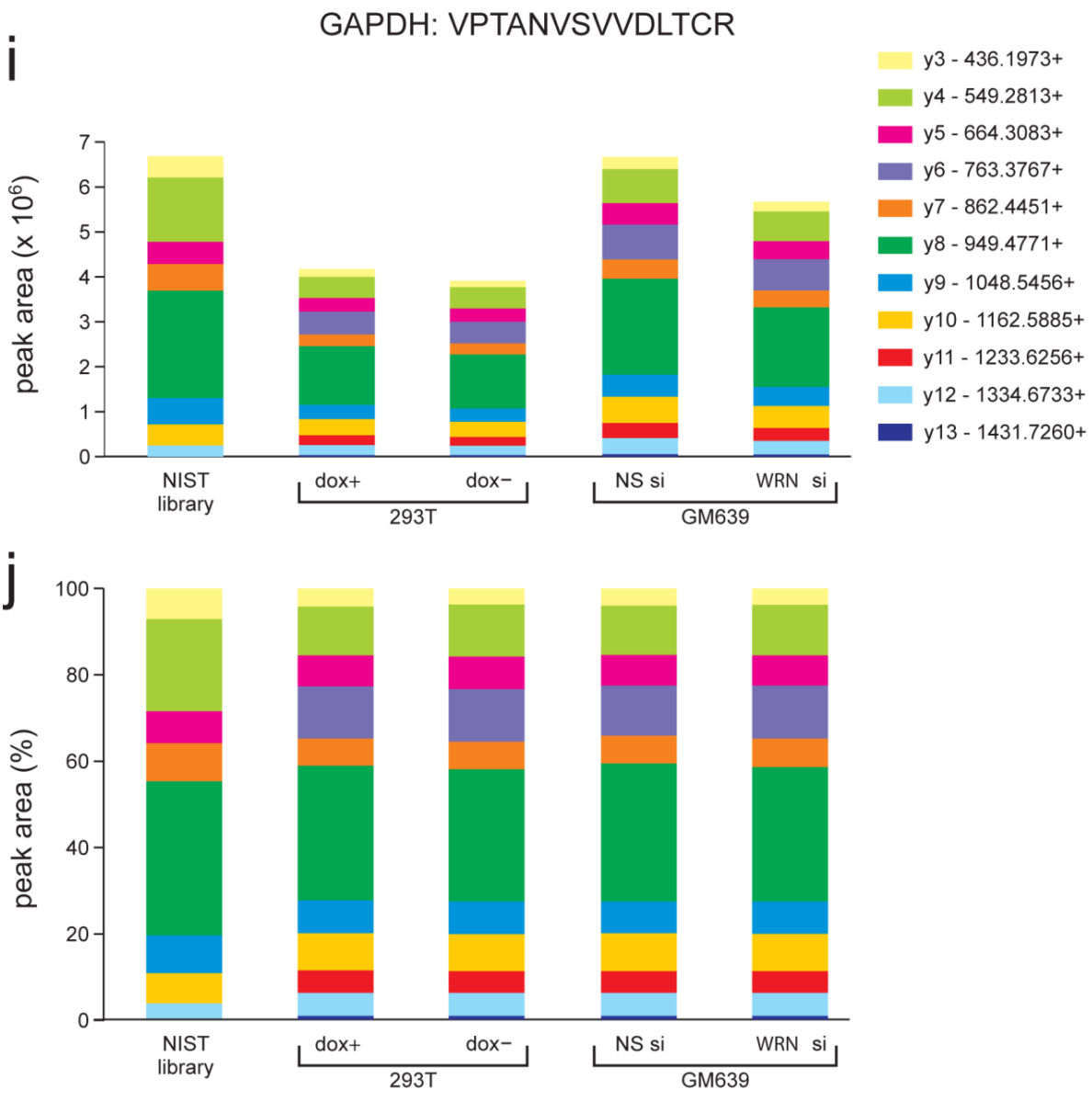

Supplementary Figure A.9: Target protein-specific ion ratios are verified against NIST spectral library, and maintained in samples expressing different amounts of WRN protein. Sample nomenclature is explained in legend for **Supplementary Figure 8**.
Absolute and normalized ion ratios are demonstrated for WRN peptides CTETWSLNSLVK, LLSAVDILGEK, and AAMLAPLLEVIK in panels (**a – f**), as well as GAPDH peptides VPTANVSVVDLTCR and IISNASCTTNCLAPLAK in panels (**g – j**).

Supplementary figure 10

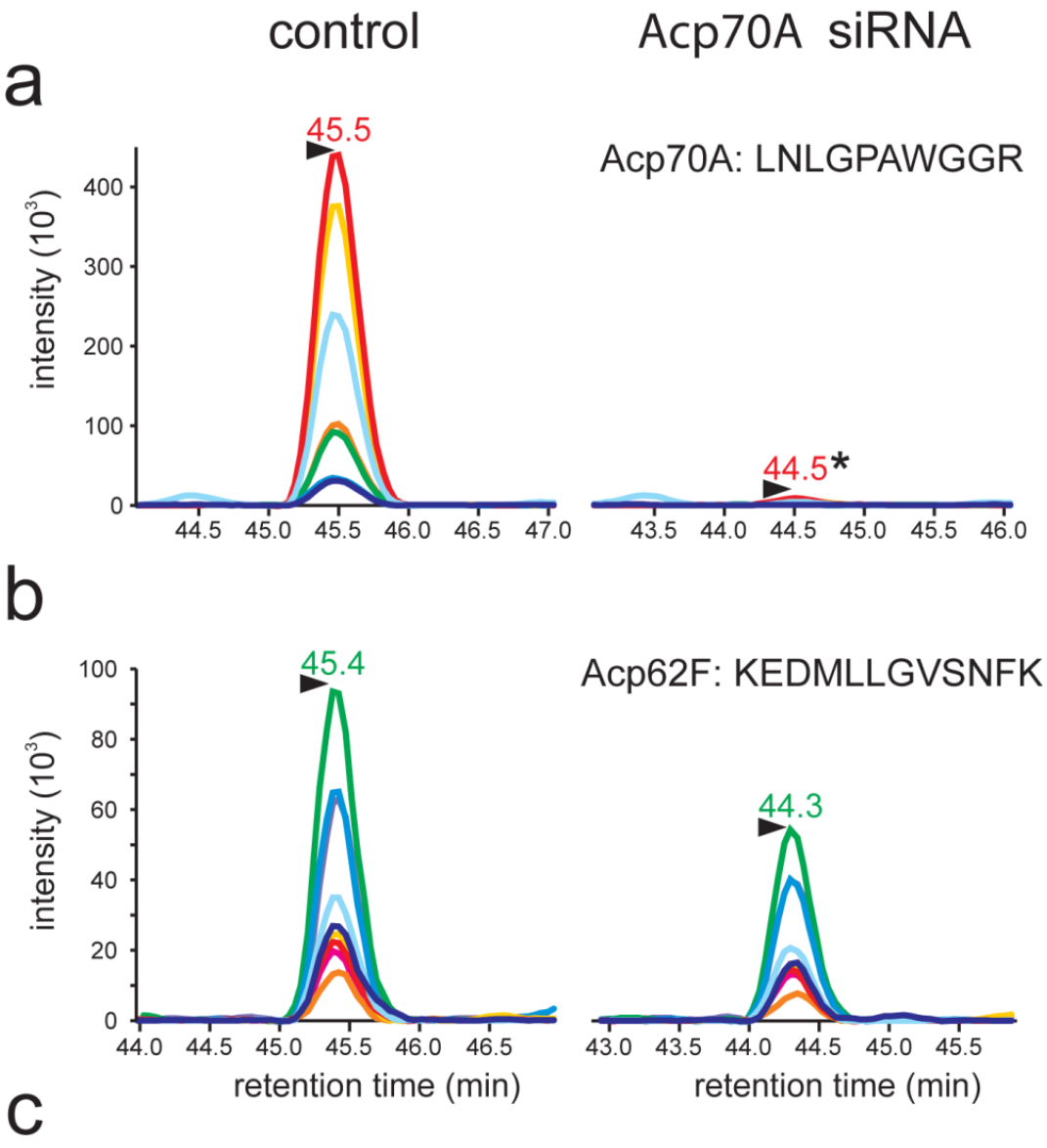

c

Acp70A peptide	/	Acp62F peptide	Acp70A depletion (%)
LNLGPAWGGR	/	KEDMLLGVSNFK	>99*

Supplementary figure 10

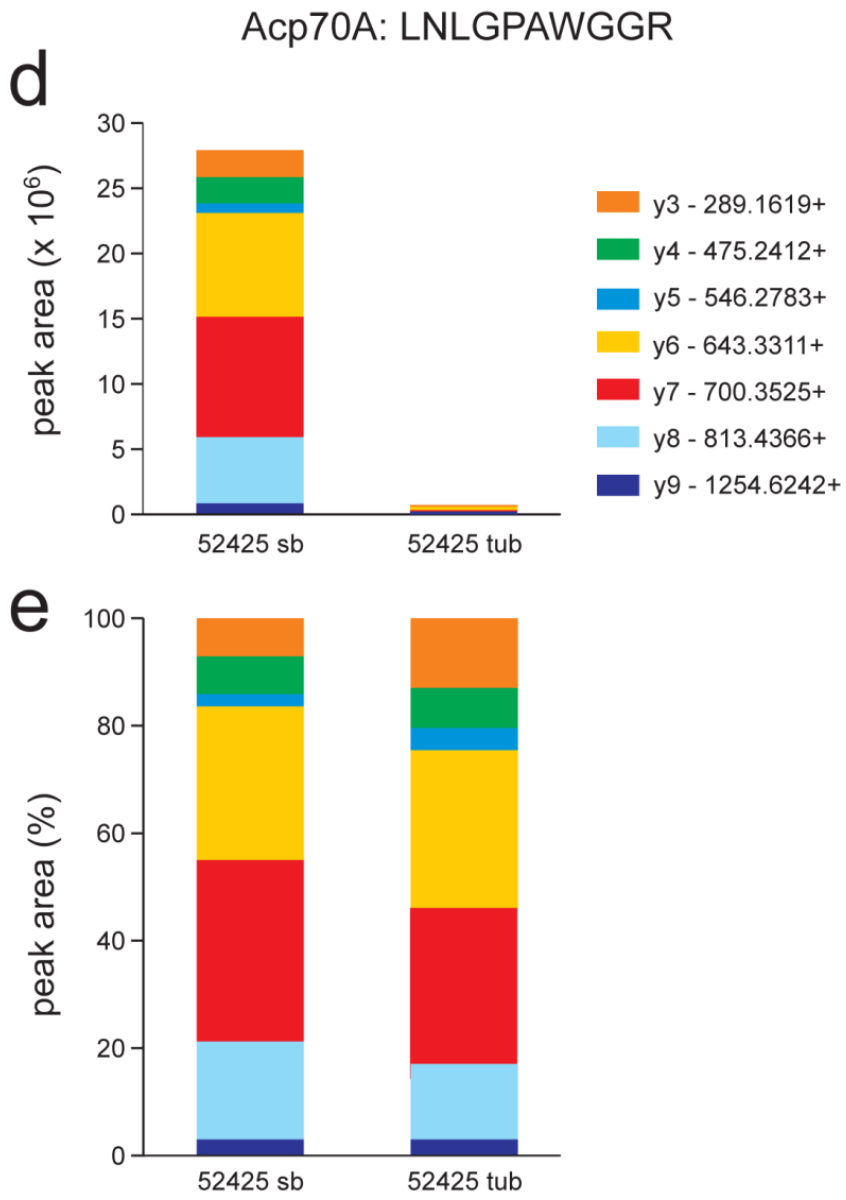

Supplementary figure 10

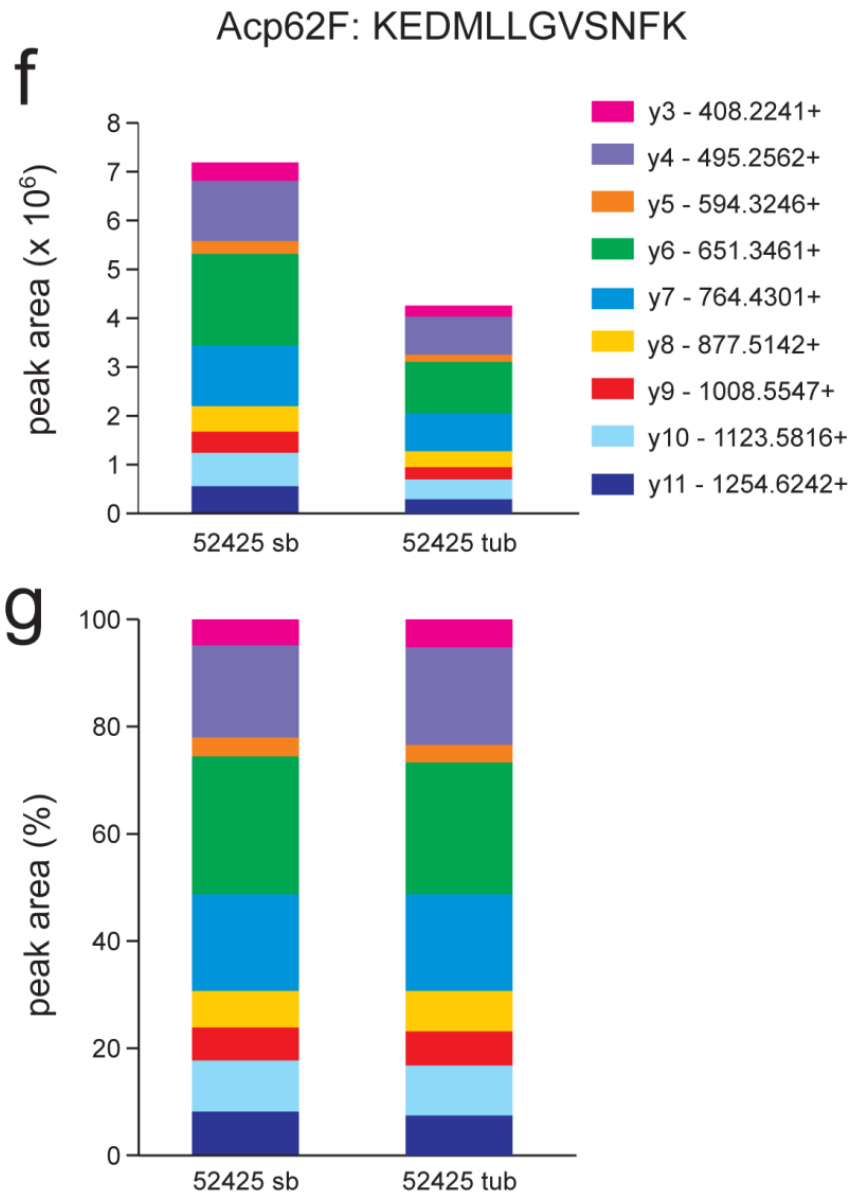

Supplementary Figure A.10: Ion chromatograms depicting RNAi-mediated depletion of accessory gland seminal fluid protein Acp70A from whole *Drosophila*. (**a**) SRM ion chromatograms for Acp70A peptide LNLGPAWGGR at *m/z* 520.8. (**b**) corresponding ion chromatograms for control protein Acp62F peptide KEDMLLGVSNFK at *m/z* 690.3. (**c**) quantitation of percent depletion of

RNAi target protein Acp70A versus Acp62F control based on SRM results. Peptide intensities were normalized against internal standard Acp62F within each sample, then compared between depleted and control samples to quantify Acp70A depletion. Residual signal in ion chromatograms for peptide LNLGPAWGGR (*) is derived from contaminants that are not Acp70A-derived (see text), and thus have been excluded from quantitation. Panels (**d**) and (**e**) show absolute and normalized ion ratios for Acp70A peptide LNLGPAWGGR, and (**f**) and (**g**) show absolute and normalized ion ratios for Acp62F peptide KEDMLLGVSNFK.

Supplementary figure 11

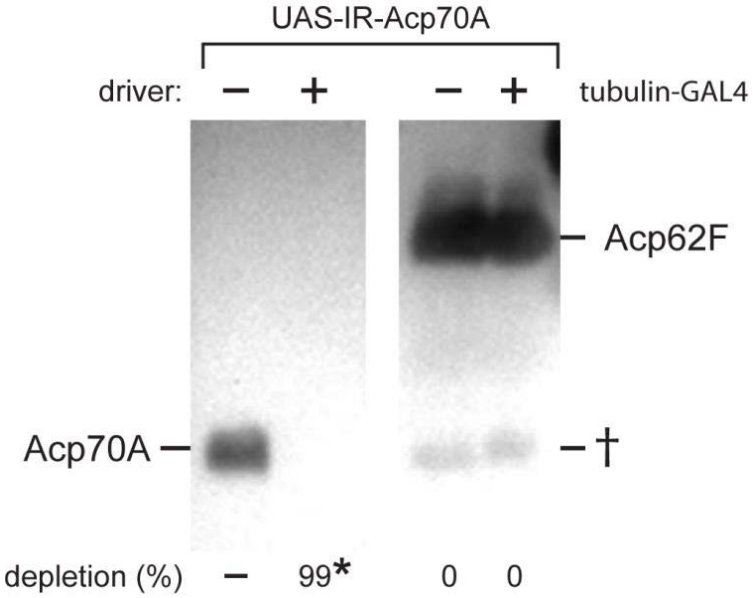

Supplementary Figure A.11: Western blot analysis of RNAi-mediated depletion of accessory gland seminal fluid protein Acp70A from whole *Drosophila*. Left panel: Acp70A was detected in control (*tubulin-GAL4* driver-minus (−) flies but not in RNAi expressing (+) flies (see Methods). Right panel: Internal control protein Acp62F, in contrast, was detected in both samples. A cross-reacting band detected by the anti-Acp62F antibody is denoted by a dagger (†). The asterisk (*) indicates percent Acp70A-specific depletion normalized to Acp62F in the same samples analyzed in **Supplementary Figure 10**.

Supplementary figure 12

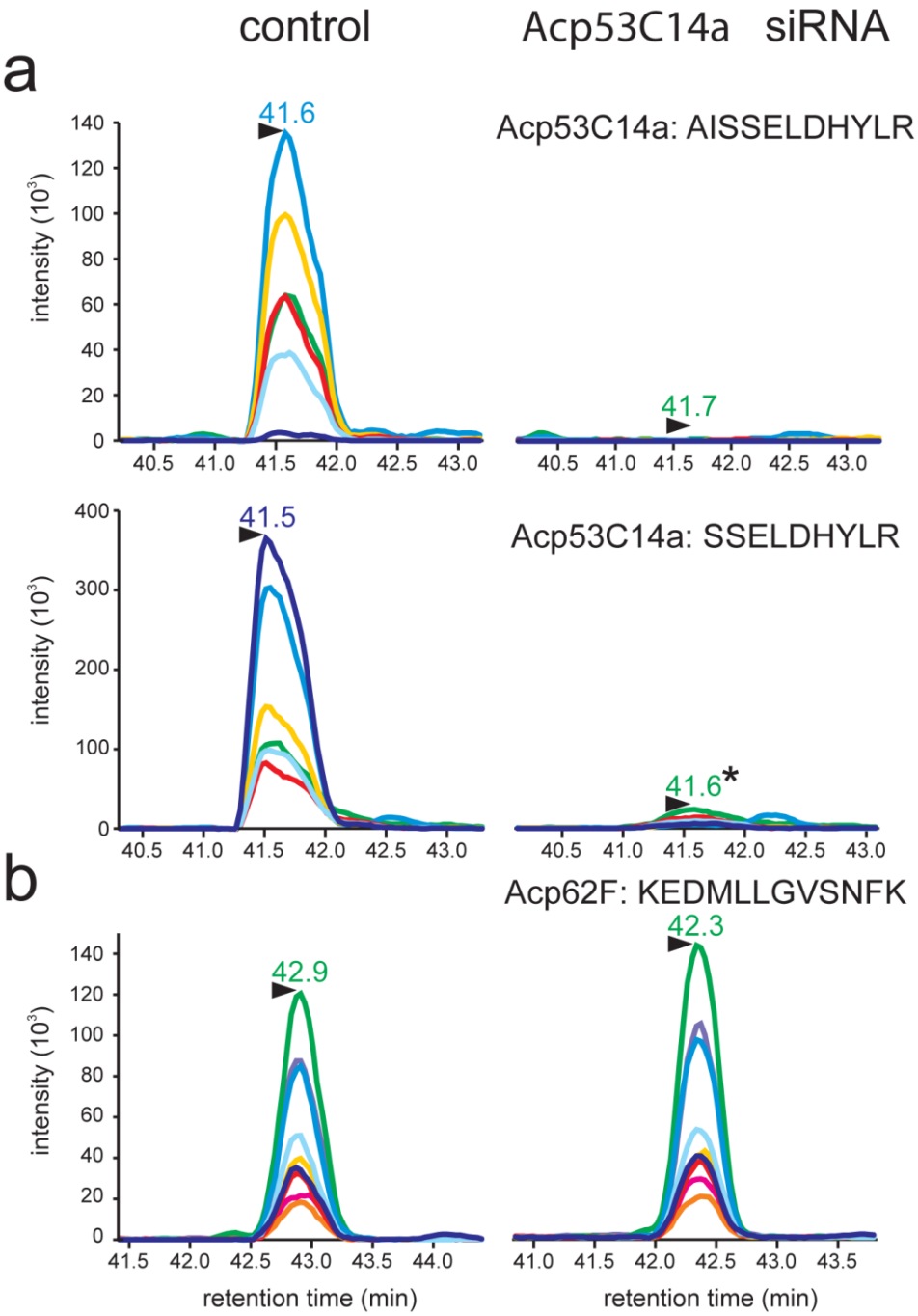

c

Acp53C14a peptide	/	Acp62F peptide	Acp53C14a depletion (%)
AISSELDHYLR	/	KEDMLLGVSNFK	93
SSELDHYLR	/	KEDMLLGVSNFK	>99*

Supplementary figure 12

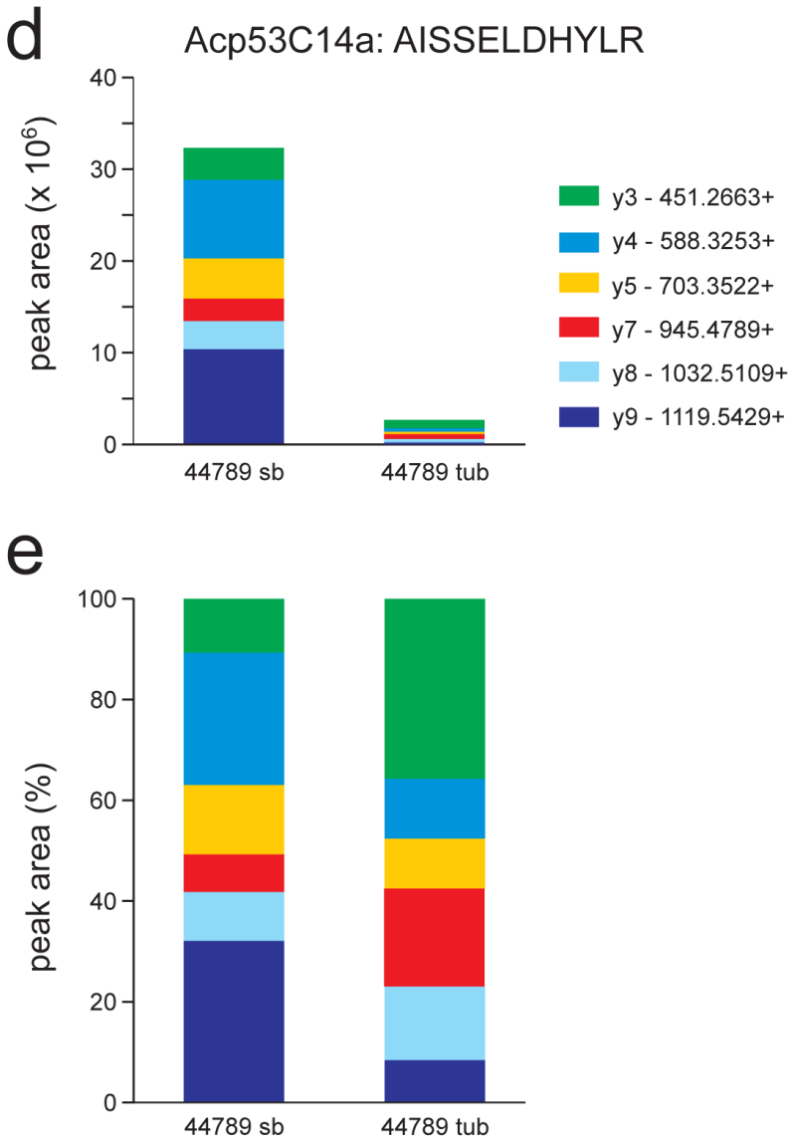

Supplementary figure 12

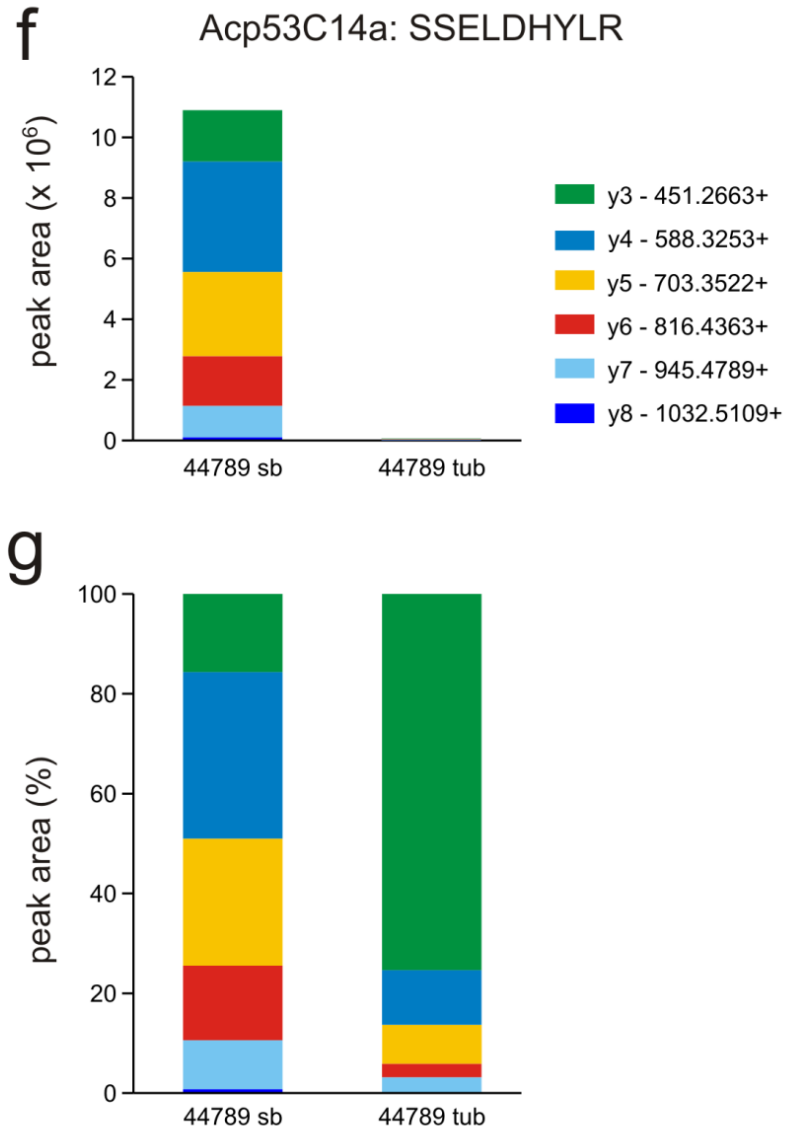

Supplementary figure 12

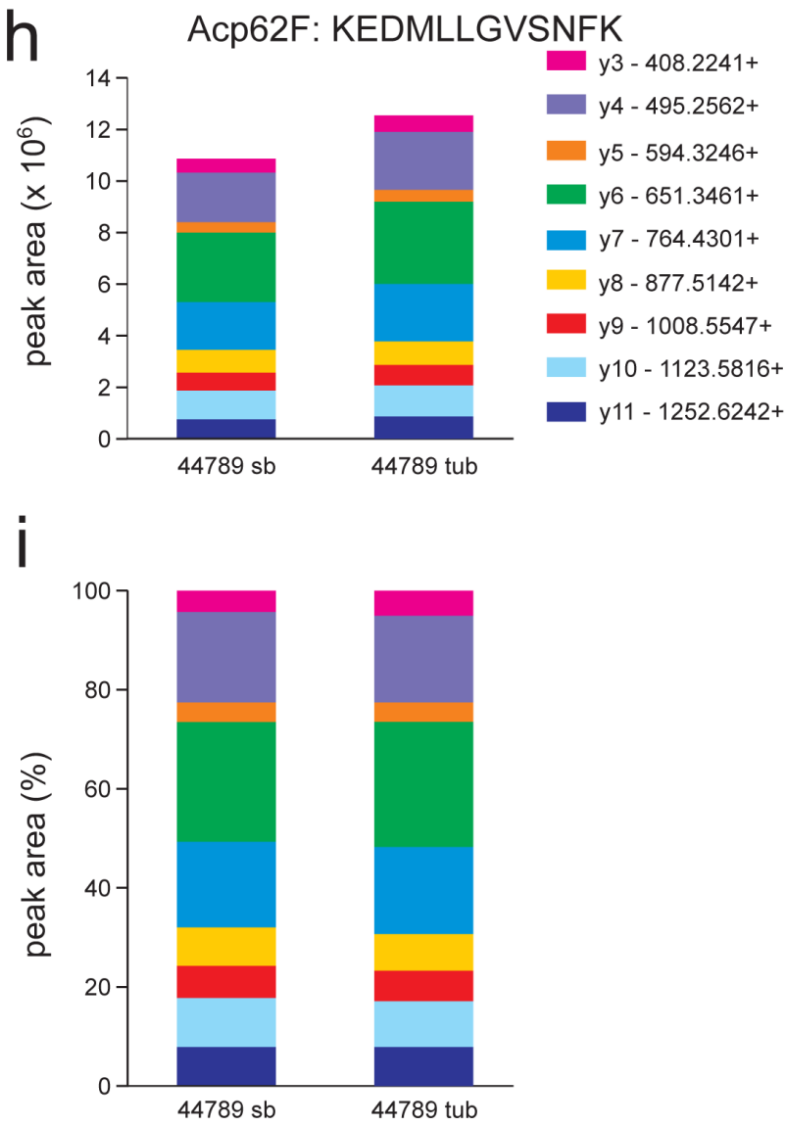

Supplementary Figure A.12: Ion chromatograms depicting RNAi-mediated depletion of accessory gland seminal fluid protein Acp53C14a from whole *Drosophila*. SRM ion chromatograms for (**a**) Acp53C14a peptides AISSELDHYLR at *m/z* 652.3 and SSELDHYLR at *m/z* 560.3 in flies expressing no (left column) or an *Acp53C14a*-specific siRNAi (right column), or for (**b**) control protein Acp62F peptide KEDMLLGVSNFK at *m/z* 690.3. (**c**) quantitation of percent depletion of

RNAi target protein Acp53C14a target peptide versus Acp62F control peptide. Peptide intensities were again normalized against internal standard Acp62F, then compared between depleted and control samples to quantify percent depletion of Acp53C14a. Residual signal in ion chromatograms for peptide SSELDHYLR (*) represents contaminants that are not Acp53C14a-derived, and thus have been excluded from quantitation.
Panels (**d**) and (**e**) show absolute and normalized ion ratios for Acp53C14a peptide AISSELDHYLR, (**f**) and (**g**) show absolute and normalized ion ratios for Acp53C14a peptide SSELDHYLR, and panels (**h**) and (**i**) show absolute and normalized ion ratios for Acp62F peptide KEDMLLGVSNFK.

Appendix B: Supplementary data from Chapter 4.

Contained here are all Supplementary data referenced in Chapter 4.

Supplementary tables:

Supplementary Table 1A: all nuclear proteins with SAINT score ≥0.9 in SH-WRN (+DMSO)

Supplementary Table 1B: all nuclear proteins with SAINT score ≥0.9 in SH-WRN (+CPT)

Supplementary figures:

Supplementary Figure B1: Full map of pFTSH-WRN plasmid

Supplementary Figure B2: complete GO_CC dendrogram (p-value cutoff 1E-2), as imported from CompGO. Input data is from **Supplementary Table 1A** as sample (1) and **Supplementary Table 1B** as sample (2).

Supplementary Figure B3: complete GO_BP dendrograms (p-value cutoff 1E-5), as imported from CompGO. Input data is from **Supplementary Table 1A** as sample (1) and **Supplementary Table 1B** as sample (2).

Supplementary Table 1A: Nuclear proteins that were found to interact with SH-WRN when sample was treated with DMSO. These proteins were identified in profiling analysis, and then analyzed by SAINT program to identify interacting partners that passed a significance threshold of Max SAINT score >=0.9. Nuclear localization was determined by Gene Ontology filtering. Proteins that are novel and were not previously reported to interact with WRN are identified in column "New ID", and are marked with a *. The protein results were cross-validated using CRAPome to determine overlap with frequently detected proteins in proteomics experiments. The overlap is presented, and marked with #.

Saint Bait	IPI	PreyGeneID	New ID	frequency of CRAPome detection	PreyGeneName	Description	(+DMSO) Total Spec	Number Rep	(+DMSO) SAINT score
WRN	IPI00002460	310	*	7 / 343	ANXA7	annexin A7	121	3	1
WRN	IPI00002495		*	1 / 343	EPN1	epsin 1	84	3	1
WRN	IPI00003310	5439	*	5 / 343	POLR2J	polymerase (RNA) II (DNA directed) polypeptide J, 13.3kDa	61	3	1
WRN	IPI00004860	5917	*	62 / 343	RARS	arginyl-tRNA synthetase	52	3	1
WRN	IPI00005154	6749		44 / 343	SSRP1	structure specific recognition protein 1	33	3	1
WRN	IPI00005705	5501	*	75 / 343	PPP1CC	protein phosphatase 1, catalytic subunit, gamma isoform	25	3	1
WRN	IPI00007283	5433	*	8 / 343	POLR2D	polymerase (RNA) II (DNA directed) polypeptide D	24	3	1
WRN	IPI00007423	10541	*	17 / 343	ANP32B	similar to Acidic leucine-rich nuclear phosphoprotein 32 family member B, PHAPI2 protein, protein SSP29	11	3	1
WRN	IPI00009713	6662	*		SOX9	SRY (sex determining region Y)-box 9	614	3	0.998
WRN	IPI00009727	58524	*		DMRT3	doublesex and mab-3 related transcription factor 3	406	3	0.998
WRN	IPI00010120	1488	*	6 / 343	CTBP2	C-terminal binding protein 2	280	3	0.998
WRN	IPI00011268	22913		37 / 343	RALY	RNA binding protein, autoantigenic (hnRNP-associated with lethal yellow homolog)	267	3	0.998
WRN	IPI00011756	4211	*		MEIS1	Meis homeobox 1	42	3	0.998
WRN	IPI00011916	7965	*	35 / 343	AIMP2	aminoacyl tRNA synthetase complex-interacting multifunctional protein 2; stromal antigen 3-like 3	41	3	0.998
WRN	IPI00012345	6431	*	84 / 343	SRSF6	splicing factor, arginine/serine-rich 6; similar to arginine/serine-rich splicing factor 6	16	3	0.998
WRN	IPI00013485	6187	*	143 / 343	RPS2	ribosomal protein S2	42	3	0.996
WRN	IPI00014938	84324	*	42 / 343	SARNP	SAP domain containing ribonucleoprotein	19	3	0.996
WRN	IPI00015953	9188		123 / 343	DDX21	DEAD (Asp-Glu-Ala-Asp) box polypeptide 21	18	3	0.996
WRN	IPI00017669	6605	*	13 / 343	SMARCE1	SWI/SNF related, matrix associated, actin dependent regulator of chromatin, subfamily e, member 1	16	3	0.996
WRN	IPI00019848	3054	*	26 / 343	HCFC1	host cell factor C1 (VP16-accessory protein)	11	3	0.996
WRN	IPI00020928	7019		13 / 343	TFAM	transcription factor A, mitochondrial	9	3	0.996
WRN	IPI00025057	103	*	30 / 343	ADAR	adenosine deaminase, RNA-specific	26	3	0.994
WRN	IPI00025277	10016	*	18 / 343	PDCD6	aryl-hydrocarbon receptor repressor; programmed cell death 6	15	3	0.994
WRN	IPI00026219	29894	*	33 / 343	CPSF1	cleavage and polyadenylation specific factor 1, 160kDa	9	3	0.994
WRN	IPI00026260	4831	*	95 / 343	NME2	non-metastatic cells 2, protein NM23B	59	3	0.99
WRN	IPI00026970	11198		39 / 343	SUPT16H	suppressor of Ty 16 homolog (S. cerevisiae)	52	3	0.99
WRN	IPI00026993	6045	*	12 / 343	RNF2	ring finger protein 2	18	3	0.988
WRN	IPI00029095	7027	*	3 / 343	TFDP1	transcription factor Dp-1	13	3	0.988
WRN	IPI00032201	5888		1 / 343	RAD51	RAD51 homolog (RecA homolog, E. coli)	25	3	0.986
WRN	IPI00157304	23648	*		SSBP3	single stranded DNA binding protein 3; hypothetical LOC100131851	9	3	0.98
WRN	IPI00163849	58513	*		EPS15L1	epidermal growth factor receptor pathway substrate 15-like 1	25	3	0.976
WRN	IPI00215965	3178	*	201 / 343	HNRNPA1	heterogeneous nuclear ribonucleoprotein A1	8	3	0.976
WRN	IPI00216592	3183	*	127 / 343	HNRNPC	heterogeneous nuclear ribonucleoprotein C (C1/C2)	11	3	0.972
WRN	IPI00216691	5216	*	93 / 343	PFN1	profilin 1	213	3	0.964
WRN	IPI00219037	3014		171 / 343	H2AFX	H2A histone family, member X	15	3	0.96
WRN	IPI00219084	5970	*	1 / 343	RELA	v-rel reticuloendotheliosis viral oncogene homolog A	28	3	0.956
WRN	IPI00220301	9588	*	96 / 343	PRDX6	peroxiredoxin 6	8	3	0.956
WRN	IPI00293616	8653		136 / 343	DDX3Y	DEAD (Asp-Glu-Ala-Asp) box polypeptide 3, Y-linked	145	3	0.954
WRN	IPI00296337	5591		114 / 343	PRKDC	similar to protein kinase, DNA-activated, catalytic polypeptide; protein kinase, DNA-activated, catalytic polypeptide	11	3	0.954
WRN	IPI00305289	3832	*	112 / 343	KIF11	kinesin family member 11	171	3	0.952
WRN	IPI00334587	3182	*	144 / 343	HNRNPAB	heterogeneous nuclear ribonucleoprotein A/B	23	3	0.952

WRN	IPI00337602	284695	*	31 / 343	ZNF326	zinc finger protein 326	14	3	0.952
WRN	IPI00376317	23644	*	14 / 343	EDC4	enhancer of mRNA decapping 4	12	3	0.95
WRN	IPI00384444	3861	*	230 / 343	KRT14	keratin 14	29	3	0.948
WRN	IPI00396378	3181	*	197 / 343	HNRNPA2B1	heterogeneous nuclear ribonucleoprotein A2/B1	14	3	0.948
WRN	IPI00409671	11325	*	20 / 343	DDX42	DEAD (Asp-Glu-Ala-Asp) box polypeptide 42	118	3	0.944
WRN	IPI00419880	6189		141 / 343	RPS3A	ribosomal protein S3A	10	3	0.942
WRN	IPI00457114	9922	*	1 / 343	IQSEC1	IQ motif and Sec7 domain 1	5	3	0.942
WRN	IPI00465070	8968	*	88 / 343	HIST1H3F	histone cluster 1, H3	12	3	0.928
WRN	IPI00465248	2023	*	155 / 343	ENO1	enolase 1, (alpha)	37	3	0.926
WRN	IPI00465387	157313	*	7 / 343	CDCA2	cell division cycle associated 2	17	3	0.926
WRN	IPI00550021	6122	*	113 / 343	RPL3	ribosomal protein L3; similar to 60S ribosomal protein L3 (L4)	7	3	0.924
WRN	IPI00550363	8407	*	96 / 343	TAGLN2	transgelin 2	27	3	0.922
WRN	IPI00550451	5499	*	75 / 343	PPP1CA	protein phosphatase 1, catalytic subunit, alpha isoform	9	3	0.918
WRN	IPI00556494	29079	*		MED4	mediator complex subunit 4	10	3	0.916
WRN	IPI00640981	23352	*	21 / 343	UBR4	ubiquitin protein ligase E3 component n-recognin 4	9	3	0.916
WRN	IPI00641829	7919	*	84 / 343	DDX39B	HLA-B associated transcript 1	88	3	0.914
WRN	IPI00789551		*	116 / 343	MATR3	matrin 3	13	3	0.912
WRN	IPI00854786		*		BAT2	HLA-B associated transcript 2	19	3	0.906
WRN	IPI00908873	9221	*	61 / 343	NOLC1	nucleolar and coiled-body phosphoprotein 1	15	3	0.902
WRN	IPI00909560		*		PKM	similar to Pyruvate kinase, isozymes M1/M2, CTHBP	5	3	0.902

Table B.1: List of all nuclear proteins with SAINT score ≥0.9 in SH-WRN (+DMSO)

Supplementary Table 1B: Nuclear proteins that were found to interact with SH-WRN when sample was treated with CPT. These proteins were identified in profiling analysis, and then analyzed by SAINT program to identify interacting partners that passed a significance threshold of Max SAINT score >=0.9. Nuclear localization was determined by Gene Ontology filtering. Proteins that are novel and were not previously reported to interact with WRN are identified in column "New ID", and are marked with a *. The protein results were cross-validated using CRAPome to determine overlap with frequently detected proteins in proteomics experiments. The overlap is presented, and marked with #.

Saint Bait	Prey	PreyGeneID	New ID	frequency of CRAPome detection	PreyGeneName	Description	(+CPT) Total Spec	Number Rep	(+CPT) Max SAINT
WRN	IPI00012074	10236	*	129 / 343	HNRNPR	heterogeneous nuclear ribonucleoprotein R	130	3	1
WRN	IPI00012066	5094	*	126 / 343	PCBP2	poly(rC) binding protein 2	127	3	1
WRN	IPI00004860	5917	*	62 / 343	RARS	arginyl-tRNA synthetase	52	3	1
WRN	IPI00017334	5245		58 / 343	PHB	prohibitin	35	3	1
WRN	IPI00020928	7019		13 / 343	TFAM	transcription factor A, mitochondrial	33	3	1
WRN	IPI00550363	8407	*	96 / 343	TAGLN2	transgelin 2	32	3	1
WRN	IPI00220301	9588	*	96 / 343	PRDX6	peroxiredoxin 6	21	3	1
WRN	IPI00782992	23524	*	85 / 343	SRRM2	serine/arginine repetitive matrix 2; hypothetical LOC100132779	21	3	1
WRN	IPI00005154	6749		44 / 343	SSRP1	structure specific recognition protein 1	17	3	1
WRN	IPI00293616	8653		136 / 343	DDX3Y	DEAD (Asp-Glu-Ala-Asp) box polypeptide 3, Y-linked	16	3	1
WRN	IPI00015806	9330	*	8 / 343	GTF3C3	general transcription factor IIIC, polypeptide 3, 102kDa	12	3	1
WRN	IPI00640981	23352	*	21 / 343	UBR4	ubiquitin protein ligase E3 component n-recognin 4	225	3	0.998
WRN	IPI00014456	6801	*	3 / 343	STRN	striatin, calmodulin binding protein	32	3	0.998
WRN	IPI00216730	317772	*	164 / 343	HIST2H2AB	histone cluster 2, H2ab	23	3	0.998
WRN	IPI00019848	3054	*	26 / 343	HCFC1	host cell factor C1 (VP16-accessory protein)	19	3	0.998
WRN	IPI00012578	3840	*	25 / 343	KPNA4	karyopherin alpha 4 (importin alpha 3)	18	3	0.998
WRN	IPI00018534	8340	*	160 / 343	HIST1H2BL	histone cluster 1, H2bl	70	3	0.996
WRN	IPI00465248	2023	*	155 / 343	ENO1	enolase 1, (alpha)	27	3	0.996
WRN	IPI00011916	7965	*	35 / 343	AIMP2	aminoacyl tRNA synthetase complex-interacting multifunctional protein 2; stromal antigen 3-like 3	16	3	0.996
WRN	IPI00784161	6830	*	24 / 343	SUPT6H	suppressor of Ty 6 homolog (S. cerevisiae)	136	3	0.994
WRN	IPI00644712	2547		114 / 343	XRCC6	X-ray repair complementing defective repair in Chinese hamster cells 6; similar to ATP-dependent DNA helicase II, 70 kDa subunit	416	3	0.99
WRN	IPI00291608		*	11 / 343	PCNP	PEST proteolytic signal containing nuclear protein	28	3	0.988
WRN	IPI00005024	10514	*	70 / 343	MYBBP1A	MYB binding protein (P160) 1a	25	3	0.988
WRN	IPI00292894	55720	*	24 / 343	TSR1	TSR1, 20S rRNA accumulation, homolog (S. cerevisiae)	63	3	0.986
WRN	IPI00384444	3861	*	230 / 343	KRT14	keratin 14	8	3	0.986
WRN	IPI00216457	723790	*	206 / 343	HIST2H2AA4	histone cluster 2, H2aa3; histone cluster 2, H2aa4	9	3	0.984
WRN	IPI00465028	7167	*	75 / 343	TPI1	TPI1 pseudogene; triosephosphate isomerase 1	8	3	0.98
WRN	IPI00298731	5514	*	18 / 343	PPP1R10	protein phosphatase 1, regulatory (inhibitor) subunit 10	39	3	0.978
WRN	IPI00375441	8880	*	22 / 343	FUBP1	far upstream element (FUSE) binding protein 1	28	3	0.976
WRN	IPI00456722	253959	*	1 / 343	RALGAPA1	GTPase activating Rap/RanGAP domain-like 1	22	3	0.972
WRN	IPI00419585	5478	*	131 / 343	PPIA	similar to TRIMCyp; peptidylprolyl isomerase A (cyclophilin A)	11	3	0.972
WRN	IPI00550821	79869	*	36 / 343	CPSF7	cleavage and polyadenylation specific factor 7, 59kDa	24	3	0.97
WRN	IPI00002495		*	1 / 343	EPN1	epsin 1	11	3	0.97
WRN	IPI00479786	8570	*	71 / 343	KHSRP	KH-type splicing regulatory protein	205	3	0.968
WRN	IPI00010120	1488	*	6 / 343	CTBP2	C-terminal binding protein 2	16	3	0.968
WRN	IPI00218570	5224	*	48 / 343	PGAM2	phosphoglycerate mutase 2 (muscle)	7	3	0.968
WRN	IPI00789551		*	116 / 343	MATR3	matrin 3	150	3	0.966
WRN	IPI00295485	22824	*	37 / 343	HSPA4L	heat shock 70kDa protein 4-like	11	3	0.964
WRN	IPI00304589	85456	*	7 / 343	TNKS1BP1	tankyrase 1 binding protein 1, 182kDa	9	3	0.964
WRN	IPI00414656	4794	*		NFKBIE	nuclear factor of kappa light polypeptide gene enhancer in B-cells inhibitor, epsilon	24	3	0.962
WRN	IPI00020194	8148	*	109 / 343	TAF15	TAF15 RNA polymerase II, TATA box binding protein (TBP)-associated factor, 68kDa	12	3	0.962
WRN	IPI00909560		*		PKM	similar to Pyruvate kinase, isozymes M1/M2, CTHBP	27	3	0.96
WRN	IPI00216592	3183	*	127 / 343	HNRNPC	heterogeneous nuclear ribonucleoprotein C (C1/C2)	335	3	0.958

WRN	IPI00000846	1108		28 / 343	CHD4	chromodomain helicase DNA binding protein 4	40	3	0.958
WRN	IPI00742127		*	201 / 343	HNRNPA1	heterogeneous nuclear ribonucleoprotein A1	167	3	0.956
WRN	IPI00296337	5591		114 / 343	PRKDC	similar to protein kinase, DNA-activated, catalytic polypeptide; protein kinase, DNA-activated, catalytic polypeptide	342	3	0.954
WRN	IPI00249267		*	182 / 343	H2AFZ	H2A histone family, member Z	10	3	0.954
WRN	IPI00376317	23644	*	14 / 343	EDC4	enhancer of mRNA decapping 4	9	3	0.954
WRN	IPI00215978	661	*		POLR3D	polymerase (RNA) III (DNA directed) polypeptide D, 44kDa	13	3	0.952
WRN	IPI00328319	5928	*	92 / 343	RBBP4	hypothetical LOC642954; retinoblastoma binding protein 4	7	3	0.952
WRN	IPI00221235	23279	*	12 / 343	NUP160	nucleoporin 160kDa	27	3	0.948
WRN	IPI00414482	2975	*	10 / 343	GTF3C1	general transcription factor IIIC, polypeptide 1, alpha 220kDa	17	3	0.942
WRN	IPI00299517	23172	*		FAM175B	family with sequence similarity 175, member B	28	3	0.938
WRN	IPI00644431	10212		84 / 343	DDX39A	DEAD (Asp-Glu-Ala-Asp) box polypeptide 39	17	3	0.934
WRN	IPI00550021	6122	*	113 / 343	RPL3	ribosomal protein L3; similar to 60S ribosomal protein L3 (L4)	82	3	0.932
WRN	IPI00556594	55596	*	16 / 343	ZCCHC8	zinc finger, CCHC domain containing 8	11	3	0.932
WRN	IPI00373877	284695	*	31 / 343	ZNF326	zinc finger protein 326	6	3	0.932
WRN	IPI00026970	11198		39 / 343	SUPT16H	suppressor of Ty 16 homolog (S. cerevisiae)	17	3	0.93
WRN	IPI00297655	4853	*	4 / 343	NOTCH2	Notch homolog 2 (Drosophila)	7	3	0.93
WRN	IPI00009727	58524	*		DMRT3	doublesex and mab-3 related transcription factor 3	8	3	0.928
WRN	IPI00032201	5888		1 / 343	RAD51	RAD51 homolog (RecA homolog, E. coli) (S. cerevisiae)	33	3	0.926
WRN	IPI00167941	23195	*	12 / 343	MDN1	MDN1, midasin homolog (yeast)	16	3	0.926
WRN	IPI00158615	57187		23 / 343	THOC2	THO complex 2	11	3	0.926
WRN	IPI00171199	5684	*	45 / 343	PSMA3	proteasome (prosome, macropain) subunit, alpha type, 3	6	3	0.926
WRN	IPI00002460	310	*	7 / 343	ANXA7	annexin A7	62	3	0.924
WRN	IPI00760620	664709	*		HNRNPA1P10	heterogeneous nuclear ribonucleoprotein A1-like	241	3	0.922
WRN	IPI00017303	4436		19 / 343	MSH2	mutS homolog 2, colon cancer, nonpolyposis type 1 (E. coli)	5	3	0.916
WRN	IPI00176903	284119	*	13 / 343	PTRF	polymerase I and transcript release factor	6	3	0.91
WRN	IPI00028109	84661	*	21 / 343	DPY30	dpy-30 homolog (C. elegans)	9	3	0.906

Table B.2: List of all nuclear proteins with SAINT score ≥0.9 in SH-WRN (+DMSO)

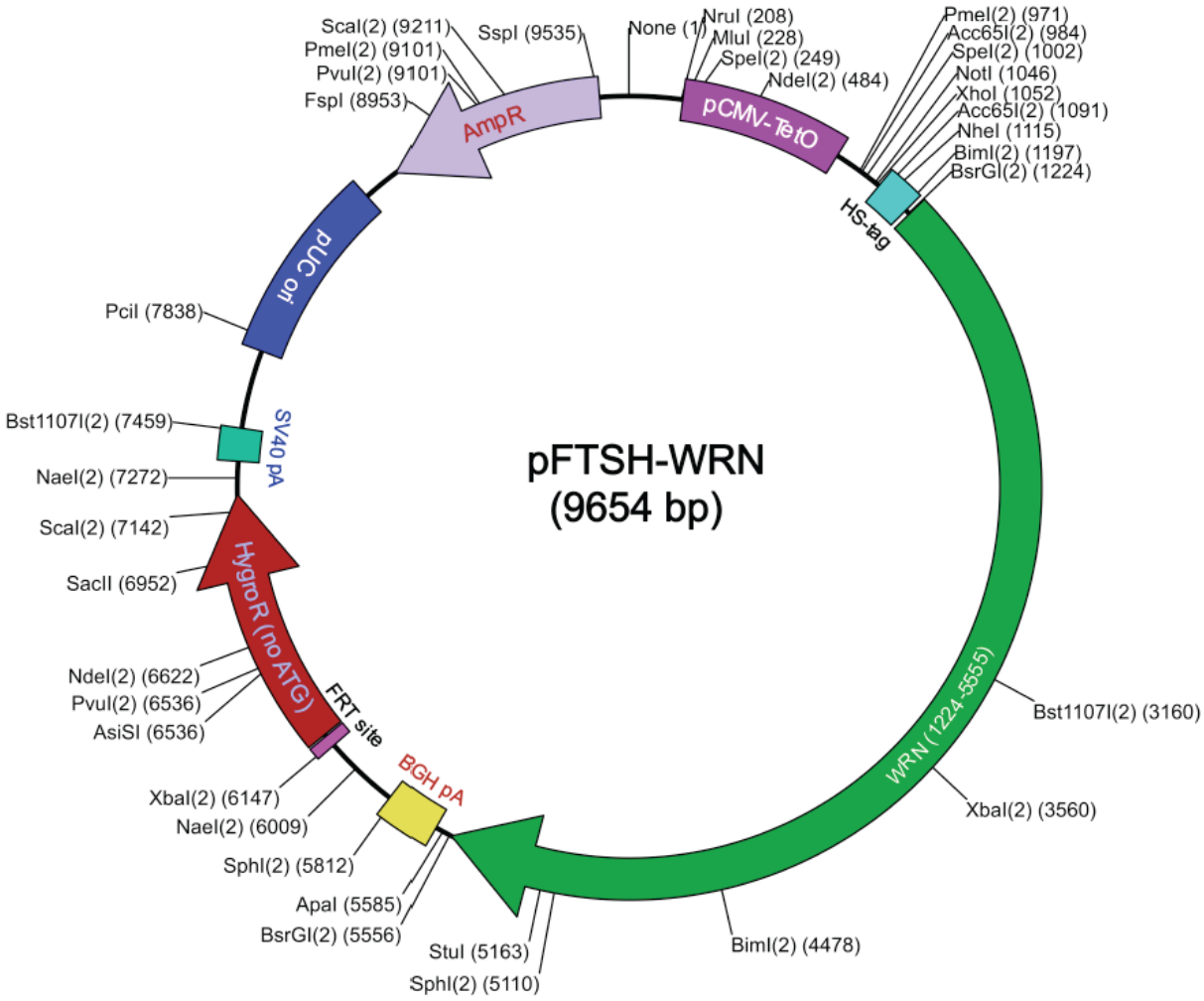

Supplementary Figure B.1: Nuclear proteins that were found to interact with SH-WRN when sample was treated with DMSO. These proteins were identified in profiling analysis, and then analyzed by SAINT program to identify interacting partners that passed a significance threshold of Max SAINT score >=0.9. Nuclear localization was determined by Gene Ontology filtering. Proteins that are novel and were not previously reported to interact with WRN are identified in column "New ID", and are marked with a *. The protein results were cross-validated using CRAPome to determine overlap with frequently detected proteins in proteomics experiments. The overlap is presented, and marked with #.

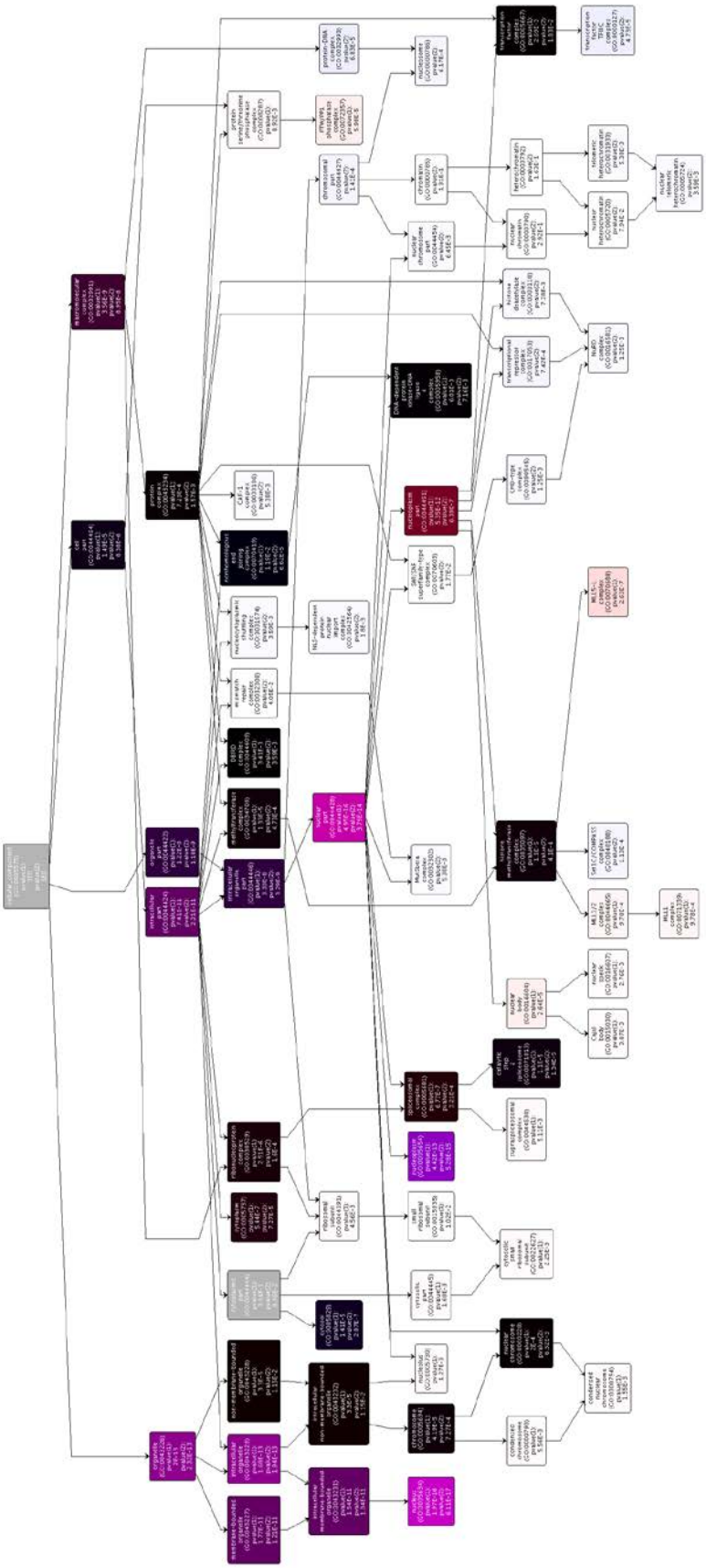

Supplementary Figure B.2: Full-size dendrogram demonstrating the dominant gene ontology categories by cellular component between WRN-enriched samples that were treated either with control DMSO (trending blue) or CPT (trending red).

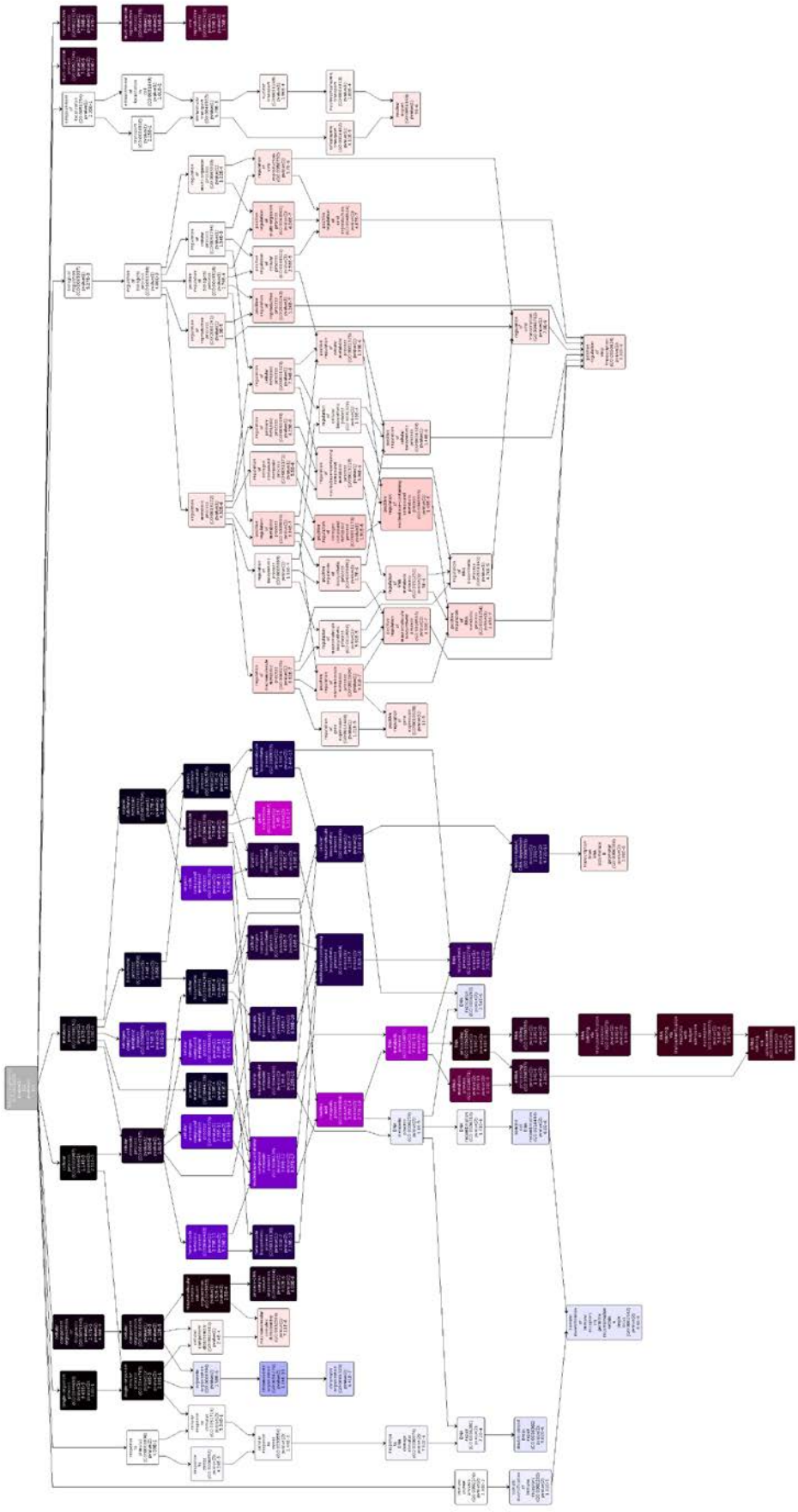

Supplementary Figure B.3: Full-size dendrogram demonstrating the dominant gene ontology categories by biological process between WRN-enriched samples that were treated either with control DMSO (trending blue) or CPT (trending red).
Appendix b fold changes

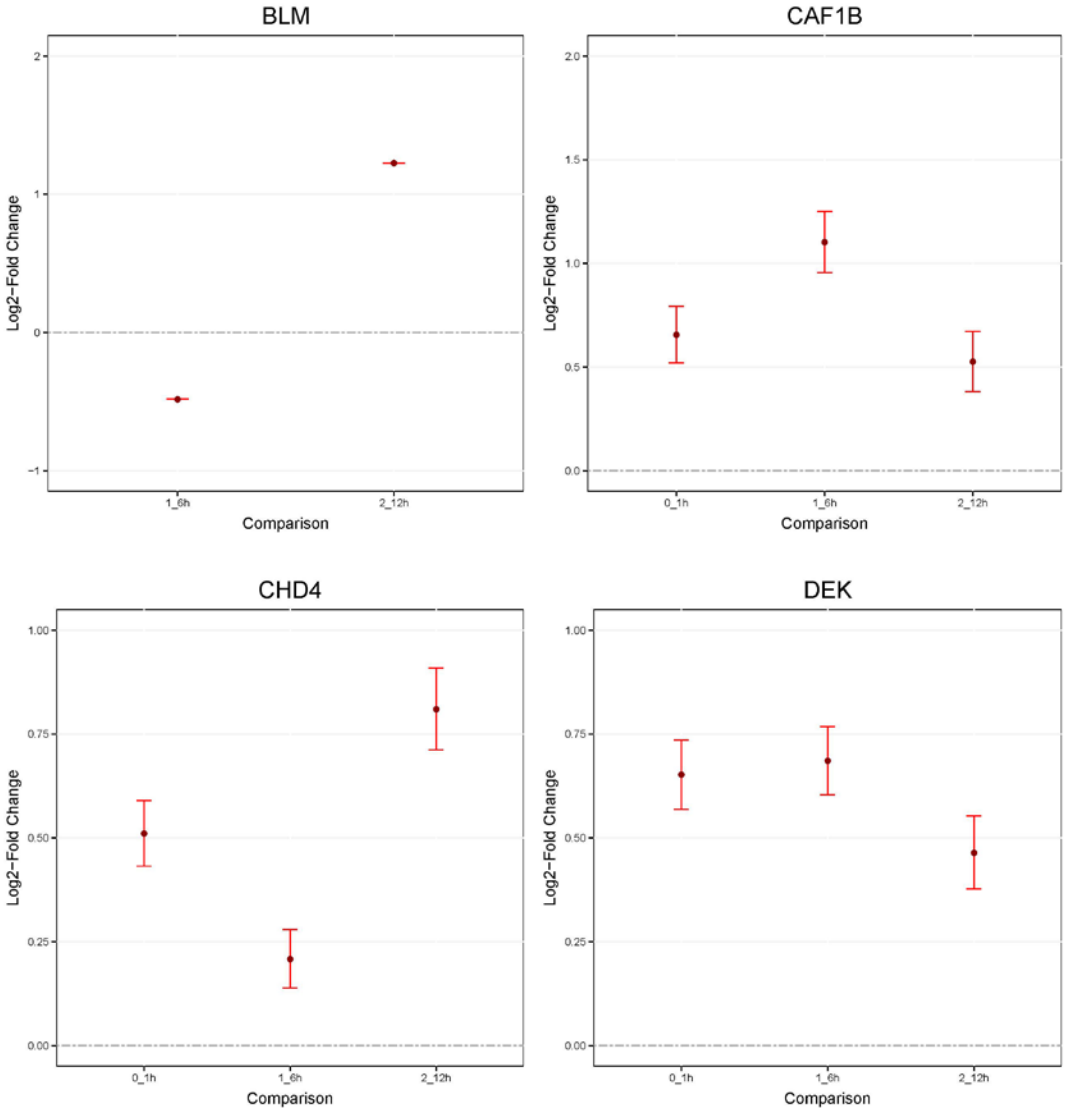

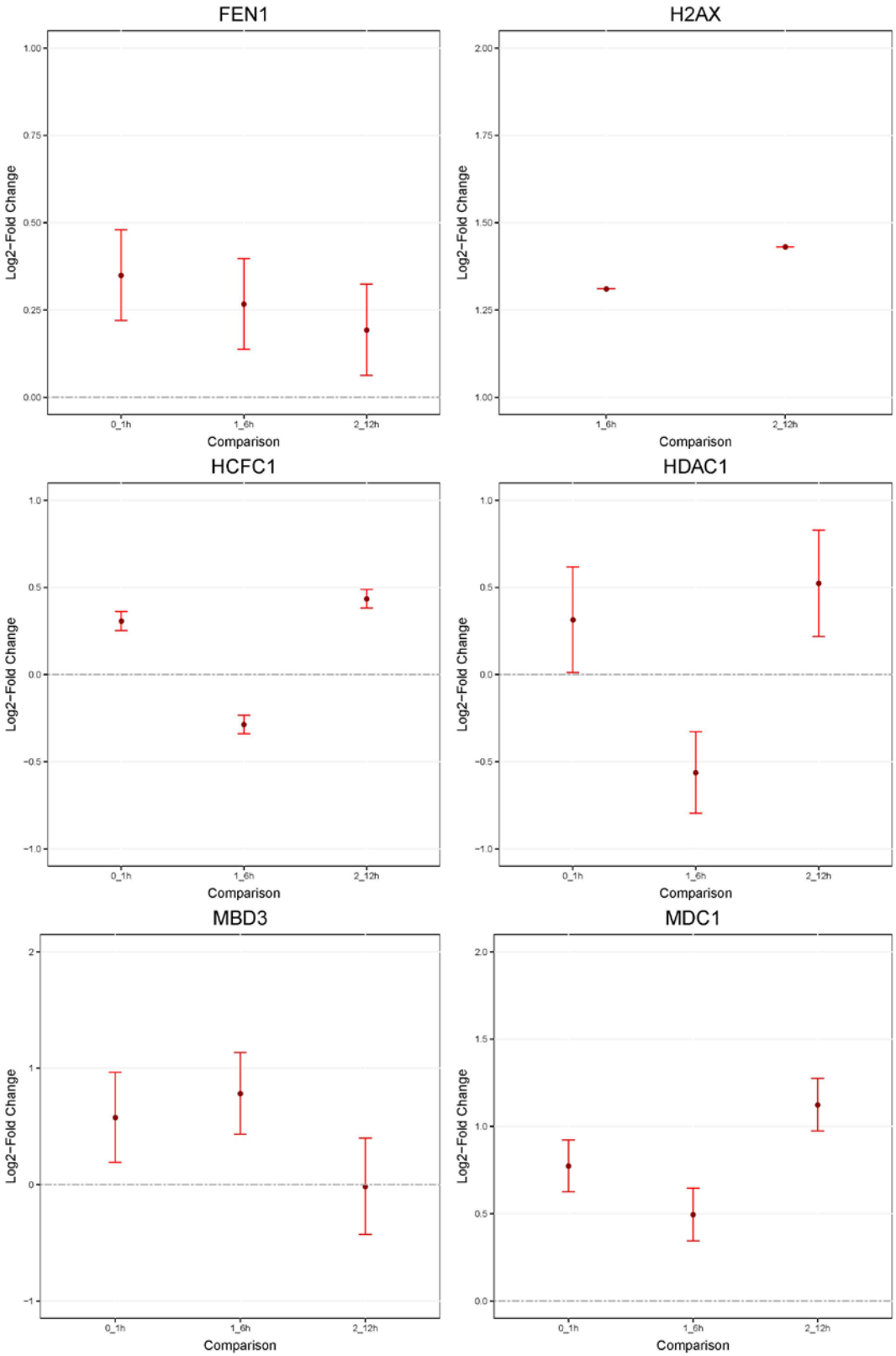
FEN1
H2AX
HCFC1
HDAC1
MBD3
MDC1
Log2−Fold Change
Comparison
0_1h
1_6h
2_12h

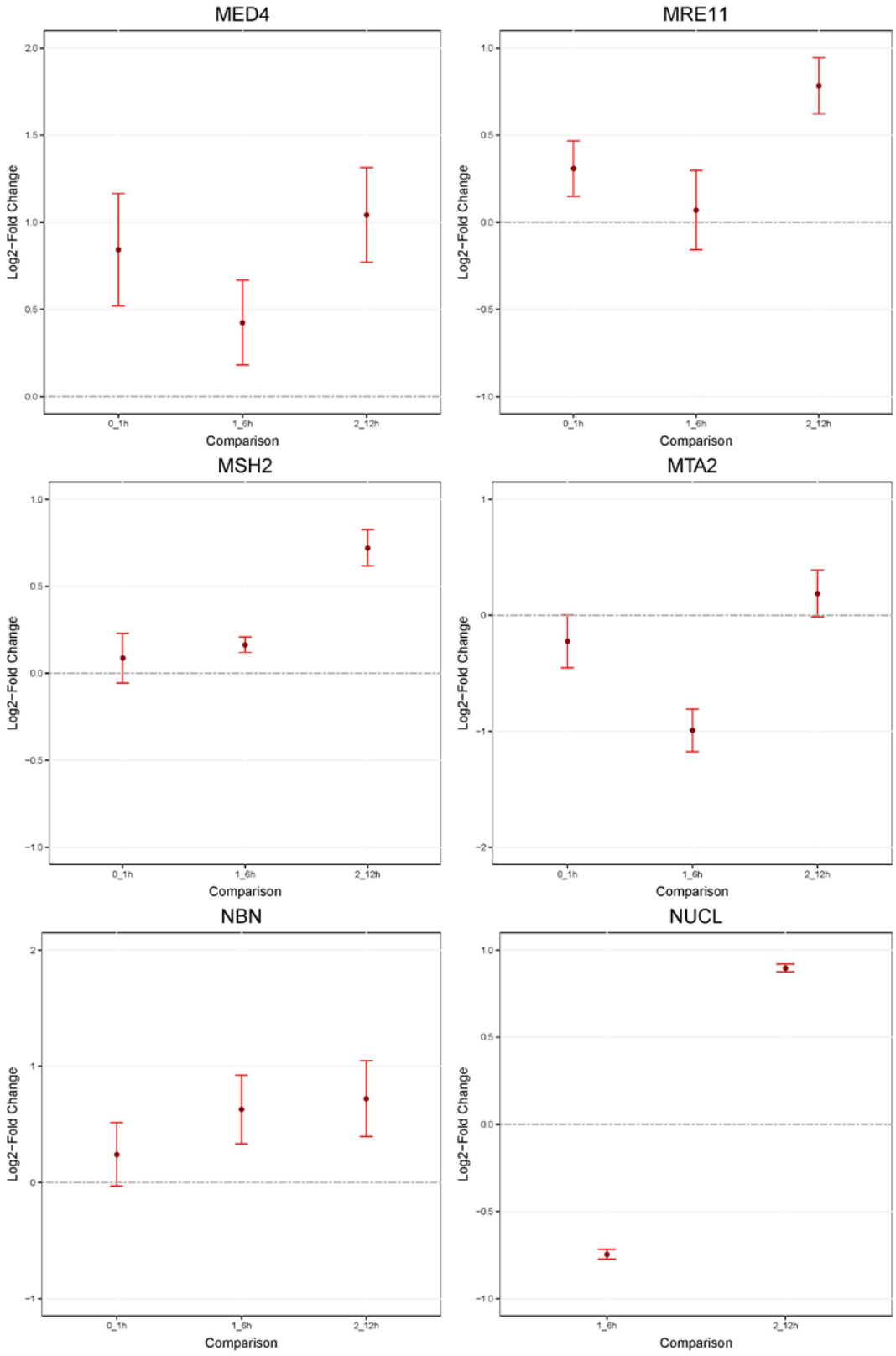
MED4
MRE11
MSH2
MTA2
NBN
NUCL
Log2−Fold Change
Comparison
0_1h
1_6h
2_12h

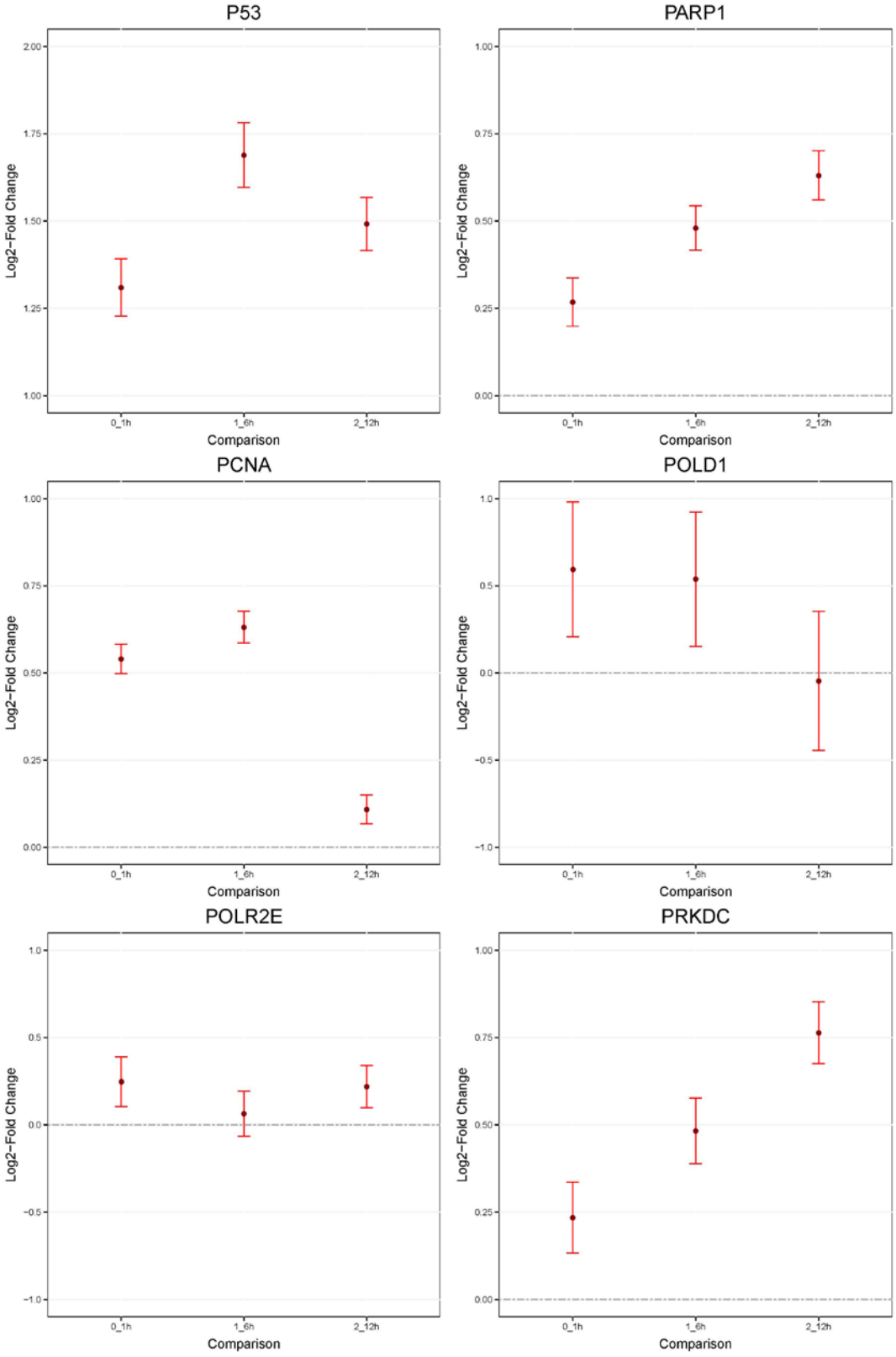
P53
PARP1
PCNA
POLD1
POLR2E
PRKDC
Log2−Fold Change
Comparison
0_1h
1_6h
2_12h

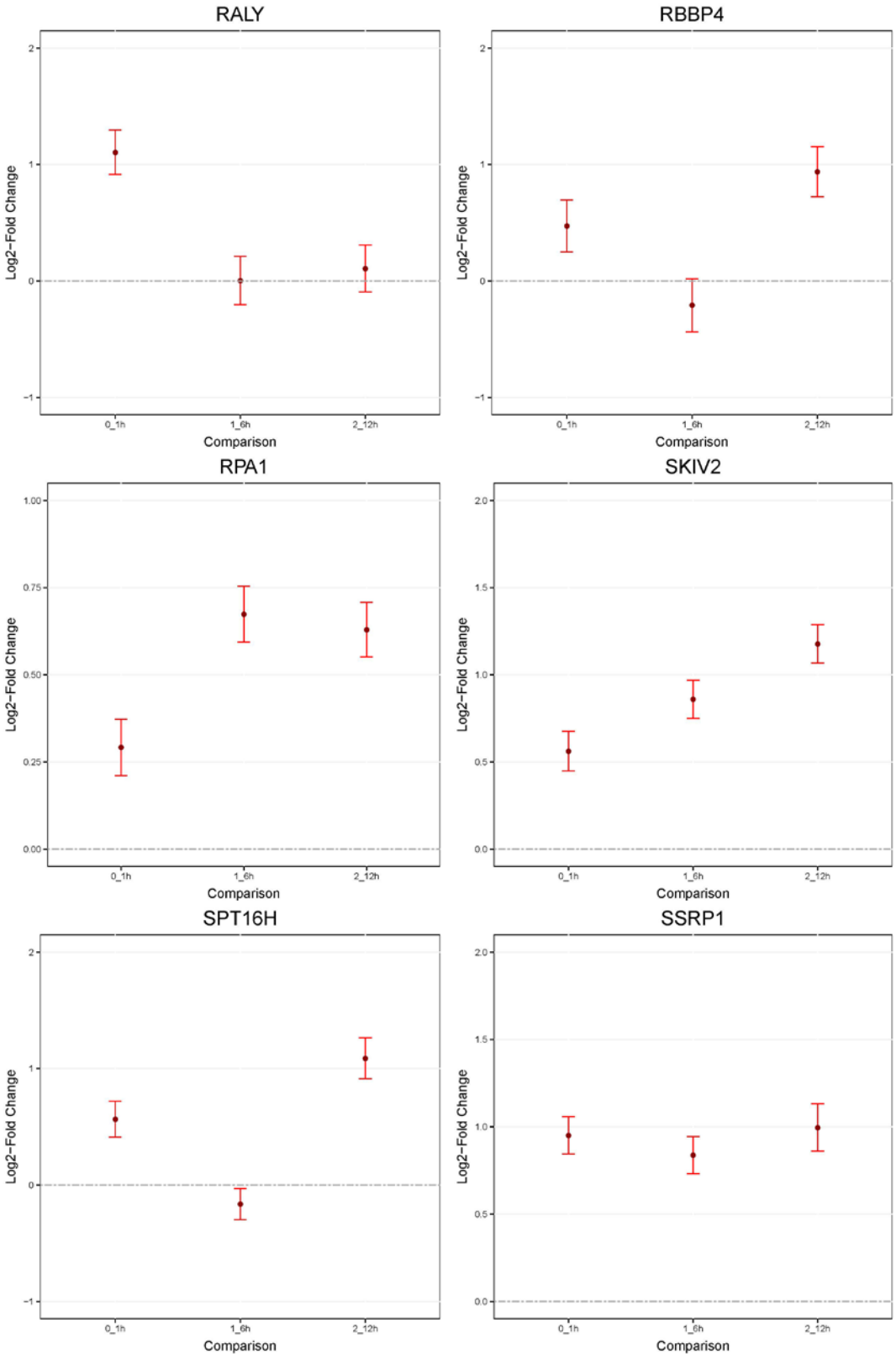
RALY
RBBP4
RPA1
SKIV2
SPT16H
SSRP1
Log2−Fold Change
Comparison
0_1h
1_6h
2_12h

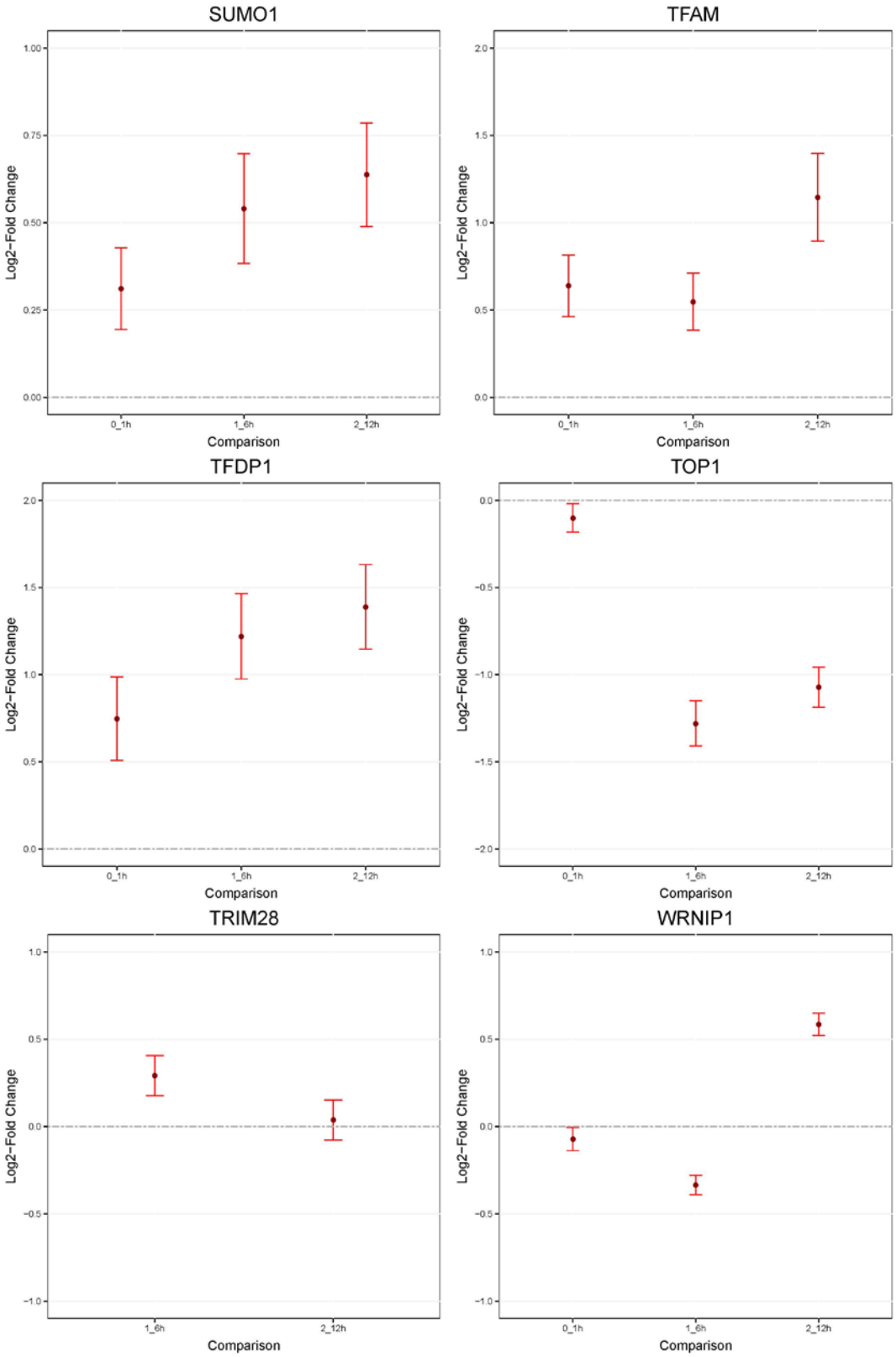
SUMO1
TFAM
TFDP1
TOP1
TRIM28
WRNIP1
Log2−Fold Change
Comparison
0_1h
1_6h
2_12h

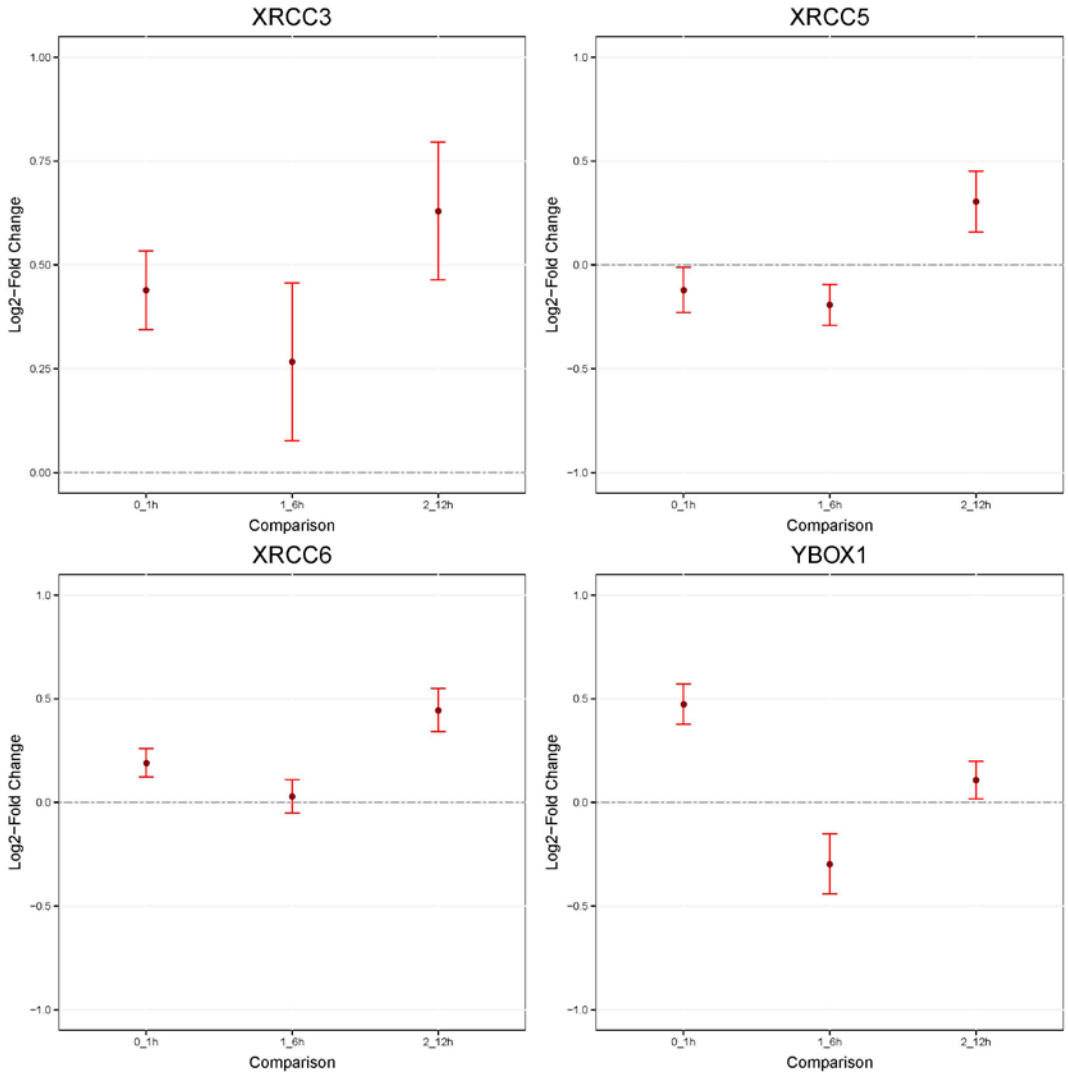

Supplementary Figure B.4: all data as exported from MSstats on protein association dynamics between WRN and its potential interaction partners

Appendix C: Preliminary data showing localization patterns of WRN domain delection mutants

All images show anti-HA staining for target protein and overlay with DAPI

Localization of domain-deletion mutants of WRN show unique distribution patterns, some of which closely mimic the distribution of SH-tagged wild-type WRN, and some localizing to other cellular compartments.This is important preliminary data for using these constructs for comparative studies.

SH-nLacZ

- Appears to localize mostly to the nucleus, but cytoplasmic staining is also very visible
- Uniform staining in most cells

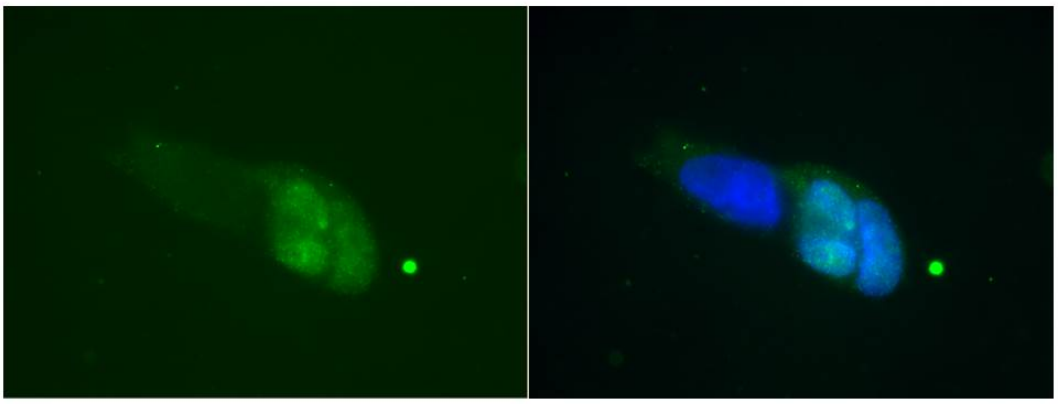

SH-nLacZ

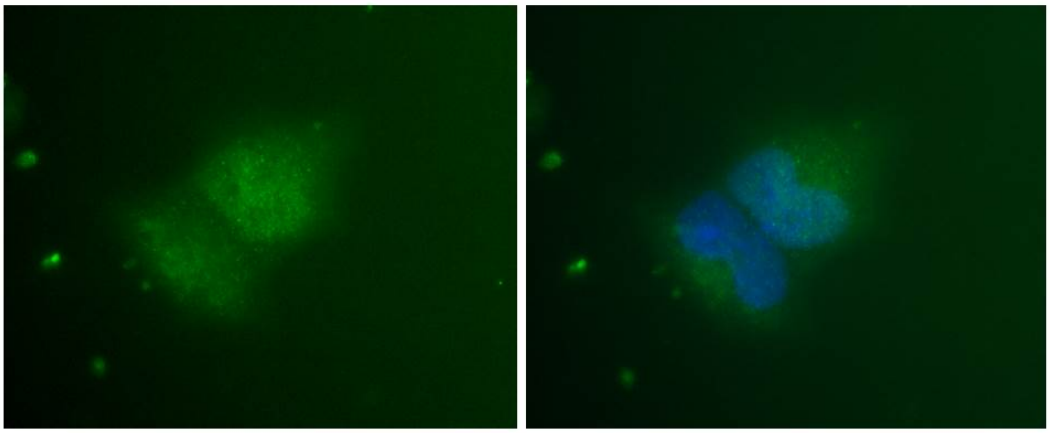

SH-nLacZ

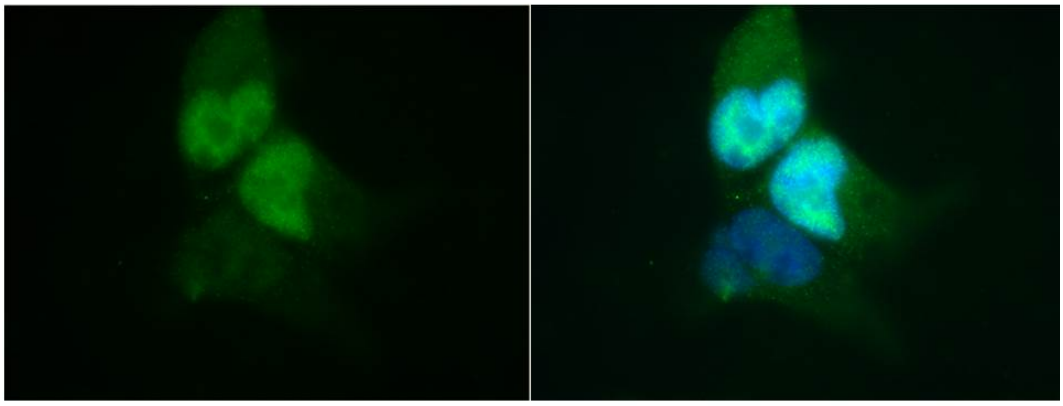

SH-WRN (WT)

- Localizes to the nucleus, in focal pattern
- ~30-35% of all cells showed staining

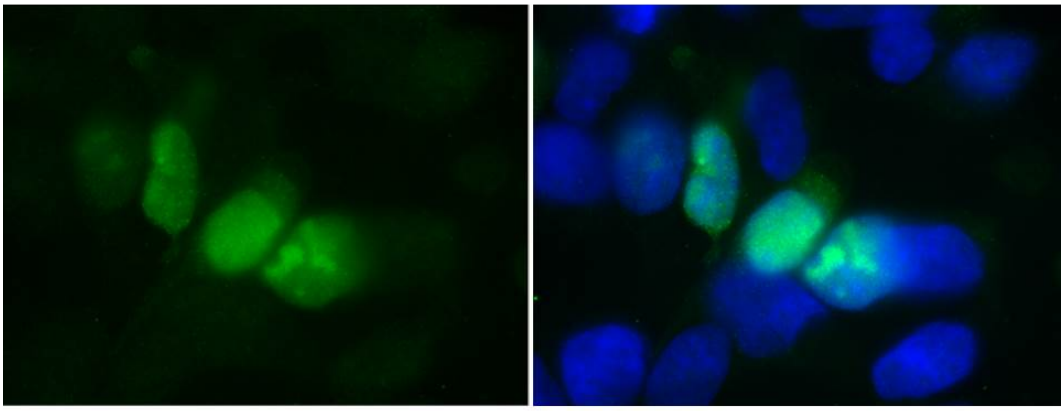

SH-WRN (WT)

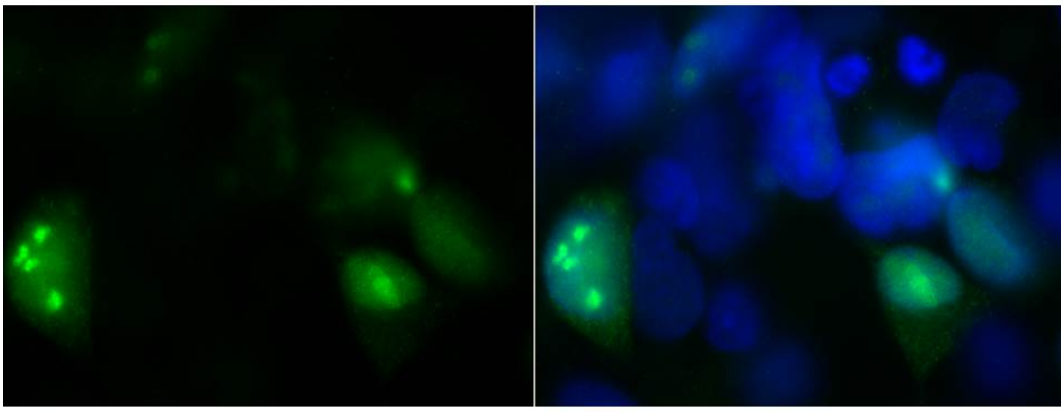

SH-WRN (WT)

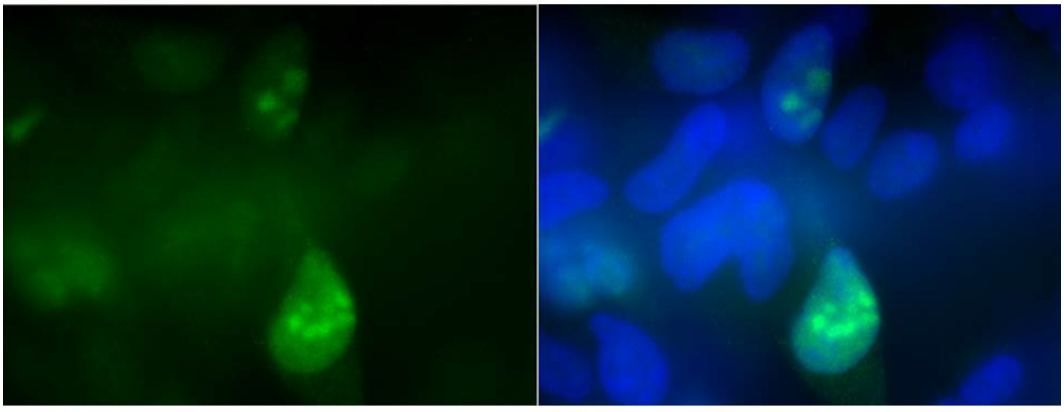

SH-WRN ExoΔ

- Localizes to the nucleus, in very clear focal pattern
- ~35% of all cells showed staining

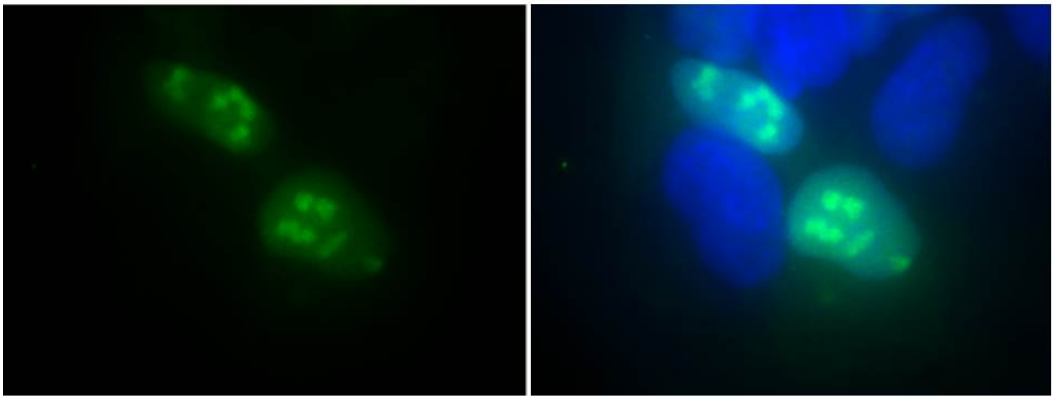

SH-WRN ExoΔ

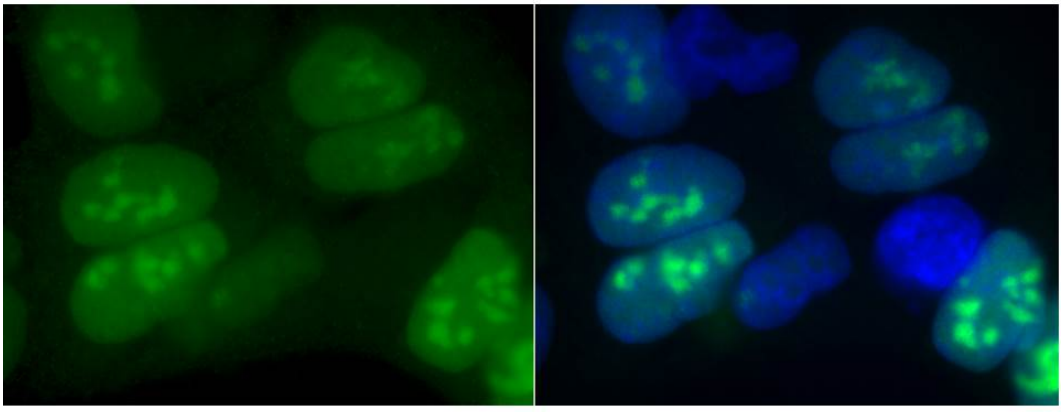

SH-WRN ExoΔ

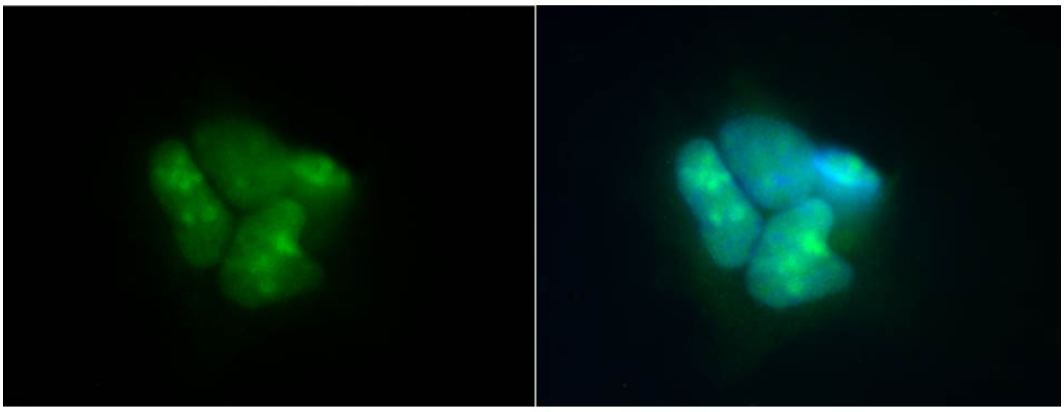

SH-WRN MultiΔ

- Diffuse staining in the nucleus, and strong staining in the cytoplasm
- ~80% of all cells showed staining

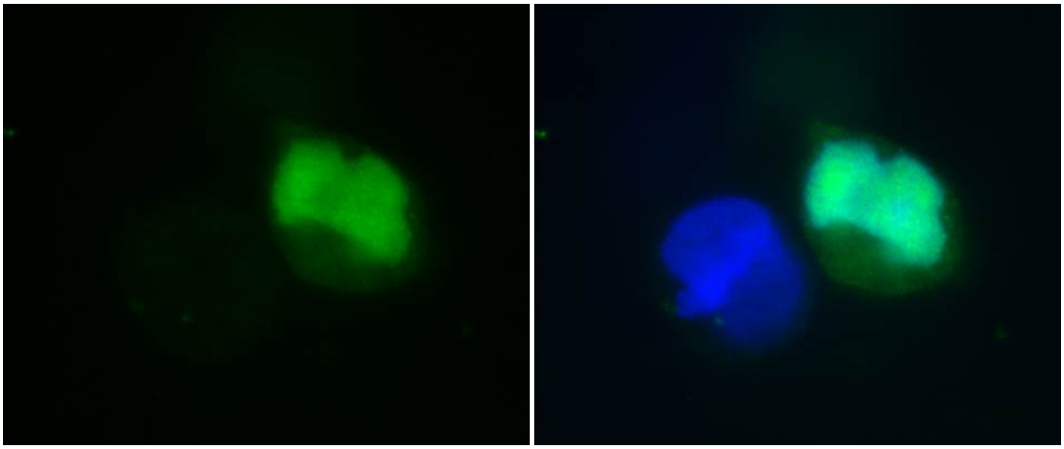

SH-WRN MultiΔ

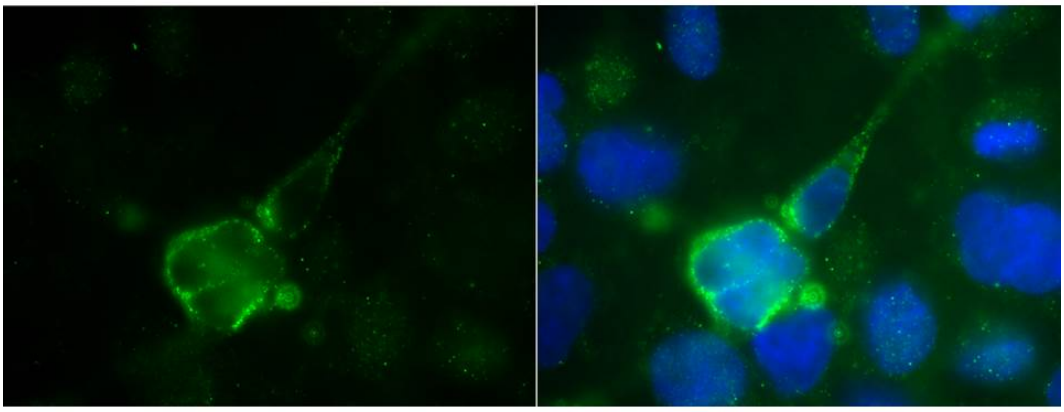

SH-WRN MultiΔ

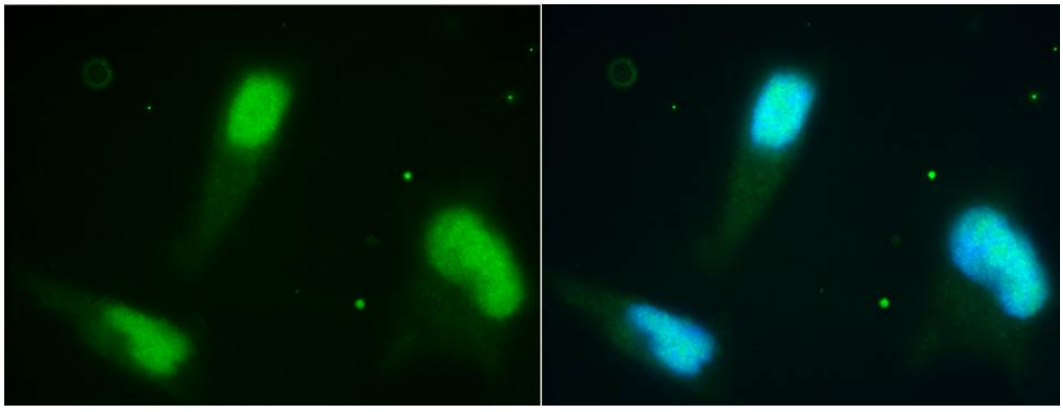

SH-WRN HRDCΔ

- Mostly cytoplasmic staining
- >80% of all cells showed staining

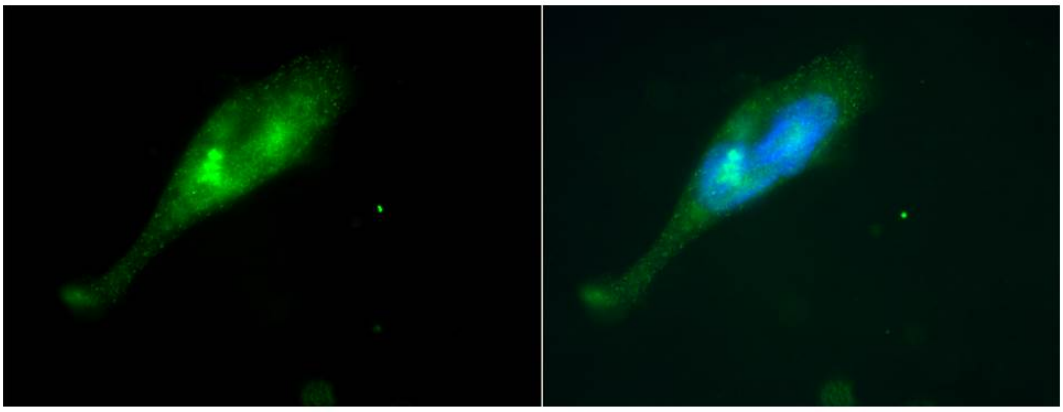

SH-WRN HRDCΔ

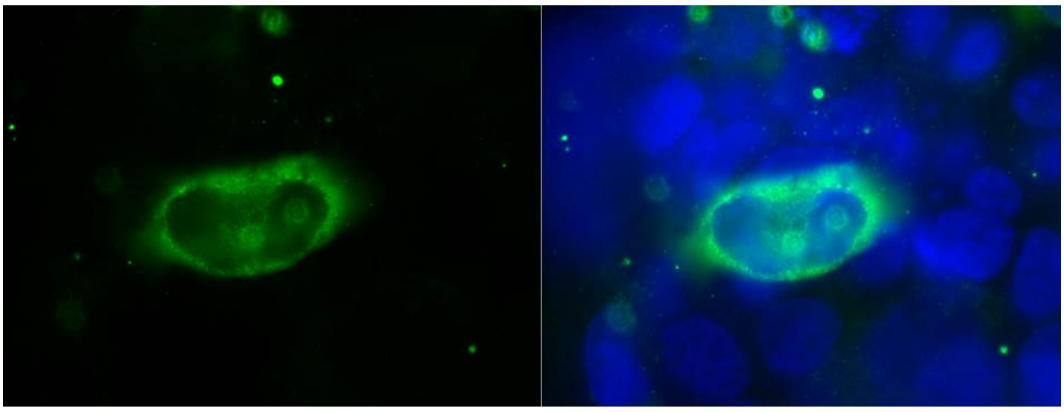

SH-WRN HRDCΔ

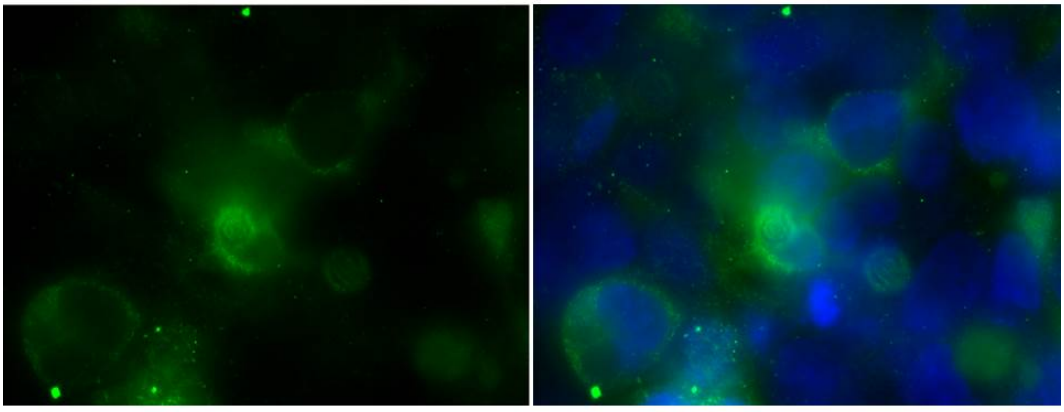

Vita

Veronika A. Glukhova was born in Obninsk, near Moscow, Russia, to two engineers. Her mother holds an M.S. in Computer Engineering, and her father holds an M.S. degree in Nuclear Physics and Engineering. In 1981 her family moved to Ukraine, where her parents worked at the Chernobyl Nuclear Power Plant. In 1986, following the accident, the family was evacuated and eventually moved to Kiev, where they lived for 9 years before emigrating to the United States in 1995.

Her parents' profession and general interest in sciences, strong focus on science and mathematics education in the Soviet Union, and early childhood events have all contributed to Veronika's interest in science and medicine. After graduating from Hanford High School in Richland, WA, she studied Cell Biology at Western Washington University and received her B.S. in 2003. During the course of her study she was a recipient of multiple fellowships to pursue undergraduate research in the Pacific Northwest National Laboratory and Brookhaven National Laboratory. These experiences provided more than involvement in cutting-edge research; they also offered the knowledge and familiarity with research environment.

While doing research in environmental microbiology under tutelage of Dr. Yuri Gorby at PNNL, Veronika became involved in a side project with the lab of Dr. Richard D. Smith, for mass spectrometric analysis of microbial proteins. This project and subsequent move to the Smith lab was the beginning of a new pursuit and a newfound interest in biochemistry and analytical chemistry. In 2004 Veronika moved to Seattle to work at the Fred Hutchinson Cancer Research Center with Dr. Samir Hanash, where she oversaw LC-MS method development and implementation for analysis of human plasma and serum samples. Veronika began her graduate studies at the Department of Pathology at the University of Washington School Of Medicine in

Fall of 2006, under Dr. Raymond J. Monnat Jr, applying her knowledge of MS to study protein interaction network of the WRN protein. Dual advising under Dr. Michael MacCoss allowed access to best instrumentation and valuable interaction with other MS specialists.

Upon graduation, Veronika plans to begin post-doctoral work in the laboratory of Dr. Richard James at Seattle Children's Research Institute, Center for Immunity and Immunotherapies.